

**Examination of the Mechanism of Corrosion  
Inhibition by  $\text{Ca}(\text{NO}_2)_2$ - and  $\text{Ca}(\text{NO}_3)_2$ -based  
Admixtures in Concrete**

**by**

**Laura Mammoliti**

**A thesis  
presented to the University of Waterloo  
in fulfilment of the  
thesis requirement for the degree of  
Doctor of Philosophy  
In  
Mechanical Engineering**

**Waterloo, Ontario, Canada, 2001**

**©Laura Mammoliti, 2001**



**National Library  
of Canada**

**Acquisitions and  
Bibliographic Services**

**395 Wellington Street  
Ottawa ON K1A 0N4  
Canada**

**Bibliothèque nationale  
du Canada**

**Acquisitions et  
services bibliographiques**

**395, rue Wellington  
Ottawa ON K1A 0N4  
Canada**

*Your file Votre référence*

*Our file Notre référence*

**The author has granted a non-exclusive licence allowing the National Library of Canada to reproduce, loan, distribute or sell copies of this thesis in microform, paper or electronic formats.**

**The author retains ownership of the copyright in this thesis. Neither the thesis nor substantial extracts from it may be printed or otherwise reproduced without the author's permission.**

**L'auteur a accordé une licence non exclusive permettant à la Bibliothèque nationale du Canada de reproduire, prêter, distribuer ou vendre des copies de cette thèse sous la forme de microfiche/film, de reproduction sur papier ou sur format électronique.**

**L'auteur conserve la propriété du droit d'auteur qui protège cette thèse. Ni la thèse ni des extraits substantiels de celle-ci ne doivent être imprimés ou autrement reproduits sans son autorisation.**

**0-612-65250-5**

**Canada**

**The University of Waterloo requires the signatures of all persons using or photocopying this thesis. Please sign below and give address and date.**

## **Abstract**

**Chloride-induced corrosion is responsible for the deterioration of many reinforced concrete structures such as roads, bridges, parking garages and marine structures. Calcium nitrite ( $\text{Ca}(\text{NO}_2)_2$ ) inhibitors are increasingly becoming the weapon of choice to address this problem. However, while many studies have shown these inhibitors to be effective in the short term, the lack of understanding of the mechanism of inhibition, and hence of their effectiveness after the many years normally taken for chlorides to penetrate the concrete cover, has made many jurisdictions wary of their use. Previous investigations show mixed results regarding the effectiveness of this inhibitor and most research within a concrete environment has simply determined the time to initiate corrosion and the subsequent corrosion rate without addressing the chemical reactions that may be occurring between the concrete and the inhibitor. A hypothesis for the mechanism by which calcium nitrite delays the onset of chloride-induced corrosion of reinforcing steel in concrete involving these reactions is proposed which is based on previous work by the researcher.**

**In the present investigation, a series of experiments were conducted to examine the effect of two commercially available calcium nitrite inhibitors (designated CN1 and CN2, respectively) and laboratory grade calcium nitrate. Studies of steel in synthetic concrete pore solution and of cement paste were conducted. Two types of cement were used: white Type 50 and grey Type 10 (Ordinary Portland Cement – OPC). Corrosion measurements in synthetic concrete pore solution found that none of the inhibitors inhibited or delayed the onset of corrosion. These tests also showed that a solid precipitate containing chlorides forms in all solutions, with the highest chloride concentration being in the precipitate from the solution containing CN1. Raman spectroscopy was used to determine the composition of the passive film formed on samples immersed in the control solution (Control) and CN1 solution both with and without exposure to chlorides. CN1 was found to have no beneficial effect to the passive layer formed.**

**Mercury intrusion porosimetry determined the effect of the admixtures on the total, capillary and gel porosities of two types of hardened cement pastes containing admixtures (Type 50 White and Type 10 Grey), both prior to and after exposure to a 2 % chloride ponding**

**solution. Inhibitors had the greatest effect on the gel porosity, decreasing the proportions compared to the Control mixes both before and after exposure to 2 %  $\text{Cl}^-$  ponding solution. Acid soluble chloride titration showed that all mixes had lower total chloride concentrations than expected based on the volume of ponding solution absorbed by cylinders. This indicates that water is entering the sample at a faster rate than chlorides.**

**Three forms of bound chlorides were detected by thermal analysis: Friedel's salt, calcium hydroxychloride and  $\text{Cl}^-$  in the C-S-H. The latter forms were found only in the cylinders made from OPC, and were highest in concentration in the OPC paste made with CN1. A sequence for formation of bound chlorides is proposed based on these observations and other currently unpublished research.**

**Using pore solution expression, it was determined that only a minor fraction of the admixed nitrites or nitrates is present in the pore water, indicating that nitrite and nitrate are incorporated into the solid cement hydration products. Chloride concentrations in ponded cylinders were also found to be disproportionate to the amount of ponding solution absorbed.**

**The results of the various tests indicate that the mechanism of inhibition by calcium nitrite is an increased binding of the chlorides in the solid phases of the cement paste, thereby removing them from the pore solution where they are able to break down the passive film on the reinforcing steel. However, significant differences were found between the chemistry and structure of the pastes made from white cement and OPC indicating that the assumption that inhibitors will affect all concretes in the same fashion is incorrect.**

## **Acknowledgements**

**I wish to express my appreciation to my supervisor, Dr. Carolyn Hansson, on a personal and professional level. Not only did she provide invaluable assistance regarding the scope of this thesis, she continued to have faith in me when I had lost faith in myself. Her guidance and support were critical to the completion of this document and my growth as a researcher and human being.**

**Special thanks must also be extended to Dr. Eric Reardon, Dr. Marios Ioannidis and Monique Hobbs, who provided technical information at the “eleventh hour”. Their help proved invaluable in my time of need and will not be forgotten. I’d also like to thank the technical staff at the University of Waterloo, in particular Tracy Fowler, Randy Fagan, Marek Odziemkowski, Norval Wilhelm, Ralph Dickhout, and Marius Van Reenen. I’d also like to thank the secretarial staff of Mechanical Engineering, in particular Susan Spaetzle, for their assistance throughout the years.**

**Where would I be without my partners in crime, Tracy Marcotte, Sean Monkman and Oliver Geprægs, whose support, both technically and personally, made many moments bearable and even enjoyable. I only hope that I am fortunate enough to work with these individuals again. We make a great team. I’d also like to thank my fellow graduate students in the “Tower Block”, both past and present, for enduring my rantings and ravings over the past five years: Per Munther, Beth Reyburn, Kevin Spencer, Jeff McIsaac, Ryan Strom, Troy D’Hondt, Tam Nguyen and Shelley Carter-Schofield.**

**I wouldn’t be writing this today if it weren’t for the constant and unwavering support and encouragement of family: my parents, Rosa and Pasquale Mammoliti, my brothers and sister, Sam, Sergio, and Maria, my sisters-in-law, Linda Vieregge and Wendy Mammoliti, and my niece and nephew, Jessica and Travis. Of course, the animals in my life must also get some credit for maintaining my sanity: Bugs, Spider, Dorian, Hobo and especially Tiger and Merv, who loved me no matter what – particularly when I gave them milk or treats in the middle of the night!**

**Finally, words cannot convey how indebted I am to my husband, Fred Bakker. Your patience, understanding, support and love throughout this period made this experience all the more rewarding. I cannot imagine my life without you.**

**Financial support was generously provided from the Natural Sciences and Engineering Research Council of Canada (NSERC), Materials and Manufacturing Ontario (MMO), Cement Association of Canada (CAC), and the University of Waterloo in the form of scholarships and teaching assistantships.**

## Table of Contents

Abstract .....	iv
Acknowledgements.....	vi
List of Tables .....	x
List of Figures.....	xiii
Nomenclature.....	xxiii
Chapter 1: Introduction .....	1
Chapter 2: Literature Review .....	4
2.1 Concrete .....	4
2.1.1 Cement Chemistry.....	4
2.1.2 Cement Hydration .....	5
2.1.3 Chemically Bound Chlorides.....	8
2.1.4 Porosity.....	9
2.2 Corrosion of Steel in Concrete .....	10
2.2.1 Pitting Corrosion .....	13
2.3 Calcium Nitrite and Calcium Nitrate Based Inhibitors.....	16
2.4 Techniques for Characterization .....	21
2.4.1 Electrochemical Corrosion Testing.....	21
2.4.1.1 Full Cyclic Polarization .....	21
2.4.1.1.1 Limitations of Full Cyclic Polarization .....	23
2.4.1.2 Linear Polarization Resistance .....	24
2.4.1.2.1 Limitations of Linear Polarization Resistance .....	25
2.4.2 Raman Spectroscopy .....	26
2.4.3 Thermal Analysis .....	27
2.4.3.1 Thermogravimetric Analysis.....	27
2.4.3.2 Derivative Thermogravimetric Analysis.....	28
2.4.3.3 Differential Thermal Analysis.....	28
2.4.3.4 Limitations of Thermal Analysis.....	29
2.4.4 Mercury Intrusion Porosimetry.....	29
2.4.4.1 Limitations of Mercury Intrusion Porosimetry .....	30
2.4.5 Environmental Scanning Electron Microscope with Energy Dispersive X-Ray Spectroscopy .....	31
2.4.6 Potentiometric Titration .....	34
2.4.7 Pore Solution Expression .....	35
2.4.7.1 Inductively Coupled Plasma.....	36
2.4.7.2 Ion Chromatography .....	36
2.4.7.3 Alkalinity.....	37
Chapter 3: Objectives and Rationale.....	38
3.1 Alternative Mechanism for Corrosion Inhibition by $\text{Ca}(\text{NO}_2)_2$ .....	38
Chapter 4: Experimental Procedures .....	40

4.1 Materials Used.....	40
4.1.1 Cement.....	40
4.1.2 Chemical Corrosion Inhibitors.....	41
4.1.3 Deformed Reinforcing Steel.....	42
4.1.4 Synthetic Concrete Pore Solution.....	42
4.2 Sample Preparation.....	42
4.2.1 Cement Paste Cylinders.....	42
4.2.2 Corrosion Samples.....	43
4.3 Synthetic Concrete Pore Solution Tests.....	44
4.3.1 Corrosion Behaviour and Corrosion Rate Testing.....	44
4.3.2 Passive Film Analysis.....	46
4.4 Cement Paste Cylinder Testing.....	47
4.4.1 Thermal Analysis.....	48
4.4.2 Pore Size Distribution.....	51
4.4.3 Chloride Profiling.....	52
4.4.4 Pore Solution Expression.....	54
<b>Chapter 5: Synthetic Pore Solution Tests: Results and Discussion.....</b>	<b>57</b>
5.1 Corrosion Testing.....	57
5.2 Passive Film Analysis.....	65
5.2.1 Synthetic Pore Solution without Chlorides.....	65
5.2.2 Synthetic Pore Solution with Chlorides.....	67
<b>Chapter 6: Transport Properties of Cement Pastes: Results and Discussion.....</b>	<b>91</b>
6.1 Mercury Intrusion Porosimetry.....	91
6.1.1 White Cement Paste Cylinders.....	91
6.1.1.1 Unponded Cylinders.....	91
6.1.1.2 Ponded Cylinders.....	93
6.1.1.3 Comparison of Unponded and Ponded Cylinders.....	94
6.1.2 OPC Paste Cylinders.....	96
6.1.2.1 Unponded Cylinders.....	96
6.1.2.2. Ponded Cylinders.....	96
6.1.2.3 Comparison of Unponded and Ponded Cylinders.....	97
6.2 Acid Soluble Chloride Titrations.....	99
6.2.1 Ponded White Cement Paste Cylinders.....	99
6.2.2 Ponded OPC Paste Cylinders.....	100
6.2.3 Qualification of Chloride Titration Results.....	101
<b>Chapter 7: Chemical Analysis of Cement Pastes: Results and Discussion.....</b>	<b>109</b>
7.1 Thermal Analysis.....	109
7.1.1 Pure Components.....	109
7.1.2 White Cement Paste Cylinders.....	110
7.1.2.1 Unponded Cylinders.....	110
7.1.2.2 Ponded Cylinders.....	112
7.1.2.3 Comparison of Unponded and Ponded Cylinders.....	113
7.1.3 OPC Paste Cylinders.....	114
7.1.3.1 Unponded Cylinders.....	114
7.1.3.2 Ponded Cylinders.....	115



7.1.3.3 Comparison of Unponded and Ponded Cylinders .....	117
7.2 Pore Solution Expression.....	118
7.2.1 White Cement Paste Cylinders .....	119
7.2.1.1 Unponded Cylinders .....	119
7.2.1.2 Ponded Cylinders.....	120
7.2.1.3 Comparison of Unponded and Ponded Cylinders .....	123
7.2.2 OPC Paste Cylinders .....	125
7.2.2.1 Unponded Cylinders .....	125
7.2.2.2 Ponded Cylinders.....	126
7.2.2.3 Comparison of Unponded and Ponded Cylinders .....	128
<b>Chapter 8: Comparison of White and OPC Cement Pastes: Results and Discussion.....</b>	<b>146</b>
8.1 Transport Properties of Cement Pastes.....	146
8.1.1 Mercury Intrusion Porosimetry.....	146
8.1.2 Acid Soluble Chloride Titrations .....	149
8.2 Chemical Analysis of Cement Pastes .....	150
8.2.1 Thermal Analysis .....	150
8.2.2 Pore Solution Expression .....	151
<b>Chapter 9: Overall Discussion, Conclusion and Recommendations .....</b>	<b>171</b>
9.1 Overall Discussion.....	171
9.2 Conclusions .....	179
9.3 Recommendations .....	181
<b>References .....</b>	<b>182</b>
<b>Appendix A .....</b>	<b>190</b>
<b>Appendix B.....</b>	<b>208</b>
<b>Appendix C.....</b>	<b>212</b>
<b>Appendix D .....</b>	<b>228</b>
<b>Appendix E.....</b>	<b>236</b>
<b>Appendix F.....</b>	<b>245</b>

## List of Tables

<b>Table 2.1 Major constituents and composition ranges of Portland cement .....</b>	<b>4</b>
<b>Table 2.2 Typical calculated potential compound composition and application of Portland cements.....</b>	<b>4</b>
<b>Table 2.3 Typical composition of pore water from concrete made with Ordinary Portland Cement (water/cement ratio by weight ~ 0.5) .....</b>	<b>6</b>
<b>Table 2.4 Formation of hydration products from C<sub>3</sub>A.....</b>	<b>6</b>
<b>Table 2.5 Dividing radius between capillary and gel porosity.....</b>	<b>10</b>
<b>Table 4.1 Chemical analyses of cements .....</b>	<b>40</b>
<b>Table 4.2 Chemical analysis of CN1 and CN2.....</b>	<b>41</b>
<b>Table 4.3 Chemical analysis of deformed reinforcing steel.....</b>	<b>42</b>
<b>Table 4.4 Mix designs for cement paste cylinders .....</b>	<b>43</b>
<b>Table 4.5 Age at initial ponding solution exposure and duration of ponding for White and OPC paste cylinders.....</b>	<b>48</b>
<b>Table 4.6 Cylinder ages at time of thermal analysis and porosity measurements.....</b>	<b>50</b>
<b>Table 5.1 Probability of corrosion based on free potential measurement.....</b>	<b>58</b>
<b>Table 5.2 Chemical analysis of filtered synthetic pore solutions containing 8 % Cl<sup>-</sup> as NaCl .....</b>	<b>60</b>
<b>Table 5.3 Calculated and experimental results from Water Quality Tests (units = mg/L).....</b>	<b>60</b>
<b>Table 5.4 Standard Gibb's energy of formation and solubility values for selected hydroxides and nitrites .....</b>	<b>62</b>
<b>Table 5.5 Standard Gibb's energy of formation and solubility values for selected salts.....</b>	<b>63</b>
<b>Table 5.6 EDS Results of Dried Pore Solutions.....</b>	<b>64</b>
<b>Table 6.1 Average coarse, fine and total pore intrusion volumes in white cement paste cylinders .....</b>	<b>92</b>
<b>Table 6.2 Effect of inhibitors on coarse, fine and total porosity with respect of White Control.....</b>	<b>93</b>
<b>Table 6.3 Average coarse, fine and total pore intrusion volumes in ponded white cement paste cylinders .....</b>	<b>94</b>
<b>Table 6.4 Effect of inhibitors on coarse, fine and total porosity with respect to ponded white paste Control .....</b>	<b>94</b>
<b>Table 6.5 Comparison of porosity values of unponded and ponded white cement paste cylinders .....</b>	<b>95</b>
<b>Table 6.6 Volume of absorbed ponding solution for ponded white cement paste cylinders ...</b>	<b>95</b>

<b>Table 6.7 Average coarse, fine and total pore intrusion volumes in OPC paste cylinders .....</b>	<b>97</b>
<b>Table 6.8 Effect of inhibitors on coarse, fine and total porosity with respect to OPC Control.....</b>	<b>97</b>
<b>Table 6.9 Average coarse, fine and total pore intrusion volumes in ponded OPC paste cylinders .....</b>	<b>99</b>
<b>Table 6.10 Effect of inhibitors on coarse, fine and total porosity with respect of ponded OPC Control .....</b>	<b>99</b>
<b>Table 6.11 Comparison of porosity values of unponded and ponded OPC paste cylinders ....</b>	<b>99</b>
<b>Table 6.12 Volume of absorbed ponding solution for ponded OPC paste cylinders .....</b>	<b>99</b>
<b>Table 6.13 Volume of ponding solution absorbed and total chloride concentration of ponded white cement paste cylinders .....</b>	<b>100</b>
<b>Table 6.14 Volume of ponding solution absorbed and total chloride concentration of ponded OPC paste cylinders.....</b>	<b>101</b>
<b>Table 7.1 Binding capacities of OPC paste mixes.....</b>	<b>117</b>
<b>Table 7.2 Conversion of alkalinity values to pH value for White Cement Paste expressed pore solutions.....</b>	<b>121</b>
<b>Table 7.3 Relationship of Na and Cl<sup>-</sup> concentrations to the volume of absorbed ponding solution in ponded White Cement Paste cylinders .....</b>	<b>122</b>
<b>Table 7.4 Comparison of molar quantities of nitrite and nitrate from admixture and expressed solutions from Ponded White Cement Paste systems.....</b>	<b>122</b>
<b>Table 7.5 Conversion of alkalinity values in pH value for Ponded White Cement Paste expressed pore solutions .....</b>	<b>123</b>
<b>Table 7.6 pH of expressed pore solutions from Unponded and Ponded White Cement Paste Cylinders .....</b>	<b>124</b>
<b>Table 7.7 Conversion of alkalinity values in pH values for OPC Paste expressed pore solutions .....</b>	<b>126</b>
<b>Table 7.8 Relationship of Na and Cl<sup>-</sup> concentrations to the volume of absorbed ponding solution in ponded OPC Paste cylinders .....</b>	<b>126</b>
<b>Table 7.9 Comparison of molar quantities of nitrite and nitrate from admixture and expressed solutions from Ponded OPC Paste cylinders.....</b>	<b>128</b>
<b>Table 7.10 Conversion of alkalinity values in pH value for Ponded OPC Paste expressed pre solutions.....</b>	<b>128</b>
<b>Table 7.11 pH of expressed pore solutions from Unponded and Ponded OPC Paste Cylinders .....</b>	<b>131</b>
<b>Table 8.1 Average coarse, fine and total porosities from Control mixes.....</b>	<b>147</b>
<b>Table 8.2 Average coarse, fine and total porosities from CN1 mixes.....</b>	<b>147</b>
<b>Table 8.3 Average coarse, fine and total porosities from CN2 mixes.....</b>	<b>147</b>

<b>Table 8.4 Average coarse, fine and total porosities from <math>\text{Ca}(\text{NO}_3)_2</math> mixes.....</b>	<b>147</b>
<b>Table 8.5 Proportion of chloride in top 23 mm of White and OPC cylinders (g <math>\text{Cl}^-</math>/g paste) .....</b>	<b>150</b>
<b>Table 8.6 Relationship of <math>[\text{Na}^+]</math> and <math>[\text{Cl}^-]</math> to the volume of absorbed ponding solution in ponded White Cement and OPC paste cylinders.....</b>	<b>150</b>
<b>Table 9.1 Comparison of ponding duration and volume of ponding solution absorbed of MIP and Pore Solution Expression Samples.....</b>	<b>173</b>
<b>Table 9.2 Comparison of theoretical and measured total chloride content of White and OPC cylinders exposed to ponding solution .....</b>	<b>179</b>
<b>Table E.1 Analysis of expressed pore solution from White Cement Paste cylinders.....</b>	<b>236</b>
<b>Table E.2 Analysis of expressed pore solution from Ponded White Cement Paste cylinders .....</b>	<b>237</b>
<b>Table E-3 Analysis of expressed pore solution from OPC Paste cylinders .....</b>	<b>238</b>
<b>Table E-4 Analysis of expressed pore solution from Ponded OPC Paste cylinders.....</b>	<b>239</b>
<b>Table E-5 Molar quantities of cement components .....</b>	<b>240</b>
<b>Table E-6 Molar contributions of Inhibitors .....</b>	<b>240</b>
<b>Table E-7 Molar quantities of expressed pore solutions from Control White and OPC Unponded and Ponded Cylinders .....</b>	<b>241</b>
<b>Table E-8 Molar quantities of expressed pore solutions from CN1 White and OPC Unponded and Ponded Cylinders .....</b>	<b>242</b>
<b>Table E-9 Molar quantities of expressed pore solutions from CN2 White and OPC Unponded and Ponded Cylinders .....</b>	<b>243</b>
<b>Table E-10 Molar quantities of expressed pore solutions from <math>\text{Ca}(\text{NO}_3)_2</math> White and OPC Unponded and Ponded Cylinders .....</b>	<b>244</b>

## List of Figures

Figure 2.1 Mercury porosimetry curves for a Portland cement paste (w/c ratio =0.47) at various stages.....	10
Figure 2.2 Pourbaix diagram for the Fe-H <sub>2</sub> O System at 25°C .....	12
Figure 2.3 Schematic diagram of corrosion of rebar in concrete .....	13
Figure 2.4 Effect of corrosion product hydrolysis and recycling Cl <sup>-</sup> pitting corrosion.....	15
Figure 2.5 Postulated mechanism for inhibition by nitrite.....	17
Figure 2.6 Schematic of types of anodic polarization curves showing passive state, pitting corrosion and active and/or crevice corrosion.....	21
Figure 2.7 Schematic of pitting and passivation potentials an anodic polarization curve .....	22
Figure 2.8 Schematic of potential variation in full cyclic polarization.....	23
Figure 2.9 Applied current-linear polarization curve .....	25
Figure 2.10 Schematic representation of the Raman effect .....	26
Figure 2.11 Comparison of TGA and DTG curves, three of which exhibit overlapping reactions .....	29
Figure 2.12 The problem of inkbottle pores.....	31
Figure 2.13 Sources of secondary and backscattered electrons and characteristic x-rays.....	32
Figure 2.14 Characteristic x-rays.....	33
Figure 2.15 Isometric three-quarter section of pore fluid expression device.....	35
Figure 2.16 Simplified explanation of ion chromatography .....	37
Figure 4.1 Schematic representation of experiment set-up for corrosion studies .....	45
Figure 4.2 Plan view and photograph of in-situ Raman cell (60 mm diameter and 15 mm deep).....	46
Figure 4.3 Representation of procedures performed on unponded and ponded cement paste cylinders .....	49
Figure 4.4 Schematic drawing of cement paste cylinder sections for thermal analysis and porosity measurements where x=45 mm for unponded cylinders and x=25 mm for ponded cylinders.....	50
Figure 4.5 Schematic drawing of sectioning on ponding sample for Cl <sup>-</sup> titration .....	53
Figure 4.6 Pore solution expression apparatus.....	55
Figure 5.1 pH values of synthetic concrete pore solutions .....	71
Figure 5.2 Free potentials of samples immersed in Control synthetic pore solution .....	72
Figure 5.3 Free potentials of samples immersed in CN1-containing synthetic pore solution.....	72

<b>Figure 5.4 Free potentials of samples immersed in CN2-containing synthetic pore solution.....</b>	<b>73</b>
<b>Figure 5.5 Free potentials of samples immersed in Ca(NO<sub>3</sub>)<sub>2</sub>-containing synthetic pore solution.....</b>	<b>73</b>
<b>Figure 5.6 Representative cyclic polarization curves for samples immersed in Control synthetic pore solution .....</b>	<b>74</b>
<b>Figure 5.7 Representative cyclic polarization curves for samples immersed in CN1-containing synthetic pore solution .....</b>	<b>75</b>
<b>Figure 5.8 Representative cyclic polarization curves for samples immersed in CN2-containing synthetic pore solution .....</b>	<b>76</b>
<b>Figure 5.9 Representative cyclic polarization curves for samples immersed in Ca(NO<sub>3</sub>)<sub>2</sub>-containing synthetic pore solution .....</b>	<b>77</b>
<b>Figure 5.10 Comparison of representative cyclic polarization curves for samples immersed in solutions containing 8 % Cl<sup>-</sup> .....</b>	<b>78</b>
<b>Figure 5.11 Average corrosion current density vs. chloride content for synthetic pore solutions (as determined through LPR) .....</b>	<b>79</b>
<b>Figure 5.12 ESEM image of dried white deposit from Control solution (x 2000) where (1) particle and (2) spherulite.....</b>	<b>80</b>
<b>Figure 5.13 ESEM image of dried white deposit from CN1 solution (x 2000) where (1) tuber and (2) spherulite .....</b>	<b>80</b>
<b>Figure 5.14 ESEM image of dried white deposit from CN2 solution (x 2000) where (1) group and (2) spherulite .....</b>	<b>81</b>
<b>Figure 5.15 ESEM image of white crusty deposit on spout of CN1 cell (x 650).....</b>	<b>81</b>
<b>Figure 5.16 Sample surface exposed to Control pore solution prior to deposit removal (mag. 55 x) .....</b>	<b>82</b>
<b>Figure 5.17 Sample surface exposed to CN1 pore solution prior to deposit removal (mag. 55 x) .....</b>	<b>82</b>
<b>Figure 5.18 Sample surface exposed to Control pore solution after removal of surface deposit (mag. 110 x) .....</b>	<b>83</b>
<b>Figure 5.19 Sample surface exposed to CN1 pore solution after removal of surface deposit (mag. 110 x) .....</b>	<b>83</b>
<b>Figure 5.20 Raman spectra for sample in Control solution, no chlorides.....</b>	<b>84</b>
<b>Figure 5.21 Raman spectra for sample in CN1 solution, no chlorides .....</b>	<b>85</b>
<b>Figure 5.22 Comparison of shiny areas on samples in Control and CN1 solutions containing chlorides .....</b>	<b>86</b>
<b>Figure 5.23 Comparison of red areas on samples in Control and CN1 solutions containing chlorides .....</b>	<b>87</b>

<b>Figure 5.24 Comparison of black areas on samples in Control and CN1 solutions containing chlorides .....</b>	<b>88</b>
<b>Figure 5.25 Digital photographs of samples immersed in Control and CN1 pore solution containing 15 % chlorides (a) Control samples after 300 seconds at +400 mV SCE; (b) CN1 sample after 300 seconds at +400 mV SCE; (c) Control sample surface after anodic polarization in (a); (d) CN1 sample surface after anodic polarization in (b) .....</b>	<b>89</b>
<b>Figure 5.26 Raman spectra of precipitates from Control and CN1 solutions and laboratory grade Ca(OH)<sub>2</sub> .....</b>	<b>90</b>
<b>Figure 6.1 Cumulative intrusion volume vs. pore radius for average of three white cement paste cylinders .....</b>	<b>102</b>
<b>Figure 6.2 Average incremental intrusion volume vs. pore radius for white cement paste cylinders .....</b>	<b>102</b>
<b>Figure 6.3 Cumulative intrusion volume vs. pore radius for average of three ponded white cement paste cylinders .....</b>	<b>103</b>
<b>Figure 6.4 Average incremental intrusion volume vs. pore radius for ponded white cement paste cylinders .....</b>	<b>103</b>
<b>Figure 6.5 Comparison of capillary porosities of unponded and ponded white paste cylinders .....</b>	<b>104</b>
<b>Figure 6.6 Comparison of gel porosities of unponded and ponded white paste cylinders .....</b>	<b>104</b>
<b>Figure 6.7 Comparison of total porosities of unponded and ponded white paste cylinders ....</b>	<b>104</b>
<b>Figure 6.8 Cumulative intrusion volume vs. pore radius for average of three OPC cylinders .....</b>	<b>105</b>
<b>Figure 6.9 Average incremental intrusion volume vs. pore radius for OPC cylinders.....</b>	<b>105</b>
<b>Figure 6.10 Cumulative intrusion volume vs. pore radius for average of three ponded OPC cylinders.....</b>	<b>106</b>
<b>Figure 6.11 Average incremental intrusion volume vs. pore radius for ponded OPC cylinders .....</b>	<b>106</b>
<b>Figure 6.12 Comparison of capillary porosities of unponded and ponded OPC paste cylinders .....</b>	<b>107</b>
<b>Figure 6.13 Comparison of gel porosities of unponded and ponded OPC paste cylinders.....</b>	<b>107</b>
<b>Figure 6.14 Comparison of total porosities of unponded and ponded OPC paste cylinders....</b>	<b>107</b>
<b>Figure 6.15 Chloride profiles for ponded white cement paste cylinders .....</b>	<b>108</b>
<b>Figure 6.16 Chloride profiles for ponded OPC paste cylinders .....</b>	<b>108</b>
<b>Figure 7.1 DTG of synthesized Friedel's salt.....</b>	<b>132</b>
<b>Figure 7.2 DTG of hydrated pure C<sub>3</sub>S .....</b>	<b>132</b>
<b>Figure 7.3 DTG of hydrated pure C<sub>3</sub>A and gypsum .....</b>	<b>132</b>
<b>Figure 7.4 DTG of White Cement Paste cylinders .....</b>	<b>133</b>

<b>Figure 7.5 Total peak areas of White Cement Paste cylinders.....</b>	<b>133</b>
<b>Figure 7.6 DTG of ponded White Cement Paste cylinders.....</b>	<b>134</b>
<b>Figure 7.7 Total peak areas of ponded White Cement Paste cylinders .....</b>	<b>134</b>
<b>Figure 7.8 DTG of OPC Paste cylinders.....</b>	<b>135</b>
<b>Figure 7.9 Total peak areas of OPC Paste cylinders.....</b>	<b>135</b>
<b>Figure 7.10 DTG of ponded OPC Paste cylinders.....</b>	<b>136</b>
<b>Figure 7.11 Total peak areas of ponded OPC Paste cylinders .....</b>	<b>136</b>
<b>Figure 7.12a Enhanced DTG for ponded Control OPC Paste cylinder .....</b>	<b>137</b>
<b>Figure 7.12b Enhanced DTG for ponded CN1 OPC Paste cylinder.....</b>	<b>137</b>
<b>Figure 7.12d Enhanced DTG for ponded CN2 OPC Paste cylinder.....</b>	<b>138</b>
<b>Figure 7.12d Enhanced DTG for ponded Ca(NO<sub>3</sub>)<sub>2</sub> OPC Paste cylinder .....</b>	<b>138</b>
<b>Figure 7.13 Total peak areas of various bound chloride forms in ponded OPC Paste cylinders .....</b>	<b>139</b>
<b>Figure 7.14a Analysis of expressed pore solution from unponded White Cement Paste cylinders: Cl<sup>-</sup>, SO<sub>4</sub><sup>2-</sup> and SiO<sub>2</sub><sup>-</sup> .....</b>	<b>140</b>
<b>Figure 7.14b Analysis of expressed pore solution from unponded White Cement Paste cylinders: Ca<sup>2+</sup>, K<sup>+</sup> and Na<sup>+</sup> .....</b>	<b>140</b>
<b>Figure 7.15 Alkalinity of expressed pore solutions from unponded White Cement Paste cylinders .....</b>	<b>140</b>
<b>Figure 7.16a Analysis of expressed pore solution from ponded White Cement Paste cylinders: SO<sub>4</sub><sup>2-</sup>, Ca<sup>2+</sup> and SiO<sub>2</sub><sup>-</sup> .....</b>	<b>141</b>
<b>Figure 7.16b 16a Analysis of expressed pore solution from ponded White Cement Paste cylinders: Cl<sup>-</sup>, NO<sub>2</sub><sup>-</sup>, NO<sub>3</sub><sup>-</sup>, K<sup>+</sup> and Na<sup>+</sup> .....</b>	<b>141</b>
<b>Figure 7.17 Alkalinity of expressed pore solutions from ponded White Cement Paste cylinders .....</b>	<b>141</b>
<b>Figure 7.18a Comparison of expressed pore solution analyses of unponded and ponded White Cement Paste Cylinders: SO<sub>4</sub><sup>2-</sup>, SiO<sub>2</sub><sup>-</sup> and Ca<sup>2+</sup> .....</b>	<b>142</b>
<b>Figure 7.18b Comparison of expressed pore solution analyses of unponded and ponded White Cement Paste Cylinders: K<sup>+</sup> and Na<sup>+</sup> .....</b>	<b>142</b>
<b>Figure 7.19a Analysis of expressed pore solutions from unponded OPC Paste cylinders: Cl<sup>-</sup>, SO<sub>4</sub><sup>2-</sup>, Ca<sup>2+</sup> and SiO<sub>2</sub><sup>-</sup> .....</b>	<b>143</b>
<b>Figure 7.19b Analysis of expressed pore solutions from unponded OPC Paste cylinders: K<sup>+</sup> and Na<sup>+</sup> .....</b>	<b>143</b>
<b>Figure 7.20 Alkalinity of expressed pore solutions from unponded OPC Paste cylinders.....</b>	<b>143</b>
<b>Figure 7.21a Analysis of expressed pore solutions from ponded OPC Paste cylinders: Cl<sup>-</sup>, K<sup>+</sup> and Na<sup>+</sup> .....</b>	<b>144</b>



<b>Figure 7.21b Analysis of expressed pore solutions from ponded OPC Paste cylinders: NO<sub>2</sub><sup>-</sup>, SO<sub>4</sub><sup>2-</sup>, NO<sub>3</sub><sup>-</sup>, Ca<sup>2+</sup> and SiO<sub>2</sub><sup>-</sup> .....</b>	<b>144</b>
<b>Figure 7.22 Alkalinity of expressed pore solutions from ponded OPC Paste cylinders.....</b>	<b>144</b>
<b>Figure 7.23a Comparison of expressed pore solution analyses of unponded and ponded OPC Paste cylinders: SiO<sub>2</sub><sup>-</sup> and Ca<sup>2+</sup> .....</b>	<b>145</b>
<b>Figure 7.23b Comparison of expressed pore solution analyses of unponded and ponded OPC Paste cylinders: K<sup>+</sup>, Na<sup>+</sup> and SO<sub>4</sub><sup>2-</sup> .....</b>	<b>145</b>
<b>Figure 8.1 Average cumulative intrusion volume vs. pore radius for Control cylinders.....</b>	<b>156</b>
<b>Figure 8.2 Average cumulative intrusion volume vs. pore radius for CN1 cylinders .....</b>	<b>156</b>
<b>Figure 8.3 Average cumulative intrusion volume vs. pore radius for CN2 cylinders .....</b>	<b>157</b>
<b>Figure 8.4 Average cumulative intrusion volume vs. pore radius for Ca(NO<sub>3</sub>)<sub>2</sub> cylinders.....</b>	<b>157</b>
<b>Figure 8.5 Average incremental intrusion volume vs. pore radius for Control cylinders.....</b>	<b>158</b>
<b>Figure 8.6 Average incremental intrusion volume vs. pore radius for CN1 cylinders .....</b>	<b>158</b>
<b>Figure 8.7 Average incremental intrusion volume vs. pore radius for CN2 cylinders .....</b>	<b>159</b>
<b>Figure 8.8 Average incremental intrusion volume vs. pore radius for Ca(NO<sub>3</sub>)<sub>2</sub> cylinders.....</b>	<b>159</b>
<b>Figure 8.9 Volume of ponding solution absorbed by ponded White Cement and OPC Paste cylinders .....</b>	<b>160</b>
<b>Figure 8.10 Chloride profiles for Control White Cement and OPC Paste cylinders.....</b>	<b>161</b>
<b>Figure 8.11 Chloride profiles for CN1 White Cement and OPC Paste cylinders .....</b>	<b>161</b>
<b>Figure 8.12 Chloride profiles for CN2 White Cement and OPC Paste cylinders .....</b>	<b>162</b>
<b>Figure 8.13 Chloride profiles for Ca(NO<sub>3</sub>)<sub>2</sub> White Cement and OPC Paste cylinders.....</b>	<b>162</b>
<b>Figure 8.14 DTG of Control cylinders.....</b>	<b>163</b>
<b>Figure 8.15 DTG of CN1 cylinders .....</b>	<b>163</b>
<b>Figure 8.16 DTG of CN2 cylinders .....</b>	<b>164</b>
<b>Figure 8.17 DTG of Ca(NO<sub>3</sub>)<sub>2</sub> cylinders.....</b>	<b>164</b>
<b>Figure 8.18 DTG of Control cylinders containing 2 % admixed chlorides .....</b>	<b>165</b>
<b>Figure 8.19a Analysis of expressed pore solutions from Control cylinders: SO<sub>4</sub><sup>2-</sup>, SiO<sub>2</sub><sup>-</sup> and Ca<sup>2+</sup> .....</b>	<b>166</b>
<b>Figure 8.19b Analysis of expressed pore solutions from CN1 cylinders: SO<sub>4</sub><sup>2-</sup>, SiO<sub>2</sub><sup>-</sup> and Ca<sup>2+</sup> .....</b>	<b>166</b>
<b>Figure 8.19c Analysis of expressed pore solutions from CN2 cylinders: SO<sub>4</sub><sup>2-</sup>, SiO<sub>2</sub><sup>-</sup> and Ca<sup>2+</sup> .....</b>	<b>167</b>
<b>Figure 8.19d Analysis of expressed pore solutions from Ca(NO<sub>3</sub>)<sub>2</sub> cylinders: SO<sub>4</sub><sup>2-</sup>, SiO<sub>2</sub><sup>-</sup> and Ca<sup>2+</sup> .....</b>	<b>167</b>

<b>Figure 8.20a Analysis of expressed pore solutions from Control cylinders: <math>K^+</math>, <math>Na^+</math>, <math>NO_2^-</math>, <math>NO_3^-</math> and <math>Cl^-</math> .....</b>	<b>168</b>
<b>Figure 8.20b Analysis of expressed pore solutions from CN1 cylinders: <math>K^+</math>, <math>Na^+</math>, <math>NO_2^-</math>, <math>NO_3^-</math> and <math>Cl^-</math> .....</b>	<b>168</b>
<b>Figure 8.20c Analysis of expressed pore solutions from CN2 cylinders: <math>K^+</math>, <math>Na^+</math>, <math>NO_2^-</math>, <math>NO_3^-</math> and <math>Cl^-</math> .....</b>	<b>169</b>
<b>Figure 8.20d Analysis of expressed pore solutions from <math>Ca(NO_3)_2</math> cylinders: <math>K^+</math>, <math>Na^+</math>, <math>NO_2^-</math>, <math>NO_3^-</math> and <math>Cl^-</math> .....</b>	<b>169</b>
<b>Figure 8.21 pH values of expressed pore solutions .....</b>	<b>170</b>
<b>Figure 9.1 Sequence of chloride binding in White Cement and OPC pastes .....</b>	<b>175</b>
<b>Figure 9.2 Composition-activity diagram of the AFm family at <math>\sim 25^\circ C</math> .....</b>	<b>177</b>
<b>Figure 9.3 Explanation of pH reduction in ponded cement paste cylinders .....</b>	<b>177</b>
<b>Figure A.1 Cyclic polarization curves of three samples immersed in Control, 0% <math>Cl^-</math> solution .....</b>	<b>190</b>
<b>Figure A.2 Cyclic polarization curves of three samples immersed in Control, 1% <math>Cl^-</math> solution .....</b>	<b>190</b>
<b>Figure A.3 Cyclic polarization curves of three samples immersed in Control, 2% <math>Cl^-</math> solution .....</b>	<b>191</b>
<b>Figure A.4 Cyclic polarization curves of three samples immersed in Control, 3% <math>Cl^-</math> solution .....</b>	<b>191</b>
<b>Figure A.5 Cyclic polarization curves of three samples immersed in Control, 4% <math>Cl^-</math> solution .....</b>	<b>192</b>
<b>Figure A.6 Cyclic polarization curves of three samples immersed in Control, 5% <math>Cl^-</math> solution .....</b>	<b>192</b>
<b>Figure A.7 Cyclic polarization curves of three samples immersed in Control, 6% <math>Cl^-</math> solution .....</b>	<b>193</b>
<b>Figure A.8 Cyclic polarization curves of three samples immersed in Control, 7% <math>Cl^-</math> solution .....</b>	<b>193</b>
<b>Figure A.9 Cyclic polarization curves of three samples immersed in Control, 8% <math>Cl^-</math> solution .....</b>	<b>194</b>
<b>Figure A.10 Cyclic polarization curves of three samples immersed in CN1 , 0% <math>Cl^-</math> solution .....</b>	<b>194</b>
<b>Figure A.11 Cyclic polarization curves of three samples immersed in CN1 , 1% <math>Cl^-</math> solution .....</b>	<b>195</b>
<b>Figure A.12 Cyclic polarization curves of three samples immersed in CN1 , 2% <math>Cl^-</math> solution .....</b>	<b>195</b>
<b>Figure A.13 Cyclic polarization curves of three samples immersed in CN1 , 3% <math>Cl^-</math> solution .....</b>	<b>196</b>

<b>Figure A.14 Cyclic polarization curves of three samples immersed in CN1 , 4% Cl<sup>-</sup> solution</b> .....	<b>196</b>
<b>Figure A.15 Cyclic polarization curves of three samples immersed in CN1 , 5% Cl<sup>-</sup> solution</b> .....	<b>197</b>
<b>Figure A.16 Cyclic polarization curves of three samples immersed in CN1 , 6% Cl<sup>-</sup> solution</b> .....	<b>197</b>
<b>Figure A.17 Cyclic polarization curves of three samples immersed in CN1 , 7% Cl<sup>-</sup> solution</b> .....	<b>198</b>
<b>Figure A.18 Cyclic polarization curves of three samples immersed in CN1 , 8% Cl<sup>-</sup> solution</b> .....	<b>198</b>
<b>Figure A.19 Cyclic polarization curves of three samples immersed in CN2 , 0% Cl<sup>-</sup> solution</b> .....	<b>199</b>
<b>Figure A.20 Cyclic polarization curves of three samples immersed in CN2 , 1% Cl<sup>-</sup> solution</b> .....	<b>199</b>
<b>Figure A.21 Cyclic polarization curves of three samples immersed in CN2 , 2% Cl<sup>-</sup> solution</b> .....	<b>200</b>
<b>Figure A.22 Cyclic polarization curves of three samples immersed in CN2 , 3% Cl<sup>-</sup> solution</b> .....	<b>200</b>
<b>Figure A.23 Cyclic polarization curves of three samples immersed in CN2 , 4% Cl<sup>-</sup> solution</b> .....	<b>201</b>
<b>Figure A.24 Cyclic polarization curves of three samples immersed in CN2 , 5% Cl<sup>-</sup> solution</b> .....	<b>201</b>
<b>Figure A.25 Cyclic polarization curves of three samples immersed in CN2 , 6% Cl<sup>-</sup> solution</b> .....	<b>202</b>
<b>Figure A.26 Cyclic polarization curves of three samples immersed in CN2 , 7% Cl<sup>-</sup> solution</b> .....	<b>202</b>
<b>Figure A.27 Cyclic polarization curves of three samples immersed in CN2 , 8% Cl<sup>-</sup> solution</b> .....	<b>203</b>
<b>Figure A.28 Cyclic polarization curves of three samples immersed in Ca(NO<sub>3</sub>)<sub>2</sub> , 0% Cl<sup>-</sup> solution</b> .....	<b>203</b>
<b>Figure A.29 Cyclic polarization curves of three samples immersed in Ca(NO<sub>3</sub>)<sub>2</sub> , 1% Cl<sup>-</sup> solution</b> .....	<b>204</b>
<b>Figure A.30 Cyclic polarization curves of three samples immersed in Ca(NO<sub>3</sub>)<sub>2</sub> , 2% Cl<sup>-</sup> solution</b> .....	<b>204</b>
<b>Figure A.31 Cyclic polarization curves of three samples immersed in Ca(NO<sub>3</sub>)<sub>2</sub> , 3% Cl<sup>-</sup> solution</b> .....	<b>205</b>
<b>Figure A.32 Cyclic polarization curves of three samples immersed in Ca(NO<sub>3</sub>)<sub>2</sub> , 4% Cl<sup>-</sup> solution</b> .....	<b>205</b>

<b>Figure A.33 Cyclic polarization curves of three samples immersed in <math>\text{Ca}(\text{NO}_3)_2</math> , 5% <math>\text{Cl}^-</math> solution.....</b>	<b>206</b>
<b>Figure A.34 Cyclic polarization curves of three samples immersed in <math>\text{Ca}(\text{NO}_3)_2</math> , 6% <math>\text{Cl}^-</math> solution.....</b>	<b>206</b>
<b>Figure A.35 Cyclic polarization curves of three samples immersed in <math>\text{Ca}(\text{NO}_3)_2</math> , 7% <math>\text{Cl}^-</math> solution.....</b>	<b>207</b>
<b>Figure A.36 Cyclic polarization curves of three samples immersed in <math>\text{Ca}(\text{NO}_3)_2</math> , 8% <math>\text{Cl}^-</math> solution.....</b>	<b>207</b>
<b>Figure C.1 Cumulative intrusion volume vs. pore radius for three Control White Cement Paste samples.....</b>	<b>212</b>
<b>Figure C.2 Cumulative intrusion volume vs. pore radius for three CN1 White Cement Paste samples.....</b>	<b>212</b>
<b>Figure C.3 Cumulative intrusion volume vs. pore radius for three CN2 White Cement Paste samples.....</b>	<b>213</b>
<b>Figure C.4 Cumulative intrusion volume vs. pore radius for three <math>\text{Ca}(\text{NO}_3)_2</math> White Cement Paste samples.....</b>	<b>213</b>
<b>Figure C.5 Incremental intrusion volume vs. pore radius for three Control White Cement Paste samples.....</b>	<b>214</b>
<b>Figure C.6 Incremental intrusion volume vs. pore radius for three CN1 White Cement Paste samples.....</b>	<b>214</b>
<b>Figure C.7 Incremental intrusion volume vs. pore radius for three CN2 White Cement Paste samples.....</b>	<b>215</b>
<b>Figure C.8 Incremental intrusion volume vs. pore radius for three <math>\text{Ca}(\text{NO}_3)_2</math> White Cement Paste samples.....</b>	<b>215</b>
<b>Figure C.9 Cumulative intrusion volume vs. pore radius for three Control OPC Paste samples.....</b>	<b>216</b>
<b>Figure C.10 Cumulative intrusion volume vs. pore radius for three CN1 OPC Paste samples.....</b>	<b>216</b>
<b>Figure C.11 Cumulative intrusion volume vs. pore radius for two CN2 OPC Paste samples.....</b>	<b>217</b>
<b>Figure C.12 Cumulative intrusion volume vs. pore radius for three <math>\text{Ca}(\text{NO}_3)_2</math> OPC Paste samples.....</b>	<b>217</b>
<b>Figure C.13 Incremental intrusion volume vs. pore radius for three Control OPC Paste samples.....</b>	<b>218</b>
<b>Figure C.14 Incremental intrusion volume vs. pore radius for three CN1 OPC Paste samples.....</b>	<b>218</b>
<b>Figure C.15 Incremental intrusion volume vs. pore radius for two CN2 OPC Paste samples.....</b>	<b>219</b>

Figure C.16 Incremental intrusion volume vs. pore radius for three $\text{Ca}(\text{NO}_3)_2$ OPC Paste samples.....	219
Figure C.17 Cumulative intrusion volume vs. pore radius for three Poned Control White Cement Paste samples.....	220
Figure C.18 Cumulative intrusion volume vs. pore radius for two Poned CN1 White Cement Paste samples.....	220
Figure C.19 Cumulative intrusion volume vs. pore radius for three Poned CN2 White Cement Paste samples.....	221
Figure C.20 Cumulative intrusion volume vs. pore radius for three Poned $\text{Ca}(\text{NO}_3)_2$ White Cement Paste samples.....	221
Figure C.21 Incremental intrusion volume vs. pore radius for three Poned Control White Cement Paste samples.....	222
Figure C.22 Incremental intrusion volume vs. pore radius for two Poned CN1 White Cement Paste samples.....	222
Figure C.23 Incremental intrusion volume vs. pore radius for three Poned CN2 White Cement Paste samples.....	223
Figure C.24 Incremental intrusion volume vs. pore radius for three Poned $\text{Ca}(\text{NO}_3)_2$ White Cement Paste samples.....	223
Figure C.25 Cumulative intrusion volume vs. pore radius for three Poned Control OPC Paste samples.....	224
Figure C.26 Cumulative intrusion volume vs. pore radius for three Poned CN1 OPC Paste samples.....	224
Figure C.27 Cumulative intrusion volume vs. pore radius for three Poned CN2 OPC Paste samples.....	225
Figure C.28 Cumulative intrusion volume vs. pore radius for three Poned $\text{Ca}(\text{NO}_3)_2$ OPC Paste samples.....	225
Figure C.29 Incremental intrusion volume vs. pore radius for three Poned Control OPC Paste samples.....	226
Figure C.30 Incremental intrusion volume vs. pore radius for three Poned CN1 OPC Paste samples.....	226
Figure C.31 Incremental intrusion volume vs. pore radius for three Poned CN2 OPC Paste samples.....	227
Figure C.32 Incremental intrusion volume vs. pore radius for three Poned $\text{Ca}(\text{NO}_3)_2$ OPC Paste samples.....	227
Figure D.1 DTG of two Control White Cement Paste samples.....	228
Figure D.2 DTG of two CN1 White Cement Paste samples.....	228
Figure D.3 DTG of two CN2 White Cement Paste samples.....	229
Figure D.4 DTG of two $\text{Ca}(\text{NO}_3)_2$ White Cement Paste samples.....	229

<b>Figure D.5 DTG of two ponded Control White Cement Paste samples .....</b>	<b>230</b>
<b>Figure D.6 DTG of two ponded CN1 White Cement Paste samples.....</b>	<b>230</b>
<b>Figure D.7 DTG of two ponded CN2 White Cement Paste samples.....</b>	<b>231</b>
<b>Figure D.8 DTG of two ponded Ca(NO<sub>3</sub>)<sub>2</sub> White Cement Paste samples .....</b>	<b>231</b>
<b>Figure D.9 DTG of two Control OPC Paste samples .....</b>	<b>232</b>
<b>Figure D.10 DTG of two CN1 OPC Paste samples.....</b>	<b>232</b>
<b>Figure D.11 DTG of two CN2 OPC Paste samples.....</b>	<b>233</b>
<b>Figure D.12 DTG of two Ca(NO<sub>3</sub>)<sub>2</sub> OPC Paste samples .....</b>	<b>233</b>
<b>Figure D.13 DTG of two ponded Control OPC Paste samples .....</b>	<b>234</b>
<b>Figure D.14 DTG of two ponded CN1 OPC Paste samples.....</b>	<b>234</b>
<b>Figure D.15 DTG of two ponded CN2 OPC Paste samples.....</b>	<b>235</b>
<b>Figure D.16 DTG of two ponded Ca(NO<sub>3</sub>)<sub>2</sub> OPC Paste samples .....</b>	<b>235</b>

## Nomenclature

$\gamma$	surface tension
$\theta$	contact angle
$\Delta E$	change in corrosion potential
$\gamma\text{-Fe}_2\text{O}_3$	maghemite
$\alpha\text{-Fe}_2\text{O}_3$	hæmatite
$\gamma\text{-FeOOH}$	lepidocrocite
$\alpha\text{-FeOOH}$	goethite
$\beta\text{-FeOOH}$	akagenite
$\Delta i$	change in corrosion current
AA	Atomic Absorption
AFm	monosulphate (monosulphoaluminate hydrate)
AFt	ettringite (trisulphoaluminate hydrate)
BSE	backscattered electrons
$\text{C}_2\text{S}$	dicalcium silicate
$\text{C}_3\text{A}$	tricalcium aluminate
$\text{C}_3\text{S}$	tricalcium silicate
$\text{C}_4\text{AF}$	tetracalcium aluminoferrite
CN1	calcium nitrite inhibitor (1)
CN2	calcium nitrite inhibitor (2)
$\text{C}\bar{\text{S}}$	gypsum
C-S-H	calcium silicate hydrate
D	pore diameter
dm	change in mass
dT	change in temperature
dt	change in time
DTA	differential thermal analysis
DTG	derivative thermogravimetric analysis
$E_{\text{corr}}$	corrosion or open circuit potential
EDS	energy dispersive spectroscopy
$E_i$	incident light energy
$E_n$	pitting or nucleation potential
$E_p$	passivation or protection potential
$E_s$	scattered light energy
ESEM	environmental scanning electron microscope
$E_v$	vibrational energy
$\text{Fe}_3\text{O}_4$	magnetite

<b>GRI</b>	<b>green rust 1</b>
<b>I</b>	<b>current density</b>
<b>IC</b>	<b>Ion Chromatography</b>
<b><math>i_{\text{corr}}</math></b>	<b>corrosion current</b>
<b>ICP</b>	<b>Inductively Coupled Plasma</b>
<b>LPR</b>	<b>Linear Polarization Resistance</b>
<b>m</b>	<b>mass</b>
<b>M</b>	<b>molarity (moles/L)</b>
<b>meq</b>	<b>milli-equivalent</b>
<b>MIP</b>	<b>mercury intrusion porosimetry</b>
<b>mmol</b>	<b>millimole</b>
<b>mol</b>	<b>moles</b>
<b>MRI</b>	<b>magnetic resonance imaging</b>
<b><math>\phi</math></b>	<b>diameter</b>
<b>OPC</b>	<b>ordinary Portland cement</b>
<b>P</b>	<b>pressure</b>
<b>r</b>	<b>radius</b>
<b>rebar</b>	<b>reinforcing steel bar</b>
<b>SCE</b>	<b>saturated calomel electrode</b>
<b>SE</b>	<b>secondary electrons</b>
<b>SEM</b>	<b>scanning electron microscope</b>
<b>Std. Dev.</b>	<b>standard deviation</b>
<b>T</b>	<b>temperature</b>
<b>t</b>	<b>time</b>
<b>TGA</b>	<b>thermogravimetric analysis</b>
<b><math>T_r</math></b>	<b>reference material temperature</b>
<b><math>T_s</math></b>	<b>sample temperature</b>
<b>V</b>	<b>mercury intrusion volume</b>
<b><math>V_{\text{inf}}</math></b>	<b>total volume of titrant added until inflection</b>
<b><math>V_q</math></b>	<b>original volume of sample</b>
<b><math>V_s</math></b>	<b>volume of titrant added for the samples</b>
<b><math>V_s</math></b>	<b>volume of salt standard added</b>
<b>w/c</b>	<b>water-cement ratio</b>
<b>wt.</b>	<b>weight</b>
<b>B</b>	<b>combined anodic and cathodic Tafel slopes</b>
<b><math>\beta_a</math></b>	<b>anodic Tafel slope</b>
<b><math>\beta_b</math></b>	<b>cathodic Tafel slope</b>



## **Chapter 1**

### **Introduction**

Steel-reinforced concrete is the most widely used construction material in the world, due in part to its superior physical properties and low cost. However, corrosion of the reinforcing steel bar (i.e. "rebar"), embedded within the concrete to improve its tensile strength, has become a significant structural and financial problem. It was estimated by the U.S. Strategic Highway Research Program that between \$450 to \$550 million U.S. per year (\$642 to \$786 million CAD) could be saved by correcting corrosion problems in existing bridges (Berke 1990). This estimate was made fifteen years ago and is probably conservative for today. A significant proportion of reinforcement corrosion within North America is a direct result of the use of deicing salts during winter months to maintain ice-free highways and roads, leading to an increased incidence of potholes, spalls and delaminations of reinforced highway structures such as bridge decks. Parking garages and support pillars of various structures are also affected as vehicles carry salt-containing snow and ice which subsequently melts allowing the chlorides to leach into the concrete. Also affected by salt-induced corrosion are coastal structures that are exposed to seawater and sea air containing chloride.

Corrosion protection is not typically needed for the first year of the life of the structure, but must be effective when aggressive species, such as chlorides, penetrate to the rebar surface. To prevent or delay corrosion of reinforcing steel, use is being made of epoxy-coated reinforcement, protective coating and membranes on the concrete surface, cathodic protection, concrete with very low permeability, corrosion-inhibiting chemical admixtures and combinations thereof. The addition to concrete of chemical corrosion inhibitors presents a simple, economically viable alternative to other techniques and is increasing in popularity.

Current figures estimate that it costs approximately \$1000 CAD per cubic metre of concrete to construct a new bridge (Parsons 1995). When corrosion inhibitors are used in conjunction with highly impermeable concrete, it is estimated that the cost of the structure is increased by \$52 U.S. (\$74 CAD) per cubic metre upon initial construction. However, this amount is minimal considering rehabilitation costs could require in excess of \$2600 U.S. (\$3714 CAD) per cubic metre (Tarricone 1992).

The most widely used corrosion inhibitor for concrete structures is calcium nitrite. Although this admixture has been used throughout the world for more than two decades, the exact nature of the mechanism of corrosion inhibition has been a topic of debate. Additionally, little information has been published regarding the interaction of calcium nitrite with the cement paste phase of concrete, despite the fact that this inhibitor is reported to have a set accelerating affect (Mindess 1981). In order to forecast the effectiveness of the inhibitor over the lifetime of the structure and its suitability in various environments, it is essential to have a clear understanding of the mechanism(s) of inhibition and the factors affecting its success.

Thus, the proposed research project aims to identify the mechanism(s) of inhibition using a combination of electrochemical, pore size distribution, spectroscopic and microscopic techniques. Chapter 2 provides background information regarding corrosion of steel, cement chemistry, calcium nitrite- and calcium nitrate-based inhibitors, and techniques used during experimentation, while Chapter 3 gives more detail regarding the objectives and rationale of the current investigation. Chapter 4 outlines the types of experiments conducted during the study, while Chapters 5, 6, 7, and 8 detail results and discussion regarding the effect of inhibitors on corrosion of reinforcement, transport properties of cement paste, cement

**chemistry and the effect of cement type, respectively. Chapter 9 summarizes the implications of the results of the previous four chapters, and provides conclusions and recommendations for further work.**

## Chapter 2 Literature Review

### 2.1 Concrete

#### 2.1.1 Cement Chemistry

*Concrete* is a composite material made of four common materials: cement powder, coarse and fine aggregate, and water, while *mortar* contains cement powder, fine aggregate and water and *cement paste* contains cement powder and water. The most commonly used type of cement powder, referred to as “Portland”, has five main compounds, as listed in Table 2.1.

Table 2.1 Major constituents and composition ranges of Portland cement (ACI 1995)

Compound	Composition	Abbreviation
Tricalcium silicate (alite)	$3\text{CaO}\cdot\text{SiO}_2$	$\text{C}_3\text{S}$
Dicalcium silicate (belite)	$2\text{CaO}\cdot\text{SiO}_2$	$\text{C}_2\text{S}$
Tricalcium aluminate	$3\text{CaO}\cdot\text{Al}_2\text{O}_3$	$\text{C}_3\text{A}$
Tetracalcium aluminoferrite	$4\text{CaO}\cdot\text{Al}_2\text{O}_3\cdot\text{Fe}_2\text{O}_3$	$\text{C}_4\text{AF}$
Calcium sulphate (gypsum)	$\text{CaSO}_4\cdot 2\text{H}_2\text{O}$	$\text{C}\bar{\text{S}}$
Other	Mg, Na K, and S oxides	

Different types of Portland cement can be used and which type should be dependent on the chemical and physical exposure conditions for the given structure. Table 2.2 lists the major different type of cements and their typical compound compositions.

Table 2.2 Typical calculated potential compound composition and application of Portland cements (CPCA 1995)

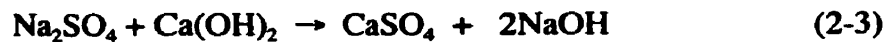
Type of Portland Cement	Application	Potential compound composition, wt. %			
		$\text{C}_3\text{S}$	$\text{C}_2\text{S}$	$\text{C}_3\text{A}$	$\text{C}_4\text{AF}$
10 Normal	General use	50	24	11	8
20 Moderate	Moderate sulphate attack	42	33	5	13
30 High-early strength	Early formwork removal; shorter curing time	60	13	9	8
40 Low-heat of hydration	Massive concrete structures	26	50	5	12
50 Sulphate resistant	Severe sulphate attack	40	40	3.5	9

### **2.1.2 Cement Hydration**

The first four major compounds mentioned in Table 2.1 react with water to give insoluble hydration products, which form the framework of the hardened concrete. The two main components,  $C_3S$  and  $C_2S$ , each react with the mixing water to form calcium-silicate hydrates.  $C_3S$  hardens quickly and is primarily responsible for the initial set and early strength of the concrete.  $C_2S$  hardens slowly and supplies strength at later stages (i.e. one week). Collectively termed “C-S-H”, these products are structurally similar but are not stoichiometrically fixed (i.e. the calcium/silica ratio and the amount of chemically combined water can vary widely). The following equations detail two possible reactions (Mehta 1986; Neville 1991):



One of the products is free, slightly soluble portlandite ( $Ca(OH)_2$ ), some of which reacts with sodium and potassium salts - minor constituents of the cement clinker - to form very soluble potassium and sodium hydroxides.



It is these hydroxides of potassium, sodium and calcium which are responsible for the highly alkaline, water-based solution - commonly referred to as “pore solution” - found in a system of randomly distributed voids within the cement paste phase of the concrete, which is composed of interconnected and isolated capillary pores and isolated gel pores (Bakker

1988). Table 2.3 shows the composition of pore water as determined by investigations by Arup (Arup 1983).

Table 2.3 Typical composition of pore water from concrete made with Ordinary Portland Cement (water/cement ratio by weight ~ 0.5) (Arup 1983)

Compound	Pore Water (mol/litre)
Na <sup>+</sup>	0.3
K <sup>+</sup>	0.6
Ca <sup>++</sup>	0.002
OH <sup>-</sup>	0.85
SO <sub>4</sub> <sup>2-</sup>	0.03
pH (calculated)	13.9

C<sub>3</sub>A hydration generates significant heat during initial hardening and contributes slightly to early strength. Several reactions are possible when C<sub>3</sub>A is combined with mixing water, depending on the amount of gypsum present, which is added to the cement during final grinding to slow down the hydration rate of C<sub>3</sub>A. The various hydration products are summarized in Table 2.4.

Table 2.4 Formation of hydration products from C<sub>3</sub>A (Mindess 1981)

Gypsum/C <sub>3</sub> A Molar Ratio	Hydration Products Formed
3.0	Ettringite
3.0 – 1.0	Ettringite + monosulfoaluminate
1.0	Monosulfoaluminate
< 1.0	Monosulfoaluminate solid solution
0	Hydrogarnet

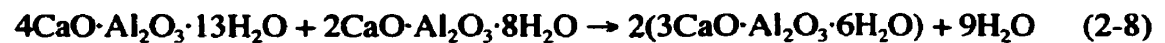
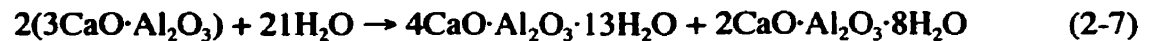
At high concentrations of gypsum, C<sub>3</sub>A reacts with gypsum and water to form ettringite or AFt (Mindess 1981):



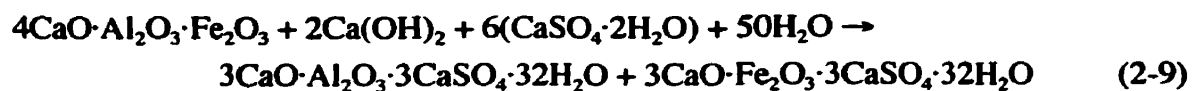
If all of the sulphate is consumed prior to complete hydration of the C<sub>3</sub>A or at intermediate concentrations of gypsum, ettringite is unstable and transforms to another compound, monosulfoaluminate hydrate or AFm, which requires less sulphate:



When small amounts or no gypsum is present, any unused C<sub>3</sub>A may react with water to form two unstable intermediate species, which further react to form hydrogarnet and water (Mindess 1981):



There is general agreement (Lea 1970; Mindess 1981; Ghosh 1983; Jawed 1983; Neville 1991; Taylor 1997) that, upon reaction with water and gypsum, C<sub>4</sub>AF reacts to form AFt and hydrogarnet, with the alumina and ferrite compounds interchangeable within the structure (Ghosh 1983):



As with C<sub>3</sub>A, at low gypsum concentrations or as gypsum is depleted, a reduction from the iron-substituted ettringite to an iron-substitute monosulphate occurs (Ghosh 1983).

### 2.1.3 Chemically Bound Chlorides

Chlorides within concrete can be introduced at the time of mixing – in contaminated aggregate, in the mixing water or as a component of admixtures – or can penetrate into the hardened concrete from the outside environment, from such sources as seawater or deicing salts. Although chlorides can cause corrosion of the reinforcing steel, only those chlorides that are “free” or dissolved within the pore solution have this potential. Chlorides do not pose a corrosion threat if they are immobilized, either within the interlayers of the calcium silicate hydrates, or by being “chemically bound” (Arya 1987).

The two main forms of chemically bound chlorides are due to the chemical reaction between tricalcium aluminate ( $C_3A$ ) and the chloride ion:



It has been shown that chloride binding is dependent on the specific surface area or fineness of the cement (Byfors 1986; Al-Gahtani 1994), as greater fineness results in a higher proportion of cement grains reacting with the mixing water. Due to the mechanism involved, it would be logical to conclude that the degree of chloride binding is dependent on the  $C_3A$  content. However, a more controversial postulate is that chloride binding is dependent on the total concentration of  $C_3A$  and  $C_4AF$  (Byfors 1986; Byfors 1986). Additionally, several researchers (Byfors 1986; Byfors 1986; Yonezawa 1988; Tritthart 1989; Al-Gahtani 1994; Suryavanshi 1994) found that a decrease in pH increased the chloride binding capacity of the cement. As an equilibrium exists between bound and free chlorides, which favours bound chlorides at lower pH values (Tritthart 1990), a shift in pH to less alkaline values would lead



to an increase in the formation of Friedel's salt. The gypsum content of the cement would also affect chloride binding (Byfors 1986; Byfors 1986), as both sulfate and chloride anions would "compete" to occupy sites within the hydrated  $C_3A$  and  $C_4AF$  phases.

#### 2.1.4 Porosity

Once hardened, concrete is considered to be composed of two phases: cement paste and aggregates. Within the cement paste matrix exists a complex pore structure – filled with either air or water – that is responsible for a variety of concrete durability properties, including permeability and strength.

Concrete is a unique material in that the range of pore sizes within the hardened cement paste spans several orders of magnitude. "Gel pores" can be considered part of the main building block of the cement paste phase - namely the hydration products of  $C_3S$  and  $C_2S$  – and constitute the bulk of the porosity within the hardened cement paste when the cement is fully hydrated (Taylor 1997). On the nanometer scale, these pores primarily influence the shrinkage and creep properties of the concrete (Mindess 1981; Mehta 1986).

Of particular interest with regards to permeability are the "capillary pores", so named because solution in these pores is subject to capillary effects (i.e. a meniscus can form) (Mindess 1981). Capillary pores result from the hydration process, essentially interstices left by unhydrated cement grains or hydration products. These pores can be isolated from one another or interconnected, in which case they are capable of transporting aggressive species, such as chlorides and carbon dioxide, to the reinforcing steel surface and within the cement paste itself. It is generally acknowledged that the greater the water:cement ratio, the larger the capillary pores, resulting in concrete of increased permeability (Mehta 1986).

Although the technical definitions of capillary and gel porosity and their roles in the cement paste matrix are agreed upon, considerable differences in opinion regarding the dividing radius between the two types of porosity exist, which are given in Table 2.5.

Table 2.5 Dividing radius between capillary and gel porosity

	Dividing radius between capillary and gel porosity
Mindess & Young (Mindess 1981)	5 nm
Mehta (Mehta 1986)	0.9 nm
Jawed et al. (Jawed 1983)	25 nm
Neville (Neville 1991)	1 nm
Vocka et al. (Vocka 2000)	15 nm

As concrete ages or matures, the total porosity of the cement paste decreases and the pore size distribution is shifted to lower pore diameters, as is demonstrated by Figure 2.1 (Taylor 1997).

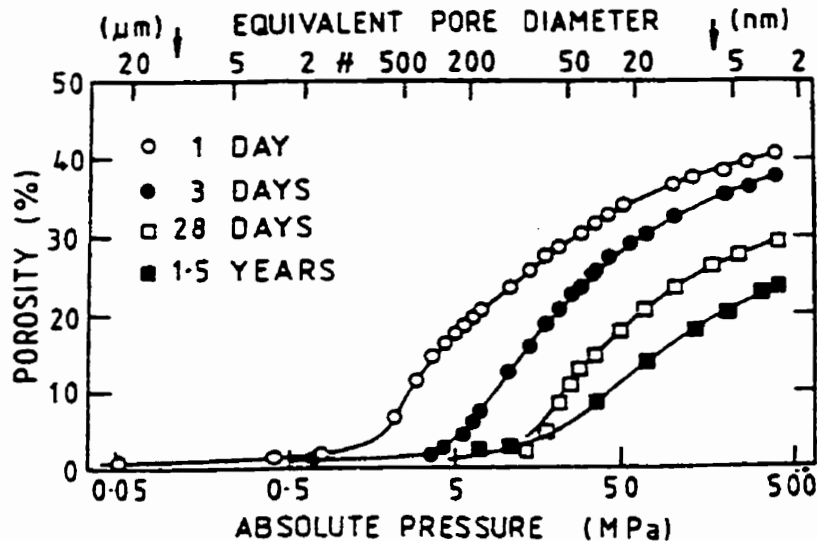


Figure 2.1 Mercury porosimetry curves for a Portland cement paste (w/c ratio = 0.47) at various stages (Taylor 1997).

## 2.2 Corrosion of Steel in Concrete

As well as providing a physical barrier to the ingress of aggressive species, concrete provides corrosion protection of embedded reinforcing steel by:

- i. formation of a protective passive film due to the alkaline nature of the pore solution in concrete;**
- ii. high electrical resistance of concrete limiting galvanic corrosion;**
- iii. formation of mineral deposits on the rebar, protecting the steel from reacting with the environment (Borgard 1990).**

**In order to initiate corrosion, mechanical failure of the mineral deposits must occur as well as breakdown of the protective passive layer (Leek 1990).**

**Concrete not exposed to any external influences usually has a pH ranging between 12.5 and 13.5 (Locke 1982; Hansson 1984). As illustrated in the Pourbaix diagram of the Fe-H<sub>2</sub>O system (Pourbaix 1974) (Figure 2.2), within this range and at potentials normally existing in concrete, insoluble, thermodynamically stable iron oxides are formed on the rebar surface upon contact with the concrete, constituting the thin passive film formed on the rebar surface.**

**Unfortunately, the protective nature of this film can be compromised by a number of factors:**

- i. the alkaline nature of the pore solution can be reduced as a result of carbonation or neutralization – due to the penetration and reaction of acidic gases (eg. CO<sub>2</sub>, SO<sub>4</sub>) from the surrounding air – resulting in general or uniform corrosion;**
- ii. the presence of aggressive ions, particularly Cl<sup>-</sup>, can lead to local breakdown of the passive film, often in the form of pitting corrosion;**
- iii. low oxygen environments (eg. submerged or underground structures) may be incapable of maintaining the passive film, causing low general/uniform corrosion.**

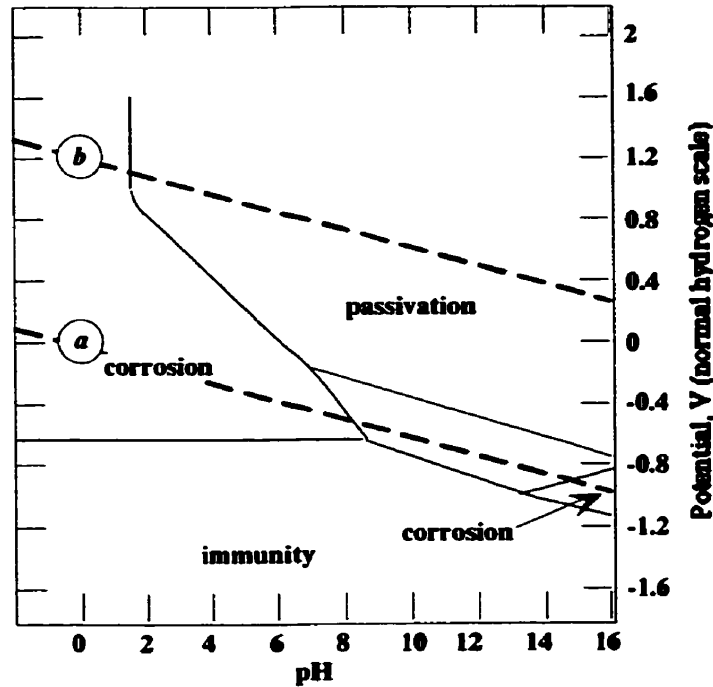
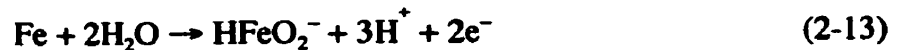
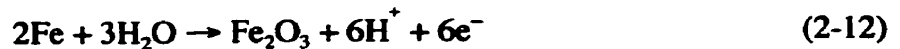


Figure 2.2 Pourbaix Diagram for the Fe-H<sub>2</sub>O System at 25°C (Pourbaix 1974).

Corrosion has long been recognized as electrochemical in nature. The corrosion process and passive film formation in concrete can be represented by the following stoichiometric equations (Hansson 1984), shown schematically in Figure 2.3 (Enevoldsen 1993):

Anodic half cell reactions (dependent on O<sub>2</sub> availability and pH near the steel surface):



Cathodic half cell reactions:



<sup>1</sup> Under the highly alkaline conditions of concrete and due to the high availability of O<sub>2</sub>, this reaction is typically considered to have a minimal influence but can occur in anaerobic concrete eg. for buried or deeply submerged concrete.

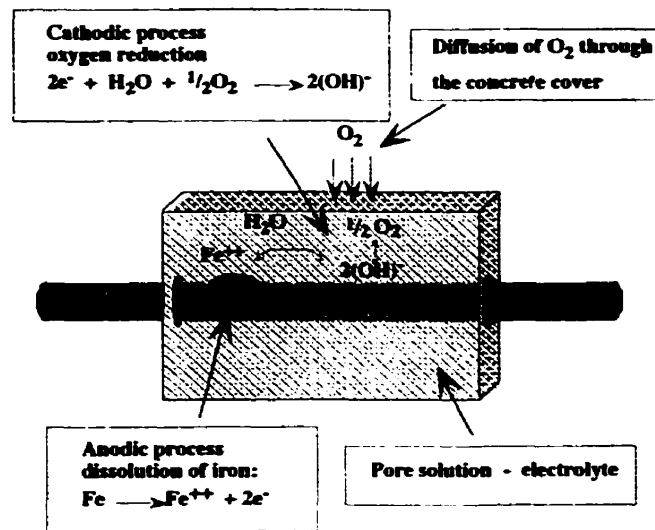


Figure 2.3 Schematic diagram of corrosion of rebar in concrete (Enevoldsen 1993).

At anodic sites, metal atoms enter the pore solution as positive ions while the free electrons travel through the metal to the cathodic sites and are consumed by electron acceptors such as dissolved oxygen or hydrogen ions. Ions then migrate through the pore solution and form corrosion products which may be soluble (eg. ferrous chloride) or insoluble (eg. rust, hydrated ferric oxide) (Page 1988).

Besides pH and availability of oxygen, a large number of factors including resistivity and porosity of the concrete, composition and metallurgical properties of the rebar, relative humidity, temperature, and the presence of aggressive ions such as chlorides, determines the rate of the corrosion processes.

### 2.2.1 Pitting Corrosion

It has been found that corrosion of reinforcement in concrete predominantly occurs as “pitting”, a form of localized attack which can result in a severance of the bar and is one of the most destructive and undetectable forms of corrosion. Since corrosion remains localised,

high corrosion rates in the pitted area result due to the micro-cell effect. The cross-section of the rebar decreases, reducing its load-bearing capacity and can lead to sudden failure of the structure.

Pitting is most commonly caused by chlorides or chlorine-containing ions (Fontana 1986).

Chlorides responsible for the corrosion process are often considered to originate from external agents, most often from deicing agents, seawater, and swimming pool chemicals.

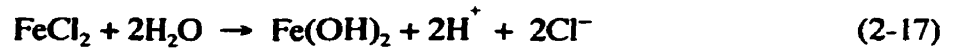
Unlike admixed chlorides (i.e. those added at the time of mixing), external chlorides are less likely to be chemically bound with the aluminate and ferrite phases of the cement paste.

These bound chlorides are considered to have a minimal influence on corrosion behaviour (Locke 1982; Locke 1986; Eglinton 1987; Benjamin 1990; Manning 1991; Enevoldsen 1993; Al-Gahtani 1994).

The exact mechanism for breakdown of passivity by chlorides is not well understood. It is known, however, that chlorides, oxygen and moisture are necessary elements in order to stimulate the pitting reactions. Pits are believed to initiate at surface discontinuities (including those caused by sulfide inclusions), insufficient inhibitor coverage, scratches in coating, and deposits of slag, scale, dust, mud, or sand (Jones 1992). Such conditions may lead to a momentarily high rate of metal dissolution, which, in turn, leads to migration of chloride ions to that particular site to maintain electro-neutrality and thus stimulating the pitting process.

On the other hand, there is general agreement on the mechanism of pit propagation. Once a pit has been initiated, the pitting process becomes autocatalytic or self-supporting. Figure 2.4

(Treadaway 1988) schematically represents this process. Rapid iron dissolution (i.e. the anodic reaction) occurs within the pit itself, while the adjacent surfaces (covered by the passive film) act as sites for oxygen reduction (i.e. the cathodic reaction). Thus, within the pit exists a high concentration of iron chloride complexes and, as a result of hydrolysis:



a high concentration of hydrogen ions, leading to a highly acidic environment within the pit, further propagating the anodic reaction. The pH at adjacent cathodic sites, on the other hand, tends to become more alkaline due to the production of hydroxide. Thus, pitting can be said to cathodically protect the rest of the rebar surface.

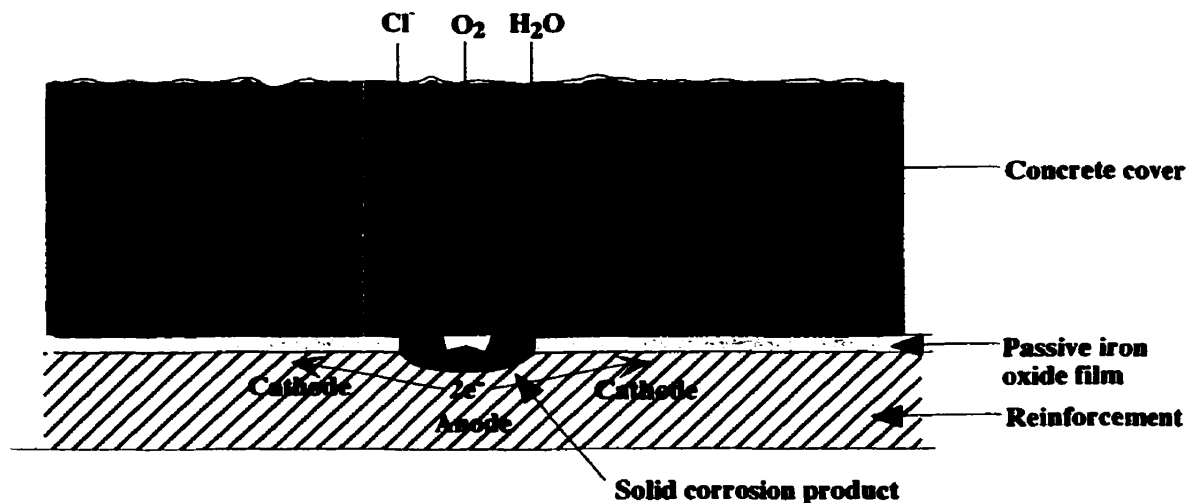


Figure 2.4 Effect of corrosion product hydrolysis and recycling  $\text{Cl}^-$  pitting corrosion (Treadaway 1988).

The intermediate iron chloride complexes are thermodynamically stable only within the highly acidic region located within the pit. As iron chlorides are water soluble, they tend to diffuse away from this zone and into the more alkaline concrete environment where they precipitate out as iron oxides. This chemical conversion is associated with a volume expansion, up to six times the volume of the original steel (Mehta 1986), leading to stresses

that cause cracking and spalling of the concrete thus leaving the concrete more permeable to further chloride ingress and carbonation.

### **2.3 Calcium Nitrite and Calcium Nitrate Based Inhibitors**

Calcium nitrite ( $\text{Ca}(\text{NO}_2)_2$ ) inhibitors are the only inhibitors in large scale commercial use in concrete structures throughout the world. This is mainly due to the fulfillment of three important criteria:

- i. they provide corrosion inhibition in the presence of chlorides;
- ii. at the recommended dosage, they are not detrimental to concrete properties;
- iii. they are available in sufficient quantities for commercial use (Berke 1989; Berke 1992).

The currently accepted mechanism of  $\text{Ca}(\text{NO}_2)_2$  inhibition is based on studies by Pyke and Cohen (Pyke 1948). Conducting tests using steel exposed to sodium nitrite and Ottawa tap water, it was determined that nitrite suppresses anodic activity and acts to repair and complete the protective oxide film already formed. Figure 2.5 schematically explains the proposed mechanism. Nitrite ion is first absorbed onto the surface and then reacts with cathodic hydrogen to form reduction products (i.e.  $\text{NH}_3$ ) and a continuous oxide layer.



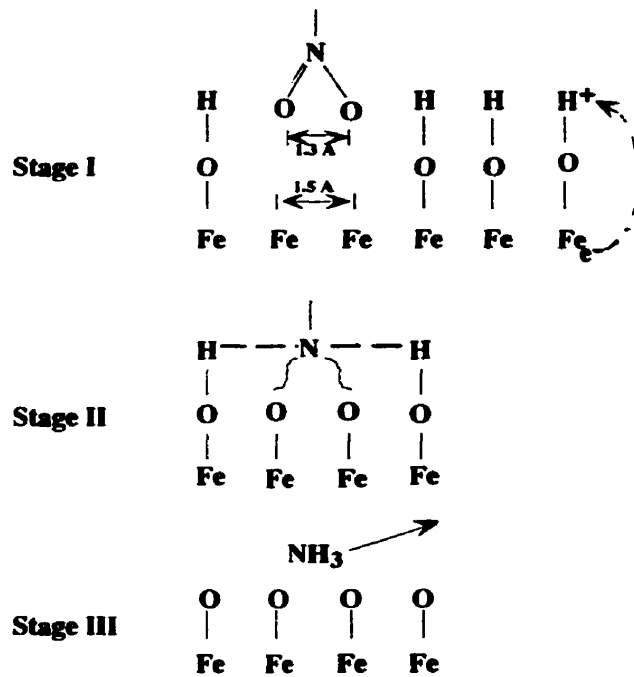
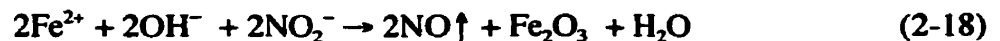


Figure 2.5 Postulated mechanism for inhibition by nitrite (Pyke 1948).

This mechanism was expanded upon by El-Jazairi and Berke (El-Jazairi 1990) as well as Berke and Weil (Berke 1992), now addressing the inhibiting mechanism of calcium nitrite in a concrete environment. As with sodium nitrite, calcium nitrite is believed to inhibit by targeting weak spots in the oxide film and reacting with the ferrous ions as follows:



or



In the presence of chlorides, the nitrite “competes” with both chloride and hydroxide ions for the free Fe<sup>2+</sup>. Over time, nitrite and/or an alkaline environment free of chlorides will reduce the number of flaws in the protective film, thus decreasing the number of available sites from which to form chloride complexes. The higher the chloride content, the more nitrite is required for protection or the more probable that chlorides will form complexes with free

iron. Only mono-layers of oxides are involved, virtually no nitrite or hydroxide is consumed in forming the initial protective oxides or hydroxides.

Extensive research has been performed to determine the effectiveness of calcium nitrite as an inhibitor for rebar in concrete (Berke 1986; Hope 1987; Hope 1989; Berke 1990; Berke 1990; El-Jazairi 1990; Tomosawa 1990; Thompson 1991; Sagoe-Crentsil 1991/92; Yilmaz 1991/92; Loto 1992; Collins 1993; Berke 1994; Berke 1994; Cigna 1994; Justnes 1994; Trepanier 1994; Mammoliti 1995). Various evaluation methods, including polarization resistance, electrochemical impedance spectroscopy, cyclic polarization, and macro-cell corrosion technique, were employed in synthetic concrete pore solution, in concrete and in mortar specimens. The majority of the studies demonstrated that calcium nitrite delayed the onset of active corrosion initiation, reduced the corrosion rate, and increased both the pit initiation potential<sup>2</sup> and the protection potential<sup>3</sup>, thus decreasing the likelihood of pitting. It was also found to have no adverse effects, when used at the recommended dosage, on the mechanical properties of hardened concrete but acted as a set accelerator. Despite all the studies performed to verify the effectiveness of calcium nitrite, minimal work has been performed to verify the mechanism of inhibition.

Nevertheless, some researchers have noted some interesting observations. Cigna et al. (Cigna 1994) found that the presence of the nitrite in concrete did not appear to hinder the initiation of corrosion, but rather appeared to stop it over time. Hope and Ip (Hope 1987), conducting tests of steel in filtered lime water, found that all specimens, prior to chloride

---

<sup>2</sup> Pit initiation potential is defined as the electrochemical potential at which new pits form and existing pits grow.

<sup>3</sup> Protection potential is defined as the electrochemical potential at which pits repassivate.

addition and upon nitrite addition, exhibited a thin silvery-white coating that adhered tightly to the steel surfaces and was suspected to be the protective ferric oxide film. Also, the effectiveness of calcium nitrite to delaying the onset of corrosion was significantly decreased when the lime solution was stored with iron filings for a period of three months. As well, the white film seen previously was not evident on samples subjected to this solution. This would tend to indicate that the nitrite ions were consumed by the iron filings.

Using analytical electron microscopy to determine the extent that  $\text{Ca}(\text{NO}_2)_2$  modified the electrochemical reactions at the steel:cement interface, Yilmaz et al. (Yilmaz 1991/92) supported the inhibition mechanism for nitrite previously postulated by El-Jazairi and Berke (El-Jazairi 1990) and Berke and Weil (Berke 1992), who conducted tests in synthetic pore solution. However, they also concluded that localized pitting due to the presence of chloride occurred because chloride ions initially present in the mixing water were likely to accumulate on the particle surface before inhibition by nitrite became effective. They also found that the effectiveness of nitrite increased with time up to about 90 days, whereafter corrosion rates remained virtually constant (Loto 1992). Thompson (Thompson 1991) tested mortar lollipop samples partially immersed in chloride solutions to simulate exposure to salt water bodies. Cylinders were cast containing both calcium nitrite and sodium molybdate, calcium nitrite alone and no inhibitor, while the ponding solution consisted only of an aqueous solution of chlorides (3.5% NaCl). It was found that the corrosion rates of cylinders containing the combined inhibitors dropped 80% after 300 days, while the rates of those containing only calcium nitrite continued to increase. Cylinders exposed to calcium nitrite alone were also the only ones to undergo pitting corrosion in the middle section of the rebars. Additionally, the corrosion rate for the control cylinders - i.e. those without inhibitor - were lower than for

those containing inhibitors, suggesting that the calcium nitrite is having the opposite effect to its intention to inhibit or reduce corrosion.

Previous investigations by Mammoliti (Mammoliti 1995) in synthetic concrete pore solution did not show an indication of film enhancement due to the presence of calcium nitrite.

However, calcium nitrite reduced the pH of synthetic pore solution from approximately 13.5 to approximately 12, lowered the chloride concentration needed to induce localized corrosion, and lowered the pitting potential. As well, immediately upon addition of the inhibitor to the pore solution, a white precipitate formed. However, studies performed simultaneously in concrete (Trepanier 1994) found that one calcium nitrite-based inhibitor increased the time to corrosion.

Justnes and Nygaard (Justnes 1994) stipulate that calcium *nitrate* ( $\text{Ca}(\text{NO}_3)_2$ ) is also an effective corrosion inhibitor. They suggest that the nitrate ( $\text{NO}_3^-$ ) inhibits by transforming ferric hydroxide ( $\text{Fe}(\text{OH})_2$ ) to ferrous hydroxide ( $\text{Fe}(\text{OH})_3$ ), which is assumed to be more protective. As the proposed mechanism is considered similar to that of corrosion inhibition by nitrite, they prefer the use of calcium nitrate as larger quantities of ferric hydroxide are oxidized to ferrous hydroxide,  $\text{Ca}(\text{NO}_3)_2$  is more readily available in large quantities and is less expensive. They also found a decrease in pH with addition of  $\text{Ca}(\text{NO}_3)_2$ , thereby increasing the  $[\text{Cl}^-]/[\text{OH}^-]$  ratio, which is considered an indication of the level of chloride needed to initiate corrosion.

## **2.4 Techniques for Characterization**

### **2.4.1 Electrochemical Corrosion Testing**

Electrochemical testing techniques are the most commonly used methods to determine various corrosion parameters, such as pitting and corrosion potentials and corrosion current densities, when examining corrosion behaviour. Two methods were utilized for this study: full cyclic polarization and linear polarization resistance.

#### **2.4.1.1 Full Cyclic Polarization**

In this technique, the electrode potential of the specimen is changed continuously while the resulting current is monitored. The applied potential is plotted vs. the logarithm of the resulting current density and the shape of the anodic portion of the curve generated, shown schematically in Figure 2.6, gives an indication of whether the sample is in the passive or active state. The pitting or nucleation potential,  $E_n$ , and the passivation or protection potential,  $E_p$ , can also be deduced from these curves, and are shown schematically in Figure 2.7 (Mammoliti 1995). Given the highly alkaline nature of concrete the only cathodic reaction of any significance will normally be that of oxygen reduction, as indicated in Figure 2.2.

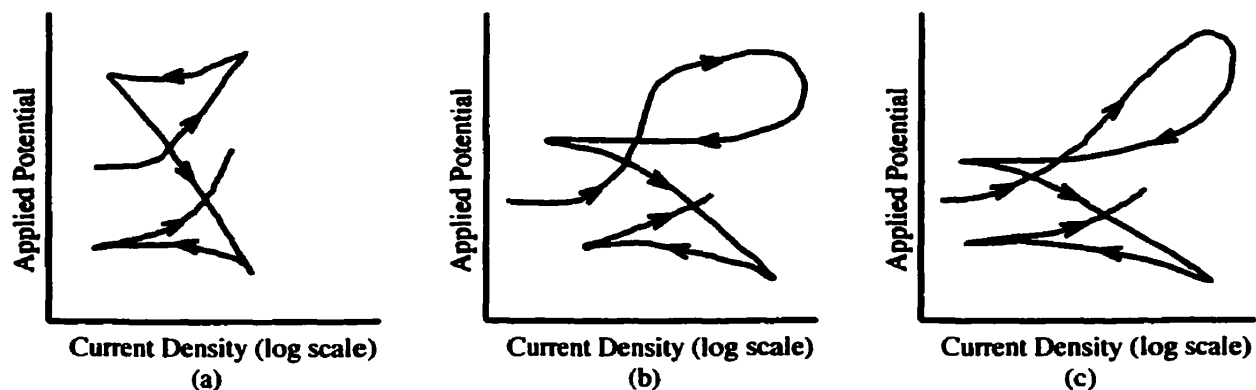


Figure 2.6 Schematic of types of anodic polarization curves showing (a) passive state, (b) pitting corrosion and (c) active and/or crevice corrosion.

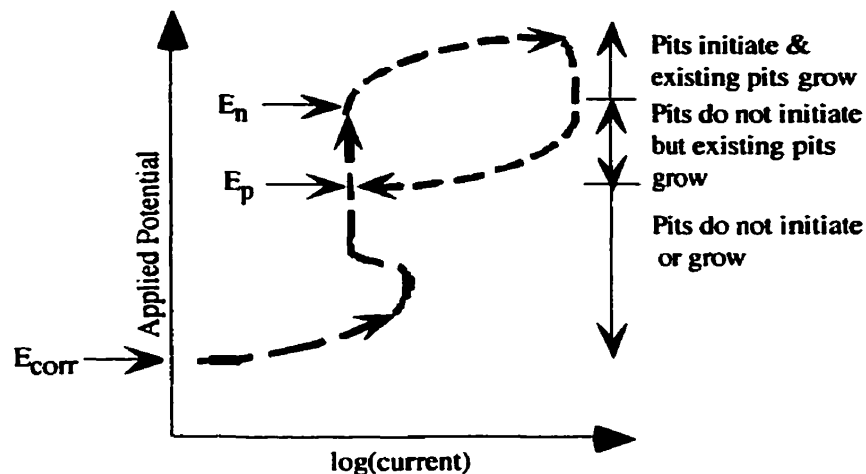


Figure 2.7 Schematic of pitting and passivation potentials on anodic polarization curve (Mammoliti 1995)

In accordance with ASTM Standard G61 (ASTM 1993), a three electrode system is used, consisting of a working electrode (i.e. sample), counter electrode (i.e. typically stainless steel or platinum wire) and a reference electrode (e.g. saturated calomel electrode-SCE), connected through a potentiostat. The working electrode is held at ground and a potential is applied to the counter electrode such that the difference in potential between the reference and working electrodes is the desired value. The resulting current between the working and counter electrodes is monitored. The experimental procedure used in the current project is shown schematically in Figure 2.8 (Mammoliti 1995). Maximum and minimum potentials of +500 mV SCE and -1000 mV SCE were used to avoid evolution of oxygen and hydrogen, respectively, as indicated in Figure 2.2. In order to minimize the effects of concentration polarization (i.e. diffusion controlled as opposed to charge transfer controlled), solutions are stirred to decrease the diffusional boundary layer.

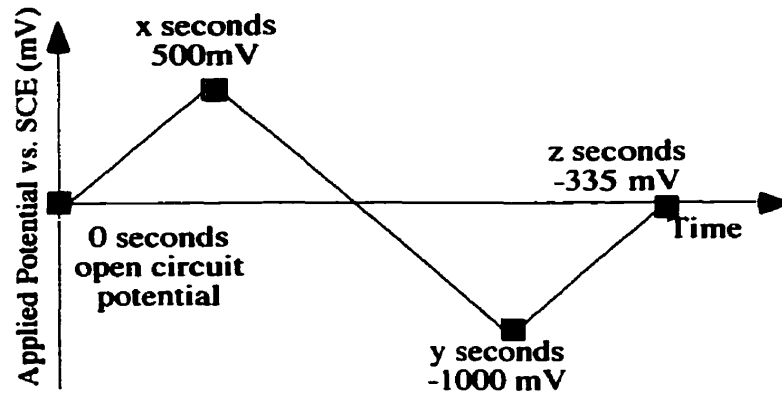


Figure 2.8 Schematic of potential variation in full cyclic polarization (Mammoliti 1995)

#### 2.4.1.1.1 Limitations of Full Cyclic Polarization

In order to obtain the data required, it is necessary to polarize the working electrode, in many cases, to potential levels that do not naturally occur under normal exposure conditions. The passive film, therefore, is undergoing constant changes, which may not be irreversible and may not be representative of service conditions. Additionally, care must be taken to not over-polarize the sample, thereby causing oxygen and hydrogen gas evolution, which can affect the corrosion process. This is accomplished by keeping the polarization between the potential limits mentioned in the previous section.

One of the main reasons that this method, although providing very useful information, is limited to laboratory experiments and is not used extensively on concrete structures in the field, is that, to generate reproducible and accurate data, a slow scanning rate is necessary. On the order of 1 mV/sec, this results in a long data collecting period, typically one hour, which is deemed “too long” when monitoring concrete structures (Hansson 1999).

### 2.4.1.2 Linear Polarization Resistance

The applied current density is an approximately linear function of the electrode potential in the range of overpotential<sup>4</sup> of 0 to  $\pm 20$  mV (Berke 1990). This relationship is shown in Figure 2.9 (Fontana 1986). By applying a small potential perturbation ( $< 20$  mV) about the corrosion potential and monitoring the current, the corrosion rate can be determined as follows (Research 1982):

$$\left(\frac{\Delta E}{\Delta i}\right)_{\Delta E \rightarrow 0} = \frac{\beta_a \beta_b}{2.3 i_{corr} (\beta_a + \beta_b)} \quad (2-20)$$

where  $\beta_a$  and  $\beta_b$  are the Tafel slopes (i.e. the slopes of the linear portions of the E vs. log i curves) of the anodic and cathodic reaction, respectively. As the slope of a linear-polarization curve is mainly a function of  $i_{corr}$  and is relatively insensitive to changes in  $\beta$  values, the above equation can be reduced to:

$$\left(\frac{\Delta E}{\Delta i}\right)_{\Delta E \rightarrow 0} = \frac{B}{i_{corr}} \quad (2-21)$$

where B is usually assigned a constant value of 0.026 mV for active corrosion of steel in concrete, determined by assuming the anodic and cathodic  $\beta$  values of 0.12 V represents the average of all corrosion systems. This assumption yields corrosion rates that differ by no more than a factor of three from the actual rates (Stern 1957).

---

<sup>4</sup>The overpotential is the difference between the applied and open circuit or corrosion potentials.



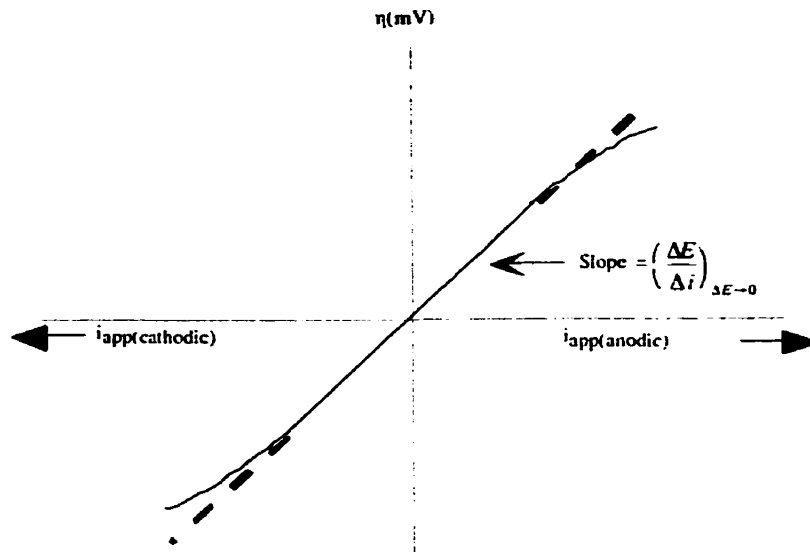


Figure 2.9 Applied current-linear polarization curve (Fontana 1986)

#### 2.4.1.2.1 Limitations of Linear Polarization Resistance

The following lists some of the assumptions and therefore, limitations associated with this technique:

- i. it assumes that the system is under activation control (i.e. thermodynamically driven);
- ii. it assumes that the metal surface is bare (i.e. no passive or inhibitor films or corrosion products) to limit charge transfer;
- iii. it assumes that the sample is corroding uniformly, that is, no localized forms of corrosion such as pitting;
- iv. it assumes that only one anodic and one cathodic reaction is taking place on the sample surface;
- v. to accurately determine current density values, knowledge of Tafel constants is needed;
- vii. it assumes that all currents are due to corrosion reactions only (Tullmin 1995).

With respect to tests in pore solution, a number of these assumptions are valid as the system can be controlled. However, when studying steel in concrete, virtually all of the assumptions are invalid. Hence, the use of this technique on steel embedded in concrete can theoretically lead to erroneous results, but has been found in practice to provide a reliable indication of the state of steel (Andrade 1978).

## 2.4.2 Raman Spectroscopy

Raman spectroscopy is based on the Raman effect, which involves the interaction of light with matter. As shown in Figure 2.10, an incident, monochromatic light (i.e. laser) illuminates the sample, and the light is scattered by the material, predominantly at the same wavelength as the original incident beam. However, a small proportion of the beam experiences a wavelength shift, which results from bonds between the material's atoms vibrating. The energy difference between the incident light ( $E_i$ ) and the scattered light ( $E_s$ ) is equal to the energy,  $E_v$ , characteristic of the vibration of the atomic or molecular bonds. Qualitative analysis of these scattered wavelengths, plotted as Raman shift ( $\text{cm}^{-1}$ ) vs. intensity, and comparison to previously generated standards, gives information regarding the chemical composition and physical state of a material.

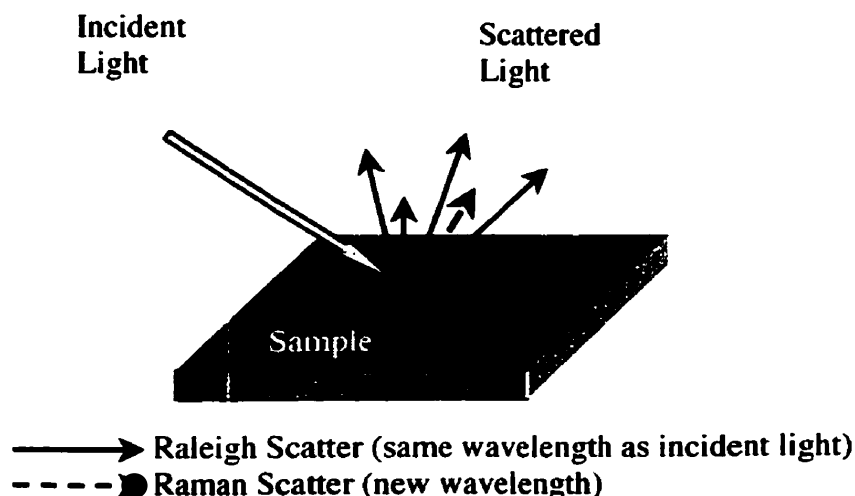


Figure 2.10 Schematic representation of the Raman effect (Shaver 2000)

Raman spectroscopy is becoming increasingly popular since little to no sample preparation is required and its ability to analyse all matter states (gas, liquid, solid). It is also possible to observe “in situ” reactions, which is particularly useful for examining corrosion films.

### **2.4.3 Thermal Analysis**

Thermal analysis is the general term used to describe a variety of techniques that study the thermal behaviour of materials. By measuring different physical or mechanical properties as a function of temperature or time, an understanding can be gained about the material's structure or chemical composition.

#### **2.4.3.1 Thermogravimetric Analysis**

Thermogravimetric analysis (TGA) measures the variation in material mass (either loss or gain) as a function of time ( $t$ ) and/or temperature ( $T$ ):

$$m = f(T \text{ or } t) \quad (2-22)$$

For this particular study, “dynamic thermogravimetry” was utilized, in which the temperature of the material is increased in a predetermined manner, usually at a linear rate, within a controlled atmosphere of helium. By measuring and plotting the resulting mass decrease or increase versus temperature or time, information regarding the chemical compound composition of the initial sample and any intermediate compounds that may form during the heating cycle is determined. Comparison of the generated plot to those of known materials facilitates identification of compounds.

The procedure involves placement of the sample – in the case of this study, crushed cement paste – into a tared platinum crucible, which is then placed on a sensitive microbalance arm. An inert reference material<sup>5</sup>, which is stable over the range of temperature to be evaluated, is placed into another tared platinum crucible, also placed on a microbalance arm. Both the

---

<sup>5</sup> In the case of this study, the reference material was considered to be the platinum crucible itself.

sample and the reference material holders are then placed into a high temperature furnace.

The room temperature mass of the sample is measured and changes in the sample mass – either mass loss or gain – are continuously monitored during the heating cycle.

#### 2.4.3.2 Derivative Thermogravimetric Analysis

As the name implies, in derivative thermogravimetric analysis (DTG) the derivative of the mass change with respect to time or temperature is measured as a function of time or temperature:

$$\frac{dm}{d(t \text{ or } T)} = f(T \text{ or } t) \quad (2-23)$$

A maximum in the DTG curve occurs at an inflection point in the corresponding TGA curve. Sequences of peaks are obtained, where the areas under the peaks are proportional to the total mass-change of the sample at that temperature.

The advantage of DTG relative to TGA is that quantitative information can be obtained regarding chemical composition of unknown materials. As well, analysis of the data present in this fashion is more sensitive to small fluctuations in mass than TGA.

#### 2.4.3.3 Differential Thermal Analysis

Differential thermal analysis (DTA) measures the difference in temperature between a sample ( $T_s$ ) and an inert reference material ( $T_r$ ) as a function of temperature or time:

$$T_s - T_r = f(T \text{ or } t) \quad (2-24)$$

The temperature change differences are due to endothermic or exothermic reactions. In general terms, endothermic effects are due to phase transitions, dehydration, reduction and

some decomposition reactions while crystallization, oxidation, and some decomposition reactions are due to exothermic effects.

#### 2.4.3.4 Limitations of Thermal Analysis

Due to the high number of phases within concrete and cement paste, some overlapping of thermal responses can occur and may be obscured in TGA. However, DTG overcomes this by emphasizing very small mass losses. This is shown in Figure 2.11 (Wendlandt 1986):

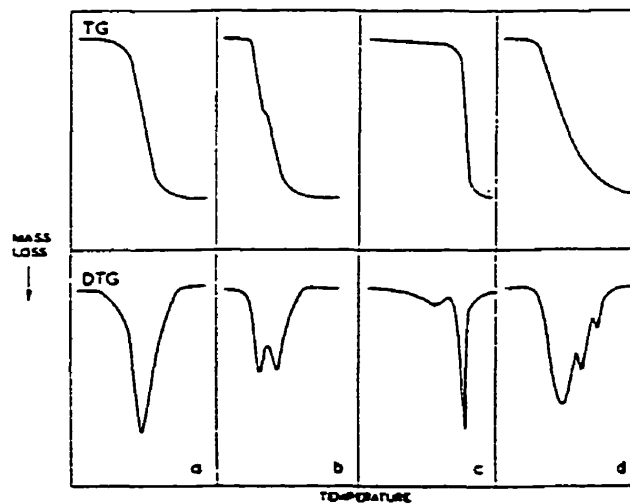


Figure 2.11 Comparison of TGA and DTG curves, three of which exhibit overlapping reactions (Wendlandt 1986)

DTA also solves this problem, as very small temperature changes can be detected, since the difference in temperature between the sample and reference material is being measured (Wendlandt 1986).

#### 2.4.4 Mercury Intrusion Porosimetry

Mercury intrusion porosimetry (MIP) is often used for determining pore size distributions within cement-based systems. The principle behind MIP is that a non-reactive, non-wetting liquid will only enter a porous solid if sufficient pressure is applied to force entrance. If it is

assumed that the pores are cylindrical, the relationship between the pressure,  $P$ , needed to force the liquid in and the pore diameter,  $D$ , is governed by the Washburn equation:

$$D = -\left(\frac{1}{P}\right) 4\gamma \cos \theta \quad (2-25)$$

where  $\gamma$  is the surface tension of the non-wetting liquid (i.e. for mercury, this value is 485 dyne  $\text{cm}^{-1}$  for most surfaces), and  $\theta$  is the contact angle between the non-wetting liquid and the pore wall (i.e. for mercury,  $130^\circ$ ). As the pressure is increased, the intrusion volume of mercury,  $V$ , is monitored by the change in capacitance between the mercury within the penetrometer column and the metal sheath surrounding the stem of the sample cell. In theory, the relationship between  $P$  and  $V$ , therefore, gives a unique characterization of pore structure.

#### 2.4.4.1 Limitations of Mercury Intrusion Porosimetry

Despite being widely used to study porosity in cement-based systems, several problems have been identified when using MIP. These have been summarized by Taylor (Taylor 1997):

- i. this method does not measure the distribution of pore sizes, but that of pore-entry sizes. If large pores can be entered only through small pores, they will be registered as small pores;
- ii. the delicate pore structure of the paste is altered by the high stress needed to intrude the mercury;
- iii. the pore structure is also altered by the removal of the pore solution prior to testing;
- iv. it is not clear whether the method registers the coarsest part of the porosity, intruded at low pressures;
- v. the assumption of cylindrical pores and of a particular contact angle may be incorrect.

A particular drawback of the technique is the assumption of cylindrical pores. Figure 2.12 demonstrates the problem of “inkbottle pores”, where bigger hollow spaces are filled through narrower connecting channels. The volumes of mercury needed to fill radii  $r_4$  and  $r_5$  would be assigned with radius  $r_3$ , as it only after penetrating the latter pore radius that the other two

chambers can be filled. This would lead to a larger proportion of small pores than is actually present within the sample.

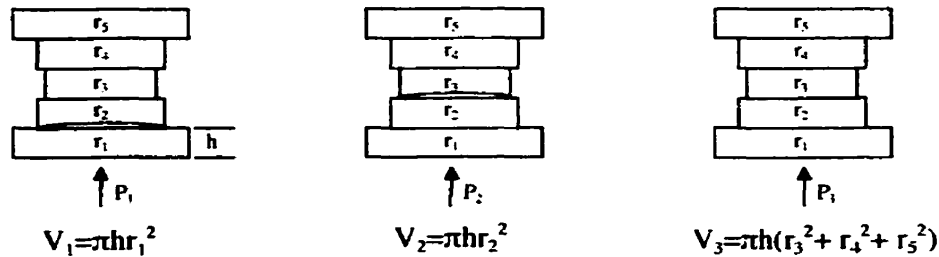


Figure 2.12 The problem of inkbottle pores (Metz 1992)

Diamond (Diamond 1988) also raises concerns that this technique assumes that pore size decreases with increasing depth into the sample and that all the pores are interconnected. Additionally, corrections to the measured intruded volume of mercury are necessary to correct for the physical compression of mercury and the machine components at high pressures and the subsequent thermal expansion of the mercury.

Despite these concerns, MIP remains the primary method of determining porosity characteristics in cement-based materials due to its ability to measure an extensive range of pore diameters.

#### 2.4.5 Environmental Scanning Electron Microscope with Energy Dispersive X-Ray Spectroscopy

The advent of the conventional Scanning Electron Microscope (SEM) allowed more detailed microstructural and chemical characterization of materials. However, it is limited in that a high vacuum ( $10^{-6}$  to  $10^{-7}$  Torr) sample environment is necessary and samples must be clean.

dry and electrically conductive. The Environmental Scanning Electron Microscope (ESEM) eliminates these disadvantages by removing the high vacuum constraint and allows analysis of samples in any physical condition. This is of particular importance when examining cement-based systems, as drying of the sample can lead to structural and microstructural changes (Mehta 1986).

The interactions between the incident beam electrons and the sample atoms can generate a variety of signals. The most commonly used signals are secondary electrons, backscattered electrons and characteristic x-rays, which originate from different volumes within the sample (Figure 2.13).

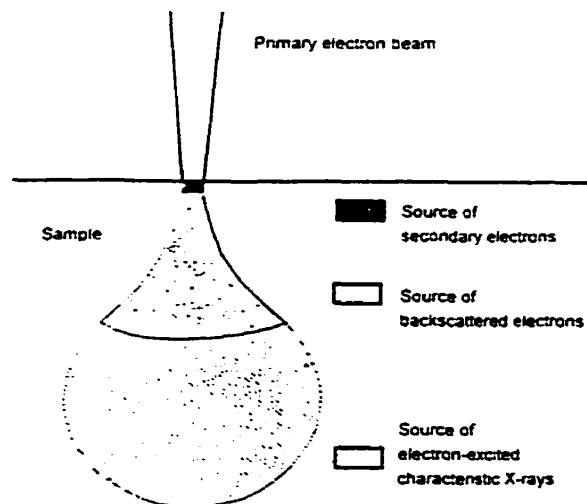


Figure 2.13 Sources of secondary and backscattered electrons and characteristic x-rays (Optics 1996)

Secondary electrons (SE) are electrons from the sample that have been ejected by interactions with the primary electrons of the beam. As they are of very low energy, they can only escape from the surface of the sample and provide imaging resolution. In a conventional SEM, this theoretically can be as high as 2 nm. In the ESEM used in the present study, the theoretical resolution limit is approximately 5 times this value (i.e. 10 nm).



**Backscattered electrons (BSE)** are incident beam electrons that have scattered back out of the sample by elastic collisions with the nuclei of sample atoms. Due to their high energy, they are emitted from a deep part of the sample and the resolution is lower. However, high atomic number nuclei backscatter more electrons and create bright areas in the generated image. Therefore, compositional information on the sample can be obtained.

**Characteristic x-rays** are generated when an inner shell electron vacancy is filled by higher energy outer shell electron (Figure 2.14). An energetic electron from the beam ejects the inner shell electron. The energy of the x-ray equals the difference between the electron energies and is characteristic of the emitting element. As most elements have multiple energy shells, x-rays of differing energies can be emitted.

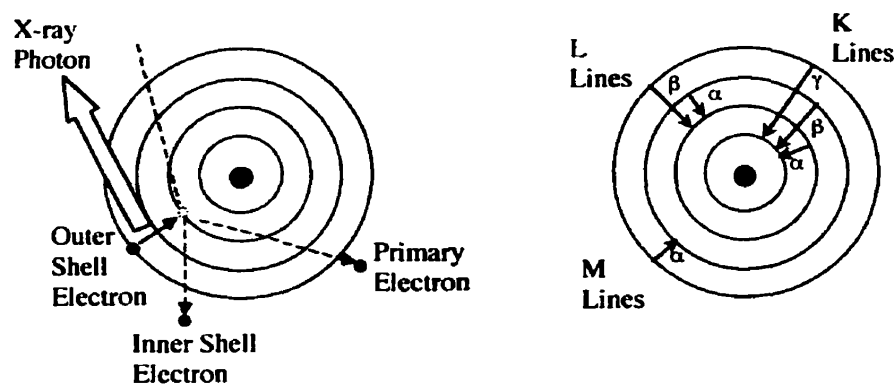


**Figure 2.14 Characteristic x-rays (Optics 1996)**

**Characteristic x-rays** can be identified and quantified through **Energy Dispersive Spectroscopy (EDS)**. An x-ray spectrometer counts and sorts the x-rays on the basis of energy. The energy level of the peak identifies the particular element while the intensity of the peak gives concentration information. Concentrations in excess of 10% by mass can be

measured confidently quantitatively, but the lower the concentration, the larger the error.

Three corrections should be made to the peak intensities in order to account for other elements in the sample that may interfere with the desired analysis. Collectively termed “ZAF”, these corrections take into consideration the effects of elements having higher atomic numbers reflecting incident electrons away from the sample before interaction with the sample (Z), absorption of x-rays by the sample itself (A), and sample x-rays stimulating the emission of other x-rays within the sample, termed “fluorescence” (F). This correction is typically incorporated into the software that operates the EDS system.

#### 2.4.6 Potentiometric Titration

The principle of titration is that the concentration of a solution, either acidic or basic, is determined by monitoring the reaction of the original solution with another solution (i.e. titrant), either basic or acidic, of known concentration. The amount of original solution is known, while the titrant is added in small increments until there is an equal number of proton acceptors as proton donors i.e. the endpoint is reached. The endpoint or inflection point is determined by either a chemical indicator, or in the case of potentiometric titration, when a sudden drop in electrochemical potential is observed.

For determination of chlorides, a silver/silver chloride electrode is used. It consists of a silver wire with AgCl(s) deposited on the surface. The solubility of the AgCl on the electrode is affected by the concentration of chloride ions in the solution, which in turn affects the potential at the electrode surface. When the titrant, a solution of silver nitrate, is added to the sample solution, silver chloride precipitates due to its very low solubility (0.000089 g/100 cc cold water), thereby decreasing the chloride concentration and potential at the electrode surface by reducing the conductivity of the solution.

Care must be taken when evaluating inflection points calculated automatically by the software. The extremely high sensitivity needed for this type of measurement inevitably leads to false identification of endpoints due to minor fluctuations in potential. Therefore, it is imperative that calculated endpoints are verified by inspection of the generated potential vs. titrant volume plot.

#### 2.4.7 Pore Solution Expression

The expression of pore fluid from hardened concrete, mortar and cement paste is based on the apparatus and technique developed by Barneyback and Diamond (Barneyback 1981).

Figure 2.15 is an isometric  $3/4$ -section diagram of the unit developed by the aforementioned authors. Details regarding the construction and operator of the apparatus are given within the same document.

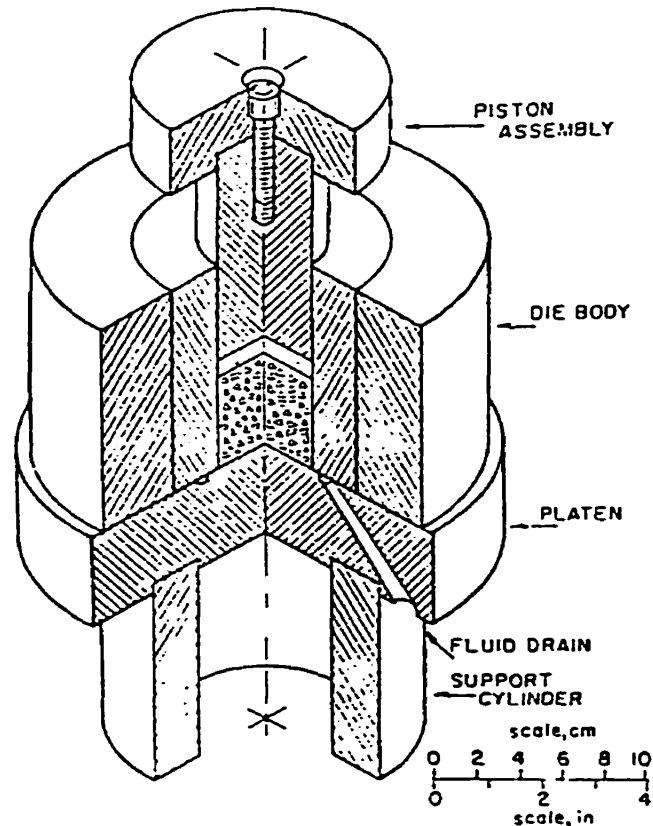


Figure 2.15 Isometric three-quarter section of pore fluid expression device (Barneyback 1981)

The amount of solution expressed is dependent on several parameters, including water:cement ratio, age of the sample, storing and exposure conditions, mix composition and applied pressure. In general, the higher the water:cement ratio and the younger the sample, the greater the amount of fluid expressed. Once the solution is collected, analysis for various anions and cations as well as the alkalinity of the solution is carried out to determine the effect of changing various parameters (eg. the addition of corrosion inhibitors) on the pore solution composition. The effect on various chemical and physical properties of the concrete, mortar or cement paste can then be determined.

#### 2.4.7.1 Inductively Coupled Plasma

This method is used to quantitatively determine the concentration of various cations (positively charge ions) within a solution. Inductively coupled plasma (ICP) involves the production of a stream of very hot, ionized gas (i.e. plasma) which dissociates, atomizes and excites the elements composing a sample that has been injected into the stream. This results in the generation of light at different wavelengths, which are dependent on the element(s) present. The intensity of light is also proportional to the concentration of the element(s) in the sample.

#### 2.4.7.2 Ion Chromatography

Ion chromatography (IC) is the separation and quantification of anions and cations by selective adsorption. Figure 2.16 is a simplified representation of the process. Essentially, the analyte solution (i.e. the sample) is mixed with an eluent (i.e. solvent) through a column, which is filled with restrictive resin containing numerous ionic exchange sites. The various ions within the analyte will have different attractions for these sites, resulting in ion separation over a period of time. The quantity of ions present is determined by measuring

the electrical conductivity generated upon emerging from the column while the identity of the ion is related to the time taken to emerge from the column.

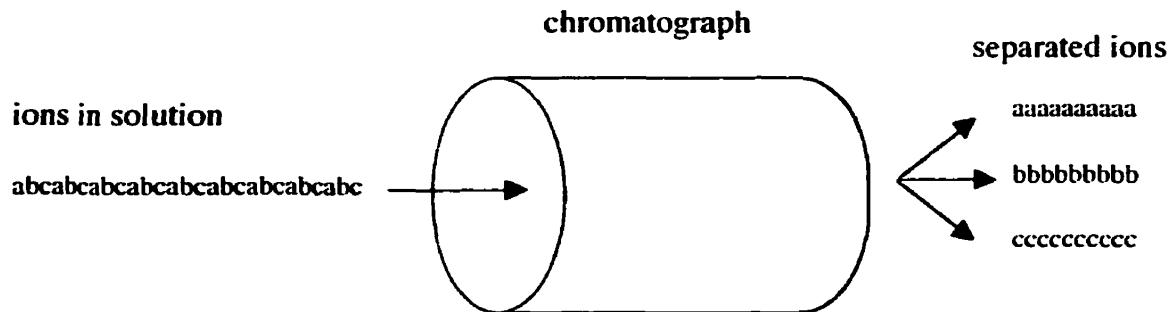


Figure 2.16 Simplified explanation of ion chromatography (Katz Analytical Services 2000)

### 2.4.7.3 Alkalinity

Alkalinity is defined as the capacity of a solution to neutralize acid. Alkalinity is primarily a function of the carbonate ( $\text{CO}_3^{2-}$ ), bicarbonate ( $\text{HCO}_3^-$ ) and hydroxide ( $\text{OH}^-$ ) concentrations.

Alkalinity is determined using potentiometric titration from the sample pH to a pH of 4.5, using either sulphuric or hydrochloride acid as the titrant. By measuring the volume of titrant used to reach specific inflection points, thereby neutralizing the sample to pre-specified pH values, the amount of each contributor to total alkalinity can be determined. Most analytical methods for determining alkalinity presuppose that hydroxides and bicarbonates can not exist simultaneously in significant quantities (Reardon 1999).

## **Chapter 3**

### **Objectives, Rationale and Strategy**

Without a clear knowledge of the mechanism of inhibition by calcium nitrite, it is difficult to predict how the inhibitor will perform under different conditions over time and what factors could possibly render the inhibitor ineffective. Hence, the objective of the proposed work is to try to determine the mechanism of corrosion inhibition by  $\text{Ca}(\text{NO}_2)_2$  and  $\text{Ca}(\text{NO}_3)_2$  in concrete. Specifically, by examining the chemical reactions occurring between concrete and calcium nitrite, it is believed that those interactions primarily responsible for the delay in corrosion initiation associated with calcium nitrite in concrete can be elucidated and therefore, the long-term effectiveness of the inhibitor evaluated.

#### **3.1 Alternate Mechanism for Corrosion Inhibition by $\text{Ca}(\text{NO}_2)_2$**

Although it has been found that  $\text{Ca}(\text{NO}_2)_2$  does delay the onset of corrosion without having an adverse short term effect on the mechanical properties, several observations suggest that an alternate or additional mechanism to that reported in the literature, may be responsible for inhibition:

- i. the majority of previous studies which examined  $\text{Ca}(\text{NO}_2)_2$  in solutions supposedly simulating the free pore water of concrete were actually performed in distilled water saturated with  $\text{Ca}(\text{OH})_2$ , which has been shown to give significantly different results than those obtained in synthetic pore solutions containing sodium and potassium hydroxide in addition to  $\text{Ca}(\text{OH})_2$  (Mammoliti 1996);
- ii. when conducting tests in synthetic pore solution, the absence of some major constituents found in concrete (i.e. the hydration products) eliminates a whole range of possible reactions;
- iii. the formation of a white precipitate observed immediately upon addition of  $\text{Ca}(\text{NO}_2)_2$  to the synthetic pore solution, which, if it occurs in concrete, may have subsequently deposited on the surface of reinforcement providing additional protection, has not been examined;
- iv. a decrease in the pH of both synthetic pore solution and pore solutions of cement (Monkman 1995) containing  $\text{Ca}(\text{NO}_2)_2$  reflects a change in the chemistry of the concrete;

- v. lower chloride threshold values for samples exposed to synthetic pore solutions containing chlorides and  $\text{Ca}(\text{NO}_2)_2$ .

Based on these observations, it is suggested by this researcher that an alternative or additional mechanism to that proposed by El-Jazairi and Berke (El-Jazairi 1990) and Berke and Weil (Berke 1992) is responsible for the delay in corrosion initiation when calcium nitrite is used as a corrosion inhibitor in concrete. The following phenomena are potential alternative mechanisms, either individually or in combination:

- i. alteration of the environment to promote increased chemical chloride binding by the concrete;
- ii. formation of a precipitate that physically blocks the capillary pores, thereby hindering the ingress of chlorides, oxygen and other aggressive species;
- iii. formation of a precipitate on the surface of steel, creating a physical barrier to the chloride reaching the steel surface and damaging the existing passive layer.

## Chapter 4 Experimental Procedures

### 4.1 Materials Used

#### 4.1.1 Cement

Two types of cement were investigated in order to determine the role of the aluminate phases of cement in interacting with the nitrites or nitrates: an ordinary portland cement (OPC) (Type 10), manufactured by Lafarge Canada in Woodstock, Ontario and a white, sulphate-resisting portland cement (Type 50), manufactured by Aalborg Portland in Denmark. The latter contained significantly less  $C_4AF$  and  $C_3A$  than the OPC. The chemical analyses of the cements, as provided by the manufacturers, are detailed in Table 4.1.

Table 4.1 Chemical Analyses of Cements

	<b>White Cement ( weight %)</b>	<b>OPC (weight %)</b>
SiO <sub>2</sub>	25.01	21.15
Al <sub>2</sub> O <sub>3</sub>	1.91	5.01
Fe <sub>2</sub> O <sub>3</sub>	0.32	2.46
CaO	69.34	64.16
MgO	0.56	2.19
Na <sub>2</sub> O	0.17	0.12
K <sub>2</sub> O	0.12	0.43
SO <sub>3</sub>	2.10	3.08
TiO <sub>3</sub>	0.09	---
Cl	0.008	---
Loss on Ignition	0.41	2.13
C <sub>4</sub> AF	1.0	7.5
C <sub>3</sub> A	4.5	9.1
C <sub>3</sub> S	73	54.4
C <sub>2</sub> S	17	19.4
CaSO <sub>4</sub>	3.6	n/a
Blaine (m <sup>2</sup> /kg)	---	368
-325 Mesh	---	90.7 % passing
Alkalis (Na <sub>2</sub> O <sub>(eq)</sub> )	0.25	0.40



#### 4.1.2 Chemical Corrosion Inhibitors

Currently, calcium nitrite-based ( $\text{Ca}(\text{NO}_2)_2$ ) inhibitors are the most widely used admixtures in concrete to combat rebar corrosion. Two separate manufacturers supplied two inhibitors, hence referred to as CN1 and CN2. However, despite having the same active ingredient, the manufacturers specify very different dosages to be used (10-30 L/m<sup>3</sup> and 3 L/m<sup>3</sup> of concrete, for CN1 and CN2, respectively), resulting in very different performances in previous synthetic pore solution and concrete studies (Trepanier 1994; Mammoliti 1996) and manufacturers of both inhibitors state that each contains approximately 30%  $\text{Ca}(\text{NO}_2)_2$  by weight. It was therefore felt necessary to independently determine the actual composition of the two inhibitors. Samples of each inhibitor were provided to Solutions Analytical Laboratory in the Department of Earth Sciences, University of Waterloo, and analyzed for nitrite ( $\text{NO}_2^-$ ), nitrate ( $\text{NO}_3^-$ ) and calcium ( $\text{Ca}$ ). Results from the analysis are shown in Table 4.2 and it is clear they contain the same active ingredients, despite differences in appearance. A laboratory grade, crystalline form of calcium nitrate ( $\text{Ca}(\text{NO}_3)_2$ ) was also examined as a potential corrosion inhibitor because of previous reports of its efficiency (Justnes 1994).

Table 4.2: Chemical Analysis of CN1 and CN2

<b>Analysis</b>	<b><math>\text{NO}_2^-</math></b>	<b><math>\text{NO}_3^-</math></b>	<b><math>\text{Ca}^{2+}</math></b>
<b>Method</b>	<b>IC*</b>	<b>IC*</b>	<b>AA**</b>
<b>Units</b>	<b>mg/L</b>	<b>mg/L</b>	<b>mg/L</b>
<b>Detection Limit</b>	<b>0.05</b>	<b>0.05</b>	<b>0.05</b>
CN1	261000	13400	113000
CN2	271000	13600	117000

\*IC = Ion Chromatography

\*\*AA = Atomic Absorption Spectroscopy

All inhibitors were added at a dosage of approximately 9% by weight of the total pore solution.

### **4.1.3 Deformed Reinforcing Steel**

For corrosion testing performed in synthetic concrete pore solutions, deformed reinforcing steel was used, having a nominal diameter of ten (10) millimetres and of composition given in Table 4.3. Chemical analysis was performed by Galt Testing Laboratories Ltd., Cambridge, Ontario.

Table 4.3 Chemical Analysis of Deformed Reinforcing Steel

<b>Element</b>	<b>Wt. %</b>
Silicon	0.23
Sulphur	0.046
Phosphorus	0.037
Manganese	0.83
Total Carbon	0.46
Nickel	0.13
Chromium	0.22
Molybdenum	0.03
Iron	Balance

### **4.1.4 Synthetic Concrete Pore Solution**

The synthetic concrete pore solution used in the corrosion experiments was similar to that used by Berke and Hicks (Berke 1990). It consisted of 0.6 M KOH, 0.3 M NaOH, and 12.50 g of solid  $\text{Ca}(\text{OH})_2$  per litre of pore solution. All chemical reagents used were of laboratory grade.

## **4.2 Sample Preparation**

### **4.2.1 Cement Paste Cylinders**

Cement paste cylinders, having dimensions of  $\text{Ø}50.8$  mm by 101.6 mm, were used in the majority of the tests performed for this study. The mixing procedure was as follows:

- i. measure dry cement powder into mixing bowl and commence mixing at low speed using a commercial mixer designed for this purpose;

- ii. over the period of one (1) minute, gradually add all mixing water (admixed with inhibitor for all inhibited samples);
- iii. allow cement powder and water to mix for one (1) minute, then cease mixing;
- iv. with a rubber spatula and/or gloved hands, remove settled cement powder clumps from bottom of mixing bowl and break apart;
- v. continue to mix at low speed for a further three (3) minutes;
- vi. turn off mixer and allow cement paste to rest for five (5) minutes;
- vii. continue mixing on low speed for a further five (5) minutes;
- viii. pour cement paste into plastic, cylindrical moulds.

The cylinders were allowed to set for approximately twenty-four (24) hours prior to being placed in a humidity room. Samples were not removed from their respective moulds to minimize leaching of cement paste constituents (i.e.  $\text{Ca(OH)}_2$ , etc.) due to a concentration gradient being established with the outside atmosphere. All samples remained in the humidity room until used in various experiments. In total, eight different mix designs were used, which varied the type of cement and the type of inhibitor. Table 4.4 details the various mix designs used in casting of the cylinders.

Table 4.4 Mix designs for cement paste cylinders

	Mix	Cement	Water	Inhibitor
White Cement	Control	1	0.45	----
	CN1	1	0.4369*	0.5 %**
	CN2	1	0.4369*	0.5 %**
	$\text{Ca(NO}_3)_2$	1	0.45	0.5 %**
OPC	Control	1	0.45	----
	CN1	1	0.4369*	0.5 %**
	CN2	1	0.4369*	0.5 %**
	$\text{Ca(NO}_3)_2$	1	0.45	0.5 %**

\* when combined with inhibitor, w/c = 0.45

\*\* 0.5 %  $\text{Ca(NO}_2)_2$  or 0.5 %  $\text{Ca(NO}_3)_2$  by weight of cement

#### 4.2.2 Corrosion Samples

Deformed reinforcing steel bars were cross-sectioned and mounted in bakelite. Each mounted section was then metallurgically polished with silicon carbide paper and diamond polished to 1  $\mu\text{m}$ . The edges of the rebar disc were painted with an epoxy – ICI Devoc

Coatings, TRU-GLAZE 4508, Components A and B – commonly used on reinforcing steel in concrete in order to reduce the likelihood of crevice corrosion, a common occurrence with this type of sample. Each sample was then drilled and tapped for insertion of a stainless steel threaded rod providing an electrical connection to the potentiostat. The rod was coated in the same epoxy previously mentioned to prevent contact with the pore solution and to minimize the occurrence of galvanic corrosion.

### **4.3 Synthetic Concrete Pore Solution Tests**

#### **4.3.1 Corrosion Behaviour and Corrosion Rate Testing**

Corrosion testing in synthetic concrete pore solutions was carried out on metallographically polished samples described in Section 4.2.2. Although not representative of rebar surfaces used in practice, this is standard laboratory corrosion practice to ensure reproducibility of sample surfaces and allow greater understanding of the corrosion process. Three (3) mounted, polished samples, each connected to a threaded stainless steel rod, were placed in each of four cells: synthetic pore solution containing no inhibitor (i.e. Control), synthetic pore solution containing CN1, synthetic pore solution containing CN2, and synthetic pore solution containing laboratory grade  $\text{Ca}(\text{NO}_3)_2$ . Inhibitors were added in dosages of 9 % volume based on the total volume of the solution. In accordance with ASTM Standard G 61 (ASTM 1993), a three (3) electrode system was used, consisting of a working electrode (sample), counter electrode (stainless steel bar) and a saturated calomel reference electrode (SCE), electrically connected through an EG&G Princeton Applied Research Potentiostat/Galvanostat 273A. A schematic representation of the experimental apparatus can be seen in Figure 4.1.

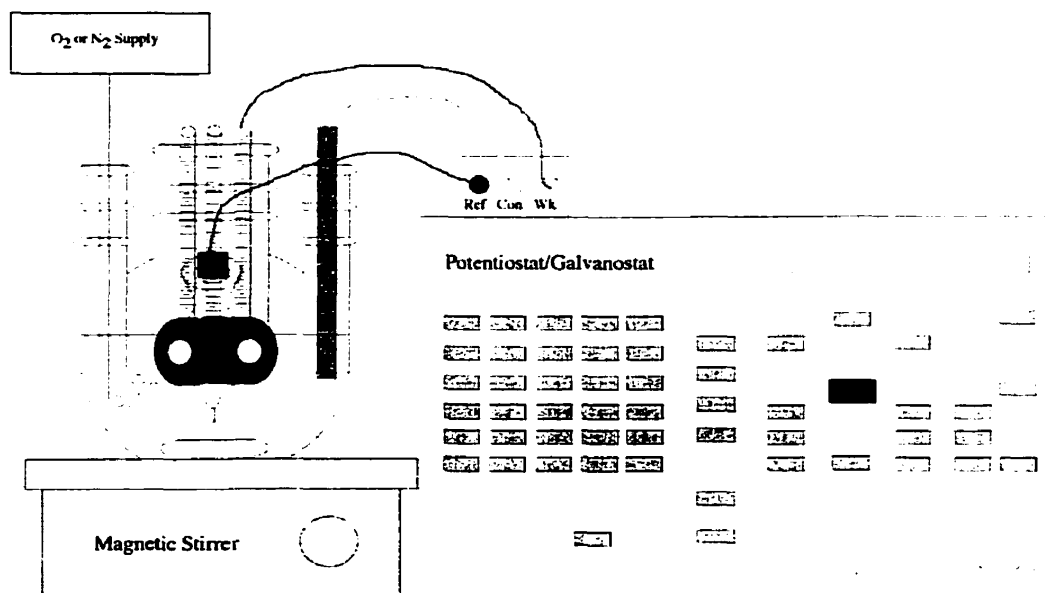


Figure 4.1 Schematic Representation of Experimental Set-up for Corrosion Studies

Samples were allowed to stabilize in their respective solutions for one (1) week prior to the first full polarization measurement. Using a scan rate of 1 mV/sec, the full polarization started from the free potential of the sample, increased to +500 mV SCE (just below the potential of oxygen evolution), decreased to -1000 mV SCE (just above the potential of hydrogen evolution), and finally returned to the free potential. Plots of applied potential vs. resulting current density on a semi-logarithmic scale were generated and from these it was determined if the samples were in the active or passive state. Chloride additions, in the form of laboratory grade sodium chloride (NaCl), of 1 %  $\text{Cl}^-$  by weight of the pore solution were made weekly to a total of 8 % and the above measurement process was repeated one week after each  $\text{Cl}^-$  addition. Weekly pH measurements were also made during this period using a pH meter. After all testing was completed, aliquots of pore solution from the Control, CN1 and CN2 cells<sup>1</sup> were sent for analysis at the Solutions Analytical Laboratory, Department of

<sup>1</sup> Aliquots from the  $\text{Ca}(\text{NO}_3)_2$  cell were not sent for analysis due to equipment problems experienced at the lab at the time.

Earth Sciences, University of Waterloo. All aliquots sent for analysis were filtered through a 0.45-micron filter to remove solids, which could alter original concentrations if allowed to dissolve upon dilution of the original volume.

#### 4.3.2 Passive Film Analysis

In-situ examination of the passive films formed in synthetic concrete pore solutions, similar in composition to that used in Section 4.1.4, with and without inhibitor additions and with and without salt additions, was performed using Raman spectroscopy. This technique has been successfully used to identify surface films formed on iron and steel alloys (Odziemkowski 1994). The experiment involved construction of a miniature corrosion cell (Figure 4.2), containing junctions to insert a graphite reference electrode, a stainless steel counter electrode, a working electrode, and a metallographically polished cross-section of No. 10 reinforcing steel mounted in bakelite.

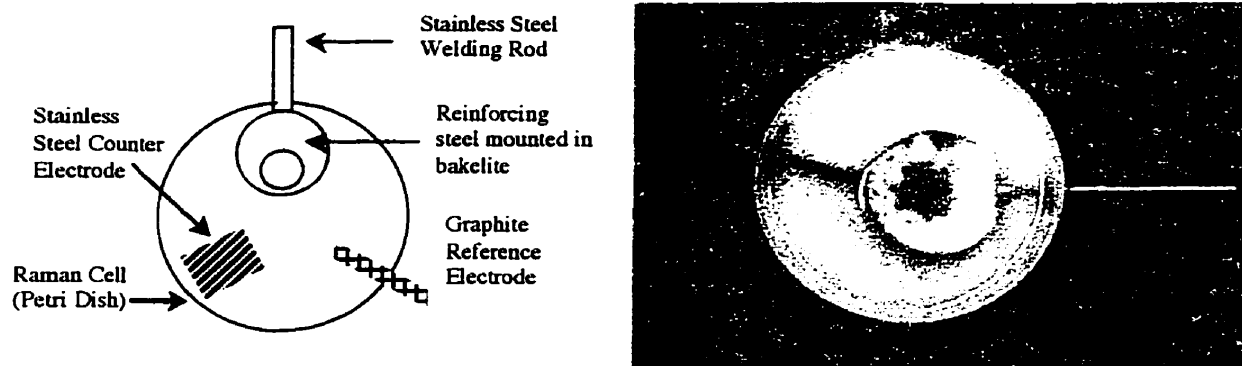


Figure 4.2 Plan view and photograph of in-situ Raman cell (60 mm diameter and 15 mm deep)

Each Raman cell was filled with one of six solutions: Control, CN1-, or CN2-containing synthetic pore solution without chlorides, or Control, CN1-, or CN2-containing synthetic pore solution with 15 %  $\text{Cl}^-$  to ensure corrosion of the sample. However, no results were obtained for the CN2 cell due to masking of peaks by the organic component in CN2.

Reinforcing steel bars in cells without chloride additions were allowed to passivate for approximately one year prior to examination to develop a sufficiently thick passive film to allow it to be identified by Raman spectroscopy, and were examined without external polarization. Samples immersed in cells with chlorides were allowed to passivate for approximately one week prior to examination, to correspond to corrosion experiments. As corrosion still had not initiated, samples required anodic polarization to potentials of +400 mV for 300 seconds was applied to induce corrosion product formation.

Raman spectra were obtained using a Renishaw 1000 microscope with a image sensor CCD camera (400 x 600 pixels) using a 30mW HeNe (632.8 nm) laser. The unit was also equipped with a motorized XYZ stage.

#### **4.4 Cement Paste Cylinder Testing**

Three cylinders from each cement paste mix described in Section 4.2.1 were exposed to a 2 % Cl<sup>-</sup> solution to provide ingress of chlorides from an external source. The ponding wells were clear, plexi-glass piping, approximately 76 mm in height and having an inside diameter of 39 mm. The wells were attached to the cylinder surfaces with 3M Five-Minute Epoxy. Rubber bands were used to secure the wells to the cylinder to facilitate better bonding between the well and the cylinder surface. The epoxy was allowed to cure for approximately twenty-four hours prior to filling the wells with salt solution. Prior to filling with ponding solution, the potential for evaporation was minimized by wrapping each cylinder in plastic wrap and masking tape. Ponding wells were refilled with more salt solution when deemed necessary by an absence of solution in the ponding well. Although not frequently, leaking of the ponding well occurred, requiring resealing of the well to the surface of the cylinder.

Approximately 40 mL of salt solution were added at the beginning of testing and at each subsequent refilling. Table 4.5 lists the ages of these cylinders at the time of first exposure to ponding solution and the duration of the ponding period.

Table 4.5 Age at initial ponding solution exposure and duration of ponding for White and OPC paste cylinders

		Age at initial exposure (days)	Duration of ponding (days)
<b>White Cement</b>	<b>Control</b>	279	412
	<b>CN1</b>	276	412
	<b>CN2</b>	275	412
	<b>Ca(NO<sub>3</sub>)<sub>2</sub></b>	275	412
<b>OPC</b>	<b>Control</b>	279	385
	<b>CN1</b>	137	390
	<b>CN2</b>	137	390
	<b>Ca(NO<sub>3</sub>)<sub>2</sub></b>	136	390

Tests involving cement paste cylinders, unponded and ponded, comprise the majority of the testing for this investigation. Figure 4.3 shows a schematic diagram of the test procedures performed on the cylinders. These include:

- i. phase identification using differential thermal analysis (DTA) and thermogravimetric analysis (TGA);
- ii. pore size distribution using mercury intrusion porosimetry (MIP);
- iii. chloride profiling using potentiometric titration with silver nitrate (AgNO<sub>3</sub>);
- iv. pore solution expression with subsequent chemical analysis using facilities at the Solutions Analytical Laboratory, Department of Earth Sciences, University of Waterloo.

#### 4.4.1 Thermal Analysis

Unponded cement paste cylindrical specimens were removed from the humidity room, while the ponding well was emptied and removed from ponded specimens, immediately prior to the thermal analysis procedure. Each specimen was cut with a diamond saw using Isopar<sup>2</sup>

<sup>2</sup> Isopar, an oil-based lubricant, was used during cutting of specimens instead of water to prevent leaching of cement phases during the sectioning procedure.



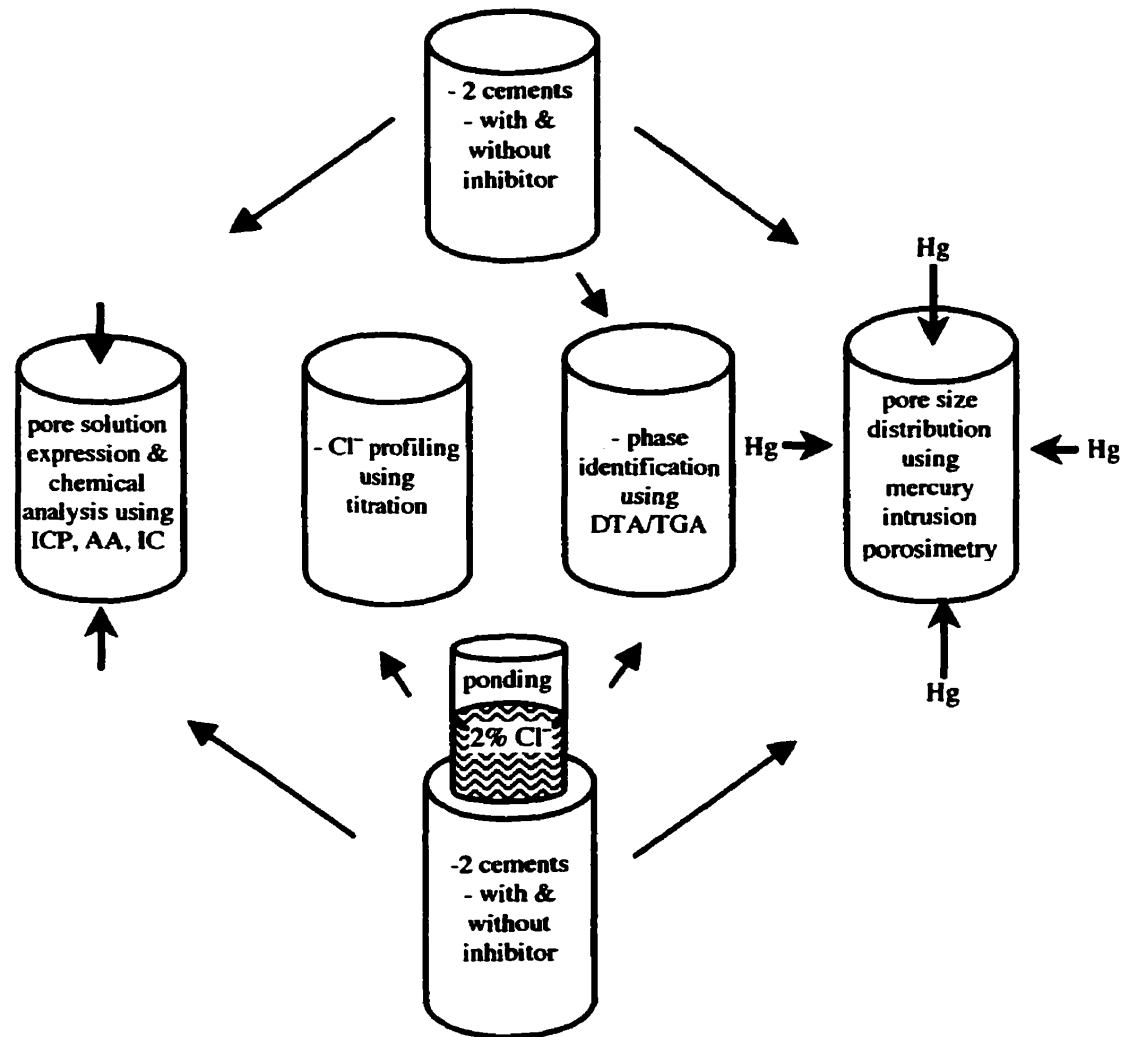


Figure 4.3 Representation of procedures performed on unponded and ponded cement paste cylinders.

lubricant, and samples for thermal analysis and porosity measurements were sectioned as illustrated in Figure 4.4, at a depth of 45 mm for unponded cylinders and 25 mm for ponded cylinders, which was selected based on chloride profiles. Since the unponded cylinders were not exposed to any external agents prior to analysis, uniform chemistry was assumed through the sample. The depth of sectioning for the ponded cylinders was based on results from chloride titration experiments. Table 4.6 lists the ages of the unponded and ponded cement paste cylinders at the time of analysis. All samples for thermal analysis were immediately

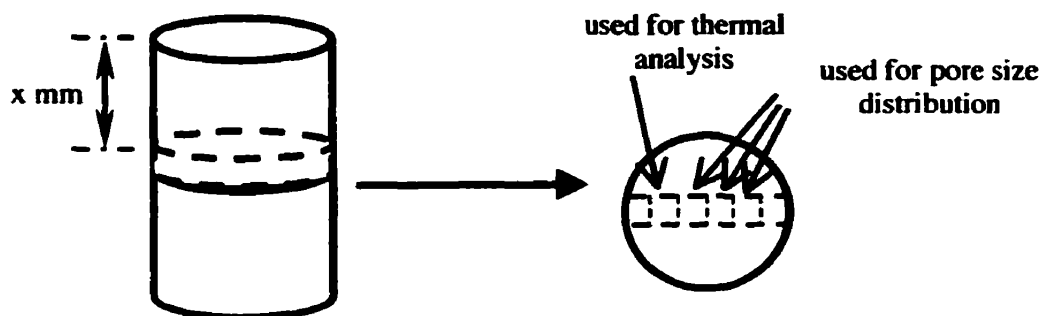


Figure 4.4 Schematic drawing of cement paste cylinder sectioning for thermal analysis and porosity measurements where  $x=45$  mm for unponded cylinders and  $x=25$  mm for ponded cylinders

Table 4.6 Cylinder ages at time of thermal analysis and porosity measurements

	White Cement		OPC	
	unponded	ponded*	unponded	ponded*
<b>Control Samples</b>	347 days	691 days	316 days	664 days
<b>CN1 Samples</b>	360 days	688 days	189 days	527 days
<b>CN2 Samples</b>	360 days	687 days	190 days	527 days
<b>Ca(NO<sub>3</sub>)<sub>2</sub> Samples</b>	371 days	687 days	209 days	526 days

\*age is a total of age at time of initial ponding solution exposure and duration of ponding

crushed to a fine powder with a mortar and pestle, and transferred to a vial for transport to the thermal analysis equipment.

Differential thermal and thermogravimetric analyses were simultaneously performed using a TA Instruments SDT 2960. All procedures were performed in a helium atmosphere at a flow rate of 120 cm<sup>3</sup>/min. Crushed sample sizes ranged from 10 to 20 mg and were placed in a platinum crucible. The temperature was increased and equilibrated at 40°C prior to commencement of the experiment, which involved heating the crushed sample to approximately 1100°C at a constant rate of 10°C/min.

During the experiment, the mass of the sample, the furnace temperature and the difference in temperature between the sample and the reference were automatically accumulated at a rate of one reading every 0.1 seconds. Analysis of the data for DTG (derivative

thermogravimetry) was performed using analytical software incorporated into the apparatus. In some instances, where anomalies occurred in the data, peak areas were determined through integration of the peak using data spreadsheet software.

#### **4.4.2 Pore Size Distribution**

Sectioning of the cement paste cylinders in preparation for mercury intrusion porosimetry is detailed in Section 4.4.1. Samples had a volume of approximately 1000 mm<sup>3</sup> and were subjected to solvent exchange by isopropyl alcohol, a procedure that exchanges alcohol for water within the pore structure of the sample. Marsh et al. (Marsh 1985) concluded that solvent replacement methods are considered less harmful than oven drying for the removal of this pore water. Measuring the mass of the samples on a daily basis monitored the degree of solvent exchange. This was continued until no significant change in mass was observed. Samples were then placed in a vacuum dessicator to remove the isopropyl alcohol and any remaining water.

A Micromeritics Pore Sizer 9310, capable of a maximum pressure of 200 MPa, was used to measure pore size distribution. Prior to measurement, samples were weighed, placed in a penetrometer, reweighed and placed into the porosimeter chamber. When the internal chamber pressure was reduced to 0.0004 MPa, the penetrometer was filled with mercury and the sample incrementally pressurized at steps of approximately 0.0075 MPa and the intruded volume of mercury was measured at each increment in pressure. At 0.15 MPa, the pressure was reduced to atmospheric pressure ( $\approx$  0.101 MPa), and the entire penetrometer assembly was reweighed. The full penetrometer was then placed in the high-pressure compartment of the apparatus, where the pressure was incrementally increased to 200 MPa, with recordings

of intruded volume of mercury made for each pressure increase. Corrected pressure and incremental intrusion volumes were used to determine pore size distributions using the Washburn equation (Section 2.4.4, pg. 30). Samples were discarded after each test due to mercury contamination.

The following assumptions were made based on the work of previous researchers (Monkman 1999):

- i. mercury/cement paste contact angle =  $130^\circ$ ;
- ii. mercury surface tension = 485 dynes/cm;
- iii. mercury density per individual sample was based on the room temperature at the time of testing and the known temperature-density relationship for mercury.

#### **4.4.3 Chloride Profiling**

Chloride profiling was performed on cement paste cylinders subjected to ponding with a 2%  $\text{Cl}^-$  solution (as NaCl), as depicted in Figure 4.3. After a suitable time elapsed for chlorides to penetrate through the cement paste, ponding wells were removed from the samples.

Samples were subsequently sectioned, as shown in Figure 4.5. The cylinder was first divided in half crosswise. The top portion was then divided in half along the diameter of the cylinder, where one half of the cylinder was used for the preparation of samples for thermal analysis and porosity measurements, as discussed in Sections 4.4.1 and 4.4.2, respectively.

The other half was sectioned again along the same axis. If cylinders were not sectioned immediately, specimens were wrapped in parafilm, sealed in a plastic bag, and placed in a refrigerator to minimise further chloride diffusion until sectioning could be completed. The quarter section was further divided into wedges approximately 7 mm thick. The remaining portion of each cylinder was also wrapped in parafilm, sealed in a plastic bag, and placed in a refrigerator to minimize further diffusion of chlorides through the sample.

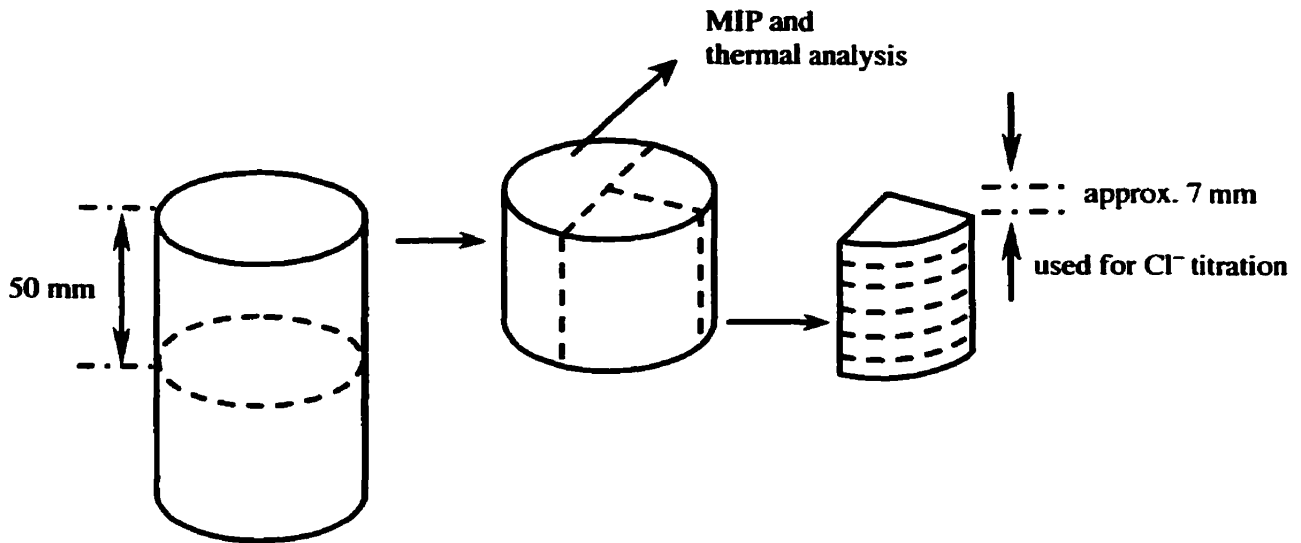


Figure 4.5 Schematic drawing of sectioning of ponding sample for  $\text{Cl}^-$  titration

The following procedure for determination of acid-soluble chlorides using potentiometric titration, which measures both free and chemically bound chlorides in the cement paste, is a modification of ASTM Standard C114 (ASTM 1997). After sectioning of the cylinder, the following steps were performed:

- 1) dry each section for 24 hours at  $105^\circ\text{C}$  to remove evaporable water;
- 2) grind each section with a mortar and pestle until powder passes through  $250\ \mu\text{m}$  sieve. Prior to grinding of each section, mortar, pestle and sieve were rinsed with 1:10 dilute nitric acid (by volume), followed by tap water, distilled water and anhydrous isopropan-2-ol alcohol;
- 3) weigh each powder to the nearest tenth of a milligram, then transfer to separate 250 mL beakers and add 120 ml dilute nitric acid;
- 4) thoroughly disperse samples with a glass stirring rod;
- 5) cover beakers with watchglasses and heat on a hotplate until a soft boil is reached, then boil for 5 minutes to release chlorides;
- 6) after boiling, remove beakers from hotplates and filter slurries through WHATMAN No. 541 filter paper into 400 mL beakers. Beakers and stirring rods were rinsed using hot distilled water at least three (3) times into the filter until all residue was removed;
- 7) wash the filtrates in the filter paper at least six (6) times with hot distilled water to remove all chlorides from solids. The filter paper was then removed from the funnel and its exterior and the funnel were rinsed three (3) times into the beaker to further remove any remaining chlorides;
- 8) if necessary, distilled water was added to the solutions to increase its volume to 250 mL. Filtrates were cooled to approximately  $23^\circ\text{C}$ ;
- 9) 50 mL of solution was titrated against  $0.05\ \text{AgNO}_3$  using a Radiometer Copenhagen TIM800 Titration Manager with ABU901 Autoburette. The automatic titrator slowly added

increments of AgNO<sub>3</sub> to determine the equivalence point of the chloride solutions. The equivalence point corresponds to the maximum change in millivolt readings occurring when the chloride solution is neutralized to a pH of about 7. In order to improve the precision of the chloride measurements, a 4 mL sample of 0.025 M NaCl solution was added to each solution. Two (2) drops of methyl orange were added to the beakers. If the indicator reveals that the solutions are not below pH 3.2, a few drops of concentrated nitric acid were added; 10) the remaining 200 mL of solution was reserved for possible future analysis.

The concentration of chlorides within the solutions was then determined using the following equations:

$$V_{sample} = V_{inf} - \frac{V_s * [salt\ solution]}{[Titrant]} \quad \& \quad [Cl^-] = \frac{V_{sample} * [Titrant]}{V_q} \quad (4-1)$$

where  $V_{sample}$  = volume of titrant added for the sample (mL)  
 $V_{inf}$  = total volume of titrant added until inflection (mL)  
 $V_s$  = volume of salt standard added (mL)  
 $[salt\ solution]$  = mean salt standard concentration (mol/L)  
 $[Titrant]$  = mean molarity of AgNO<sub>3</sub> titrant (mol/L)  
 $[Cl^-]$  = concentration of chlorides in the sample (mol/L)  
 $V_q$  = original volume of the sample (mL)

#### 4.4.4 Pore Solution Expression

This technique is based on the work Barneyback and Diamond (Barneyback 1981) in which hardened cement paste cylinders are subjected to high pressure to extract pore solution located within the porous network of the concrete. The expressed pore solution is subsequently chemically analysed for a variety of constituents. The device used in the current work, shown in Figure 4.6, is similar to that used by the aforementioned authors with some slight modifications:

- i. no support cylinder was used. The platen was placed directly onto the compression base;
- ii. the piston assembly consisted of only a piston shaft;
- iii. a rubber o-ring was fitted into a groove on the platen to prevent pore solution from leaking out;
- iv. the tolerance between the bore of the inner cylinder and the piston was approximately 0.05 mm;
- v. molybdenum disulfide (MoS<sub>2</sub>) was used as a lubricant between the bore and the piston;
- vi. a Teflon<sup>®</sup> disk and nylon disk were placed between the sample and the piston to minimize pore solution escaping through the top of the apparatus.

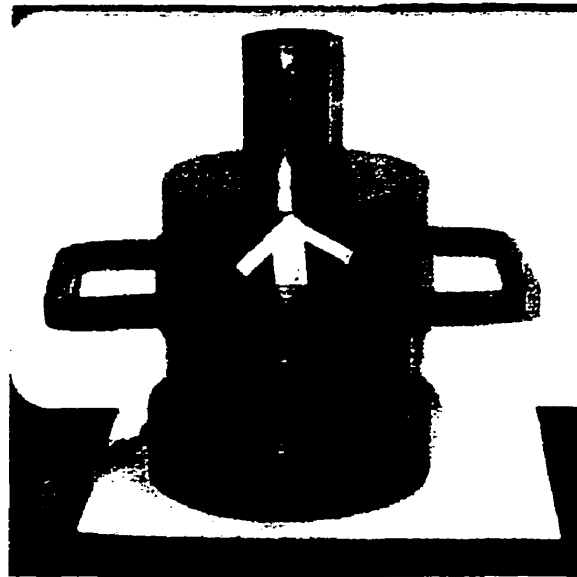


Figure 4.6 Pore solution expression apparatus

Prior to the expression of any sample, the unit was thoroughly washed with isopropyl alcohol and distilled water, then rinsed with isopropyl alcohol and dried with compressed air. The bore and the piston were lubricated with  $\text{MoS}_2$  prior to insertion of the Teflon and nylon disks and the sample. The sample remained in either its mould or under ponding conditions until ready for expression. Once assembled, a gradually increasing load was applied to the piston using a Forney Concrete Compression Tester. A total load of 1000 kN was applied to each cylinder, which corresponds to 493 MPa. Once loads of 300, 600, 900 and 1000 kN (148, 296, 444 and 493 MPa) were reached, the load was held for five (5) minutes to allow pore solution to flow into the collection syringe attached to the expression device.

Immediately after collection, the expressed pore solution was filtered through a  $0.25 \mu\text{m}$  filter to remove any solids which may dissolve in the solution, thus altering the original chemistry, weighed and diluted with distilled water. The sample was then divided in half, one aliquot having no further treatment and the other acidified with a small addition (50 or  $100 \mu\text{L}$ ) of nitric acid ( $\text{HNO}_3$ ), dependent on the volume of solution expressed. Samples

were then refrigerated until transferred to the Solutions Analytical Laboratories, located within the Department of Earth Sciences, University of Waterloo. Inductively coupled plasma (ICP), ion chromatography (IC) were used to determine the concentrations of various anions and cations while titration was used to determine the alkalinity or buffering capacity of the expressed pore solutions.



## **Chapter 5**

### **Synthetic Pore Solution Tests Results and Discussion**

#### **5.1 Corrosion Testing**

Figure 5.1 shows the pH measurements taken at each chloride level for the four solutions tested. It can be seen that upon initial addition of both calcium nitrite based inhibitors and the laboratory grade calcium nitrate, the pH decreased relative to the Control solution. This decrease in pH continued with further chloride additions. More dramatic decreases in magnitude were observed in previous studies (Mammoliti 1995), this difference in behaviour could be attributed to the pH electrodes in the tests, as their accuracy may have diminished due to over-exposure to highly alkaline solutions. Additionally, high pH (i.e pH > 11) calibration solutions were not available at the time of measurement.

Figures 5.2 through 5.5 show the free potentials of the steel samples immersed in synthetic pore solutions containing no inhibitor, CN1, CN2 or  $\text{Ca}(\text{NO}_3)_2$ , respectively, as a function of the  $\text{Cl}^-$  content of the solution. For comparative purposes, all plots have used the same range for both axes. For samples immersed in the Control solution and the two nitrite-based solutions, the free potentials become more electronegative as the chloride concentration increases. Free potentials remained virtually unchanged for samples immersed in the  $\text{NO}_3$  solution. ASTM Standard C 876-91 (ASTM 1991) states that the probability of corrosion increases as free potential becomes more negative. Table 5.1 classifies the probability of corrosion based on potential measurements in concrete according to ASTM C876-91. Based on comparison of the free potentials measured in solution and guidelines in Table 5.1, there is a 90% probability that corrosion is occurring

in the  $\text{Ca}(\text{NO}_3)_2$  solution without any added chlorides, and the state of the samples in the Control and CN2 solutions is “uncertain”. However, this was not found to be the case in these experiments; as shown in Figure 5.7, samples immersed in CN1 displayed localized corrosion activity in 8 %  $\text{Cl}^-$  solutions, whereas the samples in Control solution did not, although they solution had more noble potentials than those of Control samples. On the other hand, CN1 immersed samples should not be displaying pitting behaviour at 7%  $\text{Cl}^-$ , but corroding are nonetheless.

Table 5.1 Probability of corrosion based on free potential measurement (ASTM 1991)

Probability of Corrosion	Potential Range (mV)	
	Cu/CuSO <sub>4</sub> Reference Electrode	Saturated Calomel Reference Electrode
10 %	more “+” -200 mV	more “+” -140 mV
uncertain	-200 mV to -350 mV	-140 mV to -290 mV
90 %	more “-” -350 mV	more “-” - 290 mV

Figures 5.6 through 5.9 show representative full cyclic polarization curves of samples immersed in each of the four solutions, at chloride levels of 0 %, 6 % and 8 %. Complete cyclic polarization curves can be found in Appendix A; excellent reproducibility was achieved in the E vs. log I curves for the three samples in each of the four solutions prior to chloride additions, but there is increasing variability with increasing chloride concentration. Chloride levels of 6 % and 8 % in pore solution are equivalent to approximately 1.3 % and 1.8 %  $\text{Cl}^-$  by weight of cement<sup>1</sup>. It can be seen that, in all solutions, the curves shift to the right as the chloride concentration increases, indicative of an increase in corrosion activity. None of the samples immersed in the Control solution indicate, as mentioned below, pitting or crevice corrosion according to the

<sup>1</sup> This is based on three assumptions: (1) 100 g of cement requires 23 g of water for 100 % hydration; (2) the remaining water occupies the pore network; (3) no chlorides are contained in the hydration products, and (4) a water:cement =0.45.

**curves generated through full cyclic polarization.**

**Localized corrosion is indicated on an E/log I curve by a sharp increase in current density with increasing potential, which continues to increase even as the applied potential is reduced on the downsweep. Localized corrosion occurred on samples exposed to solutions containing calcium nitrite, where all samples in the CN1 solution showed localized corrosion in 8 % Cl<sup>-</sup> solution while, in the CN2 solution, one sample showed localized corrosion in 7 % Cl<sup>-</sup> solution, subsequently repassivating at 8 % Cl<sup>-</sup>, and another sample displayed similar behaviour at 8 % Cl<sup>-</sup>. One sample immersed in NO<sub>3</sub> solution showed localized corrosion at 6 % Cl<sup>-</sup>, repassivating at 7 % Cl<sup>-</sup>.**

**Figure 5.10 compares the cyclic polarization curves of representative samples at 8 % Cl<sup>-</sup>. In the cases of samples in CN1 and Ca(NO<sub>3</sub>)<sub>2</sub> solutions, despite having lower overall current density values compared with that of samples in the Control solution, localized corrosion has occurred. It must be remembered that current density values are calculated over the entire surface of the sample, when in actuality corrosion is occurring in a very small area. Therefore, actual current density values in the locally corroding areas of samples displaying localized corrosion are significantly higher than those indicated by the plot. This is also true of current density values calculated using linear polarization resistance measurements, which are shown in Figure 5.11. These values are averaged over the surface area of the sample and the average of three samples. It would thus appear that the presence of calcium nitrite, and to a lesser degree calcium nitrate, encourages localized forms of corrosion in synthetic concrete pore solutions under these testing conditions.**

It should be noted that some corrosion products were visually observed on the majority of the sample surfaces at a chloride level of 7 %, including one in Control solution. This is most likely indicative of the fact that although some corrosion was occurring, the average corrosion current generated was not large enough in magnitude for the equipment to detect. In future investigations, it is suggested that electrochemical noise is utilized at higher chloride levels because it is capable of detecting very early stage corrosion in the form of brief pitting with subsequent repassivation by measuring the “brief bursts of charge” associated with the removal of atoms from the metal surface (Cottis 1996).

Table 5.2 displays the composition of the filtered pore solutions containing 8 % Cl<sup>-</sup> while Table 5.3 compares these values with theoretical values calculated from the known amounts of each species added. Full calculations for Table 5.3 can be found in Appendix B.

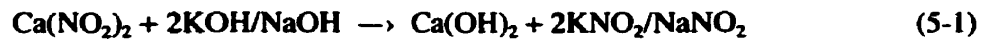
Table 5.2 Chemical analysis of filtered synthetic pore solutions containing 8 % Cl<sup>-</sup> as NaCl

Analysis	NO <sub>2</sub> <sup>-</sup>	NO <sub>3</sub> <sup>-</sup>	Cl <sup>-</sup>	Ca <sup>2+</sup>	Na <sup>+</sup>	K <sup>+</sup>	Fe*	Alkalinity
Method	IC <sup>‡</sup>	IC <sup>‡</sup>	IC <sup>‡</sup>	AA <sup>†</sup>	AA <sup>†</sup>	AA <sup>†</sup>	AA <sup>†</sup>	Titration
Det. Limit	0.05	0.05	0.05	0.05	0.02	0.02	0.05	7
Units	mg/L	mg/L	mg/L	mg/L	mg/L	mg/L	mg/L	mg/L
Control	<5	<5	80200	10.7	43600	16200	2.84	80200
CN1	23600	2230	76100	101	43500	15200	2.92	76100
CN2	23300	2720	78300	124	45800	15600	3.03	78300
* Refers to Fe <sup>2+</sup> and Fe <sup>3+</sup>								
‡ IC = Ion Chromatography								
† AA = Atomic Absorption Spectroscopy								

Table 5.3 Calculated and experimental results from Water Quality Tests (units = mg/L)

	Control Cell			CN1 Cell			CN2 Cell		
	Cal.	Exp.	%	Cal.	Exp.	%	Cal.	Exp.	%
Cl <sup>-</sup>	80012	80200	100	82171	76100	92.6	82161	78300	95.3
Ca <sup>2+</sup>	6761	10.7	0.16	16903	101	0.60	16901	124	0.73
Na <sup>+</sup>	58788	43600	74.2	59557	43500	73.0	59550	45800	76.9
K <sup>+</sup>	23549	16200	68.8	21326	15200	71.3	21324	15600	73.2
NO <sub>2</sub> <sup>-</sup>	n.a	< 5	n.a	24698	23600	95.6	24630	23300	94.6

From examination of both of these tables, several things are of particular interest. First to note is the small reduction in alkalinity of solutions containing calcium nitrite. Alkalinity is a measure of the resistance of a solution to a decrease in pH as a result of acid addition. These results confirm those observed during the course of experimentation and displayed in Figure 5.1. The initially observed pH decrease is likely a result of the precipitation of calcium hydroxide or calcium hydroxy-nitrite (Ca-OH-NO<sub>2</sub>) due to an ion exchange between the calcium supplied by the calcium nitrite and the hydroxide ions already existing in the pore solution. This is further supported by the discrepancy between the added and measured concentrations of nitrite in the CN1 and CN2 solutions. These ion exchanges can be represented by the following chemical equations:



Comparison of the standard Gibb's energy of formation for calcium, potassium and sodium hydroxides indicates that calcium hydroxide is the most stable of the three hydroxides in solid form. Additionally, due to the low solubility of calcium hydroxide, precipitation of this species would likely occur. Comparison of the standard Gibb's energy of formation of calcium, potassium and sodium nitrites are similar to those of the hydroxides, with calcium nitrite having the greatest stability in solid form and also having the lowest solubility, again suggesting that precipitation would occur. Values for the standard Gibb's energies of formation and solubilities are given in Table 5.4 (CRC 1994, Karapet'iants, 1970). A reduction in pH can lead to instability of the passive layer formed on the metal surface, and in the case of concrete, can decrease the stability of the products formed as a result of cement hydration.

**Table 5.4 Standard Gibb's energy of formation and solubility values for select hydroxides and nitrites (CRC 1994, Karapet'iants, 1970)**

	$\Delta G^{\circ}_f$ (kJ/mol)	Solubility (g/100 cc cold water)
<b>Ca(OH)<sub>2</sub></b>	-897.5	0.185
<b>KOH</b>	-379.1	107
<b>NaOH</b>	-379.5	42
<b>Ca(NO<sub>2</sub>)<sub>2</sub></b>	-617.6	45.9
<b>KNO<sub>2</sub></b>	-306.6	281
<b>NaNO<sub>2</sub></b>	-284.6	81.5

Secondly is the significant difference in calcium concentrations between the theoretical and experimentally determined values. Theoretical values are based on the assumption that there is 100 % dissociation of all calcium-based compounds in the solution. In the case of the calcium hydroxide, it is known that this will not occur due to the low solubility of Ca(OH)<sub>2</sub>. This may be explained by the fact that the solutions analyzed were filtered and as a result, values presented would not take into consideration any calcium that may have precipitated out of solution, forming a solid product. The same argument can be made for the discrepancies between the theoretical and experimental values for potassium and sodium.

Finally the results for chloride must be addressed. There appears to be a slightly lower concentration of chlorides in solutions containing calcium nitrite, despite the fact that the same mass of chlorides by weight of the total solution was added. There is also a discrepancy between the theoretical and experimental values for solutions containing calcium nitrite. This again may be due to chlorides precipitating out of the solution, which were not considered in the calculations. The fact that it only seems to occur in solutions containing calcium nitrite supports the hypothesis that calcium nitrite encourages the formation of a solid compound containing chlorides, thereby decreasing

the amount of free chloride available to destroy the passive film. Interesting to note is that precipitation of chloride species is occurring despite the lack of chloride-binding species typically found in cement-based materials, namely calcium aluminates. This suggests that another chloride form is precipitating from the solution. Table 5.5 lists the stability and solubility values of the possible chlorides that can precipitate based on the known composition of the pore solutions. Although calcium chloride is the most stable in solid form, it is also the least soluble of all the chlorides listed. It is therefore possible that sodium and potassium forms of chloride are precipitating from solution, which is supported by the experimental concentrations of the solutions.

Table 5.5 Standard Gibb's energy of formation and solubility values for selected salts (CRC 1994)

	$\Delta G^{\circ}_f$ (kJ/mol)	Solubility (g/100 cc cold water)
<b>CaCl<sub>2</sub></b>	-748.8	74.5
<b>KCl</b>	-408.5	34.4
<b>NaCl</b>	-384.1	35.7

Samples of the white precipitates formed in each of the cells were removed, dried and analyzed using energy dispersive spectroscopy (EDS) on the environmental scanning electron microscope (ESEM). Table 5.6 lists the results of this analysis while Figures 5.12 through 5.14 show the actual dried deposits. Both precipitates from the solutions containing Ca(NO<sub>2</sub>)<sub>2</sub> have a more needle-like structures than the precipitate from the Control solution. For simplicity, these structures in all solutions are designated as "spherulites". Also within each precipitate are three distinct particles of different shapes, dependent on which if any inhibitor was present in the solution. These particles are referred to as "particle" for the Control precipitate, "tuber" for the CN1 precipitate, and "group" for the CN2 precipitate. "Bulk" refers to the precipitate as a whole.

**Table 5.6 EDS Results of Dried Pore Solutions**

		<b>Oxygen (atomic %)</b>	<b>Chlorine (atomic %)</b>	<b>Potassium (atomic %)</b>	<b>Calcium (atomic %)</b>
<b>Control</b>	<b>Bulk</b>	36.5	2.8	1.3	59.4
	<b>Particle</b>	26.9	3.4	1.2	68.5
	<b>Spherulite</b>	36.2	3.0	1.4	59.4
<b>CN1</b>	<b>Bulk</b>	34.8	8.1	1.0	56.2
	<b>Tuber</b>	21.4	27.7	4.7	46.3
	<b>Spherulite</b>	36.8	2.1	0.6	60.5
<b>CN2</b>	<b>Bulk</b>	38.5	0.2	0.7	60.6
	<b>Group</b>	47.8	0.3	0.5	51.5
	<b>Spherulite</b>	41.0	0.3	0.4	58.3

Of particular interest is the significantly higher chloride percentage in the CN1 precipitate, both bulk and tuber analysis, as compared to those of the other samples. This would tend to support the postulate that calcium nitrite, at least in the case of CN1, increases the amount of chlorides that precipitate out of solution. Two likely precipitates containing chlorides that could form within the pore solution system are  $\text{CaCl}_2$  and calcium hydroxychloride ( $\text{Ca-OH-Cl}$ ) (Ramachandran 1971). Surprisingly, the same cannot be said of the CN2, despite containing the same inhibiting ingredient. This may be a result of the organic agent, believed to be “sugar”, that is added to CN2 to reduce the well known accelerating effect of calcium nitrite.

A white crusty deposit, shown in Figure 5.15, was also observed on one of the spouts of the corrosion cells containing calcium nitrite. Chemical analysis using EDS on the ESEM, gave the following chemical composition:

O: 68.8 Atomic %    Cl: Atomic 2.0 %  
 K: 27.6 Atomic %    Ca: Atomic 1.8 %

This analysis, combined with the proposed reaction between calcium nitrite and the pore solution, suggests that the precipitate is likely a combination of potassium and some form of bound chloride involving calcium and oxygen.



## **5.2 Passive Film Analysis**

### **5.2.1 Synthetic Pore Solution without Chlorides**

Figures 5.16 and 5.17 show optical images of the surfaces of rebar samples exposed to Control and CN1 solutions, respectively. Apparent on each sample is a film deposit; however, there is a marked difference between the deposits seen on the two samples. The film on the Control sample is sporadic, covering only some locations on the steel surface. The surface film on the CN1 sample appears as a more cohesive network, covering the majority of the sample surface. Portions of the metal surface are exposed on the Control sample, whereas the film on the CN1 sample covers almost all of the surface. It could, therefore, be concluded that although a physical barrier is formed on the steel surface in both solutions, the CN1 solution produces a film that provides more coverage. Although the film formed on the Control sample is  $\text{Ca}(\text{OH})_2$ , the film on the CN1 sample is more than likely the precipitate formed upon initial addition of CN1 to the synthetic pore solution, possibly  $\text{Ca-OH-NO}_2$ , as discussed in the previous section.

Figures 5.18 and 5.19 show optical images of the steel surfaces in the aforementioned solutions after the film removal, which was accomplished by gently flushing the surface of the sample with each respective pore solution. Both surfaces show some degree of localised corrosion, which is believed to have occurred after immersion in the respective solutions as each surface demonstrates different pitting behaviour. The Control sample surface displays pits of larger diameter than those observed on the CN1 sample surface. Pitting could be due to the partial coverage establishing oxygen concentration cells on the surface.

Despite the long exposure period to synthetic pore solution, the passive film formed on the samples immersed in both the Control and CN1 solutions was not thick enough for extensive analysis using Raman spectroscopy. However, limited areas of the samples did give some information regarding the composition of the passive films formed on samples immersed in these solutions. Figures 5.20 and 5.21 show Raman spectra obtained from the samples immersed in Control and CN1 pore solutions, respectively. Although analysis of the black pits on the Control sample described in the previous paragraph were obtained, information on the pits of the CN1 sample was not possible due to their small size. Peak identification is based on work by Gui and Devine (Gui 1995), Oblonsky and Devine (Oblonsky 1997), and Thierry et al. (Thierry 1991) and spectral analysis on laboratory grade samples of calcium hydroxide and the precipitates in the Control and CN1 solutions (Figure 5.26). Immediately evident is the passive film in all areas of the Control sample is composed mainly of  $\gamma\text{-Fe}_2\text{O}_3$  (maghemite) and  $\text{Fe}_3\text{O}_4$  (magnetite), irrespective of whether the spectrum was obtained from “pitted” or unpitted regions. The CN1 sample displays a variety of iron oxides on the sample surface, namely  $\gamma\text{-Fe}_2\text{O}_3$ ,  $\text{Fe}_3\text{O}_4$ ,  $\alpha\text{-Fe}_2\text{O}_3$  (hæmatite), and  $\gamma\text{-FeOOH}$  (lepidocrocite). Hence, the passive film formed in the Control solution appears more homogeneous than the passive film formed on the sample immersed in CN1 solution. However, these films were not uniform over the surface of either the samples immersed in the Control or CN1 solutions. In general, a high degree of inhomogeneity in the passive film is an indication of limited passive protection, with increased inhomogeneity resulting in increased susceptibility to corrosion. This is due to variations in corrosion potential of the individual iron species, creating potential gradients within the passive film, increasing the likelihood of localized

forms of corrosion. It is also due to lower electronic and ionic resistance of the passive film. Also apparent is that despite attempts at removal and no visual evidence of the surface deposits, Raman spectroscopy indicated some calcium hydroxide and/or precipitate remains on the surfaces of samples immersed in both solutions. This could indicate that these deposits are incorporated in the passive film itself.

Little documentation exists regarding the protective nature of different iron oxides in alkaline environments. It has been proposed by Leek (Leek 1997) that denser products such as  $\text{Fe}_3\text{O}_4$  (magnetite) are more protective than  $\alpha\text{-Fe}_2\text{O}_3$  (hæmatite), by increasing the difficulty of chloride penetration to the steel surface. If valid, this suggests that the passive film formed on the Control sample is more protective. Hansson (Hansson 2000) states the chlorides reduce the ability of the passive film to withstand the very high electric field gradients that are established across the film due to concentration cells. Leek (Leek 1990) also proposes that corrosion only begins when both protective barriers, namely the portlandite and passive layers on the steel surface are broken down. The deposit found on the CN1 immersed sample (Figure 5.17) clearly covers more of the sample surface and appears denser than that formed on the Control surface (Figure 5.16).

### 5.2.2 Synthetic Pore Solution with Chlorides

Each sample immersed in either Control or CN1 solution required anodic polarization to produce appreciable corrosion products for analysis. After polarization, distinctly coloured areas of red, black and “shiny” (i.e. areas with no apparent corrosion) were visible on each sample. Figure 5.22 shows the Raman spectra generated by the areas without pitting for samples immersed in Control and CN1 solutions containing 15%

chlorides. Immediately apparent is that the passive film of the sample immersed in CN1 pore solution is more complex than that of its counterpart in Control pore solution. The corrosion products observed were similar to those in the solutions not containing chlorides. However, present in both corroded samples and not observed in either non-corroded sample, is the iron oxide species termed “green rust”. Green rust is considered to be an intermediate corrosion product, where the initial product is  $\text{Fe}(\text{OH})_2$  and the final products can be  $\gamma\text{-FeOOH}$  (lepidocrocite),  $\alpha\text{-FeOOH}$  (goethite),  $\text{Fe}_3\text{O}_4$  or  $\beta\text{-FeOOH}$  (akagenite) or any combination thereof, all of which contains either  $\text{Cl}^-$  or  $\text{CO}_3^{2-}$ , as indicated below. The composition of green rust is not clearly defined, as it is dependent on the type of anion in the corrosive environment. Given the present system, two types of green rust can form, one incorporating chlorides while the other incorporating carbonate (Genin 1997):



Raman shifts associated with green rust are given as  $420\text{ cm}^{-1}$  and  $505\text{ cm}^{-1}$  (Odziemkowski 1998), although delineation between the chloride and carbonate forms was not specified. The latter peak is clearly evident in the spectra of both sample surfaces in the presence of chlorides. The presence of this species on surfaces where there is no visual evidence of corrosion indicates that the sample surface is in an active state.

Figure 5.23 illustrates the spectra produced for red areas on the sample surfaces immersed in Control and CN1 pore solutions. Little difference is observed between the

corrosion products formed on each sample surface despite the differences in the pore solutions. In addition, it appears that the red corrosion products on the Control sample (Figure 5.23) are identical to those of the CN1 products in the shiny area (Figure 5.22). The presence of green rust indicates that some corrosion has occurred, despite appearances to the contrary.

Figure 5.24 shows the Raman spectra obtained from the black areas of the samples immersed in Control and CN1 pore solutions. It is difficult to compare the two samples because of the high degree of background noise, likely from building vibrations, in the CN1 solution spectrum, possibly masking some of the peaks attributed to other oxides. It is highly unlikely that only green rust is present on the sample in CN2 solution in this area. As the composition of the corrosion products is similar between the black and red areas of the Control immersed sample, it is likely the same can be said of the CN1 immersed sample. Little difference is observed between corrosion products of the red and black areas of the Control immersed sample.

Digital photographs of the state of the samples immersed in the Control and CN1 pore solutions, during and after polarization at +400 mV SCE for 300 seconds are shown in Figure 5.25. Immediately apparent is the production of a rust-coloured “corrosion foam” by the sample immersed in the CN1 solution (Figure 5.25 (b)), which was not observed in Control solution (Figure 5.25 (a)). This behavioural difference is attributed to the differences in the electrolyte composition, which appears to be influencing the corrosion process. Figures 5.25 (c) and (d) show the corrosion morphology of the samples after polarization. Based on the amount of surface area affected by corrosion, the Control

sample appears to have a lower amount of damage, despite the larger pits seen on the sample surface prior to exposure to chlorides, shown in Figure 5.18.

Figure 5.26 shows the Raman spectra generated for laboratory grade  $\text{Ca}(\text{OH})_2$ , and precipitates from the CN1 solution containing 15 % chlorides and the Control solution precipitate prior to chloride addition. The only peak apparent in the Control solution is that associated with calcium hydroxide. Two other peaks at  $272 \text{ cm}^{-1}$  and  $707 \text{ cm}^{-1}$  appear in the CN1 solution containing chlorides. It is possible that these two peaks are representative of  $\text{Ca-OH-Cl}$  and  $\text{Ca-OH-NO}_2$ , however, specific conclusions cannot be made as the precipitate was not examined prior to chloride exposure.

Although it would appear that these results indicate that the CN1 solution with chloride is more detrimental to steel passivity than the Control solution with chlorides, it should be noted that in both solutions the passive film formed in the presence of chlorides and under anodic polarization. Therefore, the composition of the passive film and the dynamics of the corrosion process may vary from those circumstances where the passive film was allowed to develop for a long period of time, then exposed to chlorides.

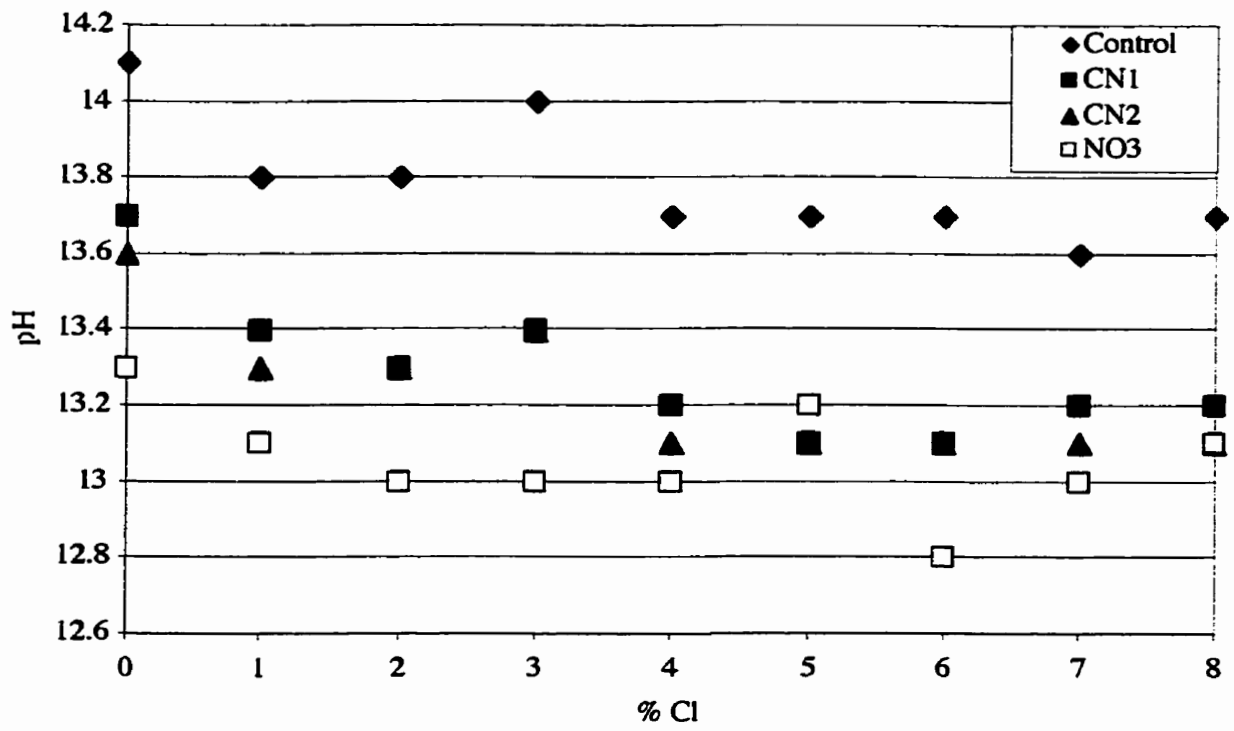


Figure 5.1 pH values of synthetic concrete pore solutions

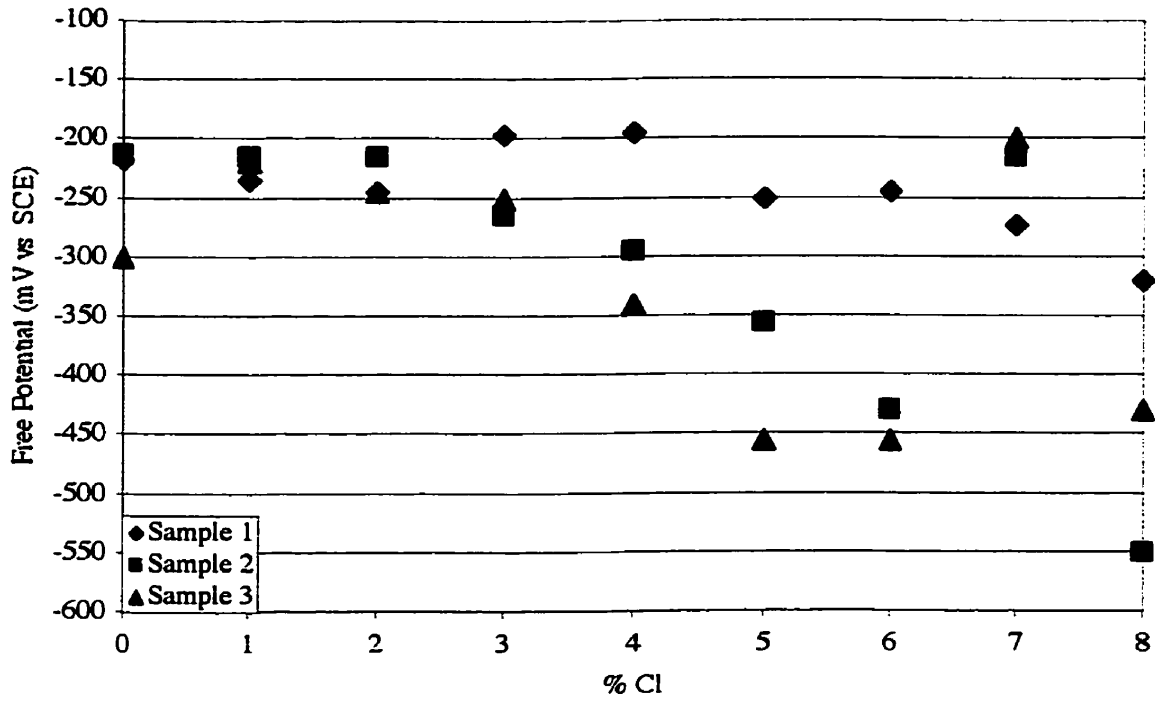


Figure 5.2 Free potentials of samples immersed in Control synthetic pore solution

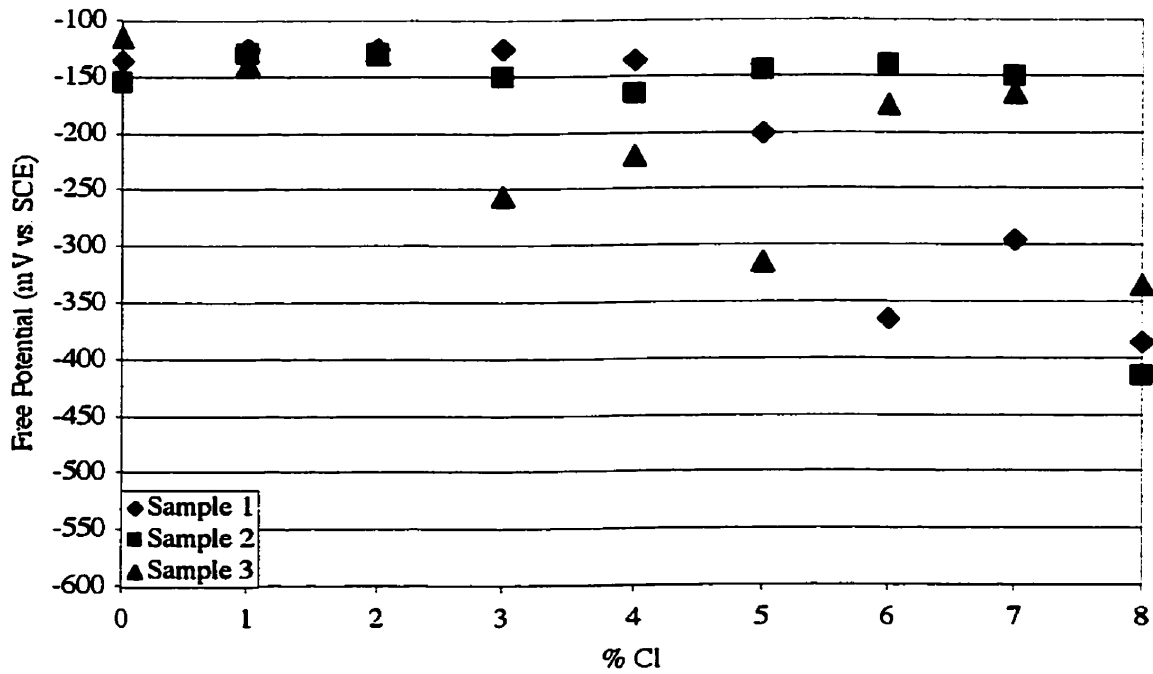


Figure 5.3 Free potentials of samples immersed in CN1-containing synthetic pore solution



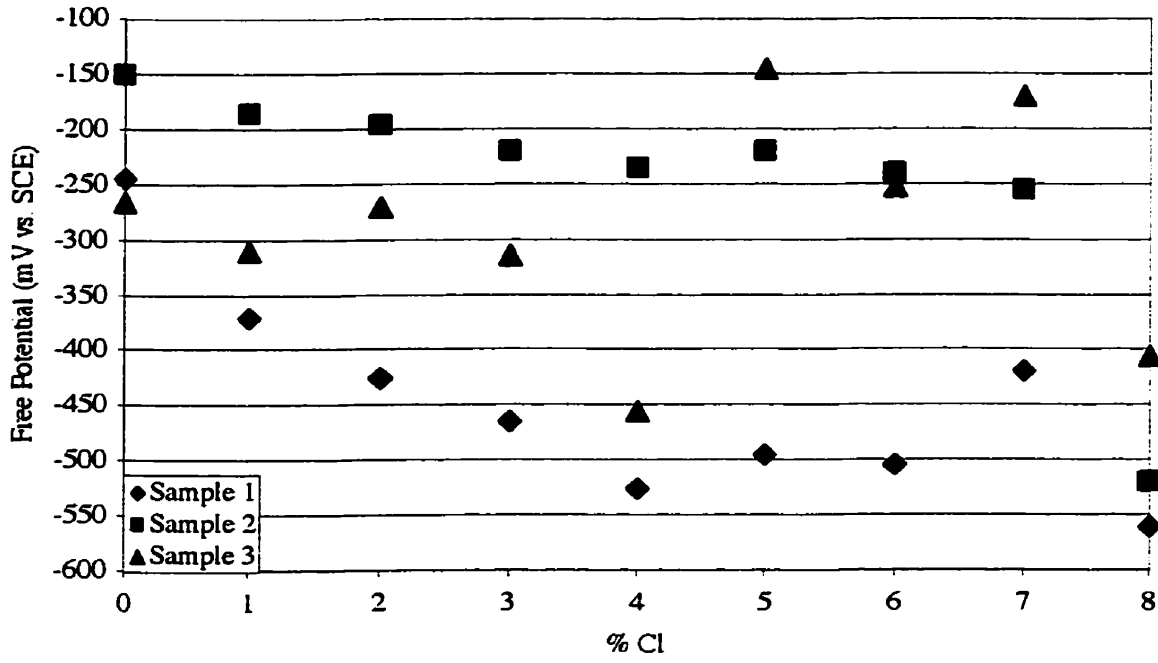


Figure 5.4 Free potentials of samples immersed in CN<sub>2</sub>-containing synthetic pore solution

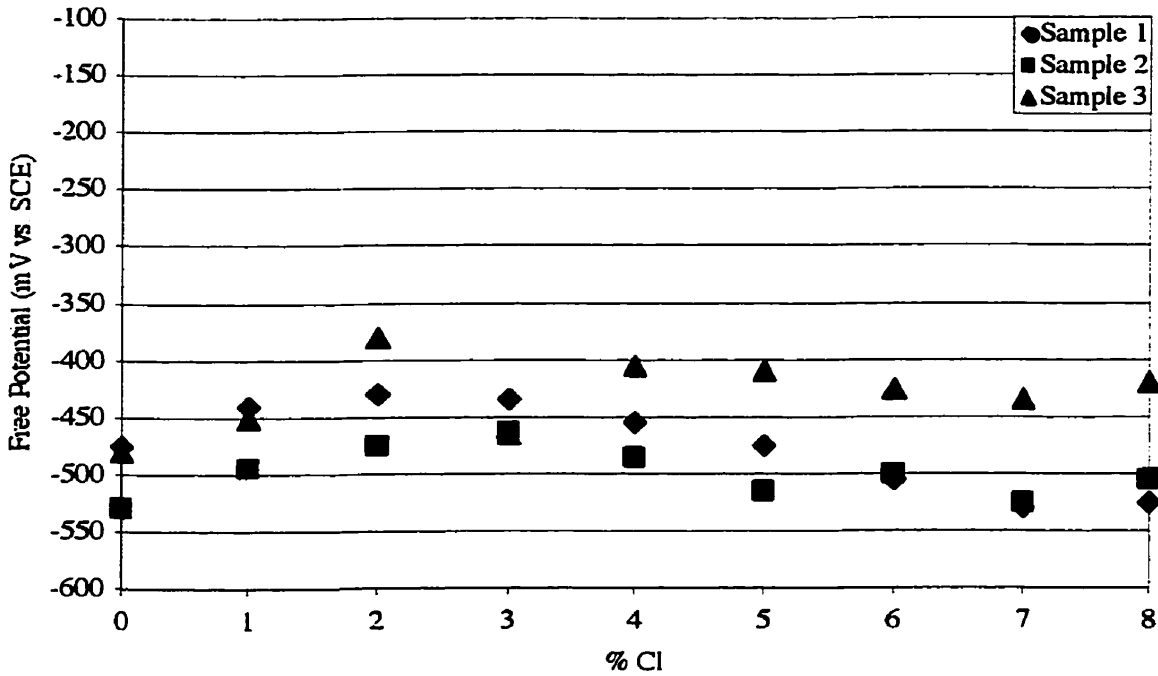


Figure 5.5 Free potentials of samples immersed in Ca(NO<sub>3</sub>)<sub>2</sub>-containing synthetic pore solution

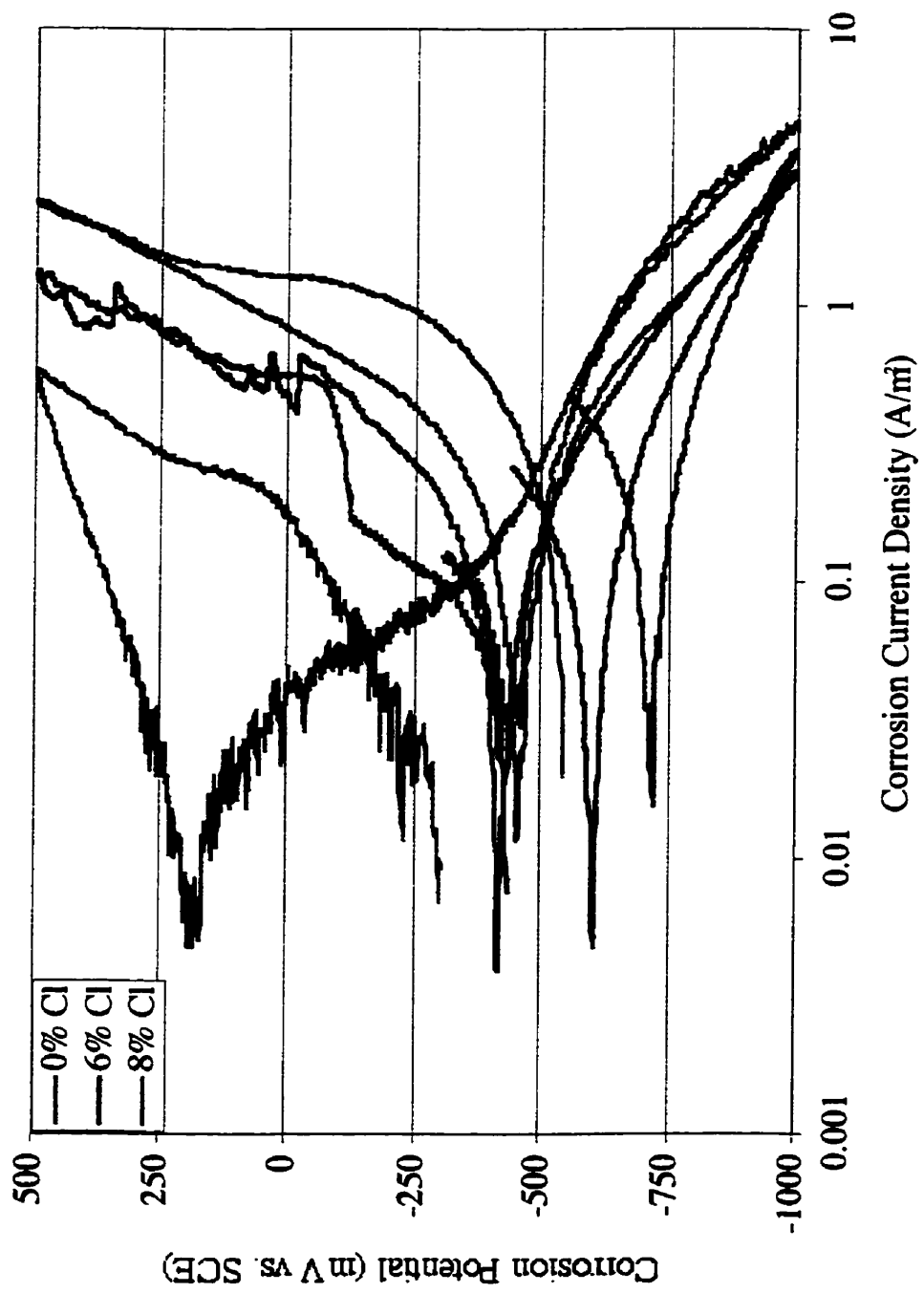


Figure 5.6 Representative cyclic polarization curves for samples immersed in Control synthetic pore solution

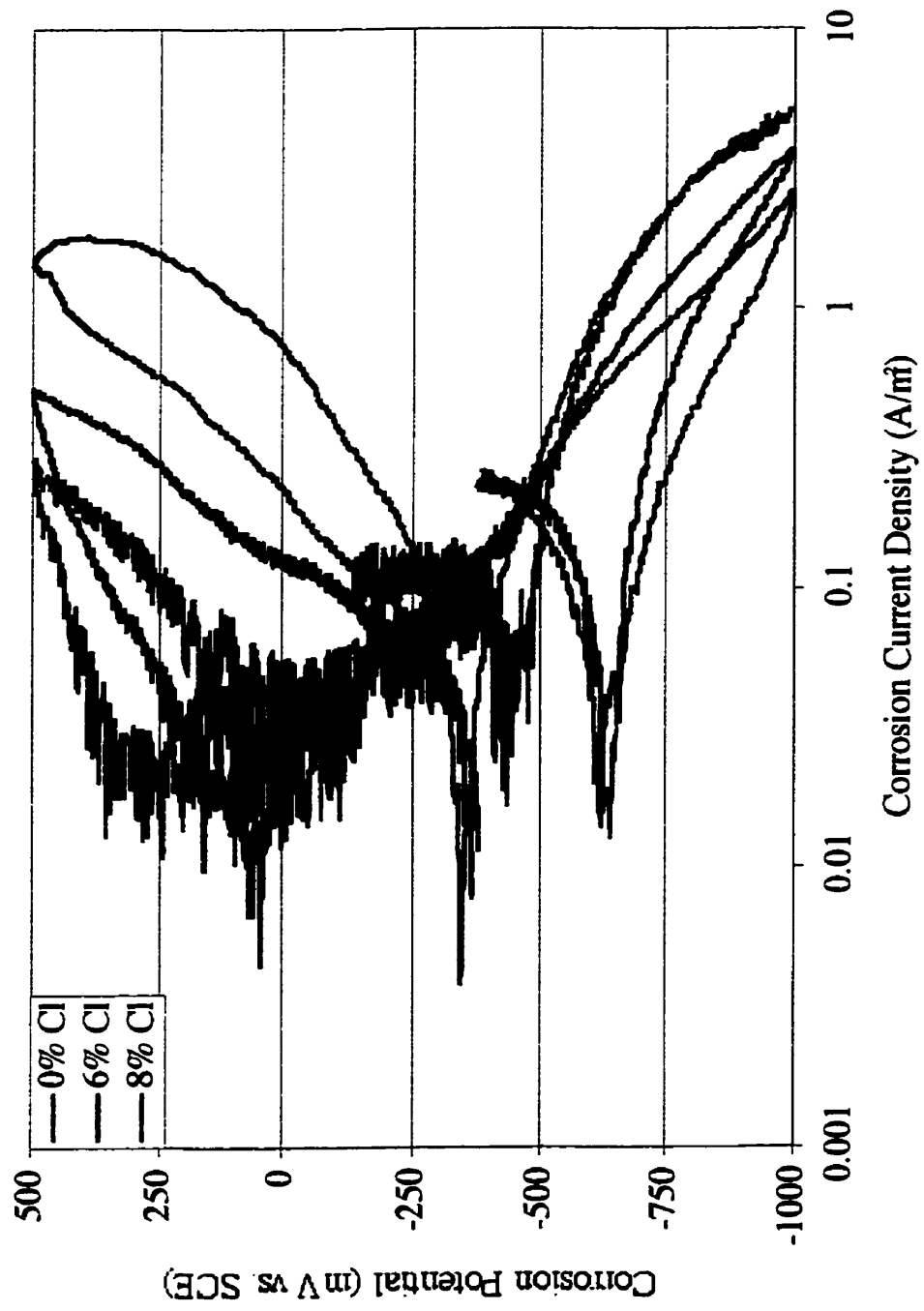


Figure 5.7 Representative cyclic polarization curves for samples immersed in CN1-containing synthetic pore solution

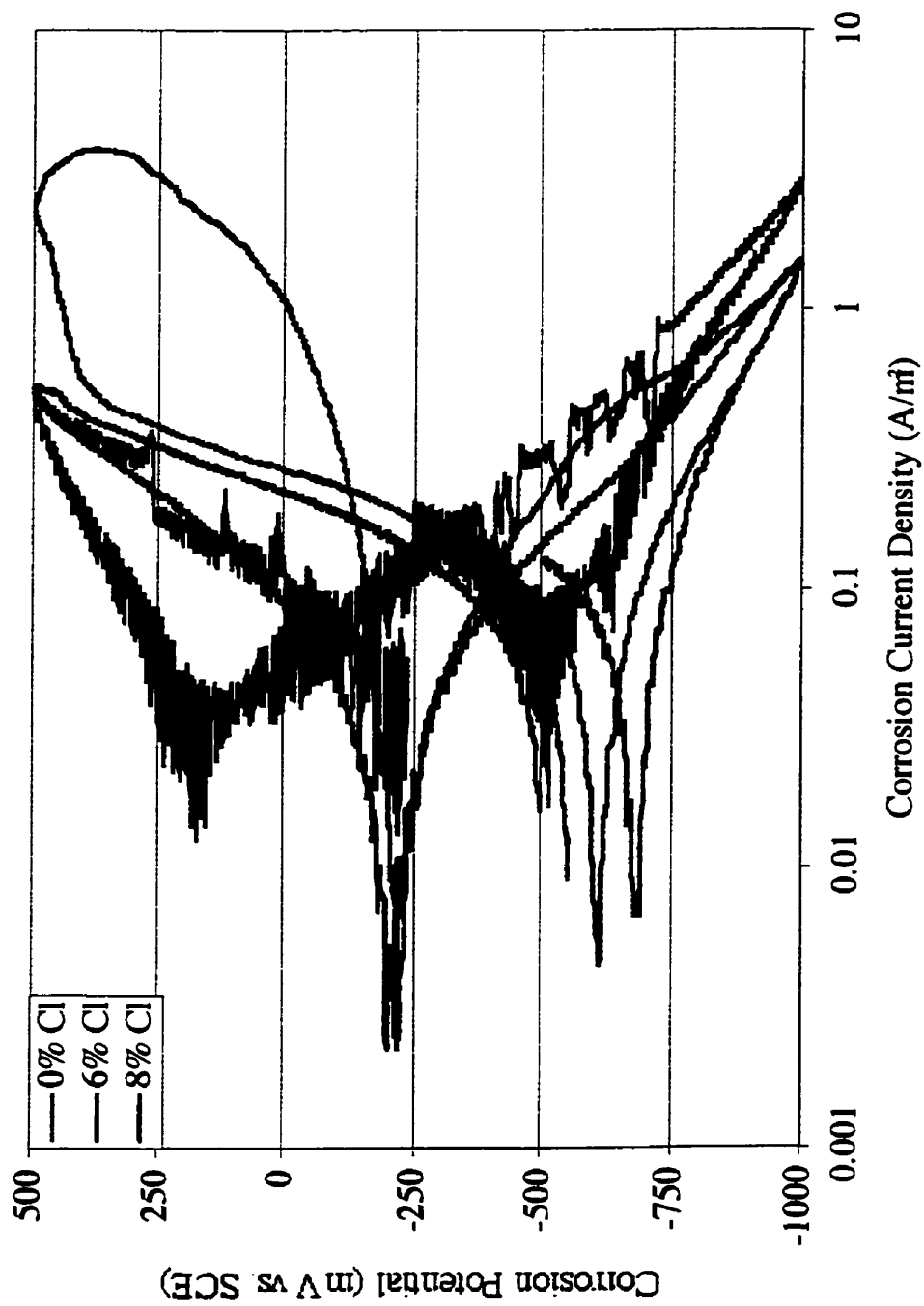


Figure 5.8 Representative cyclic polarization curves for samples immersed in CN<sub>2</sub>-containing synthetic pore solutions

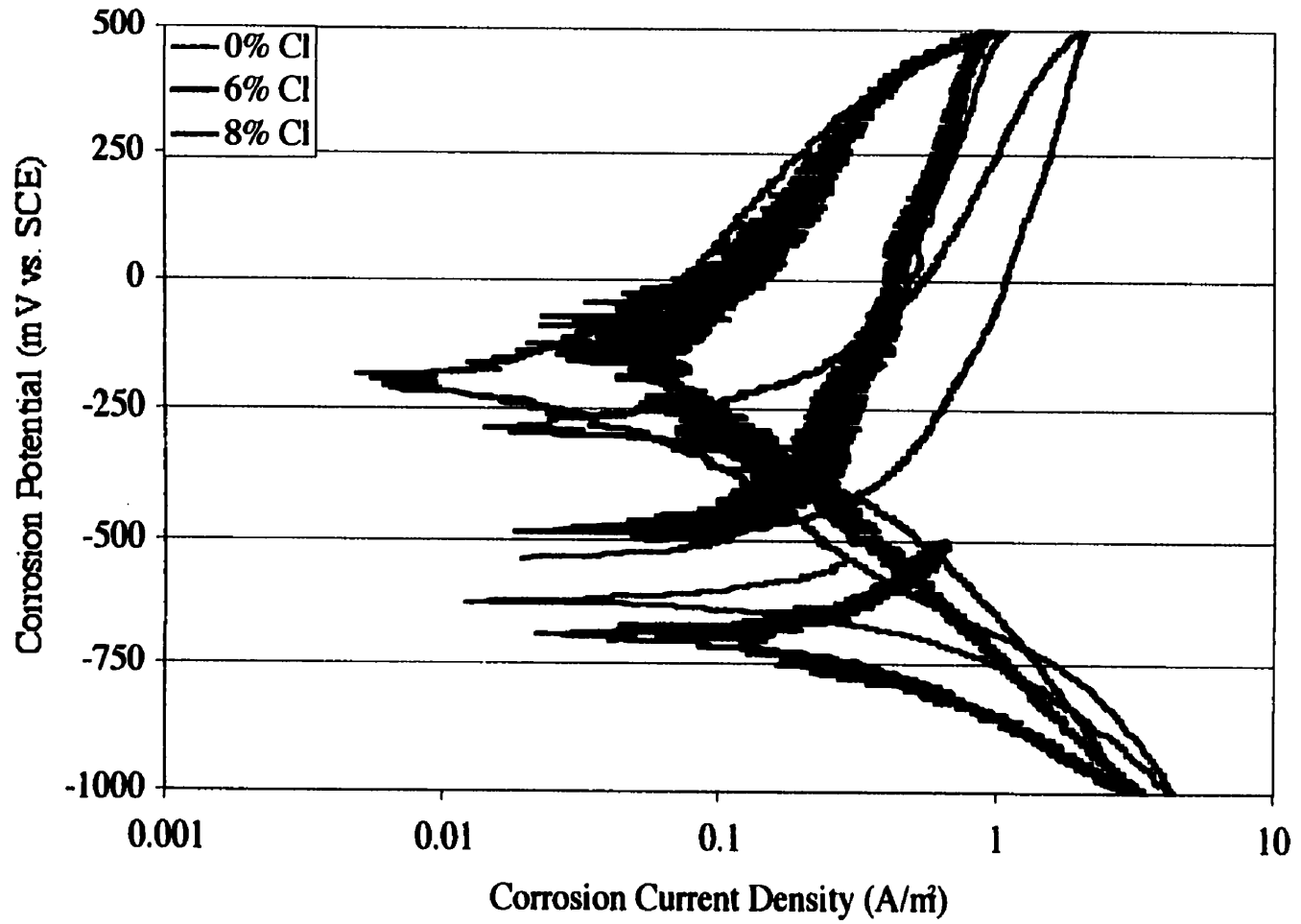


Figure 5.9 Representative cyclic polarization curves for samples immersed in  $\text{Ca}(\text{NO}_3)_2$ -containing synthetic pore solutions

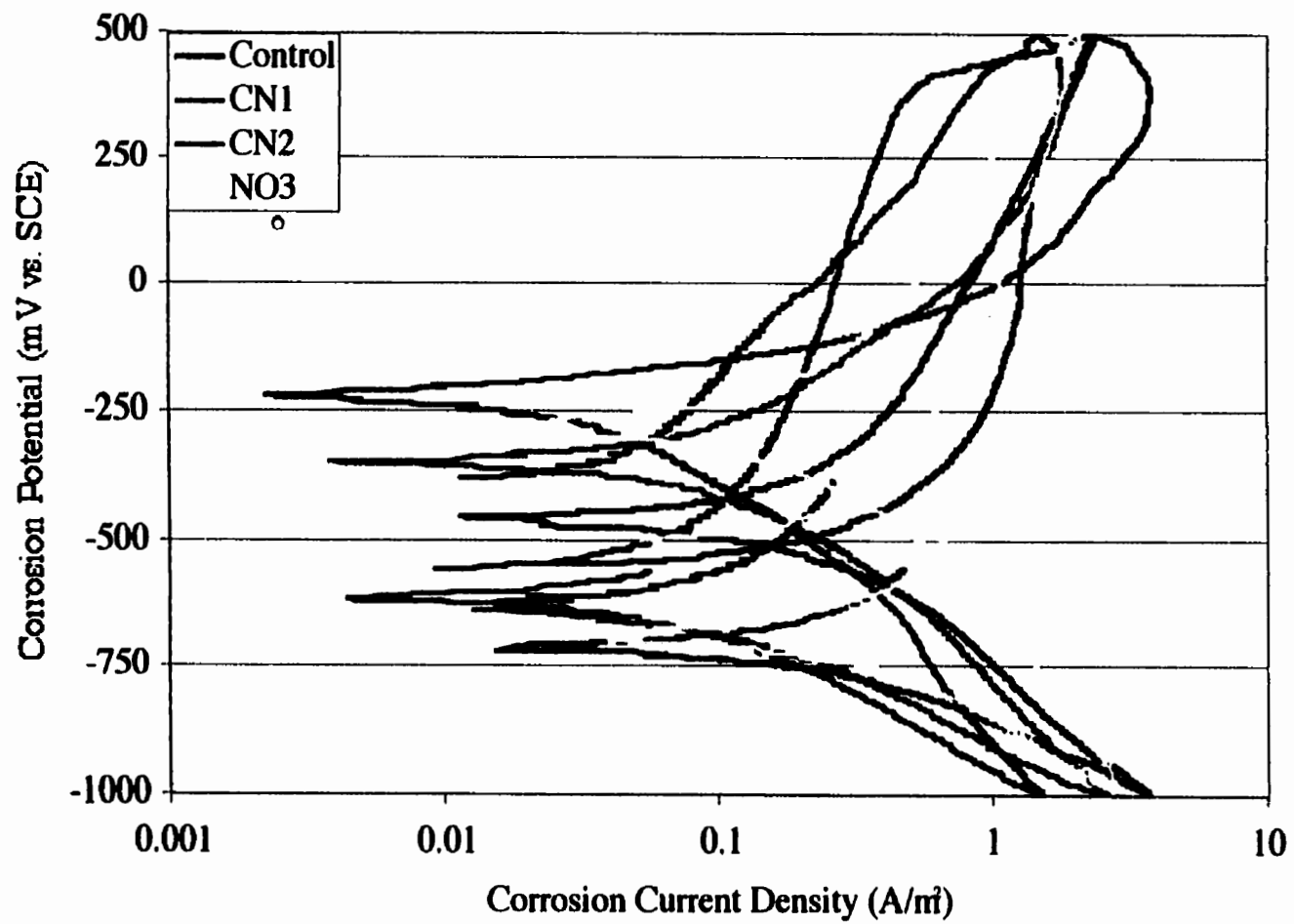


Figure 5.10 Comparison of representative cyclic polarization curves for samples immersed in solutions containing 8 % Cl<sup>-</sup>

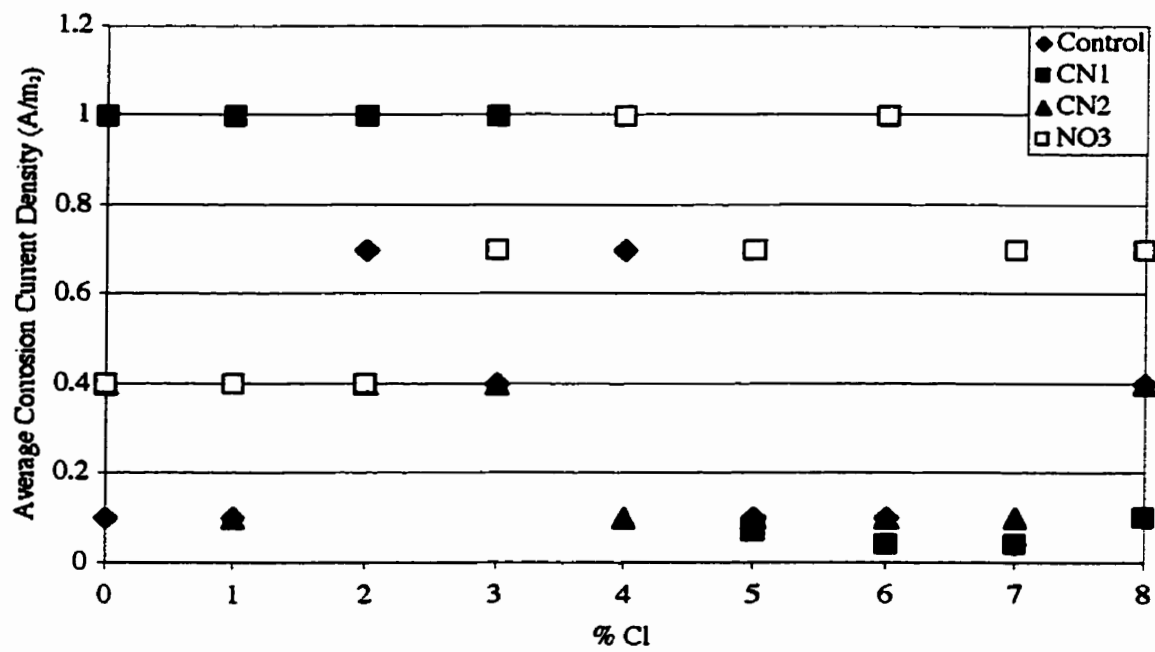
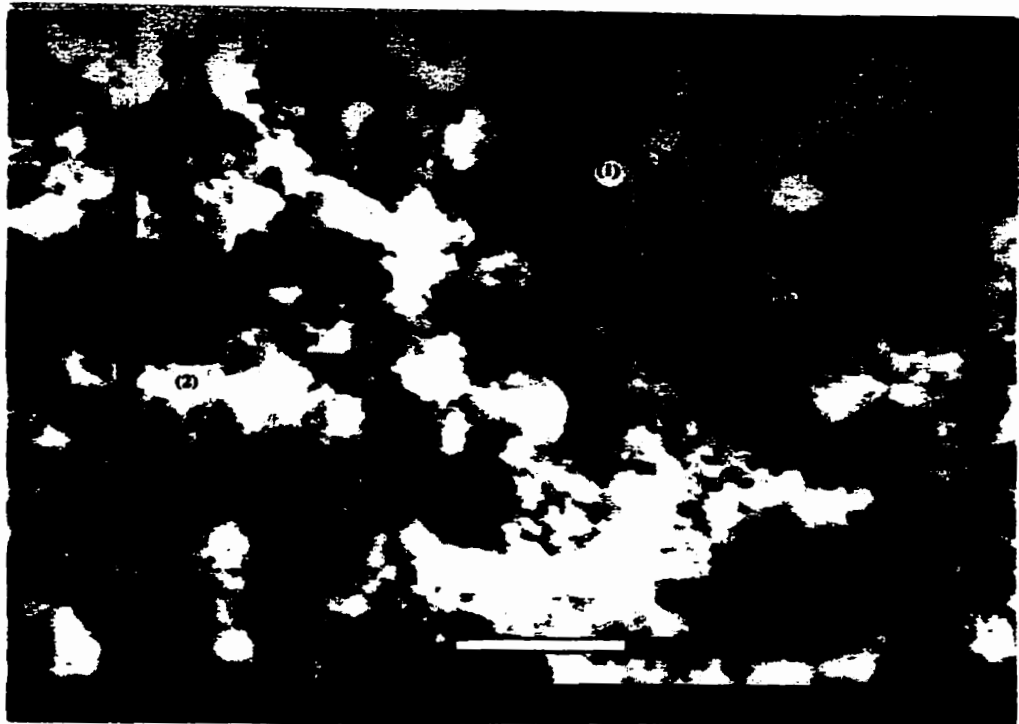
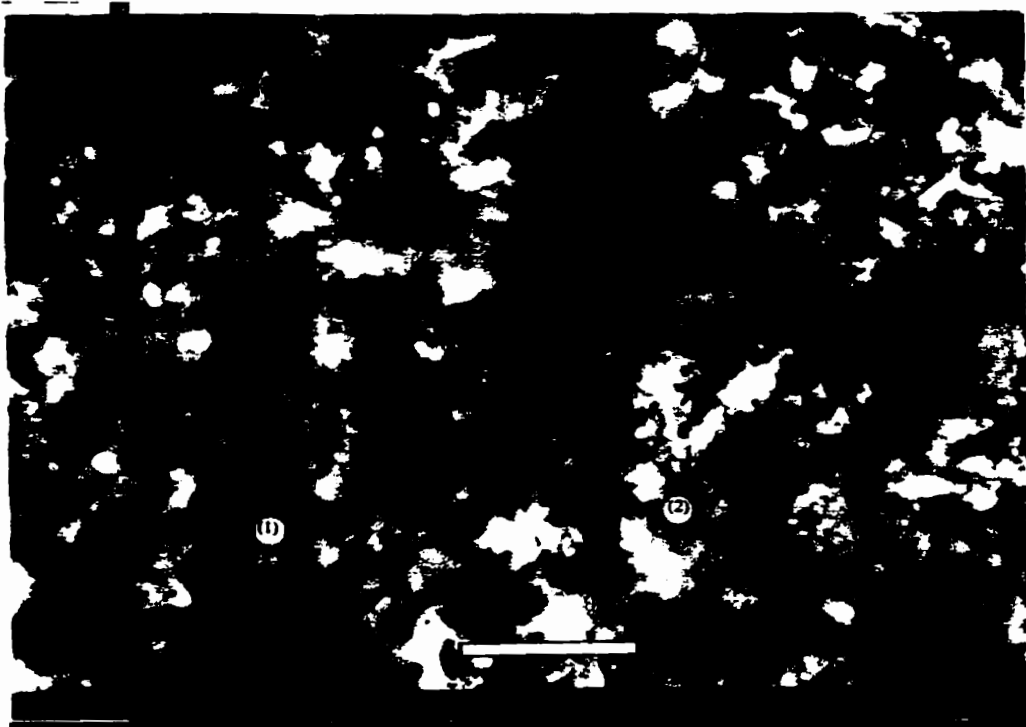


Figure 5.11 Average corrosion current density vs. chloride content for synthetic pore solutions (as determined through LPR)



**Figure 5.12 ESEM image of dried white deposit from Control solution (x 2000) where (1) particle and (2) spherulite**



**Figure 5.13 ESEM image of dried white deposit from CN1 solution (x 2000) where (1) tuber and (2) spherulite**



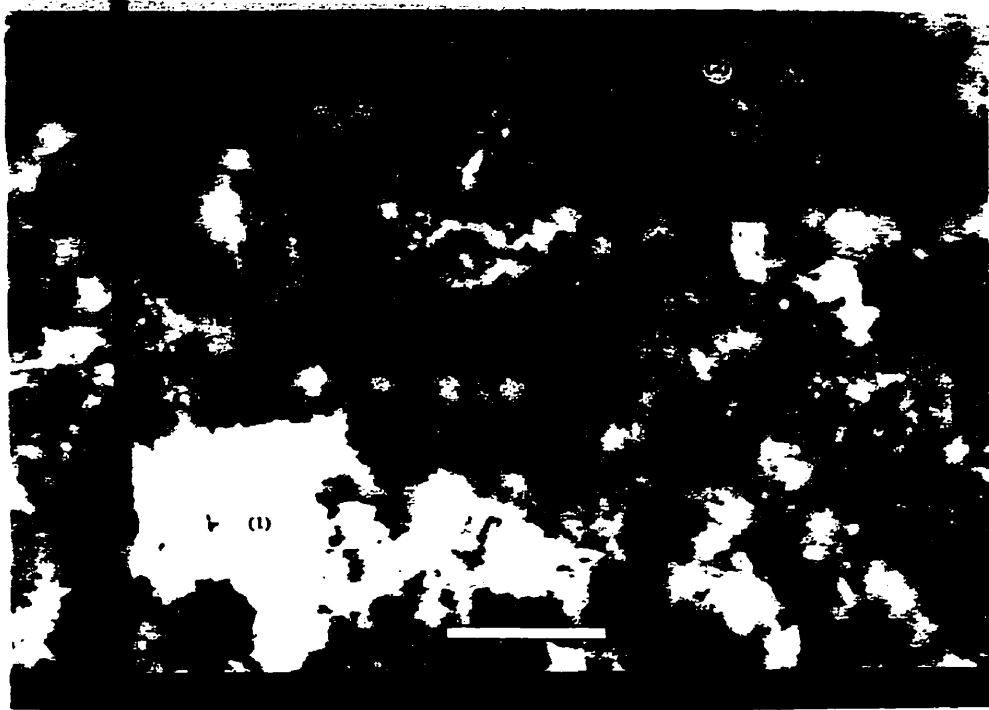


**Figure 5.14 ESEM image of dried white deposit from CN2 solution (x 2000) where (1) group and (2) spherulite**

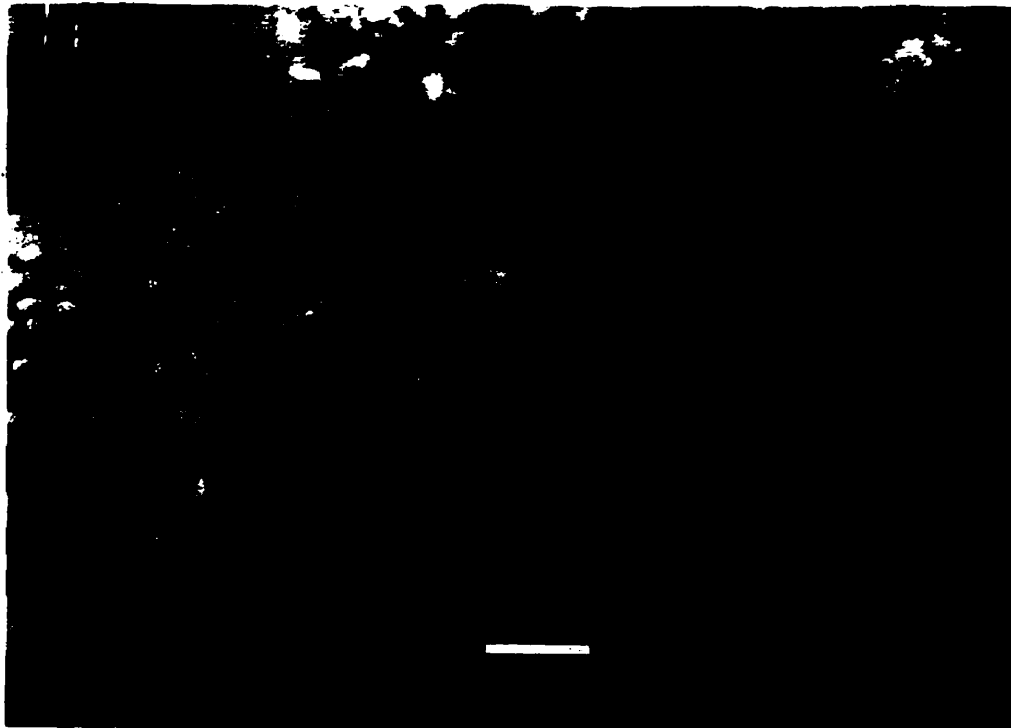


**Figure 5.15 ESEM image of white crusty deposit on spout on CN1 cell (x 650)**



**Figure 5.16** Sample surface exposed to Control pore solution prior to deposit removal (mag. 55 x).

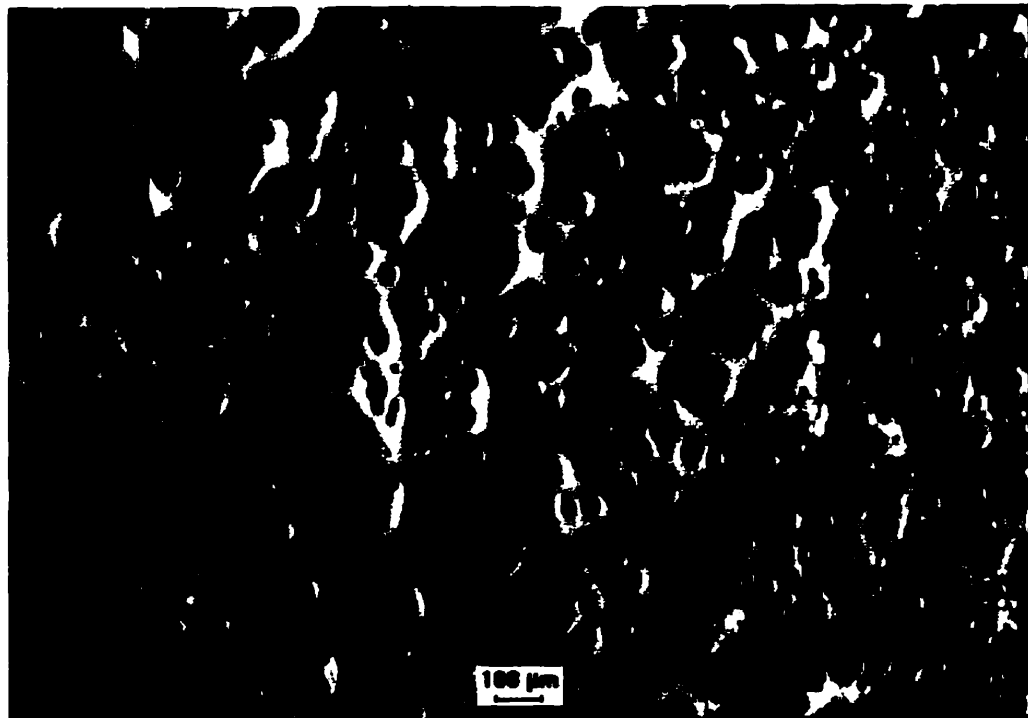


**Figure 5.17** Sample surface exposed to CN1 pore solution prior to deposit removal (mag. 55 x)

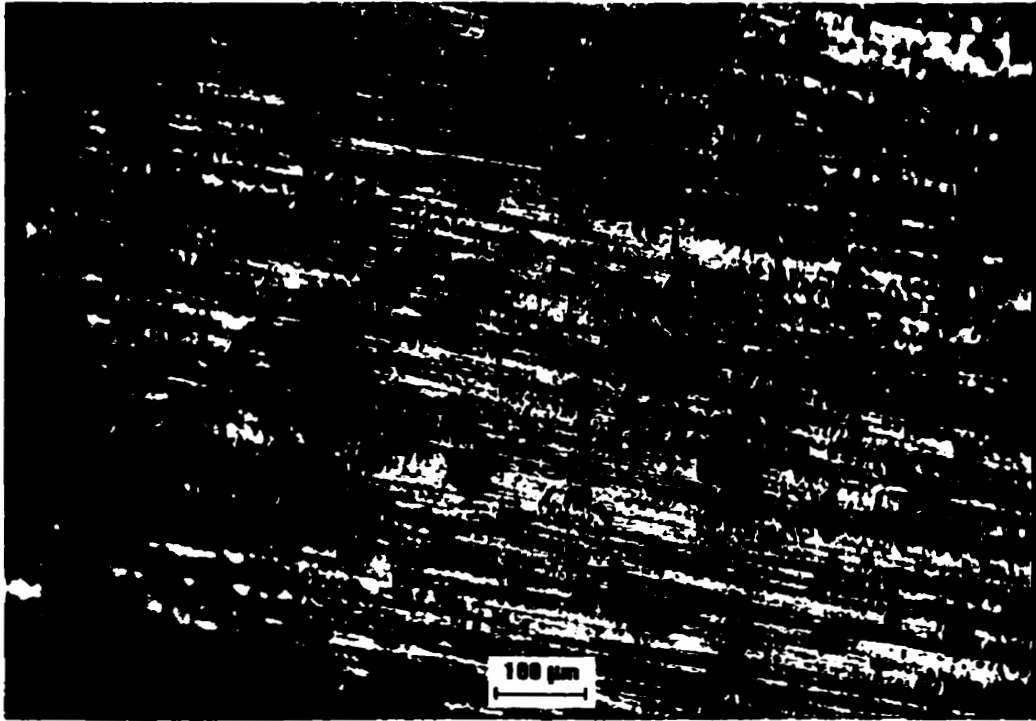


Figure 5.18 Sample surface exposed to Control pore solution after removal of surface deposit (mag. 110 x)

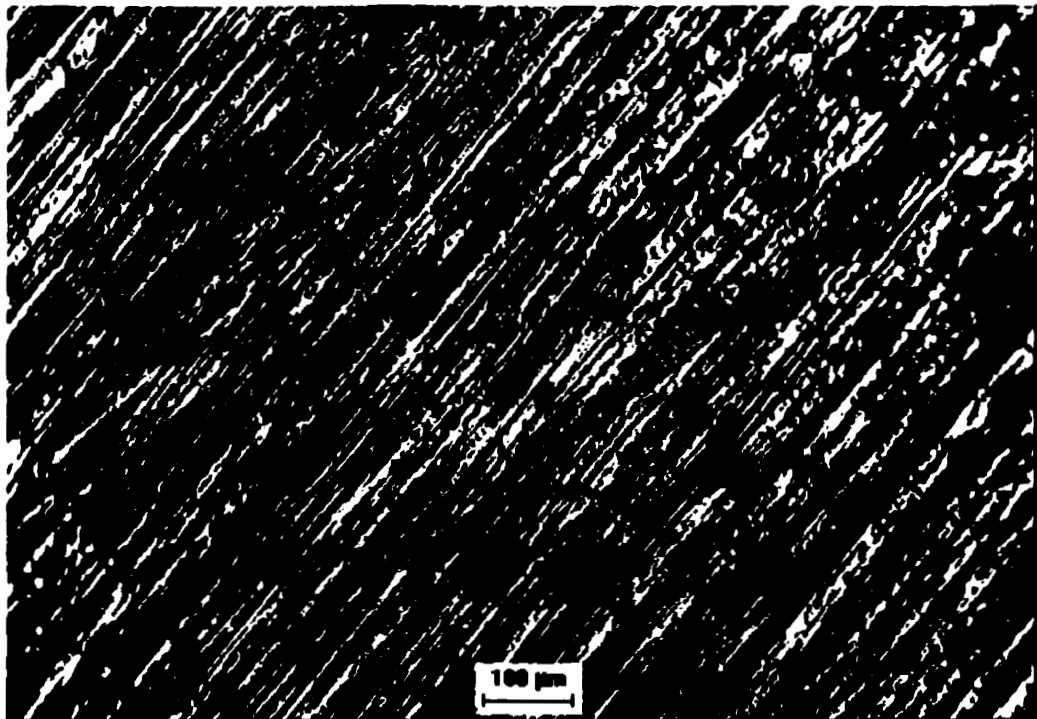


Figure 5.19 Sample surface exposed to CN1 pore solution after removal of surface deposit (mag. 110 x)

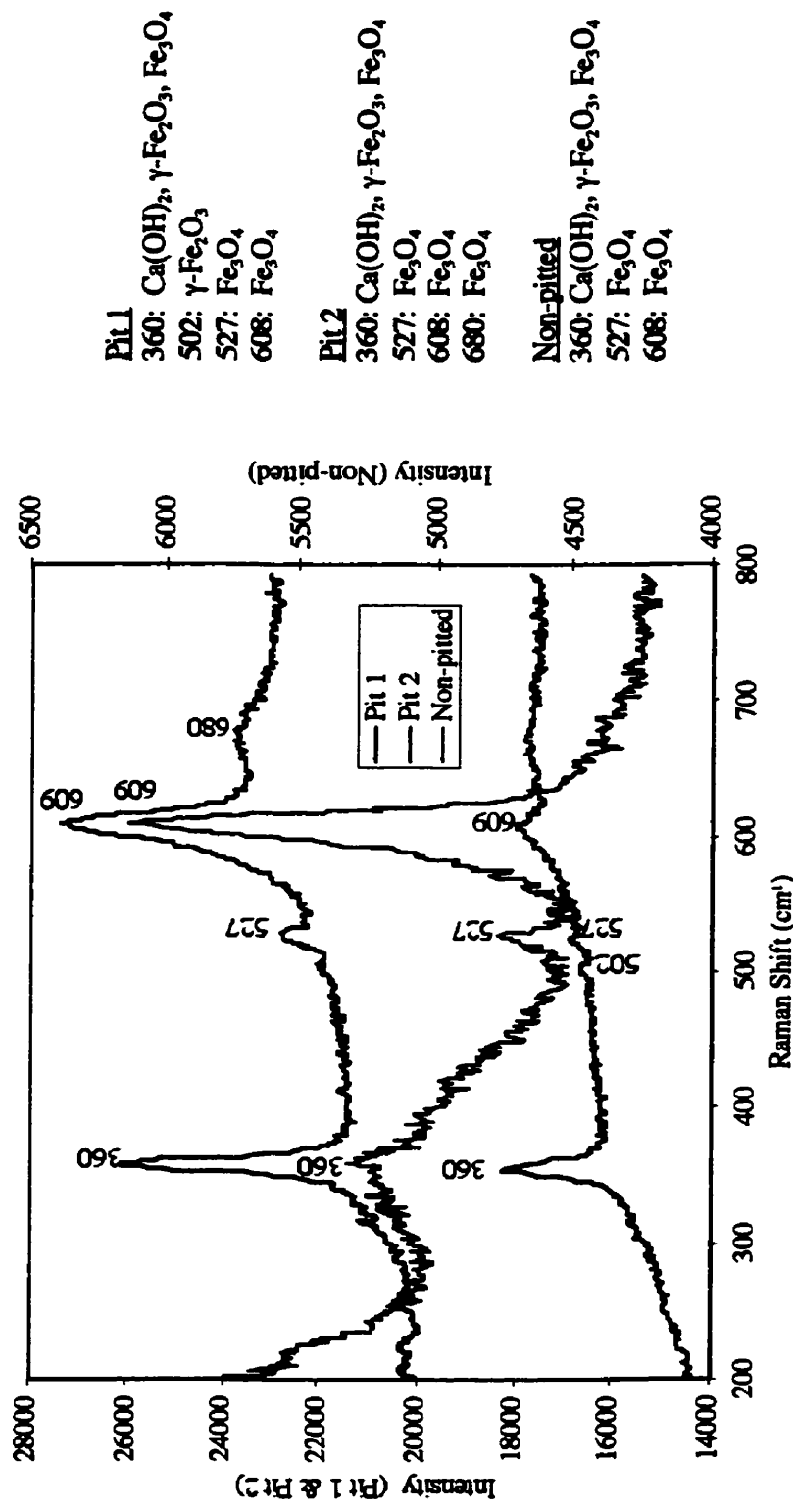


Figure 5.20 Raman spectra for sample in Control solution, no chlorides

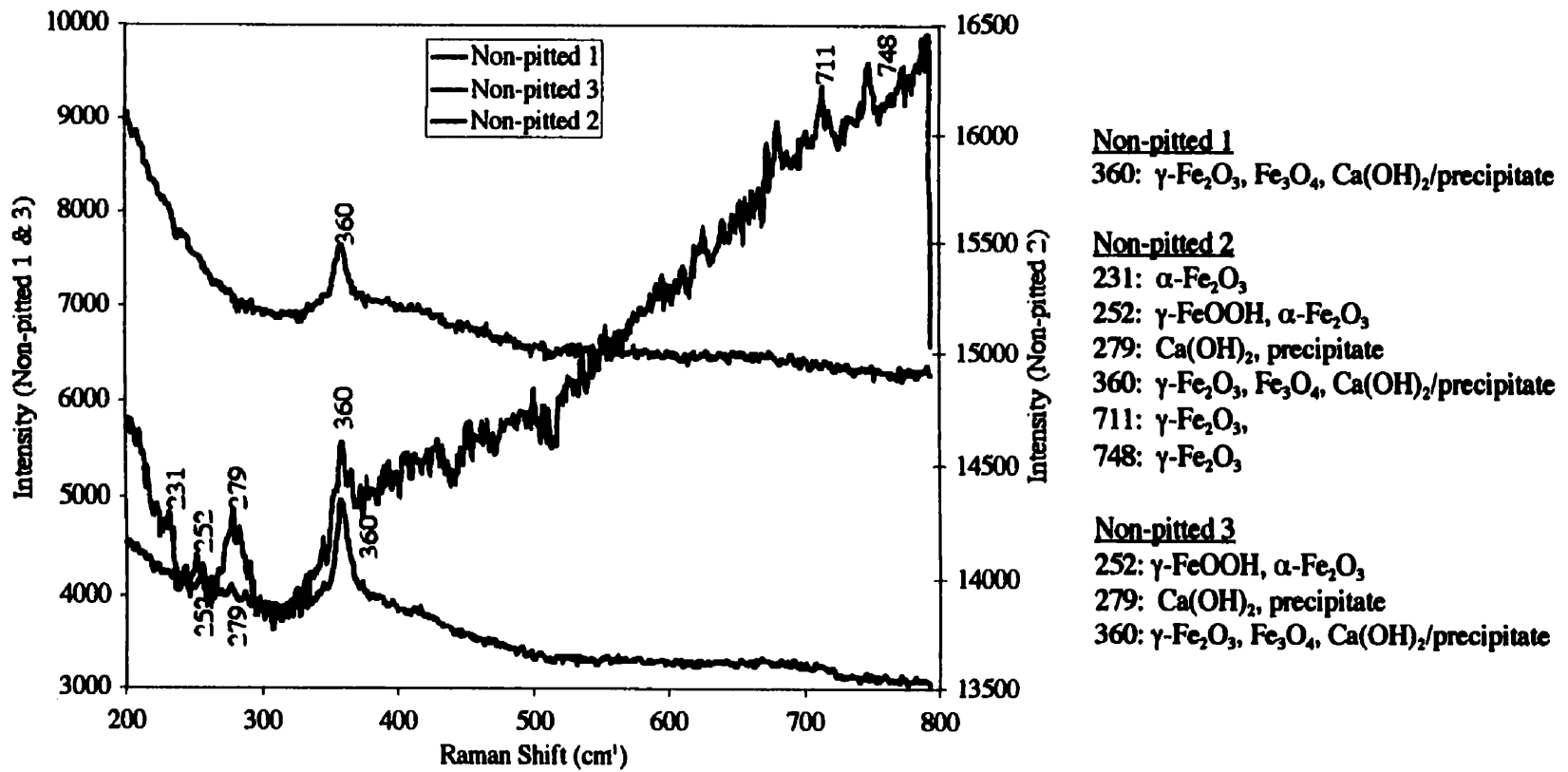


Figure 5.21 Raman spectra for sample in CN1 solution, no chlorides

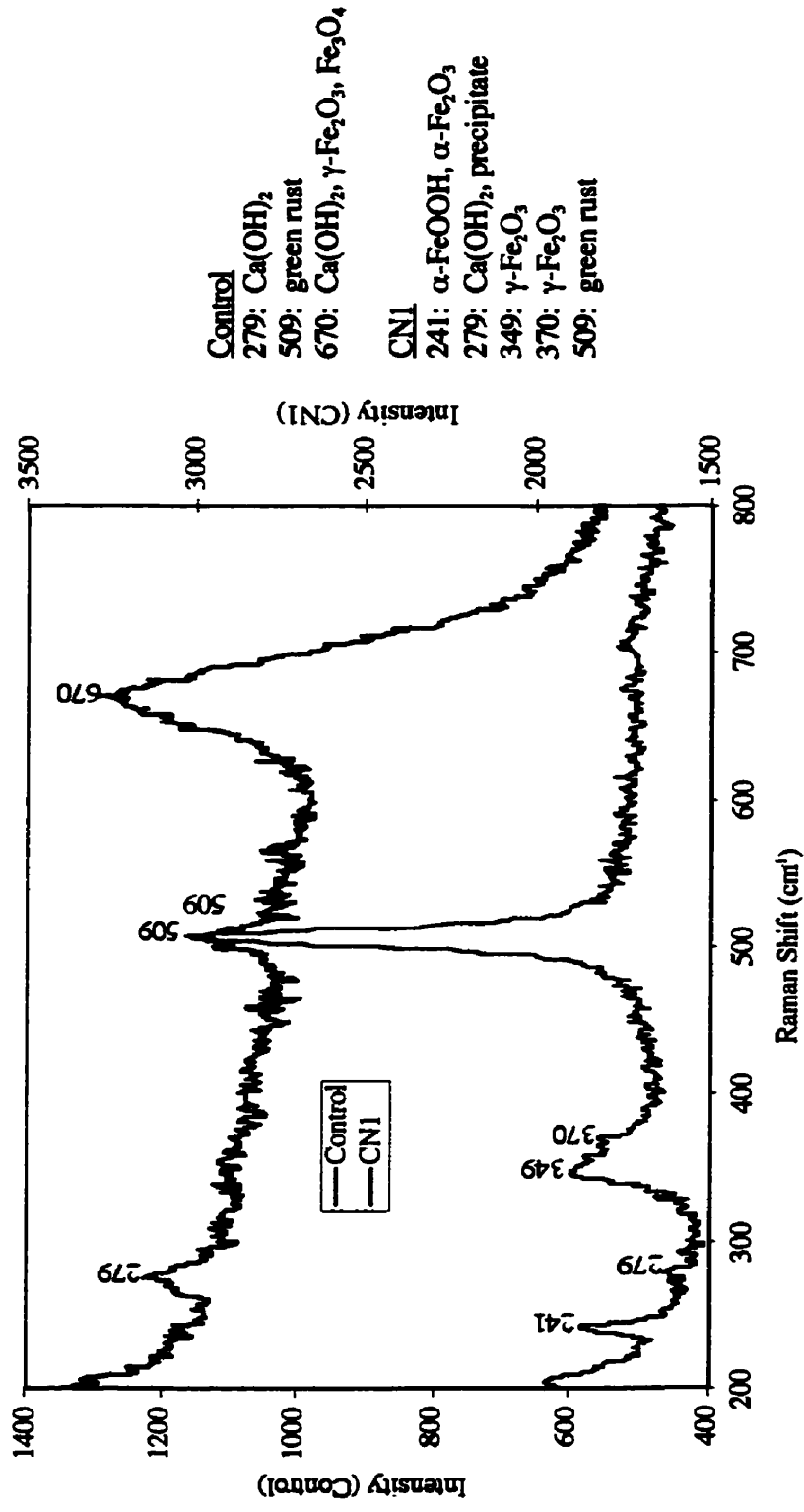


Figure 5.22 Comparison of shiny areas on samples in Control and CN1 solutions containing chlorides

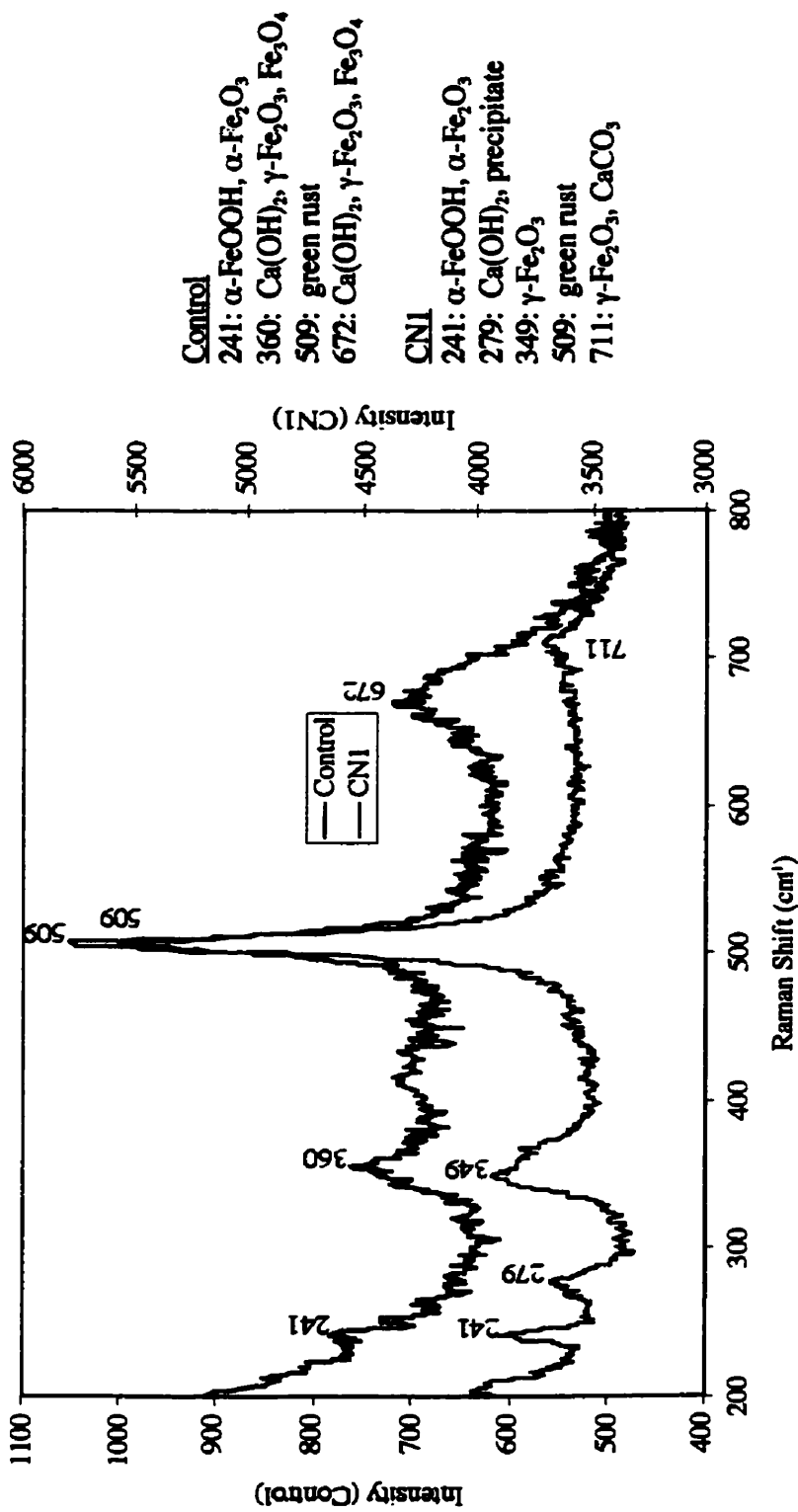


Figure 5.23 Comparison of red areas on samples in Control and CNI solutions containing chlorides

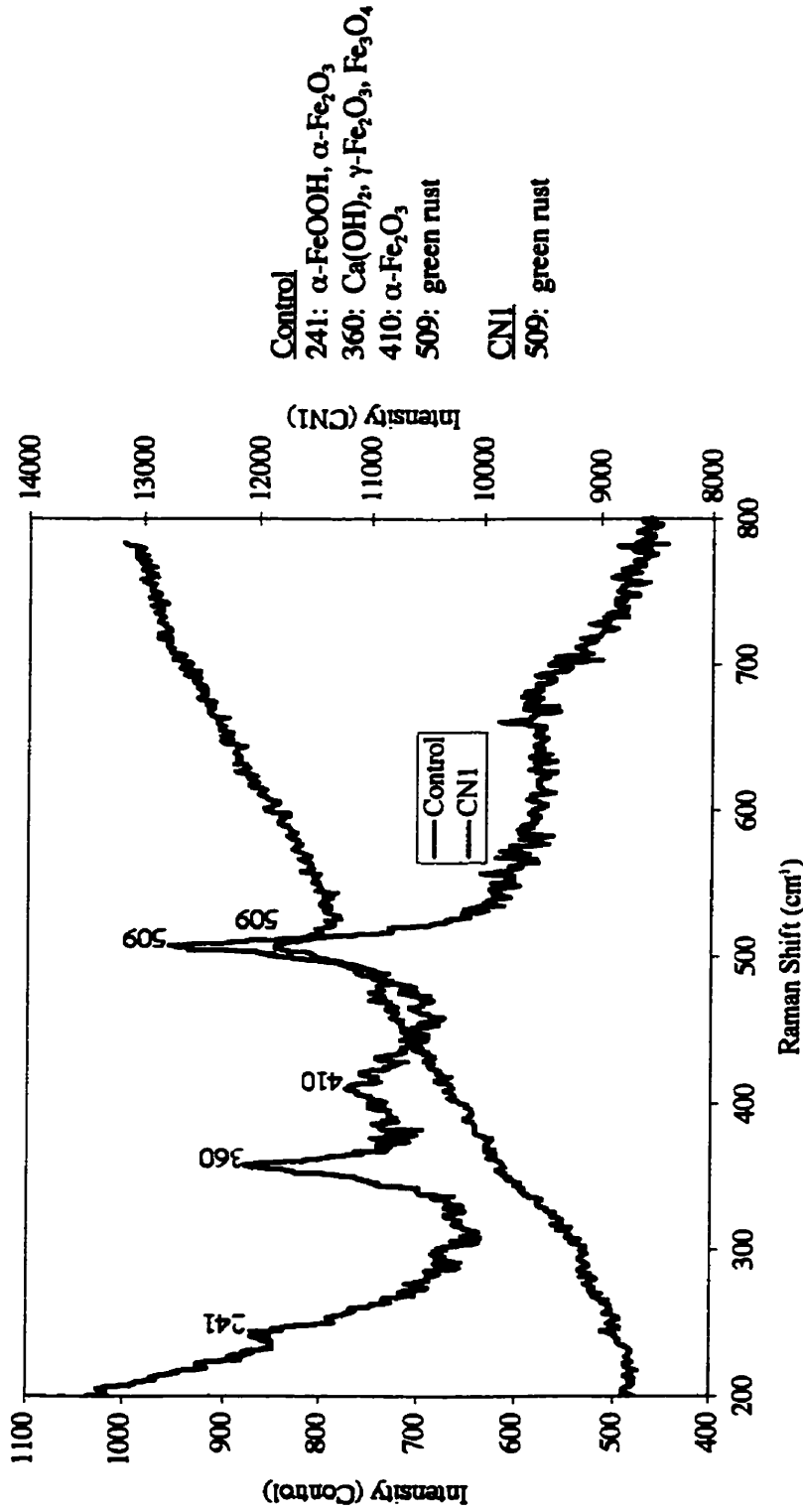
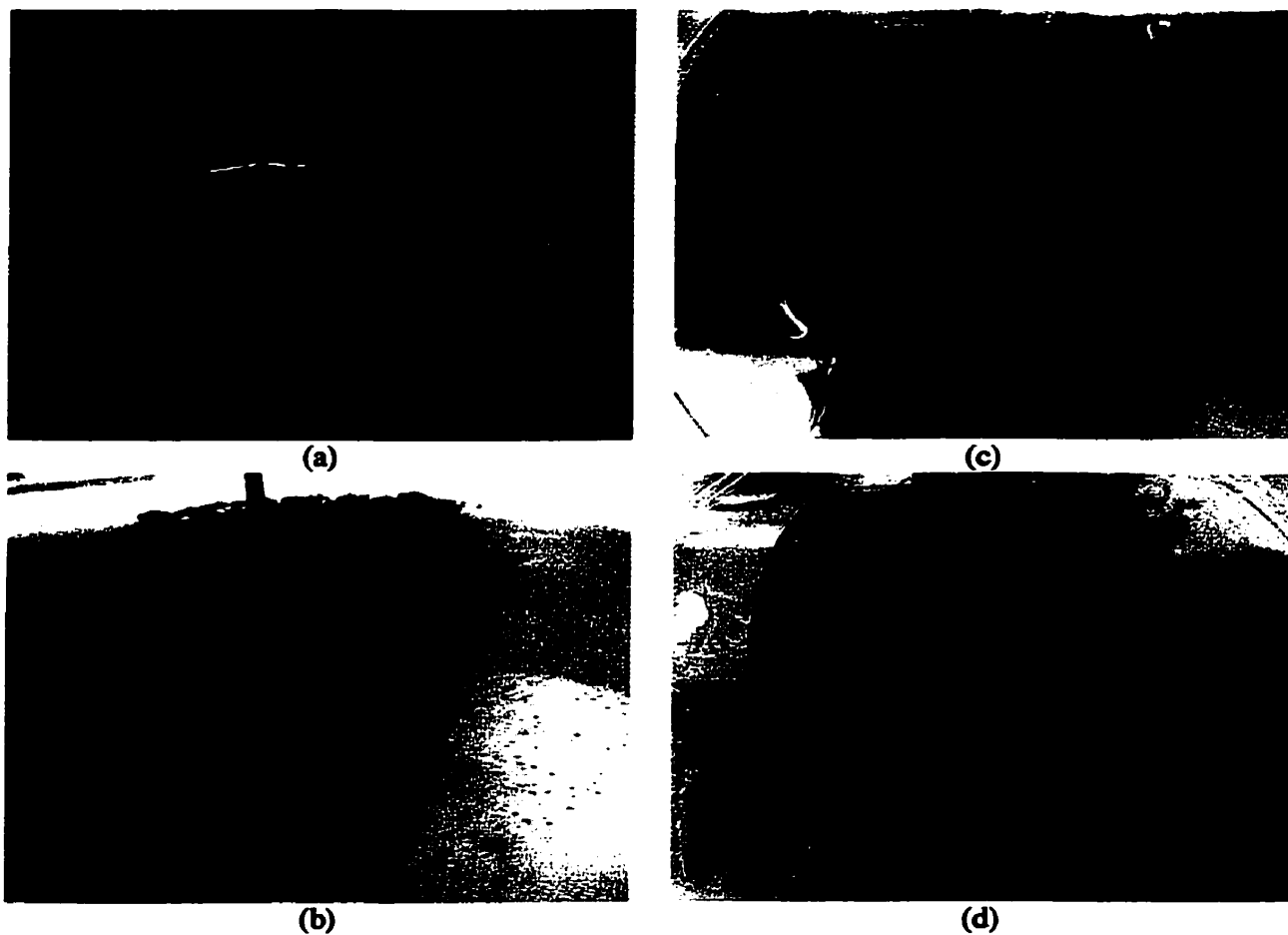


Figure 5.24 Comparison of black areas on samples in Control and CNI solutions containing chlorides





**Figure 5.25 Digital photographs of samples immersed in Control and CN1 pore solutions containing 15% chlorides**

- (a) Control sample after 300 seconds at +400 mV SCE**
- (b) CN1 sample after 300 seconds at +400 mV SCE**
- (c) Control sample surface after anodic polarization in (a)**
- (d) CN1 sample surface after anodic polarization in (b)**

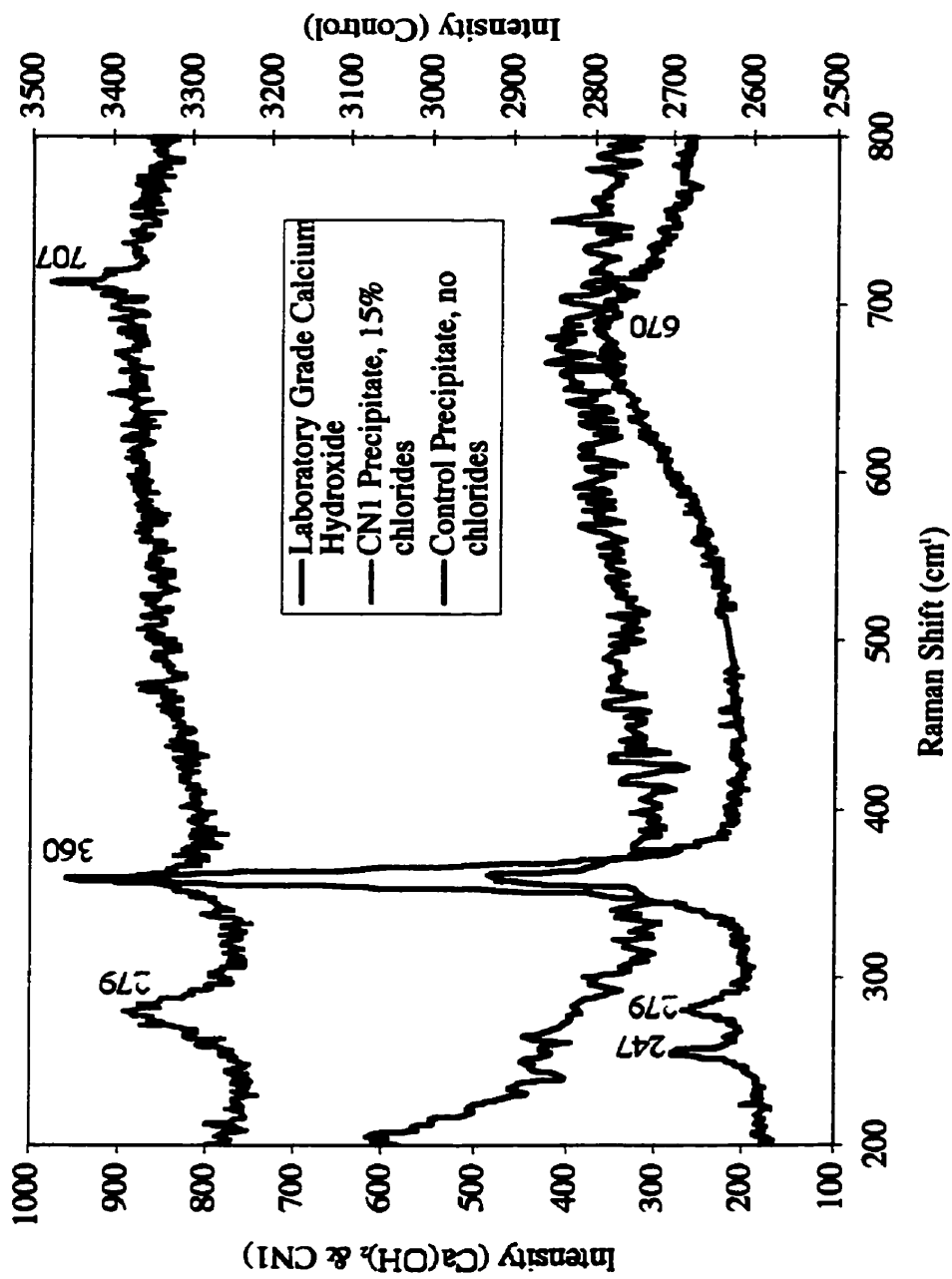


Figure 5.26 Raman spectra of precipitates from Control and CN1 solutions and laboratory grade  $\text{Ca}(\text{OH})_2$

## **Chapter 6**

### **Transport Properties of Cement Pastes**

#### **Results and Discussion**

#### **6.1 Mercury Intrusion Porosimetry**

##### **6.1.1 White Cement Paste Cylinders**

###### **6.1.1.1 Unponded Cylinders**

Cumulative intrusion volume measurements for individual specimens can be found in Appendix C, Figures C.1 to C.4. Figure 6.1 shows the average cumulative intrusion volume vs. pore radius for three specimens of each of the four white cement mixes prepared for this investigation. These and all subsequent data have been corrected for physical compression of the mercury and apparatus as well as thermal expansion of the mercury. Details regarding this correction can be found in Appendix F (Ioannidis 2001). Clearly visible from comparison of the curves is that the Control specimens have a greater total intrusion volume – and hence greater total porosity – than the specimens containing any of the inhibitors. A steep slope at the maximum intrusion pressure (i.e. smallest pore size) is evident in all mixes, suggestive of unintruded porosity, a limitation of the particular porosimeter used. The same is true for the data in Figures 6.3, 6.8 and 6.10. Also evident from Figure 6.1 is that the Control mix has a greater proportion of smaller sized pores. This is shown more clearly in Figure 6.2, where the data are replotted as the average incremental intrusion volume as a function of pore radius. Incremental intrusion volume measurements for individual specimens can be found in Appendix C, Figures C.5 to C.8. Table 6.1 separates the total intrusion volumes associated with coarse (radius  $\geq 0.1 \mu\text{m}$ ) and fine pores (radius  $< 0.1 \mu\text{m}$ ), as indicated by

the bimodal distribution in all of the incremental intrusion volume figures presented in this chapter and considering the threshold radii of each cement paste mix.

Table 6.1 Average coarse, fine and total pore intrusion volumes in white cement paste cylinders

	Coarse Pores		Fine Pores		Total Porosity		% Coarse
	Vol. (cc/g)	Std. Dev.	Vol. (cc/g)	Std. Dev.	Vol. (cc/g)	Std. Dev.	
<b>Control</b>	0.0024	0.0009	0.0752	0.0009	0.0777	0.0018	3.1
<b>CN1</b>	0.0043	0.0033	0.0553	0.0055	0.0596	0.0023	7.2
<b>CN2</b>	0.0037	0.0021	0.0613	0.0016	0.0650	0.0035	5.7
<b>Ca(NO<sub>3</sub>)<sub>2</sub></b>	0.0029	0.0017	0.0624	0.0049	0.0653	0.0055	4.4

All three inhibitors show higher coarse porosity and lower fine porosity than that observed in the Control mix. This result is consistent with the well-documented accelerating effects of both calcium nitrite and calcium nitrate.

Table 6.2 illustrates the effect of the inhibitors on coarse, fine and total porosities relative to that of Control. Although reductions in fine porosity associated with the addition of inhibitors remain relatively constant, there is significant variation in the increase in coarse porosity, dependent on the inhibitor used. The most dramatic increase is noted with the CN1 mix, followed by the CN2 and Ca(NO<sub>3</sub>)<sub>2</sub> mixes. Also interesting to note is that, despite the addition of “an organic agent” to retard the action of the calcium nitrite, CN2 appears to have an accelerating effect, albeit a lower one than that of CN1. As coarse pores are primarily responsible for the transport of agents necessary for corrosion of the reinforcing steel to the rebar surface (i.e. chlorides, oxygen), these results suggest that the addition of calcium nitrite and calcium nitrate would increase the permeability of concrete made with white cement. Holly (Holly 2001) came to the similar conclusions by examining the freezing behaviour and water dynamics of white cement paste with and without CN1 addition using combined nuclear magnetic resonance (NMR) and magnetic resonance micro-imaging (micro-MRI). These results were based, not on the radii of the

**Table 6.2 Effect of inhibitors on coarse, fine and total porosity with respect to white paste Control**

	<b>Effect on Coarse Porosity (%)</b>	<b>Effect on Fine Porosity (%)</b>	<b>Effect on Total Porosity (%)</b>
<b>CN1</b>	↑79	↓26	↓23
<b>CN2</b>	↑38	↓18	↓16
<b>Ca(NO<sub>3</sub>)<sub>2</sub></b>	↑21	↓17	↓16

pores, but on the relative intensities of water of different “mobilities” in the coarse and fine pores.

### 6.1.1.2 Poneded Cylinders

Figure 6.3 shows the average cumulative intrusion volume as a function of pore radius for three specimens from cylinders made with white cement and ponded with a 2% Cl<sup>-</sup> salt solution, while Figure 6.4 shows the average incremental intrusion volumes versus pore radius for these same samples. Cumulative and incremental intrusion volume measurements for individual specimens can be found in Appendix C, Figures C.17 to C.20 and Figures C.21 to C.24, respectively. The additions of both CN1 and calcium nitrate slightly reduce the total porosity of the cement pastes compared to the Control mix. This reduction is achieved through a decrease in the porosities associated with both categories of pores. However, although each inhibitor has an effect on total fine porosity, calcium nitrate reduces the proportion of larger fine pores and CN1 has more effect on the smaller fine pores. CN2 slightly increases total porosity through an increase in the proportion of fine pores, having virtually no effect on coarse porosity. This is more clearly shown in Tables 6.3, which compares the total, coarse and fine porosities for the mixes while Table 6.4 considers the effect of the inhibitors on these quantities.

**Table 6.3 Average coarse, fine and total pore intrusion volumes in ponded white paste cylinders**

	Coarse Pores		Fine Pores		Total Porosity		% Coarse
	Vol. (cc/g)	Std. Dev.	Vol. (cc/g)	Std. Dev.	Vol. (cc/g)	Std. Dev.	
<b>Control</b>	0.0019	0.0008	0.0488	0.0061	0.0507	0.0053	3.8
<b>CN1</b>	0.0008	0.0001	0.0453	0.0003	0.0461	0.0004	1.7
<b>CN2</b>	0.0018	0.0021	0.0507	0.0031	0.0525	0.0046	3.4
<b>Ca(NO<sub>3</sub>)<sub>2</sub></b>	0.0010	0.0008	0.0415	0.0042	0.0425	0.0048	2.4

**Table 6.4 Effect of inhibitors on coarse, fine and total porosity with respect to ponded white paste Control**

	Effect on Coarse Porosity (%)	Effect on Fine Porosity (%)	Effect on Total Porosity (%)
<b>CN1</b>	↓58	↓11	↓9
<b>CN2</b>	↓5	↑4	↑4
<b>Ca(NO<sub>3</sub>)<sub>2</sub></b>	↓47	↓15	↓16

### 6.1.1.3 Comparison of Unponded and Ponded Cylinders

Figures 6.5 through 6.7 compare the coarse, fine and total porosity values of unponded and ponded white cement paste cylinders, respectively. Immediately apparent is a reduction in total, coarse and fine porosities occurs in all mixes upon exposure to the 2 % Cl<sup>-</sup> ponding solution for 412 days. The extent of this reduction, however, is dependent on the type of inhibitor added to the mix, as is indicated in Table 6.5. This indicates that compositional differences exist between CN1 and CN2, and calcium nitrate cannot be said to interact with white cement in the same manner as calcium nitrite.

The decreases in coarse porosity upon exposure to ponding solution are beneficial with respect to limiting the pathways for aggressive species to penetrate the cement paste. All inhibitors reduce fine porosity, but to a similar or smaller degree than the reduction seen in the Control mix. However, fine porosity in these mixes is still below that observed in the Control mix. All of these data must take into consideration the volume of ponding solution absorbed by each mix, which is given in Table 6.6. Although CN1 and Ca(NO<sub>3</sub>)<sub>2</sub> had relatively the same effect on porosity values, the Ca(NO<sub>3</sub>)<sub>2</sub> mix absorbed

**Table 6.5 Comparison of porosity values of unponded and ponded white cement paste cylinders**

	Coarse Porosity (cc/g)			Fine Porosity (cc/g)			Total Porosity (cc/g)		
	No Cl	Pond	Effect	No Cl	Pond	Effect	No Cl	Pond	Effect
<b>Control</b>	0.0024	0.0019	↓21 %	0.0752	0.0488	↓35 %	0.0777	0.0507	↓35 %
<b>CN1</b>	0.0043	0.0008	↓81 %	0.0553	0.0453	↓18 %	0.0596	0.0461	↓23 %
<b>CN2</b>	0.0037	0.0018	↓51 %	0.0613	0.0507	↓17 %	0.0650	0.0525	↓19 %
<b>Ca(NO<sub>3</sub>)<sub>2</sub></b>	0.0029	0.0010	↓66 %	0.0624	0.0415	↓33 %	0.0653	0.0425	↓35 %

almost seven (7) times more ponding solution than the CN1 mix. Based on the volume of solution absorbed, CN1 is more effective at reducing porosity than Control or any of the other inhibitors. It is possible that the high level of absorption is due to a higher degree of micro-cracking in the mix made with Ca(NO<sub>3</sub>)<sub>2</sub>, although visual evidence was not apparent.

**Table 6.6 Volume of absorbed ponding solution for ponded white cement paste cylinders**

	Volume of Ponding Solution Absorbed (mL)
<b>Control</b>	9
<b>CN1</b>	6
<b>CN2</b>	8
<b>Ca(NO<sub>3</sub>)<sub>2</sub></b>	40

The reductions in porosity observed in all samples indicate that chemical reactions are occurring within all mixes upon external exposure to chlorides. One possible reaction is that between anhydrous cement grains and the water from the salt solution. However, the decrease in porosity is more probably attributable to the formation of Friedel's salt (3CaO·Al<sub>2</sub>O<sub>3</sub>·CaCl<sub>2</sub>·10H<sub>2</sub>O), trichloroaluminate hydrate (3CaO·Al<sub>2</sub>O<sub>3</sub>·3CaCl<sub>2</sub>·32H<sub>2</sub>O) and/or calcium hydroxy chloride (Ca-OH-Cl). It is more likely that the latter compound is forming, due to the abundance of Ca(OH)<sub>2</sub> and the relatively small amounts of the aluminates phases. Furthermore, the formation of Friedel's salt is simply an ion exchange and should not produce an increase in volume. The precipitation of these products would occur on the walls of the existing pores, causing narrowing or constriction of the pore

**network and/or a reduction in the number of pathways accessible to the mercury. This would also reduce access to the reinforcing steel and, in addition, chlorides would now be chemically bound and unavailable to destroy the passive film formed on the reinforcing steel.**

### **6.1.2 OPC Paste Cylinders**

#### **6.1.2.1 Unponded Cylinders**

**Figure 6.8 shows the average cumulative intrusion volume as a function of pore radius for cylinders made with ordinary Portland cement, while Figure 6.9 shows the same data plotted as average incremental intrusion volumes versus pore radius. Cumulative and incremental intrusion volume measurements for individual specimens can be found in Appendix C, Figures C.9 to C.12 and Figures C.13 to C.16, respectively. Apparent in both plots is the minimal effect on the total porosity of both calcium nitrite inhibitors as compared to the Control mix, despite a reduction in the proportion of coarse pores in each of these mixes. However, the addition of calcium nitrate reduced the proportions of both coarse and fine pores, thereby decreasing the total porosity of the mix as compared to the other three mixes. Table 6.7 gives the breakdown between coarse and fine porosity associated with each mix, while Table 6.8 shows the effect of the inhibitors on the total, coarse and fine porosity relative to those seen in the Control mix.**

#### **6.1.2.2 Ponded Cylinders**

**Figure 6.10 shows the average cumulative intrusion volume as a function of pore radius for cylinders made with ordinary Portland cement and exposed to an external source of chlorides through a 2%  $\text{Cl}^-$  salt solution, while Figure 6.11 shows the average incremental intrusion volumes versus pore radius. Cumulative and incremental intrusion**



**Table 6.7 Average coarse, fine and total pore intrusion volumes in OPC paste cylinders**

	<b>Coarse Pores</b>		<b>Fine Pores</b>		<b>Total Porosity</b>		<b>% Coarse</b>
	<b>Vol. (cc/g)</b>	<b>Std. Dev.</b>	<b>Vol. (cc/g)</b>	<b>Std. Dev.</b>	<b>Vol. (cc/g)</b>	<b>Std. Dev.</b>	
<b>Control</b>	0.0025	0.0007	0.0937	0.0052	0.0961	0.0048	2.6
<b>CN1</b>	0.0016	0.0015	0.0929	0.0044	0.0945	0.0033	1.7
<b>CN2</b>	0.0014	0.0020	0.0980	0.00004	0.0994	0.0019	1.4
<b>Ca(NO<sub>3</sub>)<sub>2</sub></b>	0.0016	0.0016	0.0801	0.0039	0.0817	0.0048	2.0

**Table 6.8 Effect of inhibitors on coarse, fine and total porosity with respect to OPC Control**

	<b>Effect on Coarse Porosity (%)</b>	<b>Effect on Fine Porosity (%)</b>	<b>Effect on Total Porosity (%)</b>
<b>CN1</b>	↓36	↓1	↓2
<b>CN2</b>	↓44	↑5	↑3
<b>Ca(NO<sub>3</sub>)<sub>2</sub></b>	↓36	↓15	↓15

volume measurements for individual specimens can be found in Appendix C, Figures C.25 to C.28 and Figures C.29 to C.30, respectively. Minimal differences exist between the total porosity of the Control and CN1 mixes, while total porosity of mixes containing CN2 and Ca(NO<sub>3</sub>)<sub>2</sub> are slightly reduced. Coarse porosity in the CN1 and Ca(NO<sub>3</sub>)<sub>2</sub> mixes are approximately two times higher than those observed in the Control and CN2 mixes, which are similar in magnitude. Tables 6.9 and 6.10 give a breakdown of the coarse, fine and total porosities of each mix and the effect of each inhibitor relative to the Control mix, reinforcing the observations shown in the aforementioned figures.

### 6.1.1.3 Comparison of Unponded and Ponded Cylinders

Figures 6.12 through 6.15 compare the coarse, fine and total porosity values of unponded and ponded OPC paste cylinders, respectively. As was observed in the case of the mixes made with white cement, a reduction in fine and total porosity occurs in all mixes with exposure to the ponding solution. However, unlike the white cement mixes, only the Control mix shows a decrease in coarse porosity with exposure to ponding solution, while

Table 6.9 Average coarse, fine and total pore intrusion volumes in ponded OPC paste cylinders

	Coarse Pores		Fine Pores		Total Porosity		% Coarse
	Vol. (cc/g)	Std. Dev.	Vol. (cc/g)	Std. Dev.	Vol. (cc/g)	Std. Dev.	
Control	0.0013	0.0006	0.0778	0.0031	0.0791	0.0034	1.6
CN1	0.0030	0.0016	0.0738	0.0037	0.0768	0.0040	3.9
CN2	0.0015	0.0013	0.0733	0.0064	0.0748	0.0059	2.0
Ca(NO <sub>3</sub> ) <sub>2</sub>	0.0027	0.0010	0.0699	0.0028	0.0726	0.0038	3.7

Table 6.10 Effect of inhibitors on coarse, fine and total porosity with respect to ponded OPC Control

	Effect on Coarse Porosity (%)	Effect on Fine Porosity (%)	Effect on Total Porosity (%)
CN1	↑131	↓5	↓3
CN2	↑15	↓6	↓6
Ca(NO <sub>3</sub> ) <sub>2</sub>	↑108	↓10	↓8

dramatic increases are observed in the CN1 and Ca(NO<sub>3</sub>)<sub>2</sub> mixes and virtually no change in the CN2 mix. Table 6.11 shows the differences in coarse, fine and total porosities between unponded and ponded mixes. Before taking the above values into consideration, the volume of ponding solution absorbed by the individual mixes, shown in Table 6.12, must also be considered.

As the Control mix absorbed the largest volume of ponding solution, the effect on coarse porosity in this mix is not as pronounced as might otherwise be concluded. Based on the volume of ponding solution absorbed, all inhibited mixes have a more significant effect on total porosity than the Control mix. The CN2 mix displays the largest effect as it absorbed the least amount of ponding solution, followed by calcium nitrate and CN1.

Table 6.11 Comparison of porosity values of unponded and ponded OPC paste cylinders

	Coarse Porosity (cc/g)			Fine Porosity (cc/g)			Total Porosity (cc/g)		
	No Cl	Pond	Effect	No Cl	Pond	Effect	No Cl	Pond	Effect
Control	0.0025	0.0013	↓48 %	0.0937	0.0778	↓17 %	0.0961	0.0791	↓18%
CN1	0.0016	0.0030	↑88 %	0.0929	0.0738	↓21 %	0.0945	0.0768	↓19%
CN2	0.0014	0.0015	↑7 %	0.0980	0.0733	↓26 %	0.0994	0.0748	↓25%
Ca(NO <sub>3</sub> ) <sub>2</sub>	0.0016	0.0027	↑69 %	0.0801	0.0699	↓13 %	0.0817	0.0726	↓11%

**Table 6.12 Volume of absorbed ponding solution for ponded OPC paste cylinders**

	<b>Volume of Ponding Solution Absorbed (mL)</b>
<b>Control</b>	46
<b>CN1</b>	31
<b>CN2</b>	6
<b>Ca(NO<sub>2</sub>)<sub>2</sub></b>	9

The discrepancies between the two calcium nitrite inhibitors may be due to the compositional differences between the two admixtures, namely the addition of “an organic compound” to CN2.

The increase in coarse porosity displayed by the mixes containing inhibitors may be explained by the introduction of micro-cracks within the cement matrix. If the inhibitors are decreasing the degree of interconnected pores within the cement paste, pressure would be exerted on the pore walls of isolated pores as they are filled. This change in porosity may also be due to the redistribution of phases due to the formation of bound chlorides.

## **6.2 Acid Soluble Chloride Titrations**

### **6.2.1 Ponded White Cement Paste Cylinders**

Figure 6.15 displays the chloride concentration of the ponded white cement paste cylinders as a function of depth into the cylinder (away from the ponding surface). The most beneficial situation from a corrosion standpoint would be a reduced chloride concentration closer to the rebar surface, where a typical concrete cover over the reinforcing steel is approximately 50 mm. A general decrease in chloride concentration with increased depth into the cylinder is observed in the Control mix and the two mixes containing calcium nitrite inhibitor, as expected. While all three inhibited mixes show higher chloride levels than Control at the surface (top 7 mm), the addition of calcium

nitrate appears to enhance the penetration of chlorides into the white cement paste, showing a relatively constant chloride concentration to about 40 mm in depth. These high concentrations can be attributed to the high volume of ponding solution absorbed by the cylinder made with nitrate inhibitor (Table 6.6).

Table 6.13 lists the volumes of ponding solution absorbed by each cylinder and their respective total chloride concentrations in the top 50 mm of the cylinder. As would be expected, total chloride concentration is dependent on the volume of ponding solution absorbed. However, despite having absorbed approximately four times more solution than the Control mix, the chloride concentration in the nitrate inhibitor paste is only twice as high as in the Control. Relatively little variation is observed between the Control mix and those mixes containing calcium nitrite. This is not surprising given that all three mixes absorbed similar volumes of ponding solution.

Table 6.13 Volume of ponding solution absorbed and total chloride concentration of ponded white cement paste cylinders

	<b>Vol. Ponding Solution Absorbed (mL)</b>	<b>Total Chloride Concentration (g Cl/g paste)</b>
<b>Control</b>	9	0.015
<b>CN1</b>	6	0.016
<b>CN2</b>	8	0.015
<b>Ca(NO<sub>3</sub>)<sub>2</sub></b>	40	0.034

### 6.2.2 Ponded OPC Paste Cylinders

Figure 6.16 shows chloride concentration with increasing depth into ponded OPC paste cylinders. All mixes show a decrease in chloride concentration with increasing penetration into the sample, however insignificant variation exists between mixes. This is confirmed by the quantities in Table 6.14, which lists the absorbed volume of ponding solution and the total chloride concentrations of the cylinders in Figure 6.16.

**Table 6.14 Volume of ponding solution absorbed and total chloride concentration of ponded OPC paste cylinders**

	<b>Vol. Ponding Solution Absorbed (mL)</b>	<b>Total Chloride Concentration (g Cl/g paste)</b>
<b>Control</b>	46	0.026
<b>CN1</b>	31	0.026
<b>CN2</b>	6	0.017
<b>Ca(NO<sub>3</sub>)<sub>2</sub></b>	9	0.017

Immediately apparent is that as a result of having absorbed the largest amounts of ponding solution, the Control and CN1 mixes have the highest total chloride concentrations. This is largely localized to the top 15 mm rather than being distributed throughout the top 40 mm, as is the case in the white cement containing nitrate. However, the CN2 and Ca(NO<sub>3</sub>)<sub>2</sub> mixes also contain high concentration of chlorides, despite having absorbed a much lower amount of ponding solution.

### **6.2.3 Qualification of Chloride Titration Results**

When considering results of chloride ion penetration into the cement paste cylinders, it must be remembered that acid soluble chlorides were measured. By dissolving the cement paste, this method measures the combined concentration of free chlorides and those that are chemically bound. It is therefore difficult to determine what proportion of the total concentration is attributable to free chlorides. With respect to corrosion of reinforcing steel, only the free chlorides are of concern. The measurement of water-soluble chlorides would have provided a better indication of the effect of calcium nitrite and calcium nitrate on free chloride concentrations, but the method is not considered as reliable. Therefore, the soluble chlorides, as determined by pore solution expression, is considered a more accurate indication of free chloride concentration. This data are reported in Chapter 7.

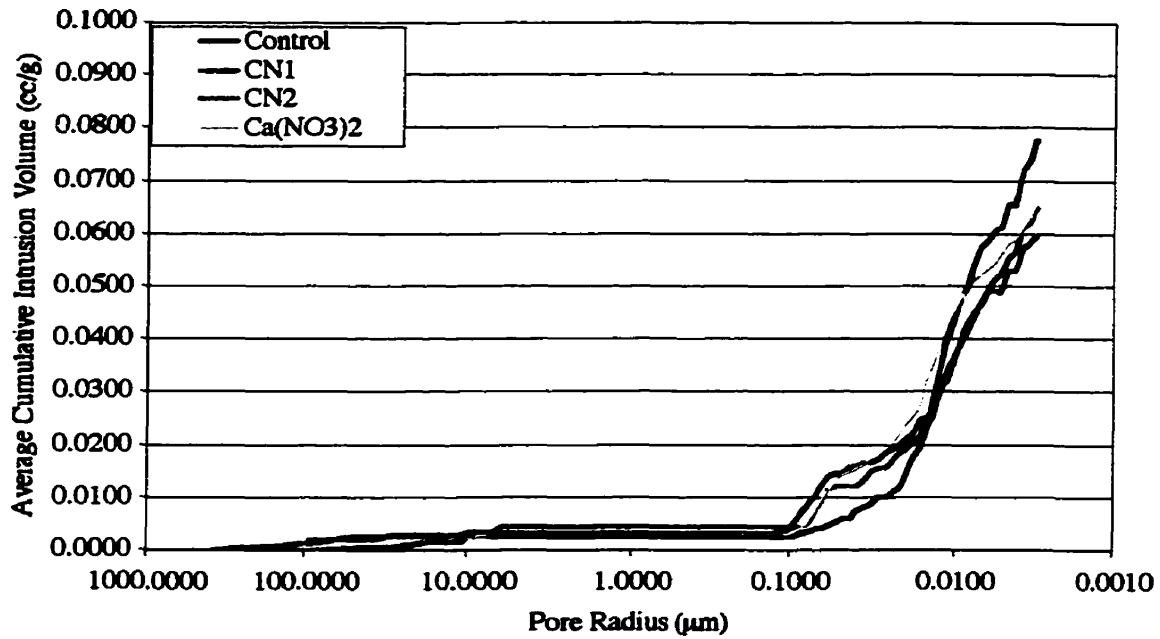


Figure 6.1 Cumulative intrusion volume vs. pore radius for average of three white cement paste cylinders

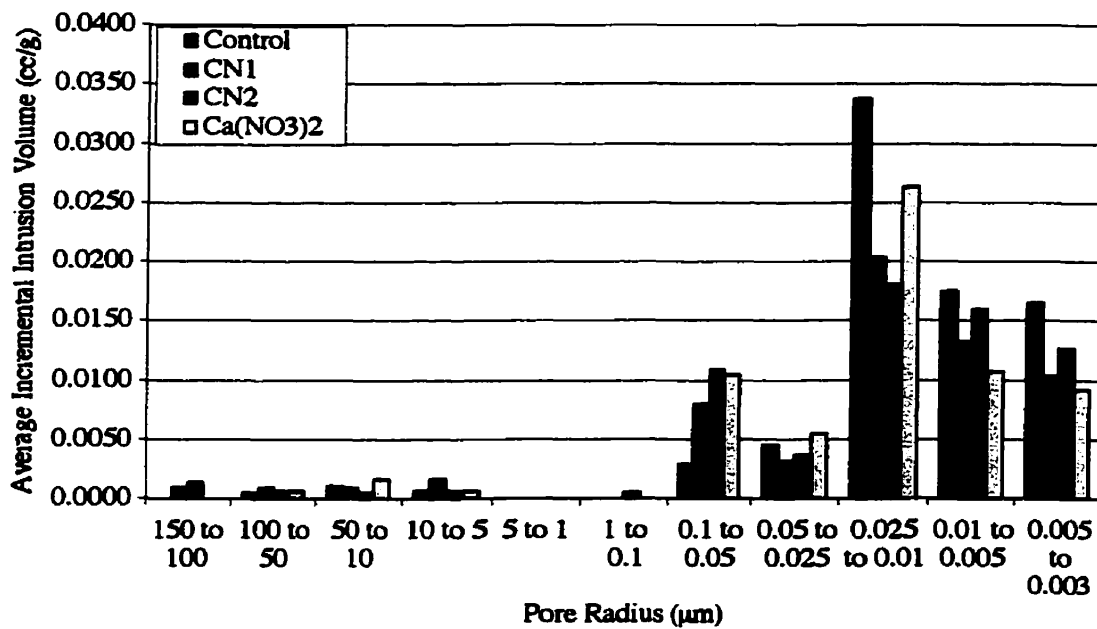


Figure 6.2 Average incremental intrusion volume vs. pore radius for white cement paste cylinders

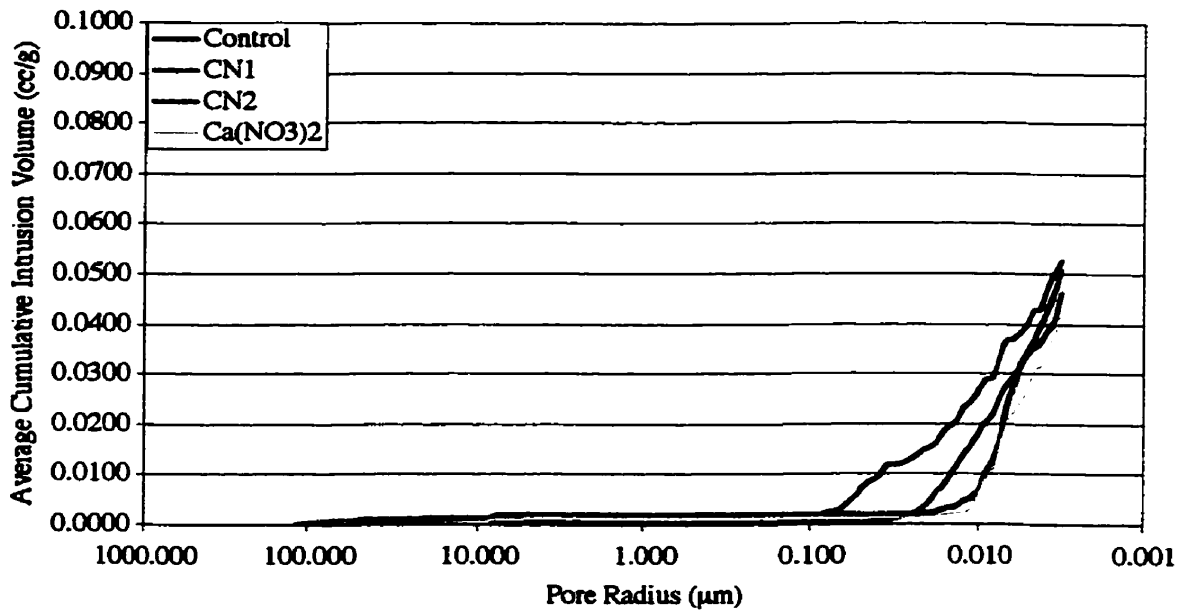


Figure 6.3 Cumulative intrusion volume vs. pore radius for average of three ponded white cement paste cylinders

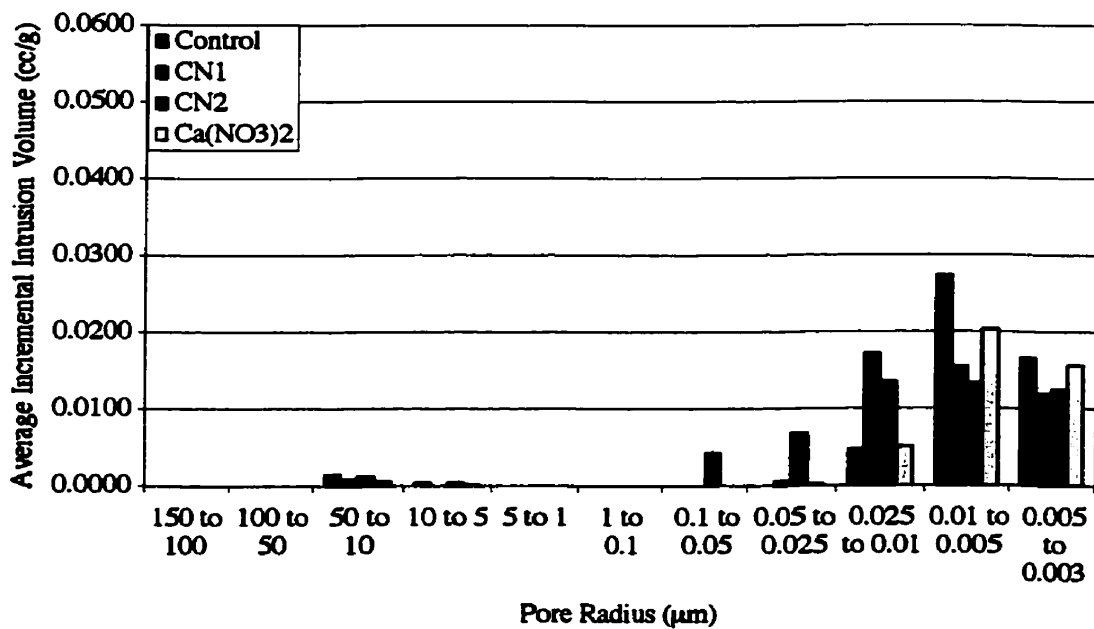


Figure 6.4 Average incremental intrusion volume vs. pore radius for ponded white cement paste cylinders

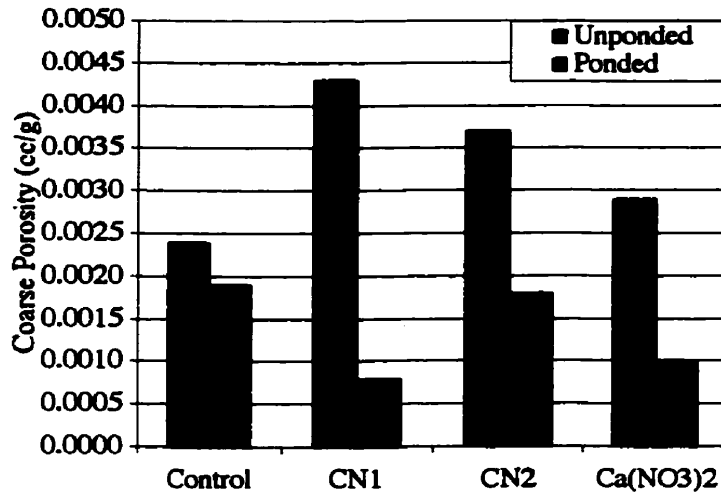


Figure 6.5 Comparison of coarse porosity of unponded and ponded white cement paste cylinders

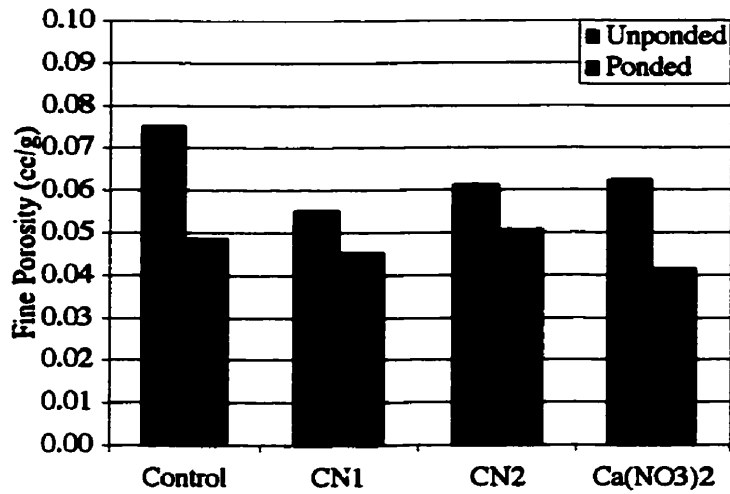


Figure 6.6 Comparison of fine porosity of unponded and ponded white cement paste cylinders

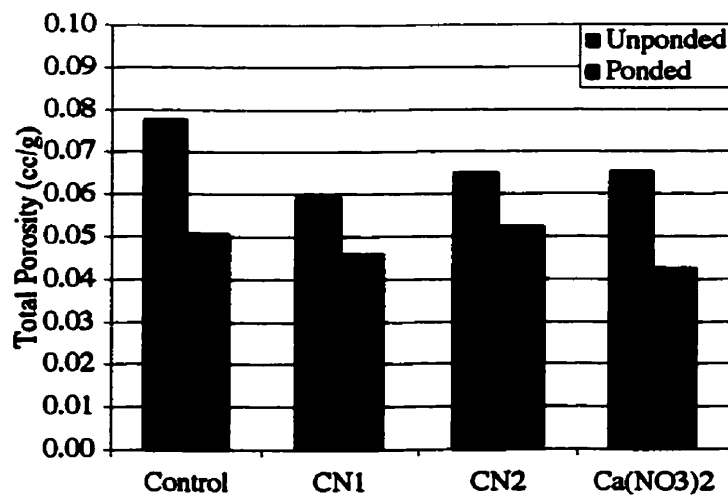


Figure 6.7 Comparison of total porosity of unponded and ponded white cement paste cylinders



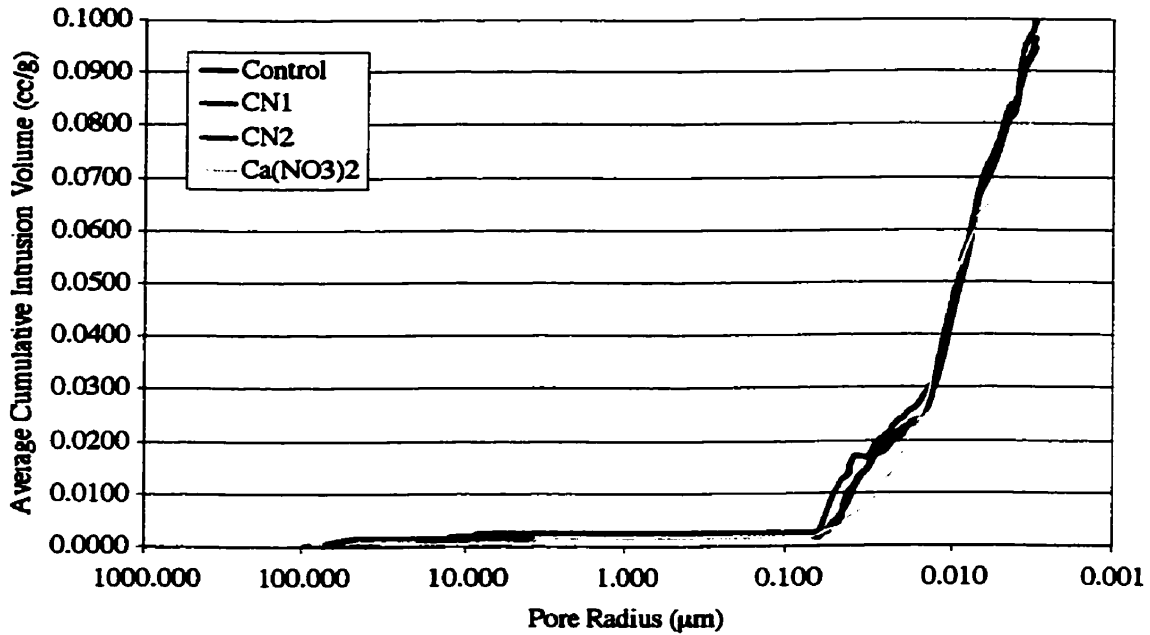


Figure 6.8 Cumulative intrusion volume vs. pore radius for average of three OPC paste cylinders

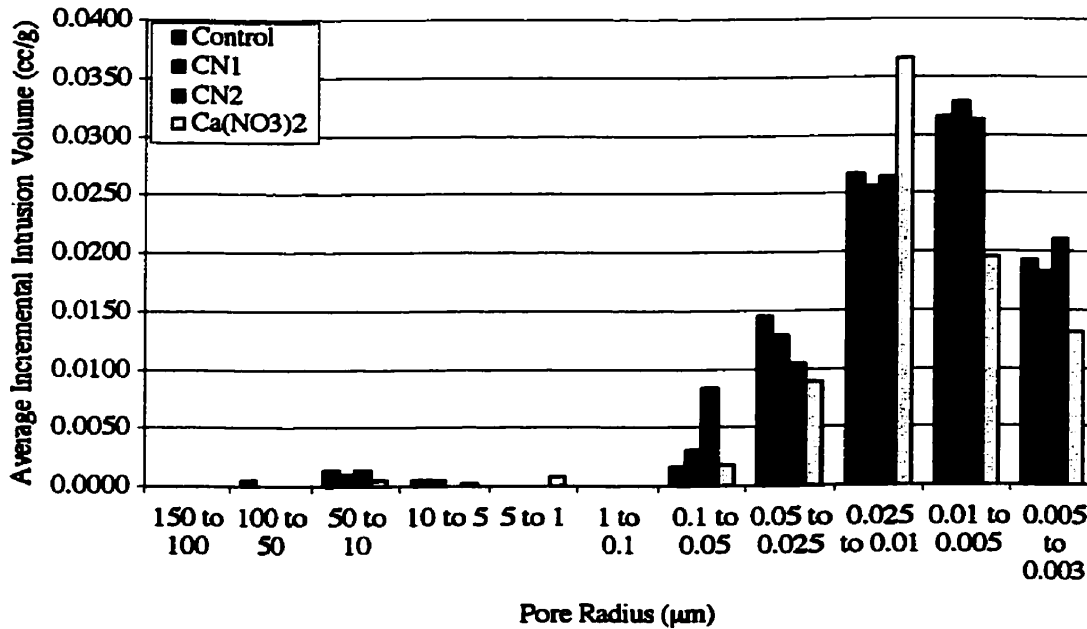


Figure 6.9 Average incremental intrusion volume vs. pore radius for OPC paste cylinders

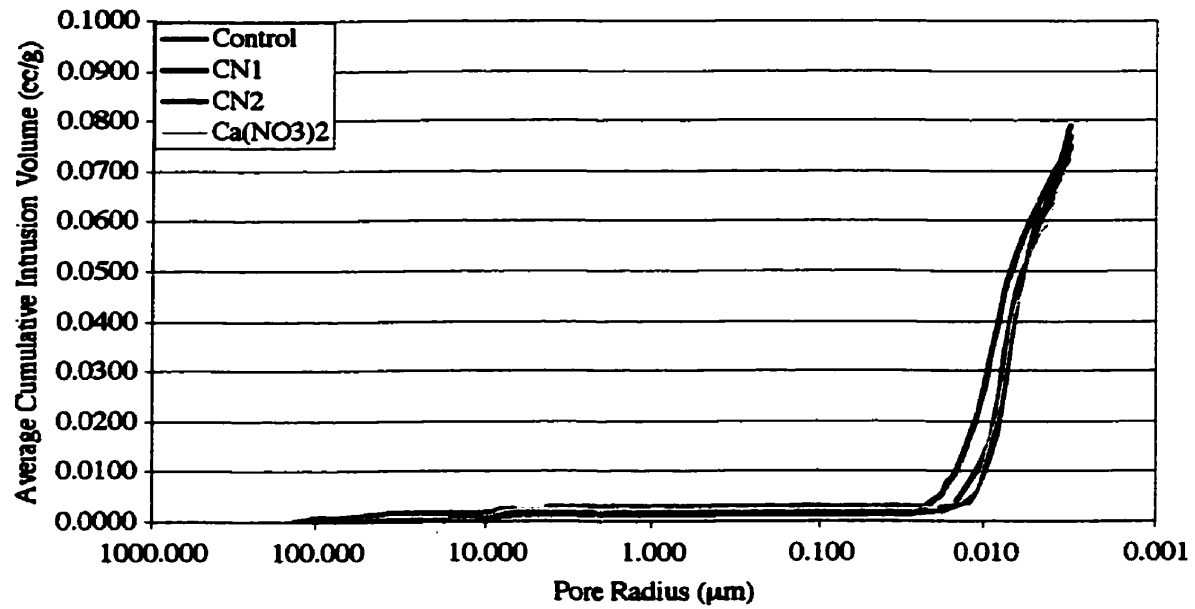


Figure 6.10 Cumulative intrusion volume vs. pore radius for average of three ponded OPC paste cylinders

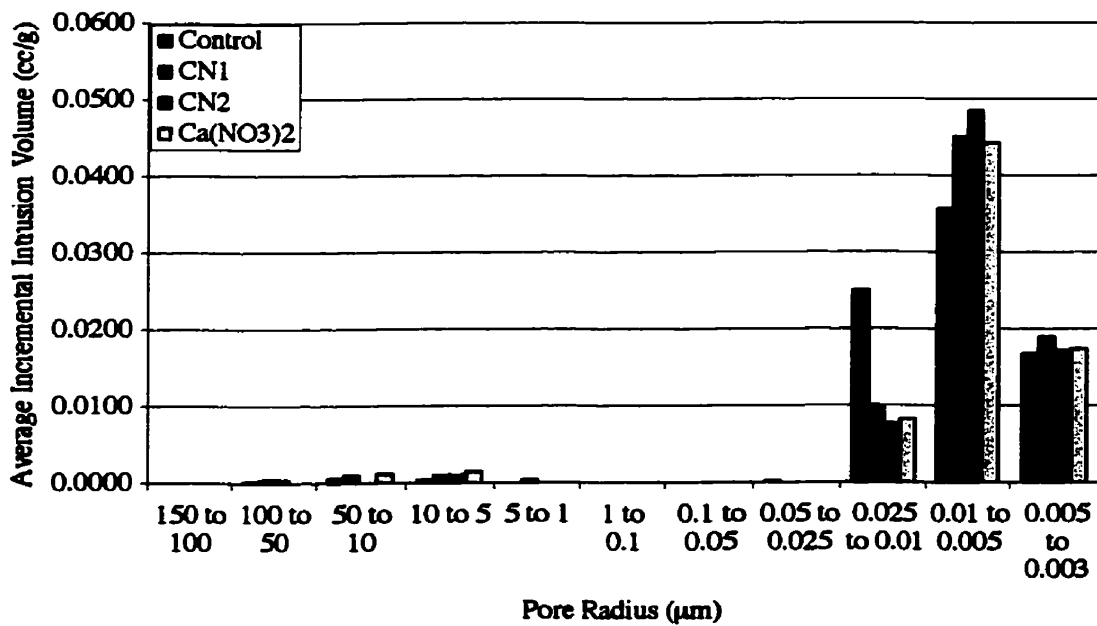


Figure 6.11 Average incremental intrusion volume vs. pore radius for ponded OPC paste cylinders

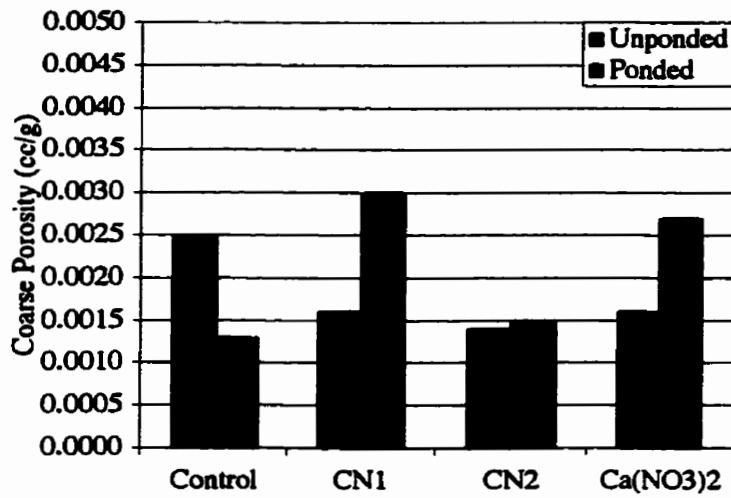


Figure 6.12 Comparison of coarse porosity of unponded and ponded OPC paste cylinders

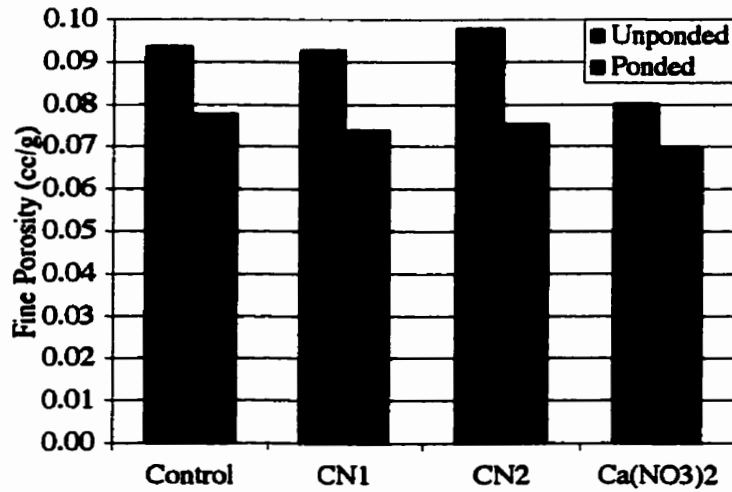


Figure 6.13 Comparison of fine porosity of unponded and ponded OPC paste cylinders

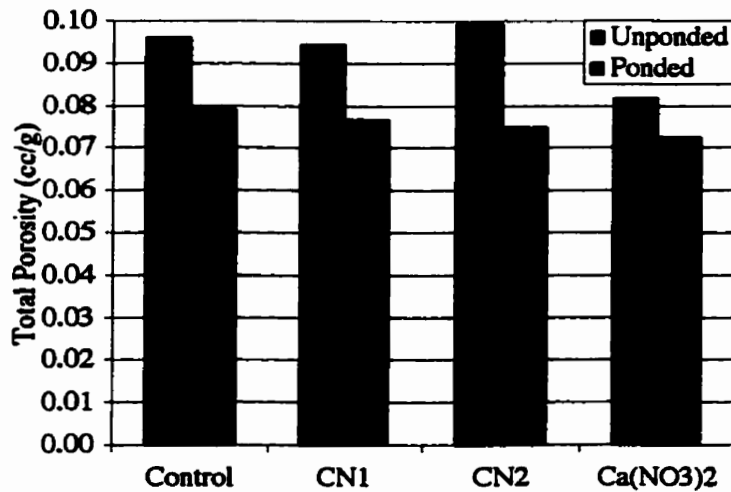


Figure 6.14 Comparison of total porosity of unponded and ponded OPC paste cylinders

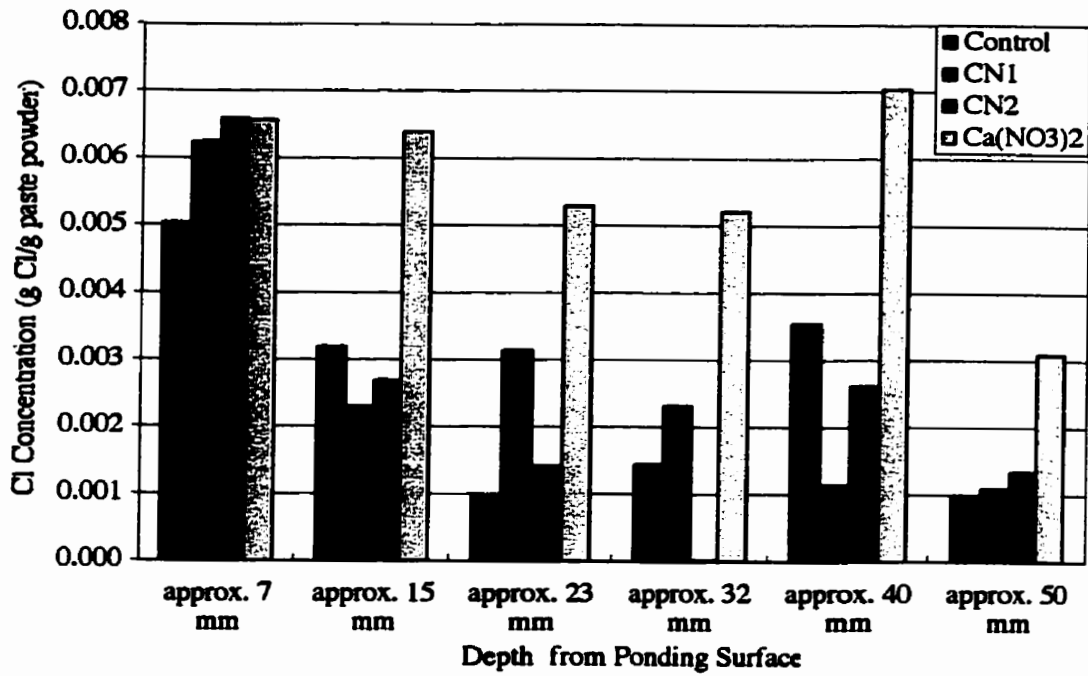


Figure 6.15 Chloride profiles for ponded white cement paste cylinders

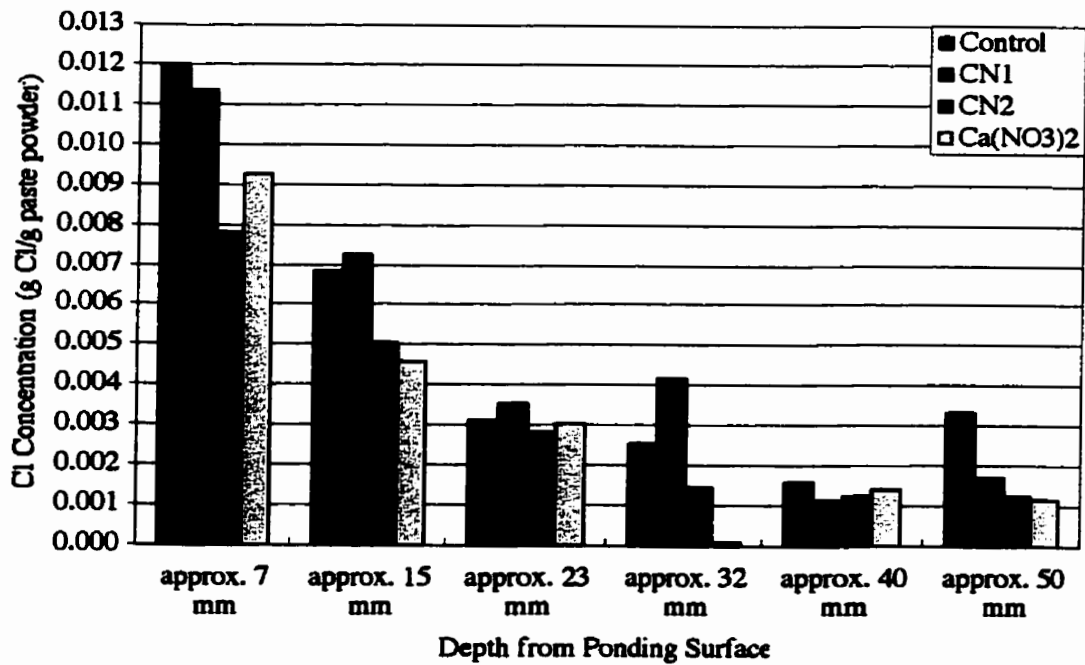


Figure 6.16 Chloride profiles for ponded OPC paste cylinders

## **Chapter 7**

### **Chemical Analysis of Cement Pastes**

#### **Results and Discussion**

#### **7.1 Thermal Analysis**

Although parallel experiments were conducted using DTA and TGA, more information was gathered through analysis of the differential thermogravimetric (DTG) plots than that generated by either the DTA and TGA curves. Consequently, the focus of this section will be on the DTG curves. It should also be noted that endothermic temperatures for the various hydration products could vary from researcher to researcher. Taylor (Taylor 1997) states that this temperature is dependent on the technique used (i.e. heating temperature, gas flow), the amount of phase present and likely the degree of crystallinity, and shifts of 10° to 20° can occur. Also apparent in all of the DTG curves is the loss in mass at the commencement of the experiment. It is believed that this mass loss is associated with the evaporation of capillary water within the cement paste, particularly as the magnitude of this mass loss is typically decreased in the second set of runs, which were performed approximately 2.5 hours after the first.

##### **7.1.1 Pure Components**

Figures 7.1 through 7.3 show representative differential thermogravimetric analysis curves generated for synthetic Friedel's salt, hydrated pure  $C_3S$  and hydrated pure  $C_3A$  and gypsum, respectively. The dominant endotherms for Friedel's salt are identified at approximately 109° and 330°. These results are similar to those of Birnin-Yauri and Glasser (Birnin-Yauri 1998), who found dominant endotherms at 120° and 290°. Skalny and Odler (Skalny 1967) however, found the dominant endotherm of Friedel's salt at a temperature of 200°, which is near a minor endotherm in the present analysis.

The products of  $C_3S$  hydration are C-S-H and calcium hydroxide, which have major endotherms at approximately  $81^\circ$  and  $425^\circ$ , respectively. Slightly different temperatures are reported by Taylor (Taylor 1997), who reports C-S-H at approximately  $100^\circ$  while studies by Skalny and Odler (Skalny 1967) observed the endotherm associated with C-S-H at approximately  $150^\circ$  and that of  $Ca(OH)_2$  at  $540^\circ$ . However, there appears to be some confusion regarding the exact nature of the decomposition at this temperature. Although it is likely that capillary and gel water is removed from the structure at these temperatures, it is unlikely that the water chemically combined in the C-S-H is being removed, as concrete is often used at temperatures well above  $150^\circ C$ . Taylor (Taylor 1997) also reports that C-S-H experiences a gradual mass loss over a temperature range of  $50^\circ C$  to  $900^\circ C$ , again suggesting that no sharp endotherm is associated with the decomposition of C-S-H.

Theoretically, the only product remaining from hydration of  $C_3A$  and gypsum in the proportions used, should be AFm, which is stoichiometrically varied in chemical composition. Dominant endotherms from this hydration reaction are identified at approximate values of  $56^\circ$ ,  $96^\circ$ ,  $155^\circ$ ,  $247^\circ$ ,  $277^\circ$ , and  $842^\circ$ . Taylor (Taylor 1997) lists a variety of endotherms associated with the AFm phase (i.e.  $85^\circ$ ,  $100^\circ$ ,  $135^\circ$ ,  $200^\circ$ ,  $290^\circ$ ,  $440^\circ$ ,  $480^\circ$ ,  $575^\circ$ ,  $715^\circ$ , and  $860^\circ$ ), which are close in value to those determined by the present thermal analysis.

### **7.1.2 White Cement Paste Cylinders**

#### **7.1.2.1 Unponded Cylinders**

Figure 7.4 shows representative differential thermogravimetric analysis curves of white cement paste cylinders. Curves for individual samples can be found in Appendix D,

Figures D.1 to D.4. Only three major endotherms are evident in all of the cement mixes. The endotherm at approximately 80° can be associated with two phenomena: the evaporation of capillary pore water (Fordham 1985) and/or the evaporation of the C-S-H gel water (Taylor 1997). Although the endotherms at 80° and 350° are coincident with endotherms associated with AFm, the low concentrations within the white cement suggest that very low volumes of this phase will form. Therefore, this endotherm at 350° is most likely associated with C-S-H, and is near the low intensity endotherm at 347° for the C-S-H in Figure 7.2. The endotherm associated with a temperature of 425° is well documented to be that of calcium hydroxide.

Figure 7.5 shows the total quantitative values for the components identified in Figure 7.4, as determined by combining the area below each endotherm of each of the samples run for each mix. The quantity from the first experiment shown as a striped region and the solid region representing the portion from the second experiment. It is very difficult to draw any conclusions regarding the significance of proportions associated with the evaporation of the capillary and gel water. Little difference is evident between mixes with regards to the proportion of C-S-H as identified at endotherm 350°. Very slightly higher levels of calcium hydroxide are formed in mixes with inhibitors, with that containing calcium nitrate showing the largest increase over Control. These small differences may be attributed to the technique used for calculation of the endotherm areas. However, this may also be a true result given the accelerating properties of both calcium nitrite and calcium nitrate. It is believed that both of these chemicals act as set accelerators on the same principle as that proposed for CaCl<sub>2</sub>. Ramachandran (Ramachandran 1971) states that when CaCl<sub>2</sub> is added to a hydrating cement there is a

reduction in alkalinity of the capillary water. The cement system then compensates by liberating more hydroxide ( $\text{Ca}(\text{OH})_2$ ) through increased hydration of  $\text{C}_3\text{S}$ , which would also lead to the formation of C-S-H. Therefore, the calcium hydroxide level may be an indication of the degree of hydration of the calcium silicate compounds. As a pH drop is also observed in synthetic pore solutions upon addition of CN1, a similar increase in  $\text{C}_3\text{S}$  hydration is likely occurring. This result also suggests that in the mixes containing these admixtures, the nitrite ion is likely interchangeable with any negatively charged ions within the C-S-H structure.

#### 7.1.2.2 Pondered Cylinders

Figure 7.6 shows representative differential thermogravimetric analysis curves of pondered white cement paste cylinders. Curves for individual samples can be found in Appendix D, Figures D.5 to D.8. Again, only three major endotherms can be resolved in these cement mixes. The first, at approximately  $80^\circ$ , is again a combination of the evaporation of capillary and gel water. A slight inflection in the DTG curve can be seen at approximately  $110^\circ$ , which is coincident with an endotherm associated with Friedel's salt as shown in Figure 7.1. However, the magnitude of the endotherm is so small that quantitative data could not be obtained. The endotherm at  $335^\circ$  can be attributed to a combination of C-S-H phase and the formation of Friedel's salt. The endotherm at  $420^\circ$  is once again attributed to  $\text{Ca}(\text{OH})_2$ .

Figure 7.7 compares quantities of identified phases in Figure 7.6 between mix compositions. Little difference is apparent between the total amount of capillary and gel water between the Control mix and that containing calcium nitrate. Little variation exists between the amount of Friedel's salt/C-S-H between the different mixes, however, as the



endotherms overlap, it is difficult to delineate between the proportions of the two phases. Slightly higher amounts of  $\text{Ca}(\text{OH})_2$  in the mix containing CN1 are observed as compared to the Control and  $\text{Ca}(\text{NO}_3)_2$  mixes, while the mix containing CN2 has a slightly lower volume than that of Control.

The small amount of Friedel's salt in the Control, CN1, and CN2 mixes is not surprising for several reasons. As stated in the previous section, the low concentration of  $\text{C}_3\text{A}$  in the white cement would result in a low volume of AFm formation, thereby limiting the amount of Friedel's salt that can form. Byfors (Byfors 1986) and Byfors et al. (Byfors 1986) found that the chloride binding capacity of concrete is related to the combined  $\text{C}_3\text{A}$  and  $\text{C}_4\text{AF}$  content of the cement. As virtually no  $\text{C}_4\text{AF}$  exists in the white cement examined, this is likely to affect the chloride binding capacity of the paste produced. As well, these mixes absorbed small volumes of ponding solution (9 mL, 6 mL, and 8 mL, respectively). This, in addition to the location of the samples tested (approximately 2 cm in depth from the ponding surface), would suggest that a limited amount of ponding solution has penetrated to this level. However, it is surprising that a higher proportion of bound chlorides are not observed in the mix containing calcium nitrate, given a higher volume of ponding solution (40 mL) was absorbed. This suggests that significant proportions of the absorbed chlorides are dissolved within the pore solution and therefore, exist in the "free" state.

### 7.1.2.3 Comparison of Unponded and Ponded Cylinders

All mixes show a significant decrease in the DTG endotherm attributed to capillary and gel water with exposure to the ponding solution. The reduction in this endotherm is likely due to the reduction of water incorporated in the calcium silicate hydrate phase.

With increasing salt content of the capillary water, a reduction in the activity of the water would result in a loss of water in the hydrated C-S-H phases (Reardon 2001). As C-S-H is not stoichiometrically fixed in composition, this result is not of great significance. It must be noted however that due to the observed evaporation of capillary water associated with this endotherm location, it is difficult to draw definitive conclusions regarding the exact occurrences at this temperature.

Due to the combination of the endotherms associated C-S-H and Friedel's salt, it is difficult to draw conclusions regarding the effect of ponding on these phases.

Slightly higher proportions of  $\text{Ca(OH)}_2$  exist in the Control and CN1 mixes upon exposure to the ponding solution, while the opposite occurs in the CN2 and  $\text{Ca(NO}_3)_2$  mixes. Further hydration of anhydrous calcium silicates may have occurred due to the ingress of more water, thereby increasing the calcium hydroxide content. However, as the quantities are relatively low, the observed changes in calcium hydroxide concentration are considered statistically insignificant.

### 7.1.3 OPC Paste Cylinders

#### 7.1.3.1 Unponded Cylinders

Figure 7.8 shows representative DTG curves of OPC paste cylinders. Curves for individual samples can be found in Appendix D, Figures D.9 to D.12. Five significant endotherms are apparent in all mix compositions. In most cases, the occurrence of each endotherm can be associated with the dehydration of two phases within the cement paste. The endotherm at  $80^\circ$  is associated with the combined evaporation of capillary and gel water. As higher concentrations of  $\text{C}_3\text{A}$  exist in the OPC cement, an increased number of

endotherms exist associated with the dehydration of its hydration products. AFm is apparent at two endotherms, namely 133° and 350°, while the dehydration of  $C_3AH_6$  occurs at 350°. The endotherm at 590° is also likely associated with AFm, as it is relatively near the AFm peak at 575° in list by Taylor (Taylor 1997). Although a peak at 575° is attributed to C-S-H in Figure 7.2, it is felt that this is likely due to AFm because of its absence in the white cement and the higher  $C_3A$  content in the OPC cement. As with white cement, the peak at 350° may also be associated with the C-S-H phase. Dehydration of calcium hydroxide is evident at the 430° endotherm.

Figure 7.9 compares quantities of phases identified in Figure 7.8 in the various mixes produced. It is difficult to draw conclusions regarding the effect of inhibitors on capillary and gel water. The addition of inhibitors to the OPC paste appears to have little effect on the production of the other phases present within the paste matrix. Minimal differences exist in the quantities of AFm and other products of  $C_3A$  hydration existing between all mix designs. Slightly higher quantities of calcium hydroxide are observed in the mixes containing CN1 and calcium nitrate, which is expected given that they are set accelerators.

#### 7.1.3.2 Ponded Cylinders

Figure 7.10 shows representative DTG curves of OPC paste cylinders exposed to ponding solution. Curves for individual samples can be found in Appendix D, Figures D.9 to D.12. The endotherm at 80° is associated with the evaporation of capillary and gel water. The endotherm at 135° is likely associated with Friedel's salt, as it is near the dominant endotherms of 109° seen in Figure 7.1 as well as that identified by Birnin-Yauri and Glasser (Birnin-Yauri 1998) at 120°. The endotherm at 350° is predominantly a

combination of the dehydration of Friedel's salt, AFm and C-S-H. Calcium hydroxide is again identified at an endotherm of approximately 430°. Ramachandran (Ramachandran 1971) identified the endotherm at 590° as indicative of the presence of calcium hydroxychloride (Ca-OH-Cl), which can lie in the range of 550° to 600°. Skalny and Odler (Skalny 1967) found a similar endotherm at approximately 640°. However, this endotherm was identified as a AFm in the unponded OPC pastes. It is also speculated by Ramachandran (Ramachandran 1971) that an endotherm at 800° may be associated with chlorides incorporated within the C-S-H phase. Fordham and Smalley (Fordham 1985) identified the 800° endotherm as the decarbonation of CaCO<sub>3</sub>. However, as the cylinders used in this experiment had limited contact with the atmosphere, it is highly unlikely that any significant level of carbonation occurred. Further evidence that this endotherm is associated with a chloride species is the lack of its presence in cylinders that were not exposed to ponding solution.

Figure 7.11 compares quantities of the first four phases identified in Figure 7.10 in the ponded OPC mixes. Slightly higher quantities of Friedel's-AFm-C-S-H phases and calcium hydroxide are present in the Control mix as compared to the inhibited mixes, which have approximately the same quantities. However, this may be due to limitations in the measurement technique.

Figures 7.12a through 7.12d show magnified representative DTG data for each of the ponded OPC paste mixes, focussing on the temperature range of 500° to 1000° to enhance the endotherms believed to be associated with calcium hydroxychloride and chloride incorporated within the C-S-H phase. Immediately apparent is the lack of an endotherm at 590° in the ponded Control mix. It is therefore likely that this endotherm is due to

calcium hydroxychloride rather than AFm. Although this endotherm is slightly less prominent in the ponded mixes containing CN2 and  $\text{Ca}(\text{NO}_3)_2$ , it is clearly present in the ponded mix containing CN1. The endotherm at  $790^\circ$  associated with Cl in C-S-H is plainly visible in all ponded mixes.

Figure 7.13 gives quantitative areas for the endotherms identified in Figure 7.12.

Although small quantities were detected, all inhibited mixes showed higher proportions of Ca-OH-Cl and Cl in C-S-H than the Control mix, with the mix containing CN1 having the highest values. This information must be considered with the volume of ponding solution absorbed by each mix. Despite having absorbed the highest volume of ponding solution (approximately 46 mL), the Control mix shows the lowest proportion of calcium hydroxychloride and Cl in C-S-H. This suggests that the presence of the inhibitors enhances the formation of these forms of bound chloride within the cement paste. If the amount of these forms of bound chlorides is compared to the volume of ponding solution absorbed by each inhibited mix, as shown in Table 7.1, all inhibited mixes show higher binding values than Control, with mixes containing CN2 and  $\text{Ca}(\text{NO}_3)_2$  the most effective at binding chlorides in these forms.

Table 7.1 Binding capacities of OPC paste mixes

	<b>Total Bound Chlorides (%/°C.min)</b>	<b>Volume Ponding Solution Absorbed (mL)</b>	<b>Bound Chlorides per Volume Ponding Solution (%/°C.min/mL)</b>
<b>Control</b>	0.012226	46	$2.7 \times 10^{-4}$
<b>CN1</b>	0.032891	31	$1.1 \times 10^{-3}$
<b>CN2</b>	0.023524	6	$3.9 \times 10^{-3}$
<b><math>\text{Ca}(\text{NO}_3)_2</math></b>	0.025083	9	$2.8 \times 10^{-3}$

### 7.1.3.3 Comparison of Unponded and Ponded Cylinders

Due to the overlapping of a significant number of phases within the DTG curves, it is

difficult to compare quantities of the majority of phases before and after exposure to ponding solution. A mass increase with  $\text{Ca(OH)}_2$  is observed in the Control mix and mixes containing calcium nitrite inhibitor, while a negligible effect is seen in the mix containing calcium nitrate. This would suggest that some degree of further hydration of unreacted calcium silicate phases is occurring, as calcium hydroxide would be a by-product of this reaction.

### **7.2 Pore Solution Expression**

Complete analyses of the expressed pore solutions for all mixes can be found in Appendix E, Tables E.1 through E.4. Cement and inhibitor molar calculations can be found in Appendix E, Tables E.5 and E.6, respectively. Conversions of expressed pore solution concentrations for all mixes can also be found in Appendix E, Tables E.7 through E.14.

In order to obtain sufficient quantities of expressed pore solution from the cement paste cylinders, it was necessary to use a whole cylinder exposed to ponding solution.

Therefore, the analyses were made on samples which were different and which absorbed different amounts of ponding solution from those used for porosimetry, titration and thermal analysis. As such, results from previous sections may not be directly comparable.

Based on the calculated amount of capillary pore solution in parallel samples, it appears that the volume of expressed solution correspond to almost all of the capillary solution in the sample. Exact calculations cannot be made because of the variation in the original porosity and in the amount of absorbed ponding solution.

## **7.2.1 White Cement Paste Cylinders**

### **7.2.1.1 Unponded Cylinders**

Figures 7.14a and 7.14b show the concentrations of key components of pore solutions expressed from white cement paste cylinders. Slightly lower chloride concentrations are observed in mixes containing inhibitor as compared to the Control mix, which may indicate that more chloride binding is occurring in the inhibited mixes. As virtually no chloride exists within the cement powder (0.008 wt. %), the source is likely the mixing water used to make the pastes. Slightly higher sulphate concentrations exist in the CN1 mix as compared to Control, while slightly lower values are detected from the other two mixes. As the only source of sulphate is from the gypsum within the cement powder, this suggests that CN1 reduces the reaction between gypsum and  $C_3A$ , thereby reducing the volume of AFt from the initial reaction. The opposite would be true for mixes containing CN2 and  $Ca(NO_3)_2$ . Sulphur levels remain relatively independent of mix design. This measurement takes into consideration all sulphur containing species, including sulphate.

As expected, higher concentrations of sodium relative to potassium are observed, which is consistent with the higher percentage of  $Na_2O$  than  $K_2O$  in the cement powder (0.17% and 0.12%, respectively). However, in both mixes containing nitrite, slightly higher concentrations of sodium and potassium are present in solution. Negligible amounts of  $SiO_2$  are present in any of the expressed pore solutions. Slightly higher concentrations of calcium are observed in the CN2 and  $Ca(NO_3)_2$  pore solutions relative to Control and CN1 pore solutions, which have very similar values.

Figure 7.15 presents the alkalinity values determined for each expressed pore solution. The concentration label “to pH 10” is attributed to the volume of acid needed to reduce

the pH of the solution to a value of 10. It is generally accepted that the ion being reduced at this level is hydroxide. Therefore, it is possible to convert the concentration into a pH value by noting that one “meq/L” is equal to one “mmol/L”. These conversions are listed in Table 7.2. Negligible changes in pH are observed for the inhibited expressed solutions as compared to the Control expressed solution. The smaller effect of the inhibitor on the pH of the pore solution within the cement paste as compared to those described in Chapter 5 for synthetic pore solutions is due to greater capacity for chemical binding in the cement than in synthetic pore solution.

Table 7.2 Conversion of alkalinity values to pH value for White Cement Paste expressed pore solutions

	Control	CN1	CN2	Ca(NO <sub>3</sub> ) <sub>2</sub>
<b>Concentration (meq/L)</b>	215	201	229	186
<b>pH</b>	13.3	13.3	13.4	13.3

#### 7.2.1.2 Poneded Cylinders

Figures 7.16a and 7.16b show the concentrations of the key components in pore solutions expressed from ponded white cement paste cylinders. It should be noted that only the top 5 cm of the cylinders were expressed, as it was felt that this portion of the cylinder would be more representative of the concrete cover, and hence, would have more effect on the corrosion of the reinforcing steel. Significantly higher levels of sulphate are present in the mix containing Ca(NO<sub>3</sub>)<sub>2</sub> as compared to the solutions from the other mixes. Calcium levels in solutions of mixes containing inhibitors are lower than that observed in the Control mix, despite an increase in total calcium concentration to the mixes as a result of inhibitor addition. Silica levels in the CN1 mix solution are relatively low compared to those observed within the other mix solutions, which are somewhat similar to one another. Potassium levels appear to remain constant despite the presence of inhibitors.



Significantly higher levels of sodium and chlorides are present in the solution expressed from the mix containing  $\text{Ca}(\text{NO}_3)_2$ . Table 7.3 relates the chloride and sodium concentrations as determined through expressed pore solution analysis to the volume of ponding solution absorbed by each cylinder. Comparison of the volumes of ponding solution absorbed show that the mix containing calcium nitrate absorbed approximately nine times more solution than the Control and CN1 mixes and approximately seven times more than the mix containing CN2. It should also be noted that despite having absorbed approximately the same volume of ponding solution, significantly less chloride is present in the expressed solution obtained from the cylinder made with mix containing CN1 inhibitor as compared to the cylinders made from the Control mix and that containing CN2. If a concentration is determined based on the volume of ponding solution absorbed, the mix containing CN1 has a lower concentration by one order of magnitude than the Control mix. As chlorides within the pore solution are considered responsible for corrosion of the reinforcing steel, lower concentrations would be advantageous. This also should demonstrate that chlorides are incorporated into solid products within the cement paste matrix since they are not present in the pore solution. Sodium concentrations, however, appear to be relatively constant between mixes and independent of the volume of ponding solution absorbed, as also indicated in Chapter 6. Therefore, the solid chloride product is associated with a cation other than sodium, the most likely candidates being calcium and/or potassium.

Low levels of nitrite are detected in the Control and  $\text{Ca}(\text{NO}_3)_2$  mixes, while low levels of nitrate are observed in the Control, CN1 and CN2 mixes. Table 7.4 compares the admixed quantities of these species to those found in the expressed solutions. In the

Table 7.3 Relationship of Na and Cl concentrations to the volume of absorbed ponding solution in ponded White Cement Paste cylinders

	Absorbed Ponding Solution (mL)	Expression Analysis (mg/L)		Conc./Sol. Absorbed (mg/L/mL)		[Conc.]/Sol. Absorbed (M/mL)	
		Na	Cl	Na	Cl	Na	Cl
Control	7	4720	831	674	119	$2.93 \times 10^{-2}$	$3.35 \times 10^{-3}$
CN1	7	4410	31.7	630	4.53	$2.74 \times 10^{-2}$	$1.28 \times 10^{-4}$
CN2	9	8420	1970	936	219	$4.07 \times 10^{-2}$	$6.17 \times 10^{-3}$
Ca(NO <sub>3</sub> ) <sub>2</sub>	62	12900	11000	586	177	$2.55 \times 10^{-2}$	$5.07 \times 10^{-3}$

cases of mixes containing CN1 and Ca(NO<sub>3</sub>)<sub>2</sub>, only a minor amount of the originally admixed nitrite or nitrate exists within the expressed pore solutions, while a slightly higher proportion exists in the pore solution from the mix containing CN2. As such low proportions of the original quantities mixed into the cement paste are present in the expressed pore solution, this suggests that the admixed nitrite or nitrate is in solid form within the cement paste matrix. The mechanism of corrosion inhibition, as proposed by the calcium nitrite manufacturers, suggests that the nitrite ion enhances the formation of the passive film on the steel surface. In order for this to occur, the nitrite ion would have to remain in a liquid state. Hence this result further supports the contention that the accepted mechanism is not the one by which corrosion inhibition is provided by calcium nitrite.

Table 7.4 Comparison of molar quantities of nitrite and nitrate from admixture and expressed solutions from Ponded White Cement Paste cylinders

	CN1		CN2		Ca(NO <sub>3</sub> ) <sub>2</sub>	
	NO <sub>2</sub>	NO <sub>3</sub>	NO <sub>2</sub>	NO <sub>3</sub>	NO <sub>2</sub>	NO <sub>3</sub>
Added (moles)	$2.2 \times 10^{-2}$	n/a	$2.2 \times 10^{-2}$	n/a	n/a	$1.7 \times 10^{-2}$
Expressed (moles)	$4.2 \times 10^{-5}$	$4.5 \times 10^{-7}$	$2.7 \times 10^{-3}$	$9.2 \times 10^{-6}$	$5.5 \times 10^{-8}$	$5.9 \times 10^{-5}$
% in Solution	0.2 %	n/a	12 %	n/a	n/a	0.3 %

Figure 7.17 shows the alkalinity values of the expressed pore solutions of the ponded white cement paste cylinders, while Table 7.5 lists the equivalent pH values based on the hydroxide concentration as specified by the term "to pH 10". While slightly higher pH

values are noted in solutions expressed from CN2 and  $\text{Ca}(\text{NO}_3)_2$  mixes compared with Control, a slightly lower value is observed for the CN1 mix. The differences between the two calcium nitrite based inhibitors suggests that although both contain the same active ingredient for corrosion inhibition, other chemical differences between the two admixtures are having dissimilar effects on the pore solution upon exposure to ponding solution.

**Table 7.5 Conversion of alkalinity values to pH values for Ponded White Cement Paste expressed pore solutions**

	<b>Control</b>	<b>CN1</b>	<b>CN2</b>	<b><math>\text{Ca}(\text{NO}_3)_2</math></b>
<b>Concentration (meq/L)</b>	79	58	81	94
<b>pH</b>	12.9	12.8	12.9	13.0

### 7.2.1.3 Comparison of Unponded and Ponded Cylinders

Figures 7.18a and 7.18b compare the concentrations of key components in the pore solutions expressed from unponded and ponded white cement paste cylinders. In all mixes, except that containing CN1, an increase in sulphate is observed in the pore solution expressed from the ponded cylinders relative to that from the unponded cylinders, while parallel trends are observed for total sulphur concentrations. This suggests that sulphate is being dissolved from the solid phases of the cement paste matrix. It is likely that this is due to chloride being bound in the form of Friedel's salt, resulting in an exchange between sulphate and chloride within the AFm structure, thereby accounting for the higher concentrations of sulphate in the expressed pore solution. Sulphate concentrations are significantly higher in the solution expressed from the calcium nitrate mix. However, as shown in Table 7.3, this pore solution also has the highest concentration of chlorides. This may indicate that the chloride binding capacity of the mix containing calcium nitrate has been exceeded. Also worthy of note is the

significant decrease in calcium concentration of all expressed solutions upon exposure to ponding solution, with the CN2 mix showing the largest decrease ( $\Delta[\text{Ca}] = 938 \text{ mg/L}$ ), followed by  $\text{Ca}(\text{NO}_3)_2$  (589 mg/L), CN1 (353 mg/L) and Control (302 mg/L). This may be a result of precipitation of calcium-containing species, possibly bound forms of chlorides (i.e. calcium hydroxychloride).

As expected, higher concentrations of sodium are observed in the solutions expressed from all the ponded mixes. As well, higher concentrations are observed in the CN2 and  $\text{Ca}(\text{NO}_3)_2$  mixes as they absorbed the largest volume of solution. Potassium and silica levels remain virtually unaffected in all mixes.

Table 7.6 compares the pH values of the expressed solutions from the unponded and ponded cylinders. All mixes experience a decrease in pH upon exposure to ponding solution, with CN1 experiencing the largest reduction. The pH drop could be due to either precipitation of hydroxides or by the dilution of the pore solution. However, the observed decrease is not proportional to the volume of ponding solution absorbed, as the ponded  $\text{Ca}(\text{NO}_3)_2$  mix absorbed the highest volume of solution (62 mL) but experienced the lowest reduction of pH. On the other hand, the ponded CN1 experienced the largest pH drop but absorbed the least amount of solution (7 mL). This would suggest that the reduction in pH is due to a dilution effect of the ponding solution.

Table 7.6 pH of expressed pore solutions from Unponded and Ponded White Cement Paste Cylinders

	Unponded	Ponded	$\Delta\text{pH}$
Control	13.3	12.9	0.4
CN1	13.3	12.8	0.5
CN2	13.4	12.9	0.5
$\text{Ca}(\text{NO}_3)_2$	13.3	13.3	0.3

## **7.2.2 OPC Paste Cylinders**

### **7.2.2.1 Unponded Cylinders**

**Figures 7.19a and 7.19b show the concentrations of the key components of the pore solutions expressed from OPC paste cylinders. Higher levels of chloride are present in the solutions expressed from the Control and CN2 mixes. This suggests that if chlorides are present at the time of mixing, cement pastes containing CN1 and  $\text{Ca}(\text{NO}_3)_2$  are more effective at binding the chlorides, thereby reducing the concentration of “free” chlorides available to breakdown the passive film on the steel surface. However, as relatively low chloride concentrations are present in all mixes, this conclusion is difficult to draw.**

**Higher levels of sulphate are present in solutions from all mixes containing inhibitors, indicating that substitution of sulphate by other anions, possibly nitrite or nitrate, in the cement paste phases is occurring. A significantly higher calcium concentration is detected in solution expressed from CN1 mix than the Control whereas those in CN2 and  $\text{Ca}(\text{NO}_3)_2$  mixes are lower than Control. This may be due to a greater degree of hydration of the calcium silicate components in the CN1 mix, due to its addition of calcium ions as the nitrite. The reduced calcium ion concentration in the CN2 solution is explained in Chapter 8.**

**Insignificant differences exist between silicate levels in expressed pore solution between the mixes. In all mixes, higher potassium than sodium levels are noted reflecting the higher initial concentration of  $\text{K}_2\text{O}$  in the original cement. Higher potassium and sodium levels are present in mixes containing inhibitors. Consequently, higher alkalinity or pH values should be seen in the expressed pore solutions from these mixes. This is indeed seen to be the case, as demonstrated in Figure 7.20 and Table 7.7.**

**Table 7.7 Conversion of alkalinity values in pH value for OPC Paste expressed pore solutions**

	<b>Control</b>	<b>CN1</b>	<b>CN2</b>	<b>Ca(NO<sub>3</sub>)<sub>2</sub></b>
<b>Concentration (meq/L)</b>	331	407	399	358
<b>pH</b>	13.5	13.6	13.6	13.6

### 7.2.2.2 Poneded Cylinders

Figures 7.21a and 7.21b show the concentrations of the key components of pore solutions expressed from ponded OPC paste cylinders. Significantly higher chloride levels are detected in mixes containing calcium nitrite inhibitors, while the opposite is true of mixes made with calcium nitrate. The same trend is noted with sodium concentrations.

However, if the volume of ponding solution absorbed is considered, as calculated in Table 7.8, an alternate picture emerges. Despite having absorbed approximately three times more ponding solution than the Control mix, the expressed solution from the CN1 mix has a relatively lower chloride concentration. A similar situation is observed with the Ca(NO<sub>3</sub>)<sub>2</sub> mix. This suggests that the mixes containing CN1 and Ca(NO<sub>3</sub>)<sub>2</sub> are more effective at chemically binding the chlorides than are the Control mix and the mix containing CN2.

**Table 7.8 Relationship of Na and Cl concentrations to the volume of absorbed ponding solution in ponded OPC Paste cylinders**

	<b>Absorbed Ponding Solution (mL)</b>	<b>Expression Analysis (mg/L)</b>		<b>Conc./Sol. Absorbed (mg/L/mL)</b>		<b>[Conc./Sol. Absorbed (M/mL)</b>	
		<b>Na</b>	<b>Cl</b>	<b>Na</b>	<b>Cl</b>	<b>Na</b>	<b>Cl</b>
<b>Control</b>	93	22300	14300	240	154	1.04 x 10 <sup>-2</sup>	4.34 x 10 <sup>-3</sup>
<b>CN1</b>	240	29500	20600	123	85.8	5.35 x 10 <sup>-3</sup>	2.42 x 10 <sup>-3</sup>
<b>CN2</b>	115	24400	31400	212	273	9.23 x 10 <sup>-3</sup>	7.70 x 10 <sup>-3</sup>
<b>Ca(NO<sub>3</sub>)<sub>2</sub></b>	120	5870	4680	49	39	2.13 x 10 <sup>-3</sup>	1.10 x 10 <sup>-3</sup>

Potassium and sodium concentrations are higher in the CN1 mix solution than in the Control mix solution, whereas the opposite is true of the solution from the Ca(NO<sub>3</sub>)<sub>2</sub> mix. Lower potassium and slightly higher sodium concentrations are detected in the solution

expressed from the CN2 mix. It is apparent from these results that each inhibited mix, although compositionally similar, reacts very differently to ponding solution containing chlorides. As both potassium and sodium are considered alkali metals, their increased concentration in the pore solution would theoretically be expected to increase the alkalinity or pH of the pore solution.

Sulphate levels in all inhibited mixes are lower than levels observed in the Control pore solution, particularly in the mix containing  $\text{Ca}(\text{NO}_3)_2$ . These decreased levels suggest that more sulphate in the inhibited mixes is in solid form, possibly as AFm.

While calcium and silicate levels vary little between the various mixes, significant differences are observed with regards to nitrite and nitrate levels. Of particular interest is the variation in nitrite concentrations of the expressed pore solutions of the CN1 and CN2 mixes. Slightly higher levels are observed in the CN2 solution, suggesting that less nitrite is incorporated in solid cement hydration products as compared to the CN1 mix. Relatively low concentrations of nitrate are also evident in the solution expressed from the mix containing  $\text{Ca}(\text{NO}_3)_2$ . Table 7.9 compares the admixed quantities of these species to those found in the expressed solutions. In the cases of mixes containing CN1 and  $\text{Ca}(\text{NO}_3)_2$ , a minor amount of the originally admixed nitrite or nitrate exists within the expressed pore solutions, while a slightly higher proportion exists in the pore solution from the mix containing CN2. Although the CN2 expressed solution contains higher nitrite concentrations than those in CN1, this amount is only a fraction of the amount originally added to the cement at mixing. Therefore, the majority of the active ingredient in all the inhibited mixes is somehow incorporated within the cement paste matrix, not in liquid form as proposed in the mechanism of inhibition specified by the manufacturers.

**Table 7.9 Comparison of molar quantities of nitrite and nitrate from admixture and expressed solutions from Poned OPC Paste cylinders**

	CN1		CN2		Ca(NO <sub>3</sub> ) <sub>2</sub>	
	NO <sub>2</sub>	NO <sub>3</sub>	NO <sub>2</sub>	NO <sub>3</sub>	NO <sub>2</sub>	NO <sub>3</sub>
<b>Added (moles)</b>	2.2 x 10 <sup>-2</sup>	n/a	2.2 x 10 <sup>-2</sup>	n/a	n/a	1.7 x 10 <sup>-2</sup>
<b>Expressed (moles)</b>	1.0 x 10 <sup>-4</sup>	1.6 x 10 <sup>-6</sup>	2.9 x 10 <sup>-4</sup>	6.2 x 10 <sup>-6</sup>	3.1 x 10 <sup>-8</sup>	2.5 x 10 <sup>-5</sup>
<b>% in Solution</b>	0.5%	n/a	1.3%	n/a	n/a	0.2%

Figure 7.22 illustrates the alkalinity values determined for the expressed pore solutions of the ponded OPC paste cylinders. The CN2 and Ca(NO<sub>3</sub>)<sub>2</sub> solutions show significantly lower alkalinity to pH 10 than the Control and CN1 solutions. Table 7.10 lists the equivalent pH values based on the hydroxide concentration as specified by the term “to pH 10”. While Control and CN1 solutions have very similar pH values, pH values for CN2 and Ca(NO<sub>3</sub>)<sub>2</sub> solutions are also similar to one another but slight lower in magnitude. This again emphasizes, that despite having the same corrosion-inhibiting ingredient, significant differences exist between CN1 and CN2.

**Table 7.10 Conversion of alkalinity values in pH value for Poned OPC Paste expressed pore solutions**

	Control	CN1	CN2	Ca(NO <sub>3</sub> ) <sub>2</sub>
<b>Concentration (meq/L)</b>	173	159	81	81
<b>pH</b>	13.2	13.2	12.9	12.9

### 7.2.2.3 Comparison of Unponded and Ponded Cylinders

Figures 7.23a and 7.23b compare the concentrations of primary pore solution constituents from unponded and ponded OPC paste cylinders. All mixes show an increase in silica concentration upon exposure to ponding solution, the largest increase being in the Control solution. A decrease in the amount of silica incorporated into the C-S-H phase may result in higher concentrations in the pore solution. However, at the highest concentration of 194 mg/L observed in the expressed Control solution, the mass of silica in the liquid represents a minor amount ( $6.28 \times 10^{-4}$  %) of the total silica in the portion of



the cylinder expressed. Therefore, the increased silica contents in the expressed pore solutions upon exposure to ponding solution are not of great significance.

In all mixes, a significant decrease in the calcium concentration is noted upon exposure to ponding solution, with the largest decrease in the mix containing CN1 ( $\Delta[\text{Ca}] = 1851$  mg/L), followed by Control (930 mg/L), CN2 (267 mg/L), and  $\text{Ca}(\text{NO}_3)_2$  (204 mg/L). As in the case of the white cement cylinders, this is indicative of precipitation of calcium-based species, probably as calcium hydroxide, from the pore solutions. As the solution from the CN1 mix had the largest drop in calcium concentration, it can be hypothesized that this mix has the greatest potential for chloride binding in the form of calcium hydroxide. Again, surprising is the difference in magnitude between the concentrations of the two calcium nitrite-based inhibitors. This is further evidence that compositional differences between the two admixtures exist, which affects their respective influence on cement paste chemistry.

Sulphate concentrations in all pore solutions increase upon exposure to ponding solution, with the largest increase occurring in the Control mix. Parallel concentration increases are observed in the total sulphur concentrations. The increase in sulphate suggests that removal of this anion from the solid cement paste products is occurring. This may be a result of the conversion of AFm to Friedel's salt, which would involve the exchange of sulphate ions for chloride ions. As higher sulphate concentrations are observed in the Control solution, this may suggest that a greater amount of chloride binding is occurring within this mix. However, it is also possible that free sulphate may also be reacting with unhydrated  $\text{C}_3\text{A}$  components, forming more AFm. Therefore reduced sulphate levels in the inhibited solutions may indicate that further hydration of unreacted  $\text{C}_3\text{A}$  has occurred.

Sodium concentrations increased in all mixes as a result of the absorption of the ponding solution. However, the concentration does not appear to be dependent on the volume of ponding solution absorbed, as shown in Table 7.8. As the Control cylinder absorbed the least amount of ponding solution, sodium concentrations as a function of the volume of ponding solution absorbed would be expected to be lower than similar values for the inhibited mixes. Instead, these values are lowest in the solutions that absorbed the most ponding solution, namely  $\text{Ca}(\text{NO}_3)_2$  and CN1, suggesting that greater precipitation of sodium is occurring in these mixes. The behaviour of potassium concentrations also varies between mixes upon ponding, increasing in concentration in the Control and CN1 mixes while decreasing in the CN2 and  $\text{Ca}(\text{NO}_3)_2$  mixes. Increases in sodium and potassium concentration in the pore solution may be a method of counteracting a decrease in pH in the pore solution. The increase in potassium concentration would have a more significant effect on increasing the pH of the pore solution, as a 0.1 M solution of KOH has a pH of 13.5, while a 0.125 M solution of NaOH has a pH of 13 (Windholz 1979).

Table 7.11 compares the pH values of the expressed solutions from the unponded and ponded cylinders. All solutions experience a pH drop upon exposure to ponding solution, with CN2 experiencing the largest drop. While similar pH values are displayed by the Control and CN1 solutions, similar values are also displayed by the CN2 and  $\text{Ca}(\text{NO}_3)_2$  solutions. As for the white cement the drop in pH also appears to be independent of the volume of ponding solution absorbed, as the CN1 cylinder absorbed the largest volume of ponding solution but has a higher pH value than the CN2 and  $\text{Ca}(\text{NO}_3)_2$  solutions. This would suggest that the drop in pH is not only an effect of dilution, but a result of the

removal of hydroxide ions from the pore solution, likely through precipitation of a solid product.

Table 7.11 pH of expressed pore solutions from Unponded and Poned OPC Paste Cylinders

	<b>Unponded</b>	<b>Poned</b>	<b><math>\Delta</math>pH</b>
<b>Control</b>	13.5	13.2	0.3
<b>CN1</b>	13.6	13.2	0.4
<b>CN2</b>	13.6	12.9	0.7
<b>Ca(NO<sub>3</sub>)<sub>2</sub></b>	13.6	12.9	0.7

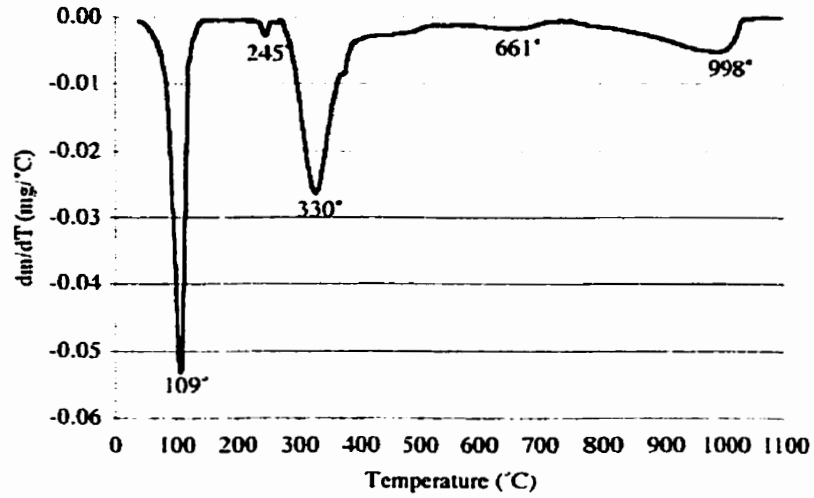


Figure 7.1 DTG of synthesized Friedel's salt

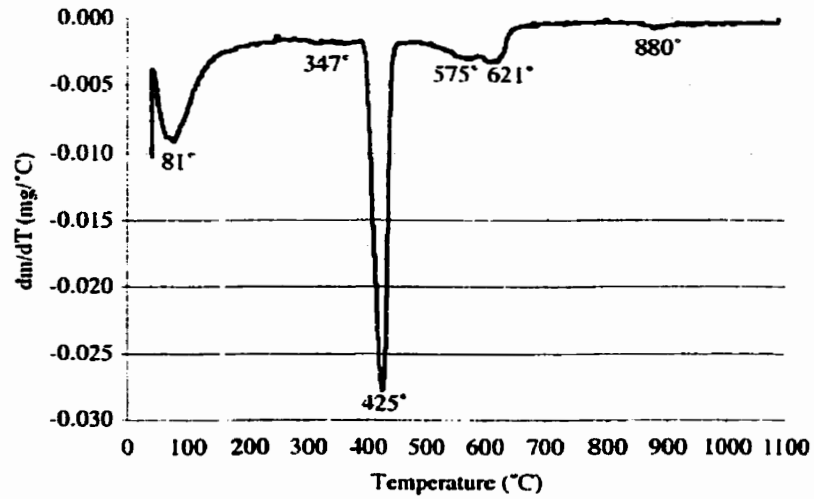


Figure 7.2 DTG of hydrated pure C<sub>3</sub>S

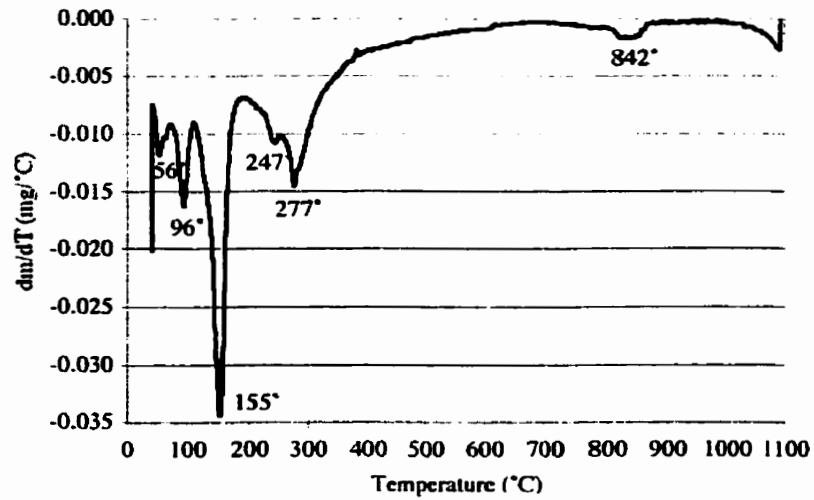


Figure 7.3 DTG of hydrated pure C<sub>3</sub>A and gypsum

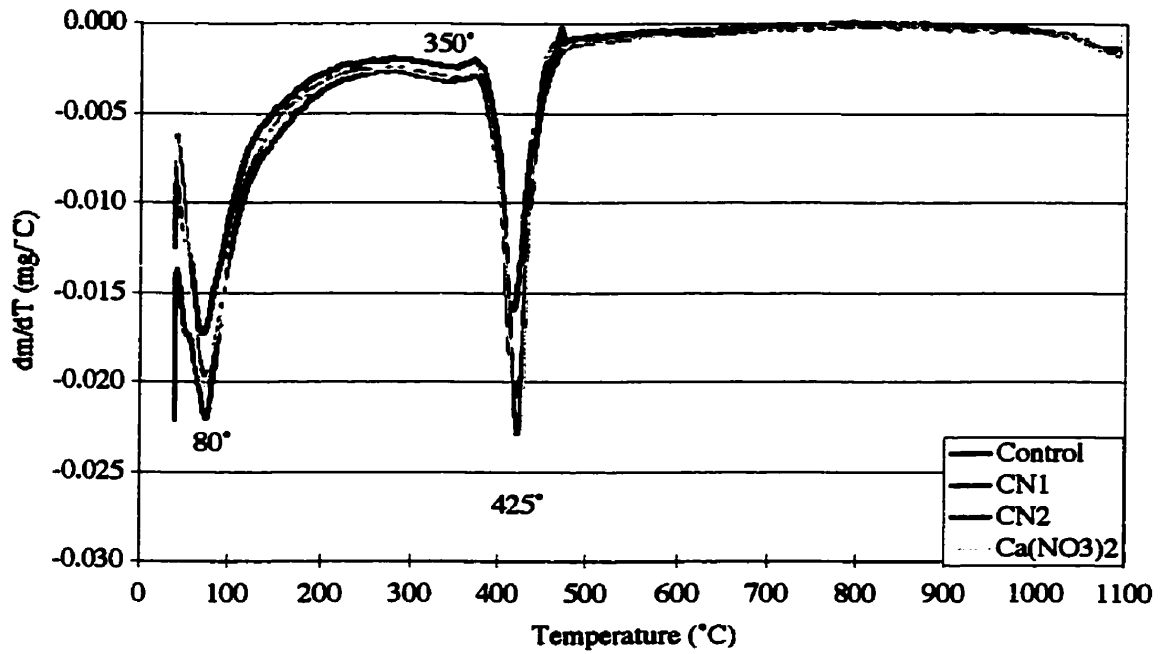


Figure 7.4 DTG of White Cement Paste cylinders

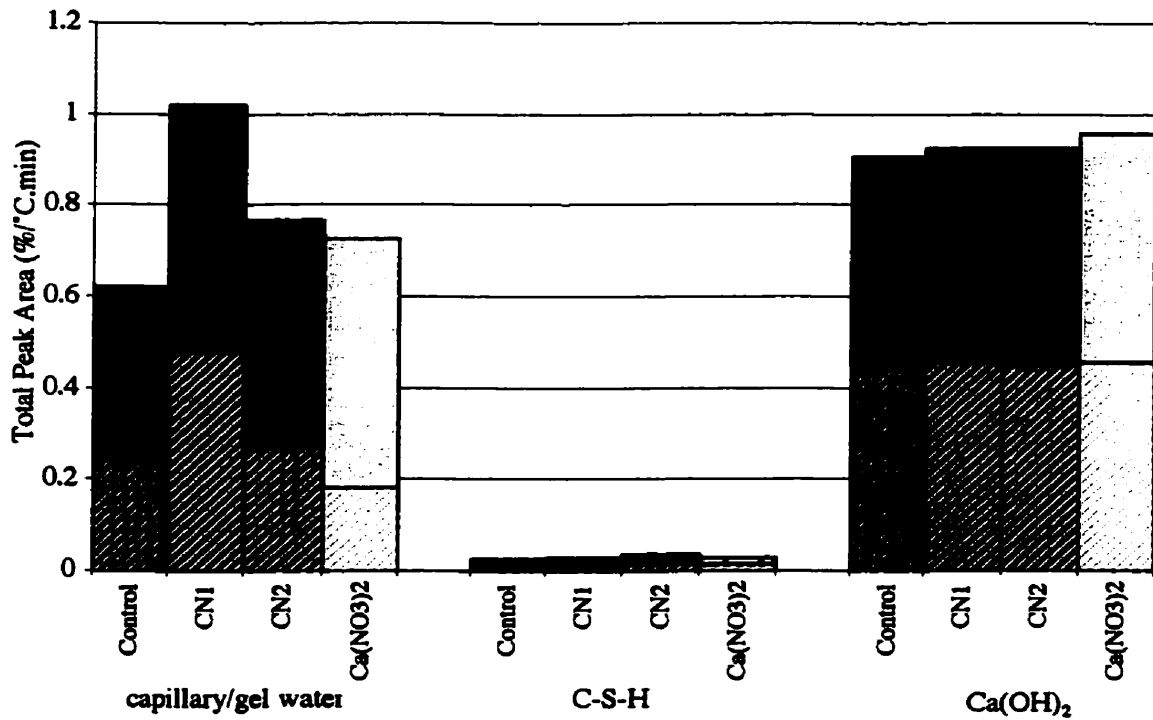


Figure 7.5 Total peak areas of White Cement Paste cylinders

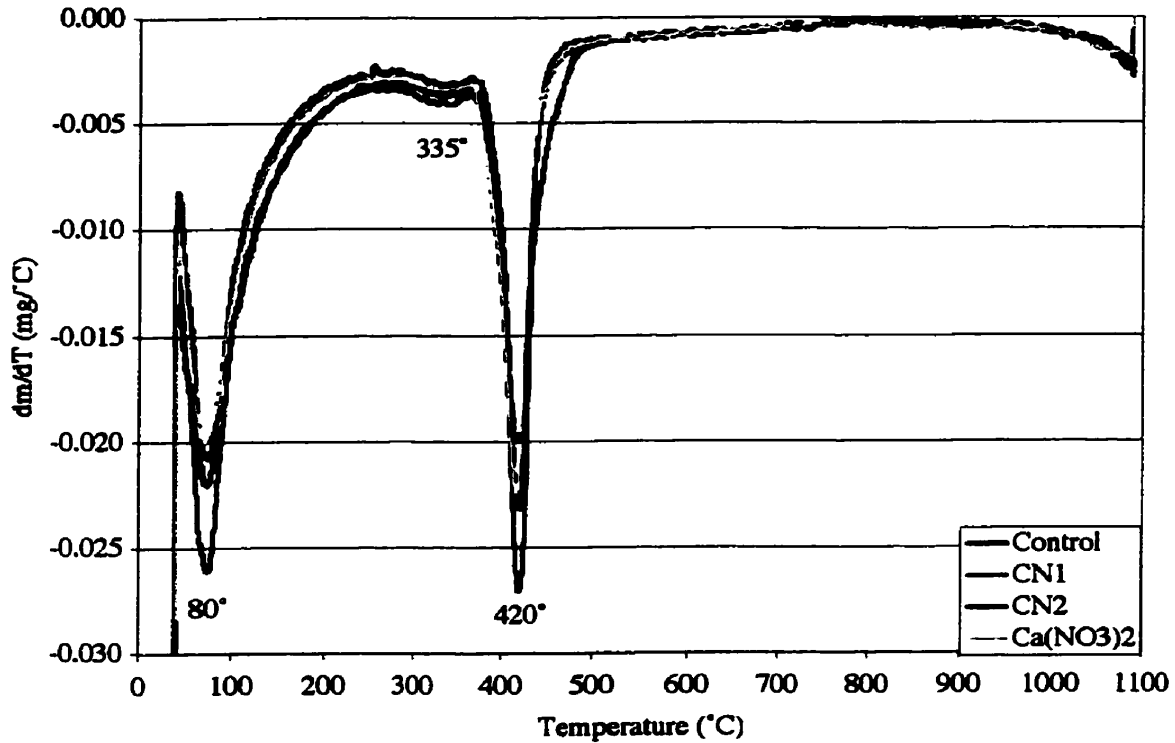


Figure 7.6 DTG of ponded White Cement Paste cylinders

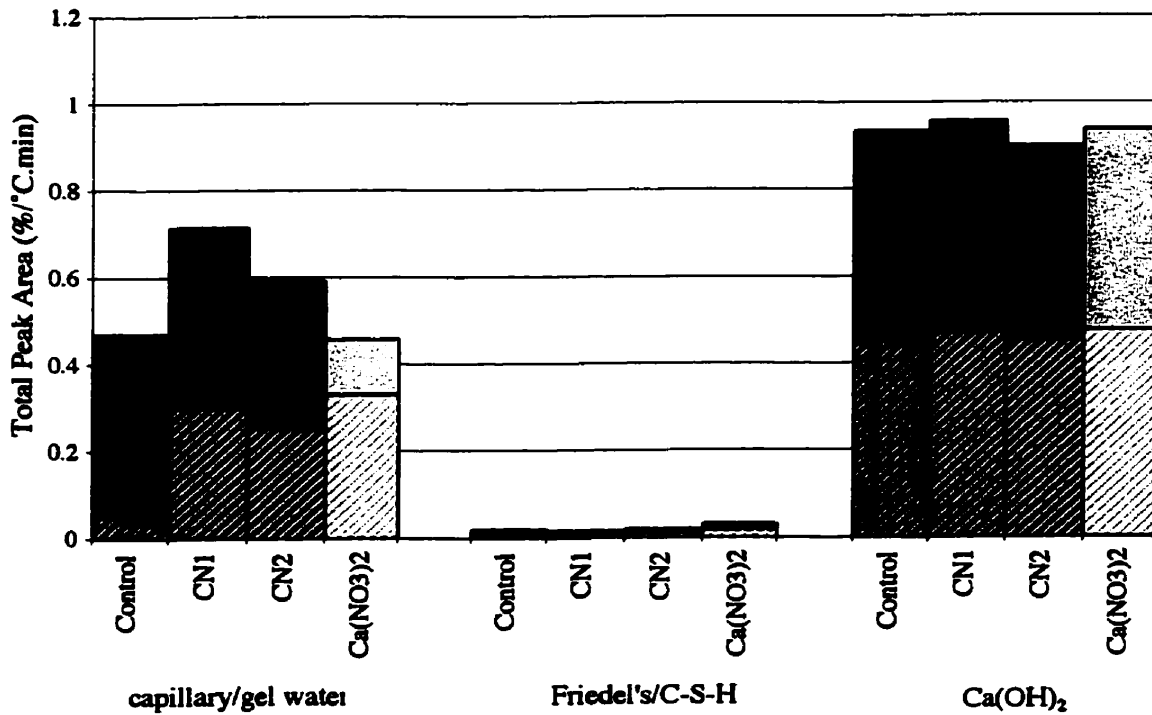


Figure 7.7 Total peak areas of ponded White Cement Paste cylinders

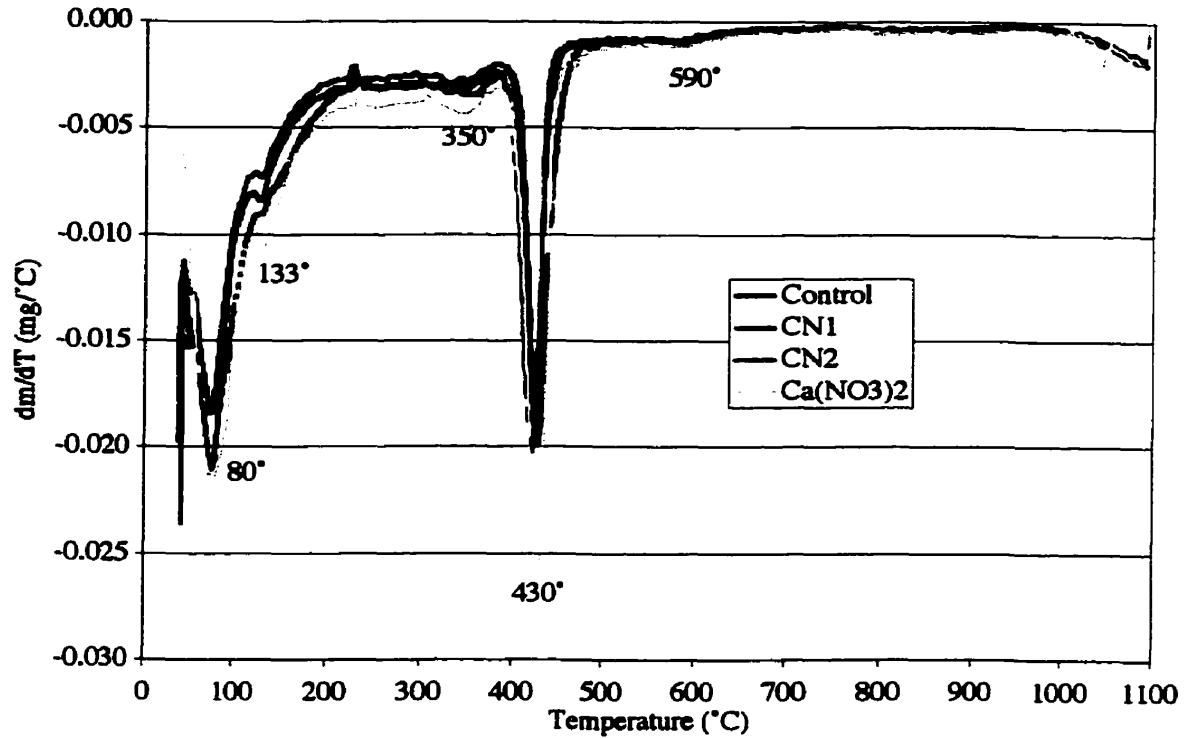


Figure 7.8 DTG of OPC Paste cylinders

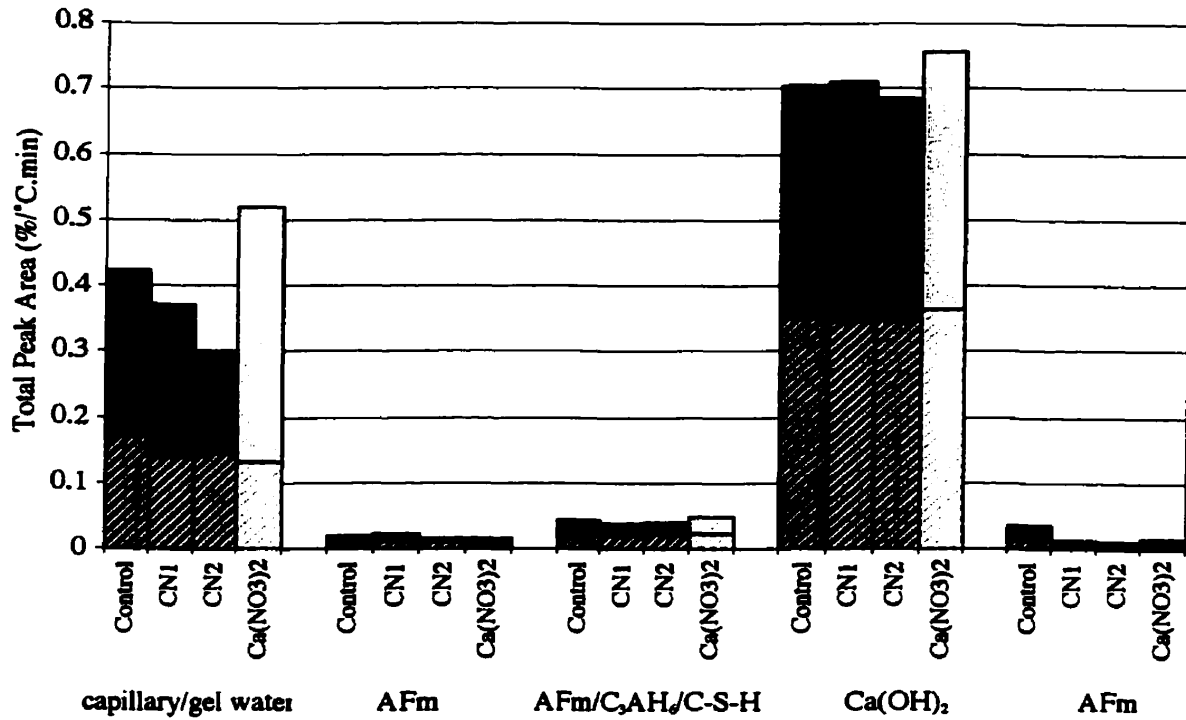


Figure 7.9 Total peak areas of OPC Paste cylinders

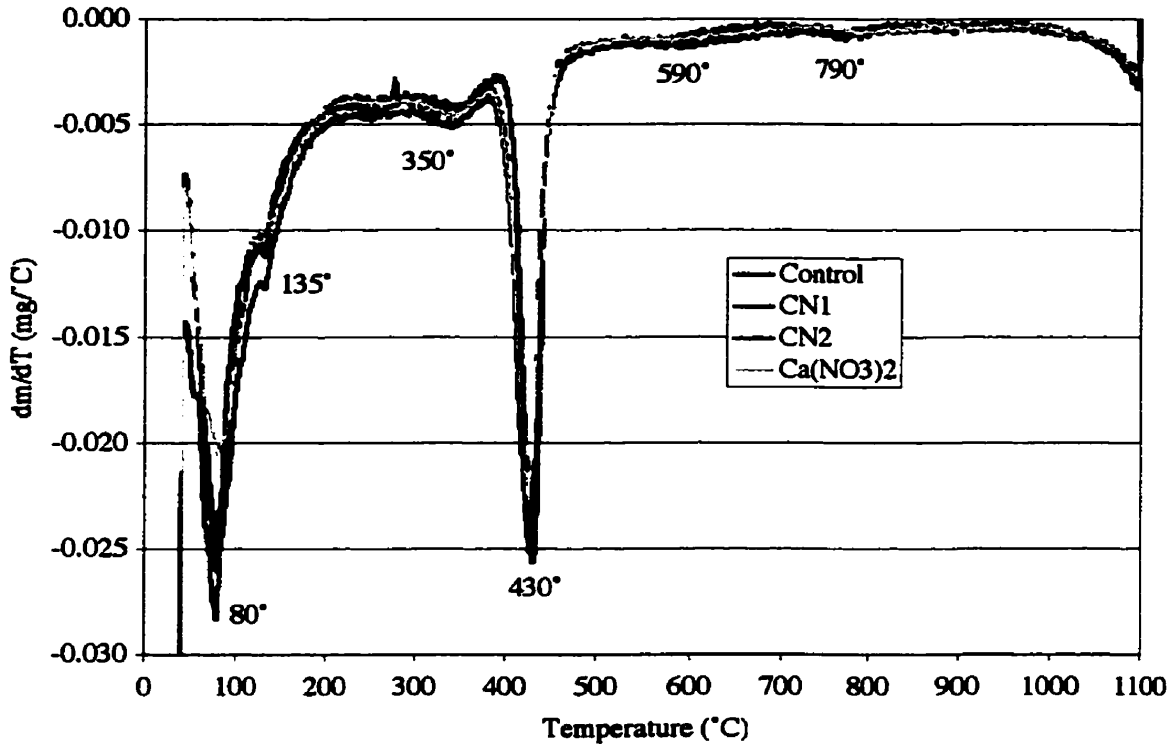


Figure 7.10 DTG of ponded OPC Paste cylinders

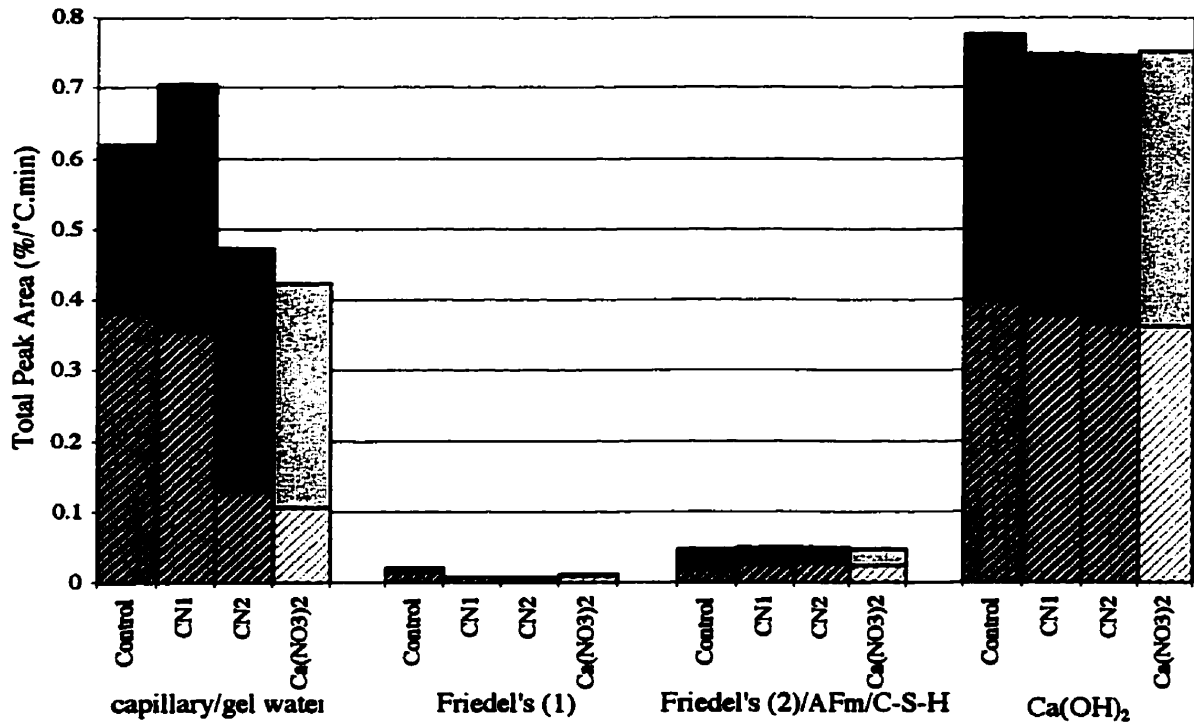


Figure 7.11 Total peak areas of ponded OPC Paste cylinders



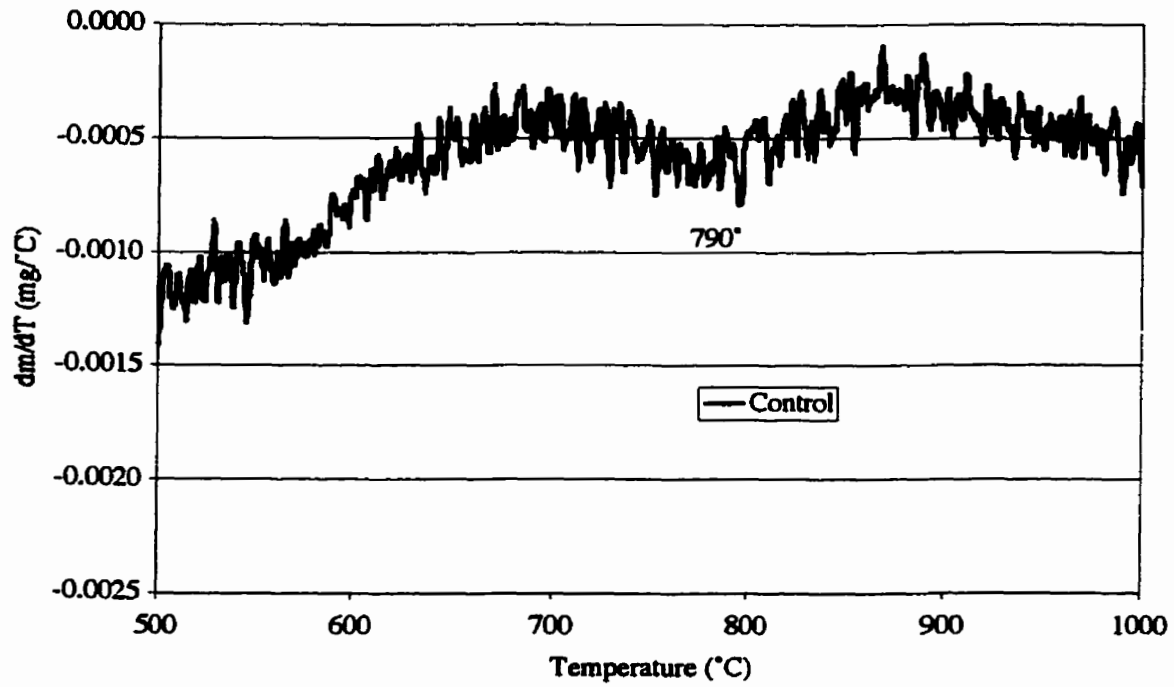


Figure 7.12a Enhanced DTG for ponded Control OPC Paste cylinder

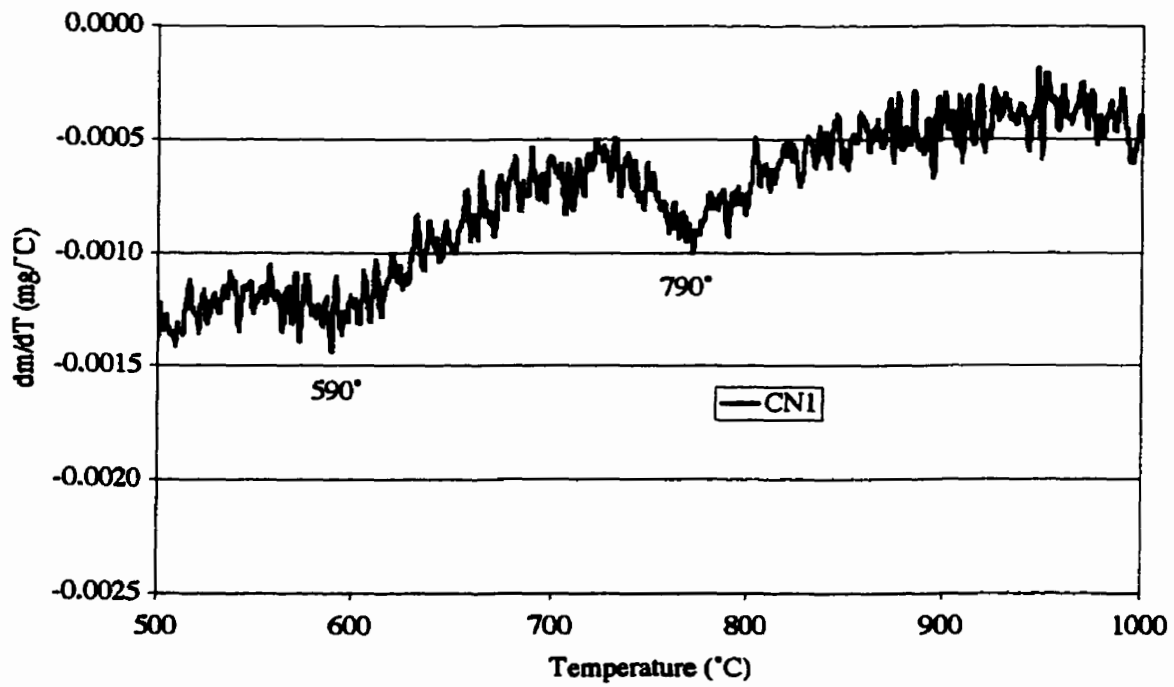


Figure 7.12b Enhanced DTG for ponded CN1 OPC Paste cylinder

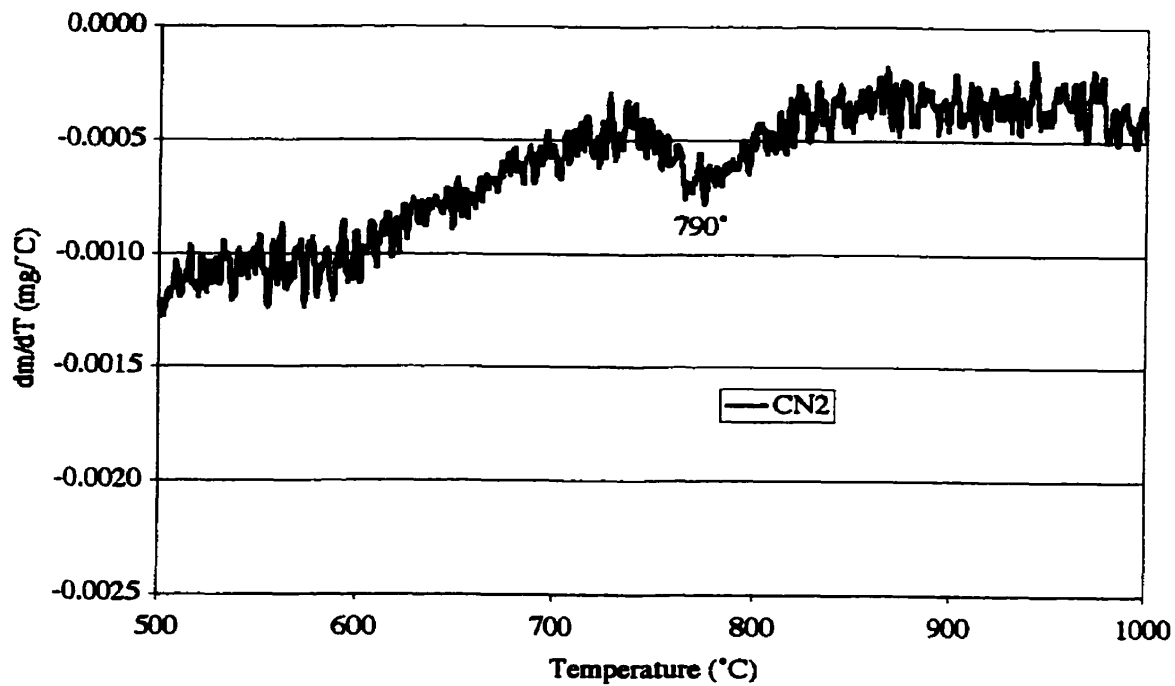


Figure 7.12c Enhanced DTG for ponded CN2 OPC Paste cylinders

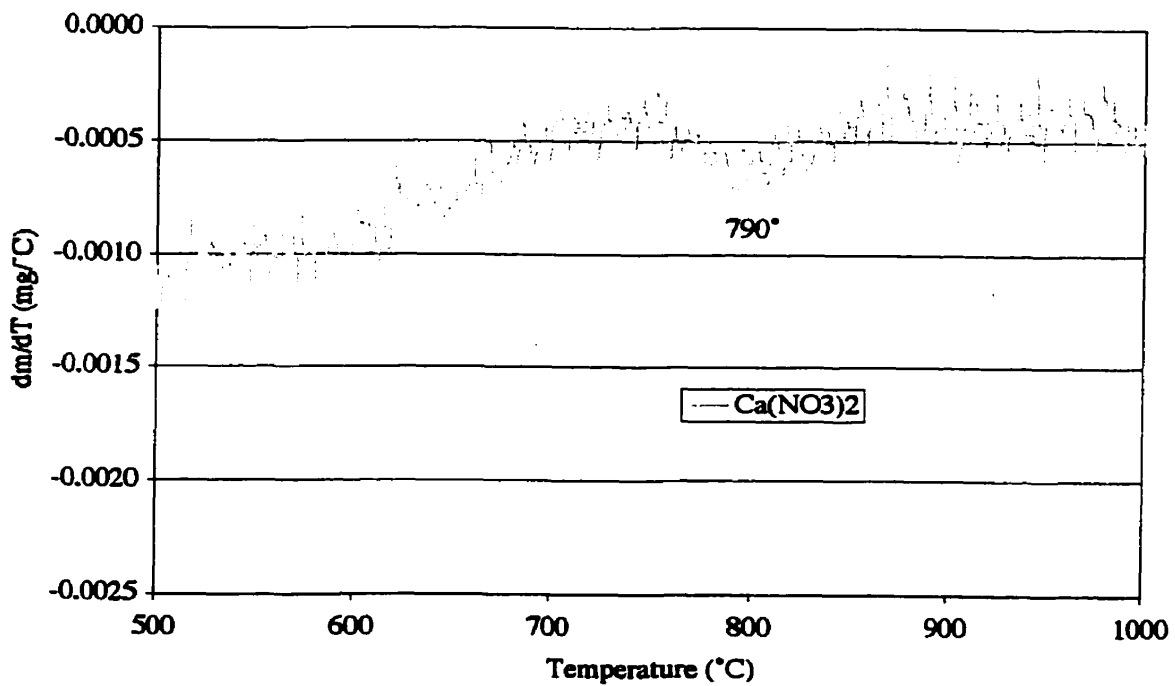


Figure 7.12d Enhanced DTG for ponded Ca(NO<sub>3</sub>)<sub>2</sub> OPC Paste cylinders

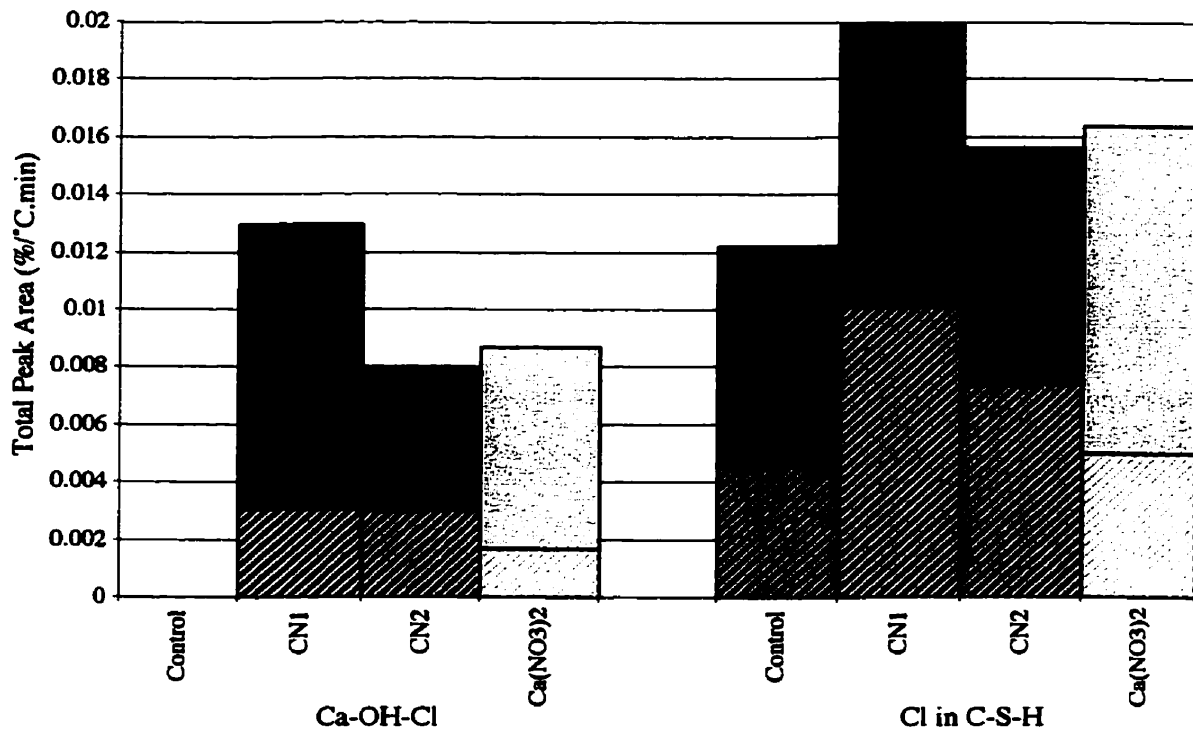


Figure 7.13 Total peak areas of various bound chloride forms in ponded OPC Paste cylinders

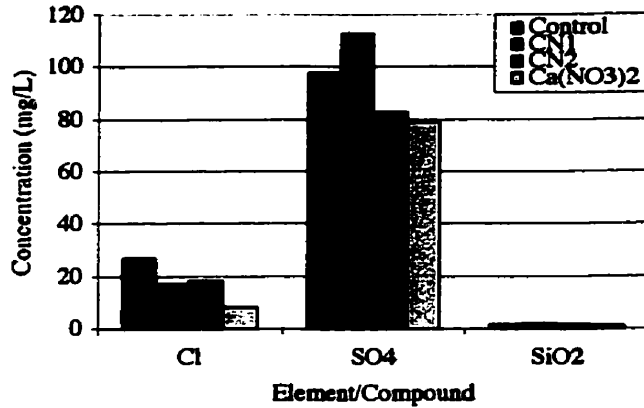


Figure 7.14a Analysis of expressed pore solution from unponded White Cement Paste cylinders:  $\text{Cl}^-$ ,  $\text{SO}_4^{2-}$  and  $\text{SiO}_2^-$

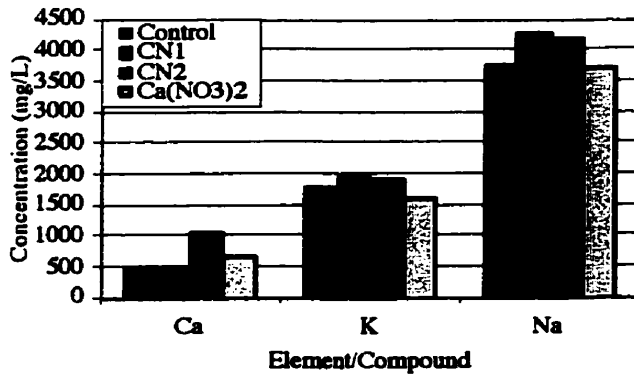


Figure 7.14b Analysis of expressed pore solution from unponded White Cement Paste cylinders:  $\text{Ca}^{2+}$ ,  $\text{K}^+$  and  $\text{Na}^+$

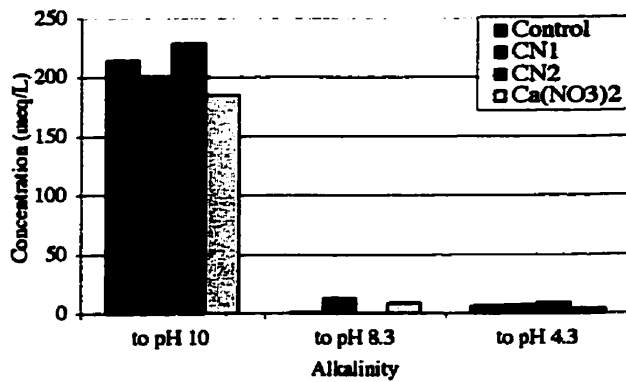


Figure 7.15 Alkalinity of expressed pore solutions from unponded White Cement Paste cylinders

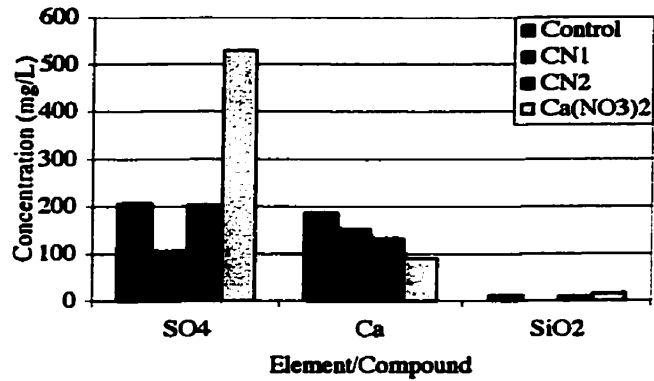


Figure 7.16a Analysis of expressed pore solutions from ponded White Cement Paste cylinders:  $\text{SO}_4^{2-}$ ,  $\text{Ca}^{2+}$  and  $\text{SiO}_2^-$

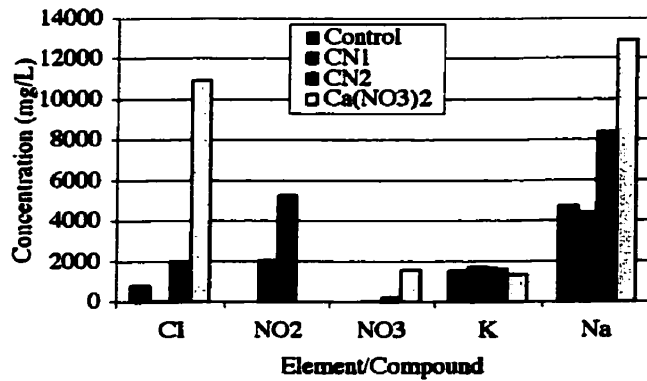


Figure 7.16b Analysis of expressed pore solutions from ponded White Cement Paste cylinders:  $\text{Cl}^-$ ,  $\text{NO}_2^-$ ,  $\text{NO}_3^-$ ,  $\text{K}^+$  and  $\text{Na}^+$

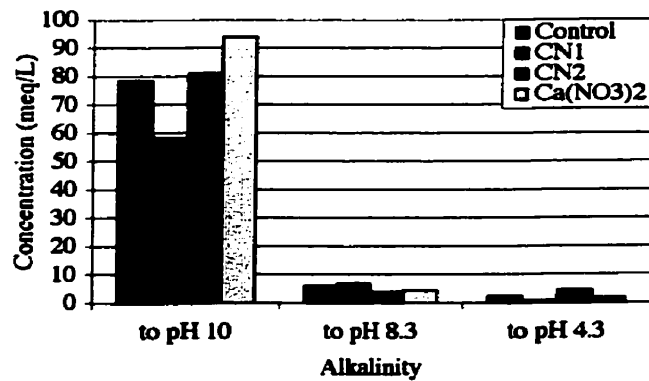


Figure 7.17 Alkalinity of expressed pore solutions from ponded White Cement Paste cylinders

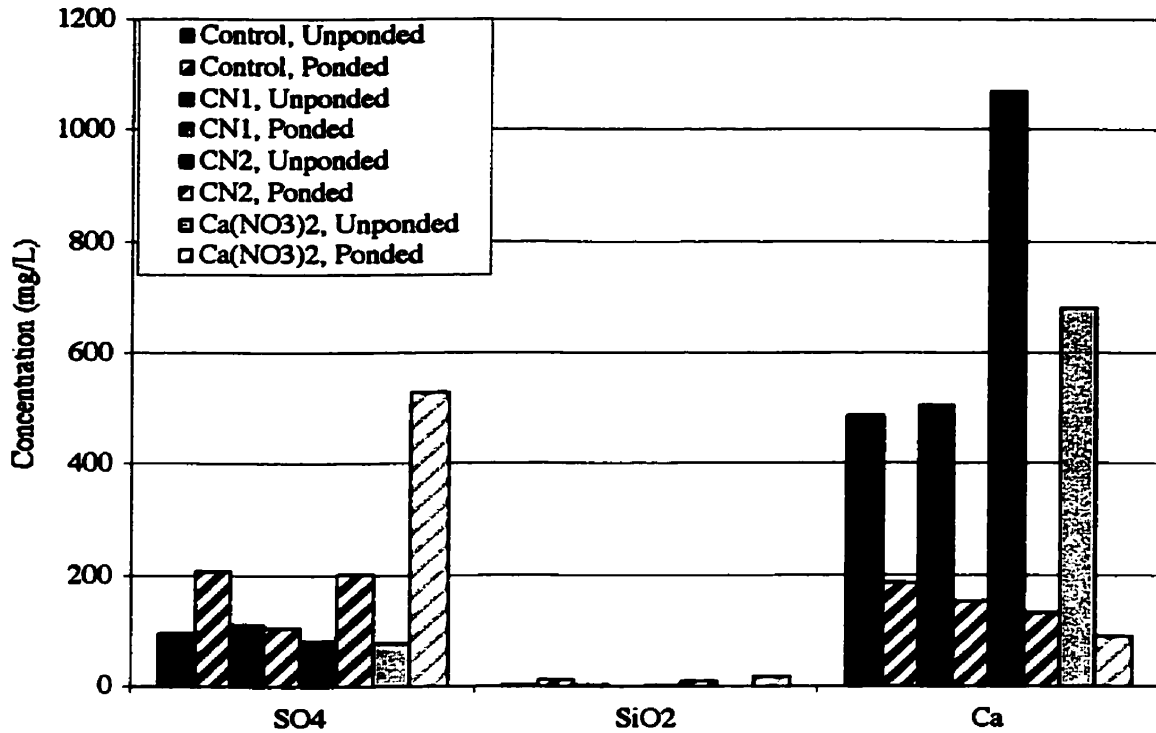


Figure 7.18a Comparison of expressed pore solution analyses of unponded and ponded White Cement Paste cylinders:  $\text{SO}_4^{2-}$ ,  $\text{SiO}_2^-$  and  $\text{Ca}^{2+}$

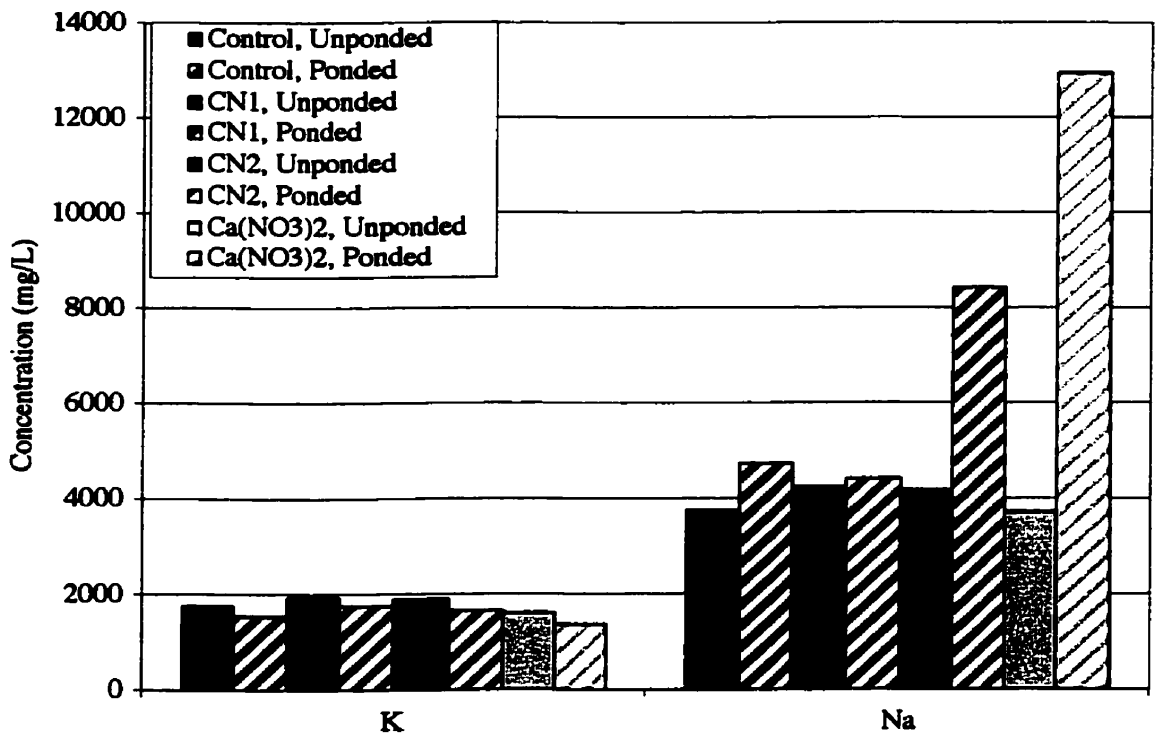


Figure 7.18b Comparison of expressed pore solution analyses of unponded and ponded White Cement Paste cylinders:  $\text{K}^+$  and  $\text{Na}^+$

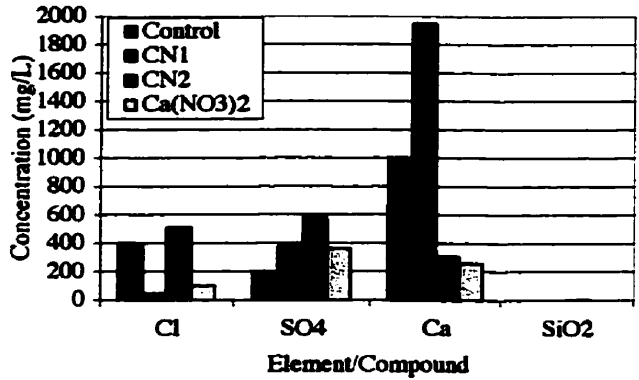


Figure 7.19a Analysis of expressed pore solutions from unponded OPC Paste cylinders:  $\text{Cl}^-$ ,  $\text{SO}_4^{2-}$ ,  $\text{Ca}^{2+}$  and  $\text{SiO}_2^-$

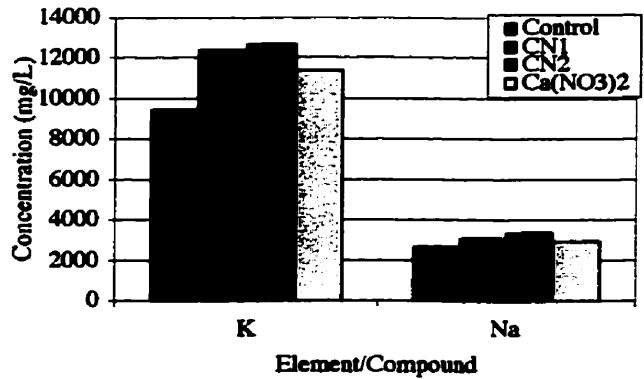


Figure 7.19b Analysis of expressed pore solutions from unponded OPC Paste cylinders:  $\text{K}^+$  and  $\text{Na}^+$

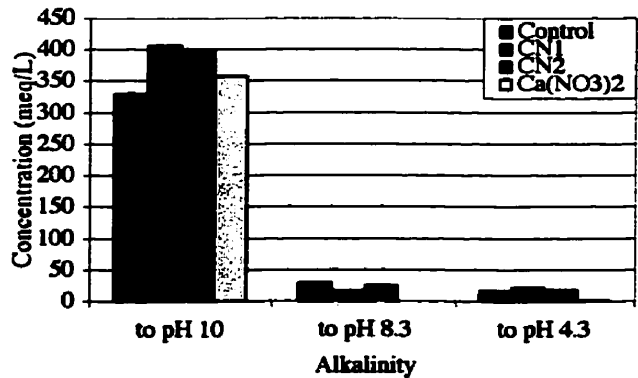


Figure 7.20 Alkalinity of expressed pore solutions from unponded OPC Paste cylinders

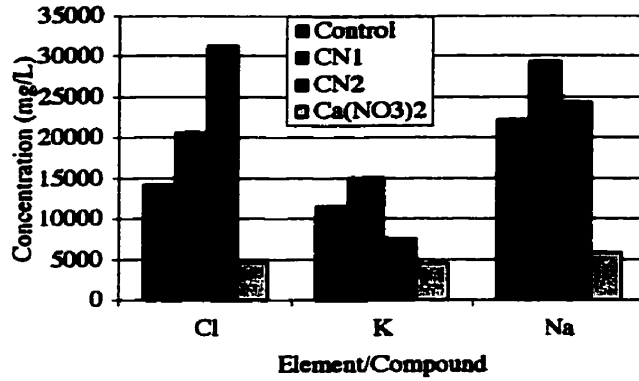


Figure 7.21a Analysis of expressed pore solutions from ponded OPC Paste cylinders:  $\text{Cl}^-$ ,  $\text{K}^+$  and  $\text{Na}^+$

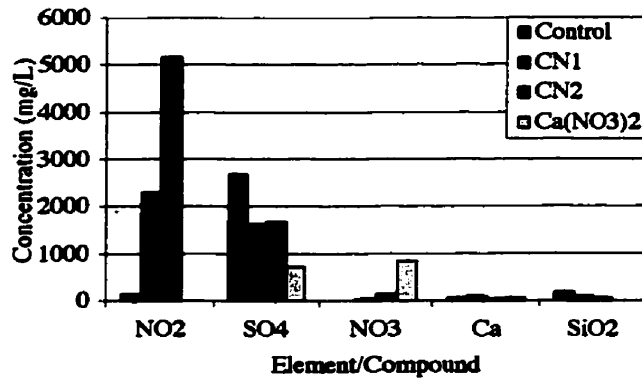


Figure 7.21b Analysis of expressed pore solutions from ponded OPC Paste cylinders:  $\text{NO}_2^-$ ,  $\text{SO}_4^{2-}$ ,  $\text{NO}_3^-$ ,  $\text{Ca}^{2+}$  and  $\text{SiO}_2^-$

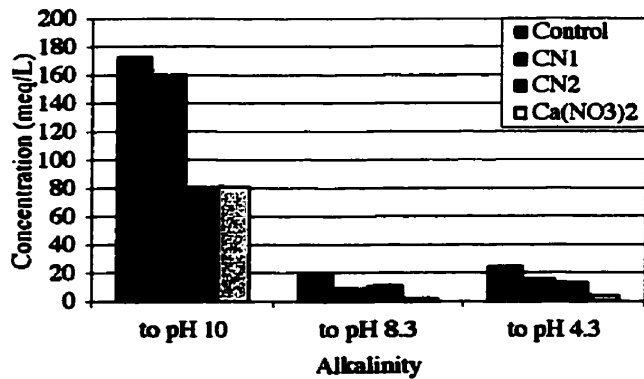


Figure 7.22 Alkalinity of expressed pore solutions from ponded OPC Paste cylinders



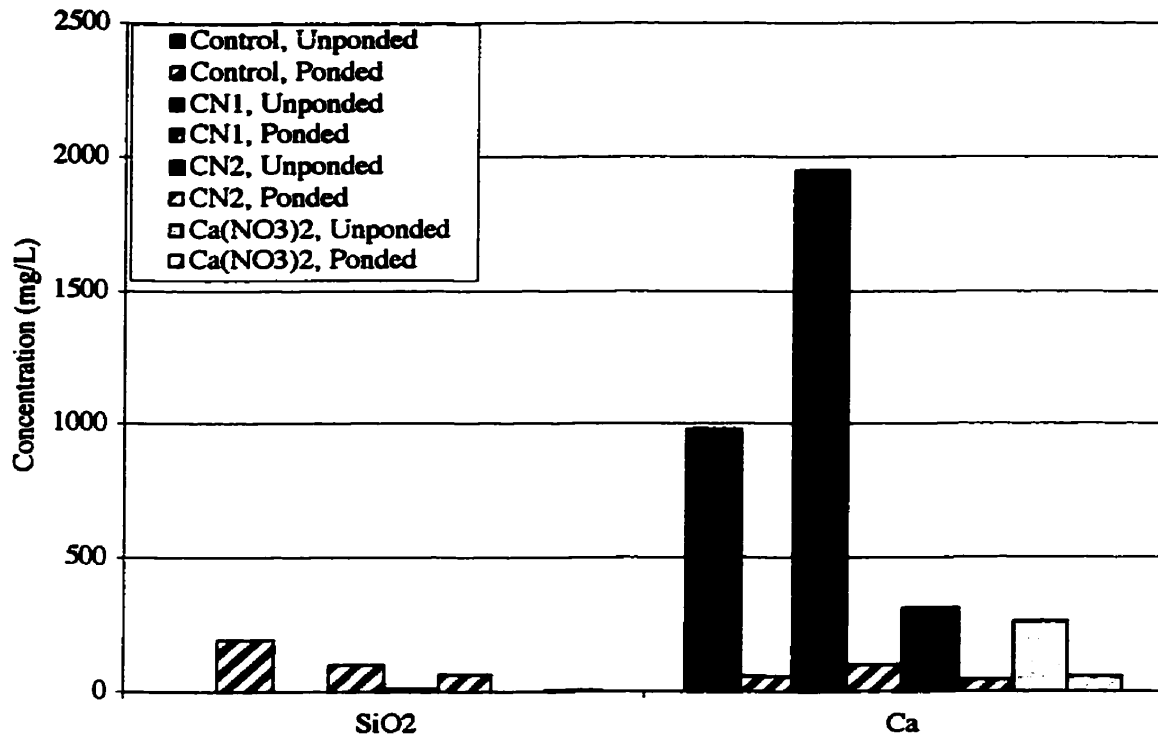


Figure 7.23a Comparison of expressed pore solution analyses of unponded and ponded OPC Paste cylinders: SiO<sub>2</sub> and Ca<sup>2+</sup>

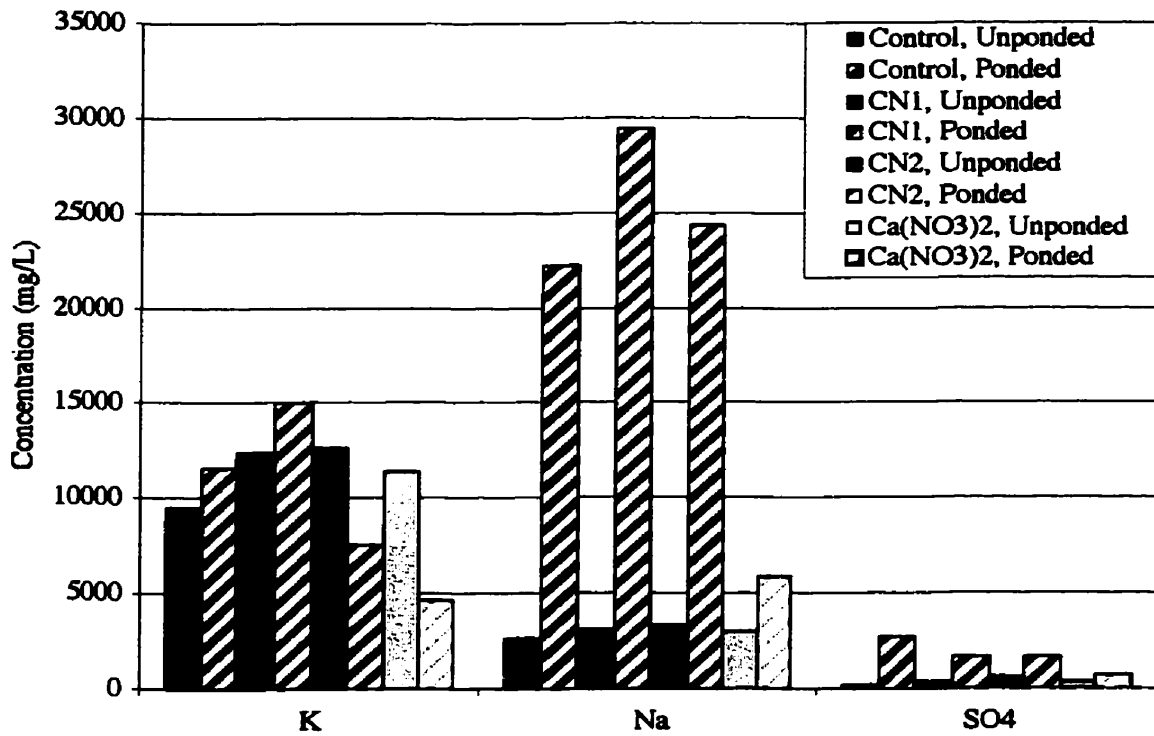


Figure 7.23b Comparison of expressed pore solution analyses of unponded and ponded OPC Paste cylinders: K<sup>+</sup>, Na<sup>+</sup> and SO<sub>4</sub><sup>2-</sup>

## **Chapter 8**

### **Comparison of White and OPC Cement Pastes Results and Discussion**

The following chapter is a reanalysis of data originally presented in Chapters 6 and 7, in order to make comparisons between white and OPC paste cylinders. Differences in the composition of the two clinkers were given in Table 4.1 on page 41.

#### **8.1 Transport Properties of Cement Pastes**

##### **8.1.1 Mercury Intrusion Porosimetry**

Figures 8.1 through 8.4 present the average cumulative intrusion volume versus average pore radius for Control, CN1, CN2 and  $\text{Ca}(\text{NO}_3)_2$  mixes made with both white and OPC cements. Comparison of these curves prior to exposure to ponding solution shows that the pastes made with OPC cement have higher total porosity than comparable mixes made with white cement. Similarly, after exposure to ponding solution, mixes made with OPC cement show higher total porosity than white cement mixes exposed to ponding solution.

Figures 8.5 through 8.8 show the distribution of the average incremental intrusion volumes as a function of pore radius for these same mixes while Tables 8.1 through 8.4 separate the total intrusion volumes into the proportion associated with coarse and fine pores, as defined in Chapter 6. In all mixes containing inhibitor, coarse porosity is greater in the white cement pastes than in the comparable OPC pastes. The Control mixes show little variation in coarse porosity with the type of cement used. It is possible that a higher degree of microcracking was present in the white mixes containing inhibitors, although no evidence was visually apparent. This may be due to autogeneous shrinkage of individual cement pastes. In all

Table 8.1 Average coarse, fine and total porosities for Control mixes

<b>Control</b>	<b>Coarse (cc/g)</b>	<b>Fine Pore (cc/g)</b>	<b>Total (cc/g)</b>	<b>% Coarse</b>
<b>White</b>	0.0024	0.0752	0.0777	3.1
<b>White, Ponded</b>	0.0019	0.0488	0.0507	3.8
<b>OPC</b>	0.0025	0.0937	0.0961	2.6
<b>OPC, Ponded</b>	0.0013	0.0778	0.0791	1.6

Table 8.2 Average coarse, fine and total porosities for CN1 mixes

<b>CN1</b>	<b>Coarse (cc/g)</b>	<b>Fine Pore (cc/g)</b>	<b>Total (cc/g)</b>	<b>% Coarse</b>
<b>White</b>	0.0043	0.0553	0.0596	7.2
<b>White, Ponded</b>	0.0008	0.0453	0.0461	1.7
<b>OPC</b>	0.0016	0.0929	0.0945	1.7
<b>OPC, Ponded</b>	0.0030	0.0738	0.0768	3.9

Table 8.3 Average coarse, fine and total porosities for CN2 mixes

<b>CN2</b>	<b>Coarse (cc/g)</b>	<b>Fine Pore (cc/g)</b>	<b>Total (cc/g)</b>	<b>% Coarse</b>
<b>White</b>	0.0037	0.0613	0.0650	5.7
<b>White, Ponded</b>	0.0018	0.0507	0.0525	3.4
<b>OPC</b>	0.0014	0.0980	0.0994	1.4
<b>OPC, Ponded</b>	0.0015	0.0733	0.0748	2.0

Table 8.4 Average coarse, fine and total porosities for Ca(NO<sub>3</sub>)<sub>2</sub> mixes

<b>Ca(NO<sub>3</sub>)<sub>2</sub></b>	<b>Coarse (cc/g)</b>	<b>Fine Pore (cc/g)</b>	<b>Total (cc/g)</b>	<b>% Coarse</b>
<b>White</b>	0.0029	0.0624	0.0653	4.4
<b>White, Ponded</b>	0.0010	0.0415	0.0425	2.4
<b>OPC</b>	0.0016	0.0801	0.0817	2.0
<b>OPC, Ponded</b>	0.0027	0.0699	0.0726	3.7

white cement mixes, a reduction in coarse porosity occurs upon exposure to ponding solution, although to varying degrees. This suggests that a new product is forming upon exposure to ponding solution. This may be due to further hydration of unreacted cement grains along the pore walls, or precipitation of species from the pore solution onto the pore walls. The behaviour with exposure to ponding solution in the OPC mixes is more complex. Only the Control mix experiences a decrease in coarse porosity with exposure to ponding solution, while all inhibited pastes show an increase to varying degrees, despite having absorbed lower volumes of ponding solution. This increase in coarse porosity in the inhibited samples may be due to the production of microcracks within the samples after

exposure to ponding solution, although no visual evidence was noted.

The vast proportion of the porosity in all mixes is fine porosity as expected from the w/c ratio, as the w/c ratio used would lead to a low volume of larger sized pores. Higher fine porosity is also apparent in all OPC pastes, unponded and ponded, as compared to similar white cement pastes. In all samples, there is a reduction in fine porosity upon exposure to ponding solution.

Figure 8.9 shows the volumes of ponding solution absorbed by white cement and OPC paste. Significantly more ponding solution was absorbed by the Control and CN1 OPC pastes than by similar mixes made with white cement, particularly in the case of the Control. This is despite the same or larger degree of coarse porosity in the unponded white cement pastes vs. OPC pastes of these mixes. This suggests a higher degree of interconnected total porosity within these OPC mixes. This may also be the case for the CN2 inhibitor, where both white cement and OPC paste CN2 mixes absorbed approximately the same amount of ponding solution, despite the coarse porosity in the white mix being more than twice that in the OPC. The white cement  $\text{Ca}(\text{NO}_3)_2$  mix, however, absorbed a larger volume of ponding solution than the similar OPC mix. Although in direct contrast to the behaviour exhibited by the Control mixes, this mix behaves as expected as the white mix had a higher degree of coarse porosity than the OPC.

The difference in porosity between the two cement pastes is likely a result of the different compositions of the original cements. The white cement has a significantly higher percentage of  $\text{C}_3\text{S}$  than the OPC cement (73% and 54.4%, respectively). It is also worthy to note that the  $\text{C}_3\text{S}$  levels in the white cement are typical of those found in Type 30, or high-

early strength or rapid hardening cements. It follows logically that concrete made from this type of cement would have higher degrees of coarse porosity due to the reduction in setting and hardening time. The higher fineness of the white cement than the OPC cement (410 m<sup>2</sup>/kg vs. 368 m<sup>2</sup>/kg) would also contribute to early setting/hardening.

### 8.1.2 Acid Soluble Chloride Titrations

Figures 8.10 through 8.13 show the chloride profiles obtained through acid soluble chloride titration of ponded white cement and OPC paste cylinders. As expected, chloride concentrations generally decrease with increasing depth into the cylinder. In order to make comparisons with the mercury intrusion porosimetry data from the previous section, only the concentrations at a depth of 23 mm (i.e. the depth of the MIP samples) are compared with MIP data. In the case of the Control, CN1 and CN2 pastes, higher chloride concentrations are observed in the OPC pastes than those observed in the ponded white cement paste mixes. This again may be indicative of the higher degree of interconnected porosity in the OPC mixes. In the case of the Ca(NO<sub>3</sub>)<sub>2</sub> mixes, the white cement paste showed the higher chloride concentration, which coincided with a higher original porosity and consequently absorbed more ponding solution.

Table 8.5 calculates the proportion of chloride concentration within the top 23 mm of the cylinder. Mixes made with OPC paste appear to retain a higher percentage of the total chloride concentration within this top level as compared to the mixes made with white cement. This would be advantageous, thereby delaying the onset of chloride-induced corrosion, as chlorides would be further away from the steel surface. However, the nitrites only have a significant effect in the white cement pastes, while little advantage of inhibitor is

Table 8.5 Proportion of chloride in top 23 mm of White and OPC cylinders (g Cl<sup>-</sup>/g paste)

<i>White</i>	<b>Control</b>	<b>CN1</b>	<b>CN2</b>	<b>Ca(NO<sub>3</sub>)<sub>2</sub></b>
<b>Top 23 mm</b>	0.00923	0.01172	0.01071	0.01829
<b>Total</b>	0.01526	0.01630	0.01471	0.03367
<b>% in top 23 mm</b>	60	72	73	54
<i>OPC</i>	<b>Control</b>	<b>CN1</b>	<b>CN2</b>	<b>Ca(NO<sub>3</sub>)<sub>2</sub></b>
<b>Top 23 mm</b>	0.01888	0.01863	0.01289	0.01388
<b>Total</b>	0.02632	0.02566	0.01689	0.01659
<b>% in top 23 mm</b>	72	73	76	84

noted in the OPC mixes.

## **8.2 Chemical Analysis of Cement Pastes**

### **8.2.1 Thermal Analysis**

Figures 8.14 through 8.17 compare the differential thermogravimetric analysis curves generated for the Control, CN1, CN2 and Ca(NO<sub>3</sub>)<sub>2</sub> mixes made with white cement and OPC pastes, both with and without exposure to ponding solution. Immediately evident, regardless of inhibitor addition, is the absence of the endotherms at 133° and 590° in the unponded and ponded white cement mixes. These were identified in Chapter 8 as associated with the AFm phase, and so its absence in white cement is not surprising given the very low C<sub>4</sub>AF (to achieve the white colour) and the low C<sub>3</sub>A content to provide sulphate resistance. In ordinary white cement, the lack of C<sub>4</sub>AF is usually compensated by additional C<sub>3</sub>A and, in such cements Bensted (Bensted 1983) states that less AFt forms during early hydration, resulting in less AFm. This is a result of the reduced solubility of sulphate due to low alkali levels within the cement.

Also absent in the ponded white cement mixes as compared to similar mixes made with OPC cement is the endotherm at 775°. Associated with chlorides incorporated in the C-S-H structure, it is possible that this phase can form in white cement but levels were insufficient

for detection. The same could be true with the endotherm associated with calcium hydroxychloride at 590°. Both endotherms are present in pastes containing 2 % admixed chlorides of both Control white cement and a Control OPC, as shown in Figure 8.18. However, also apparent is that the magnitude of the endotherm associated with Ca-OH-Cl is larger in the OPC than in the white cement paste. This suggests that the OPC paste is more efficient in producing this compound than its white cement equivalent.

### 8.2.2 Pore Solution Expression

Figures 8.19a through 8.19d and Figures 8.20a through 8.20d compare the concentrations of key components of pore solutions expressed from the different mixes prepared. Prior to exposure to ponding solution, significantly higher levels of sulphate are present in the OPC mixes as compared to those mixes made with white cement, particularly those containing calcium nitrite and calcium nitrate. This result is in agreement with Bensted (Bensted 1983), who observed that sulphate solubility in hydrated white cement is low because of the lower alkali levels. Upon exposure to ponding solution, sulphate levels increase substantially for both cement types over unponded samples, except for the white CN1 mix, with OPC demonstrating the higher concentrations. This suggests that a higher degree of sulphate replacement by chlorides in the aluminate phases is occurring in the OPC. Parallel observations are made for total sulphur concentrations.

The only trends with regards to silica concentration are noted upon exposure to ponding solution for both mixes. In white cement, Control and  $\text{Ca}(\text{NO}_3)_2$  mixes show a slight increase in concentration, while there is virtually no change noted in the CN1 and CN2 mixes. Slightly higher increases in silica concentration are noted in all ponded OPC mixes, the largest increase in the Control mix. These changes may be a result in the modification of the

calcium:silicate ratio of the C-S-H phase. As OPC expressed solutions have higher silica levels, this may indicate that the C-S-H formed in the white cement paste is higher in silica content than that formed in OPC mixes. Higher quantities of C-S-H form in white cement pastes due to the higher weight percentages of  $C_3S$  and  $C_2S$  in the initial white cement composition.

Significant differences exist with respect to calcium concentrations within expressed pore solutions, dependent on the type of cement used and the type of inhibitor added. Calcium concentrations are at least two times larger in OPC Control and CN1 pore solutions than solutions expressed from equivalent white cement paste cylinders. This observation is in agreement with Bensted (Bensted 1983), who found that lime solubility decreases in white cement due to low alkali levels. However, the opposite effect is observed in mixes containing CN2 and  $Ca(NO_3)_2$ .

The differences in behaviour between the CN1 and CN2 inhibitors gives further evidence that compositional differences exist between the two admixtures. As previously mentioned, it has been suggested that the CN2 inhibitor contains an “organic component” to minimize the well-known accelerating behaviour of calcium nitrite. Taylor (Taylor 1997) gives an excellent summary of current knowledge on sugar-based retarders. The retarding effect arises from adsorption of the sugar on the hydration product or clinker phase, thereby interfering or inhibiting growth. It is further stated that this “poisoning” of the hydration products enables calcium ions to coexist in solution with silicate, hydroxoaluminate, and hydroxoferrite ions at higher concentrations than is normally possible. From this, we would expect an increase in the calcium concentration of expressed solutions from the CN2 mixes, however this is not the case for OPC. Other research found that silicon concentrations



decrease soon after the initial 20 seconds of mixing to levels seen in unretarded mixes. Retarders in general are more effective in cements that have low aluminate concentrations, as both the aluminates and their hydration products consume disproportionate amounts of retarder. It is possible that this is the reason for the high calcium concentrations in the white but not in the OPC. The reasons for higher calcium concentrations in the white mix containing  $\text{Ca}(\text{NO}_3)_2$  are not as clear. Calcium nitrate, also a known set accelerator, would be expected to show similar behaviour as the CN1 inhibitor. However, its behaviour is parallel to that exhibited by CN2. This may be partially due to the high stability and solubility of calcium nitrate, having values of  $-742.8$  kJ/mol and  $121.2$  g/100 cc cold water, respectively (CRC 1994).

Potassium levels are significantly higher in the OPC expressed pore solutions than those expressed from white cement paste samples because of the initial higher percentage of  $\text{K}_2\text{O}$  in the OPC cement, which is approximately four times higher than that found in white cement powder. Potassium levels increase in the Control and CN1 OPC solutions with exposure of the cylinder to ponding solution, while the opposite effect is observed with CN2 and  $\text{Ca}(\text{NO}_3)_2$  solutions. This may be a reaction by the system to maintain the pH level of the pore solution, which will be discussed later.

Sodium levels in solutions expressed from cylinders prior to exposure to ponding solution are higher in the mixes made with white cement, again due to the higher initial concentration of  $\text{Na}_2\text{O}$  in the original white cement powder than in OPC (0.17% vs. 0.12%, respectively). In most cases, after exposure to ponding solution, sodium and chloride levels are a function of the volume of ponding solution absorbed by each cylinder, where mixes that absorbed higher volumes of ponding solution exhibit higher concentrations of sodium and chloride. The

exception is again observed with mixes containing  $\text{Ca}(\text{NO}_3)_2$ , where the white cement paste cylinder had a higher sodium concentration despite having absorbed lower volume of ponding solution than the OPC mix. The explanation for this not well understood at this time.

Sodium and chloride concentrations must be taken into consideration with the volume of ponding solution absorbed by each mix, as this is their primary source. Table 8.6 compares these concentrations as a function of ponding solution absorbed for the white and OPC mixes. Sodium concentrations are consistently higher in the ponded white cement pastes mixes, irrespective of inhibitor addition. In the majority of mixes, chloride concentrations are higher in the ponded OPC mixes, with the exception of the ponded white  $\text{Ca}(\text{NO}_3)_2$  mix. These results are consistent with the high total chloride concentrations obtained by titration. As these values take into consideration the volume of ponding solution absorbed, this suggests that in general the white cement mixes are more effective at reducing the concentration of free chlorides in the pore solution. The imbalance between sodium and chloride concentrations is in all probability due leaching of hydroxide while chlorides are ingressing into the cement paste, thereby maintaining charge neutrality.

Little difference in nitrite or nitrate concentration is noted in solutions expressed from ponded white cement and OPC paste cylinders.

Figure 8.21 compares the pH values of solutions expressed from unponded and ponded white cement and OPC paste cylinders. Prior to ponding, pH values of all OPC paste mixes are higher in magnitude than comparable white cement paste mixes. Although pH is an indication of the concentration of hydroxide ions, it is also a function of the concentration of

**Table 8.6 Relationship of [Na<sup>+</sup>] and [Cl<sup>-</sup>] to the volume of absorbed ponding solution in ponded White Cement and OPC paste cylinders**

		Absorbed Ponding Solution (mL)	[Conc./Sol. Absorbed (M/mL)]	
			[Na <sup>+</sup> ]	[Cl <sup>-</sup> ]
Control	White	7	$2.93 \times 10^{-2}$	$3.35 \times 10^{-3}$
	OPC	93	$1.04 \times 10^{-2}$	$4.34 \times 10^{-3}$
CN1	White	7	$2.74 \times 10^{-2}$	$1.28 \times 10^{-4}$
	OPC	240	$5.35 \times 10^{-3}$	$2.42 \times 10^{-3}$
CN2	White	9	$4.07 \times 10^{-2}$	$6.17 \times 10^{-3}$
	OPC	115	$9.23 \times 10^{-3}$	$7.70 \times 10^{-3}$
Ca(NO <sub>3</sub> ) <sub>2</sub>	White	62	$2.55 \times 10^{-2}$	$5.07 \times 10^{-3}$
	OPC	120	$2.13 \times 10^{-3}$	$1.10 \times 10^{-3}$

the alkali metals, in this case potassium and sodium. As stated in Chapter 7, potassium has a greater influence on increasing alkalinity than sodium. As OPC cement has a higher concentration of potassium than white cement, higher pH values of the expressed solutions are observed. After exposure to ponding solution, both white cement and OPC paste solutions experience a drop in pH. This is again related to the concentration of hydroxide and potassium in the mixes. A slight drop in potassium concentration results in a slight drop in the pH, as is observed in all the white cement mixes. In the ponded OPC Control and CN1 solutions, however, an increase in potassium concentration still results in a decrease in pH. However, this decrease is not as large in magnitude as the ponded OPC CN2 and Ca(NO<sub>3</sub>)<sub>2</sub> mixes, where a dramatic drop in potassium concentration occurs upon ponding.

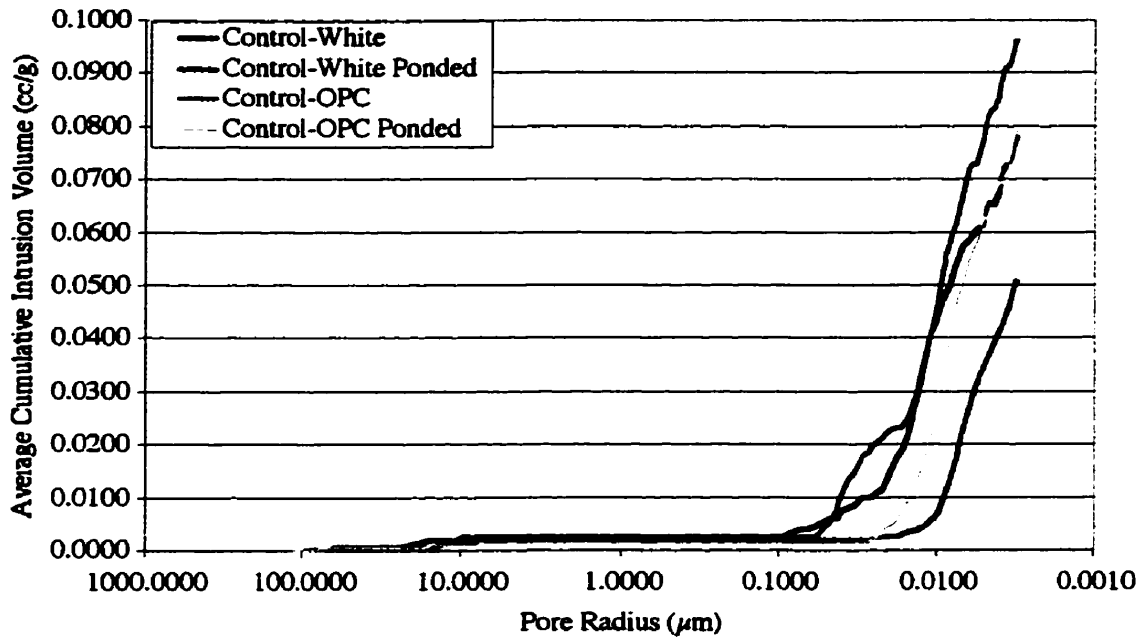


Figure 8.1 Average cumulative intrusion volume vs. pore radius for Control cylinders

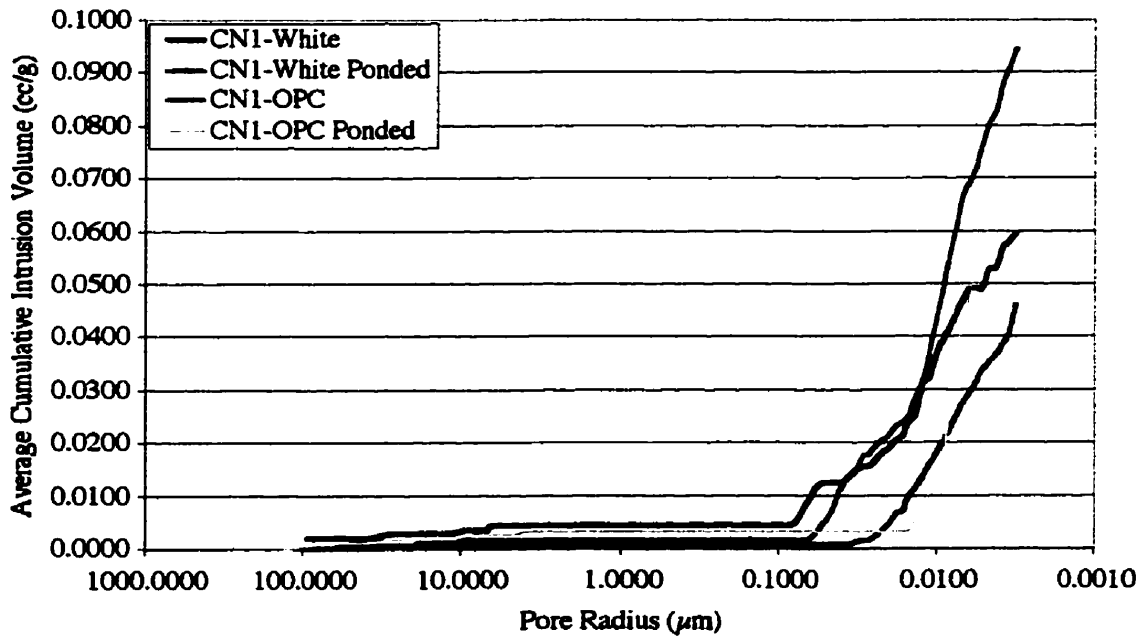


Figure 8.2 Average cumulative intrusion volume vs. pore radius for CN1 cylinders

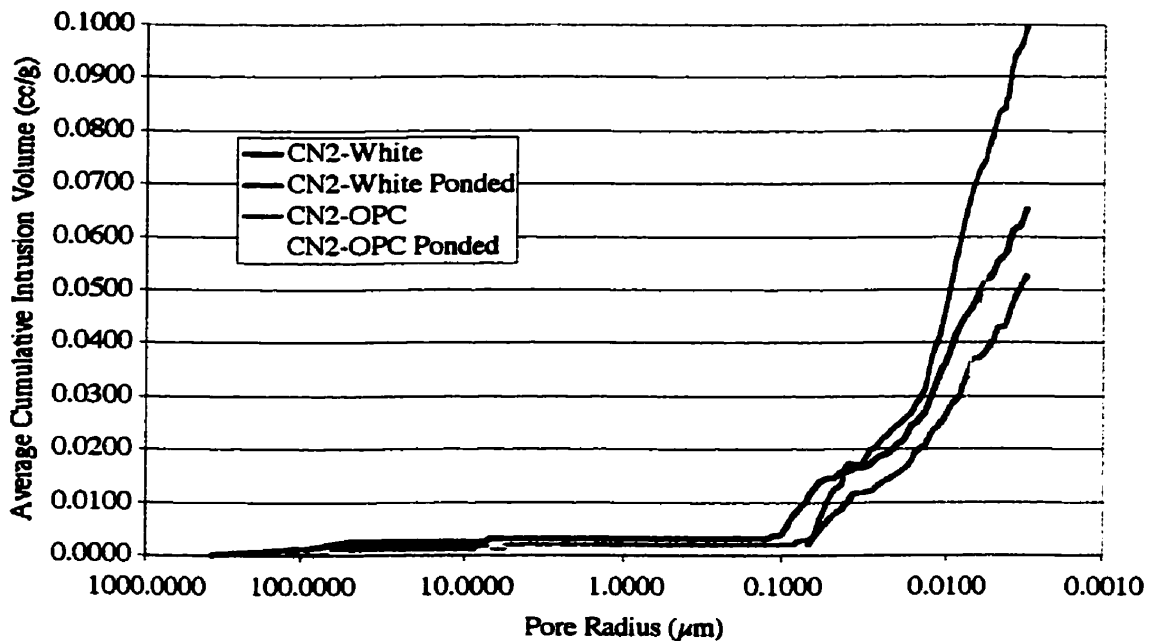


Figure 8.3 Average cumulative intrusion volume vs. pore radius for CN2 cylinders

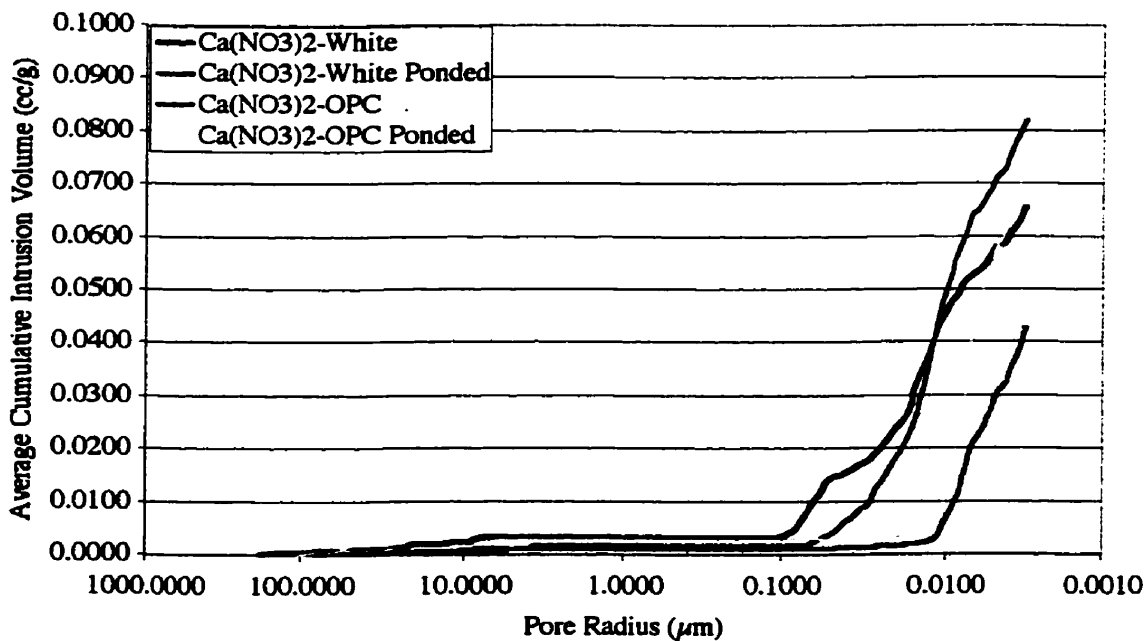


Figure 8.4 Average cumulative intrusion volume vs. pore radius for Ca(NO<sub>3</sub>)<sub>2</sub> cylinders

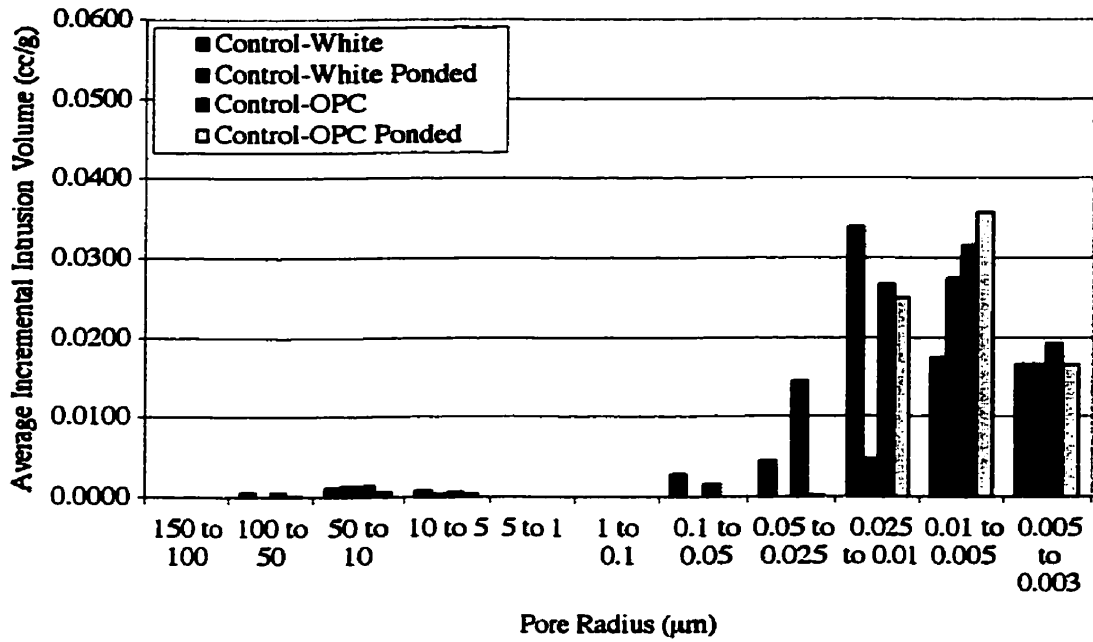


Figure 8.5 Average incremental intrusion volume vs. pore radius for Control cylinders

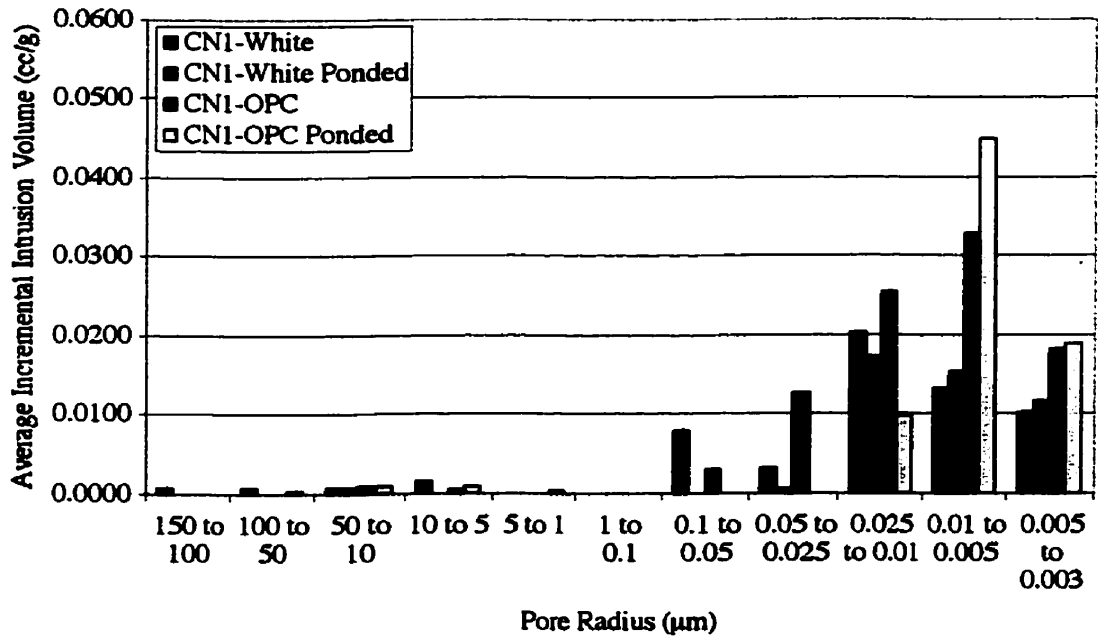


Figure 8.6 Average incremental intrusion volume vs. pore radius for CN1 cylinders

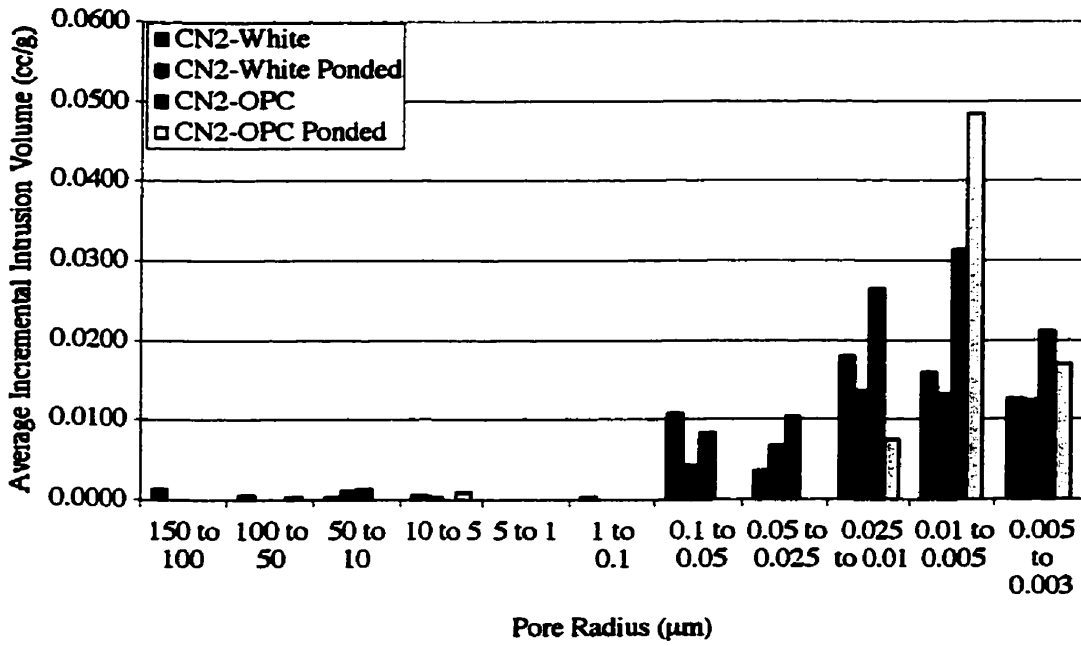


Figure 8.7 Average incremental intrusion volume vs. pore radius for CN2 cylinders

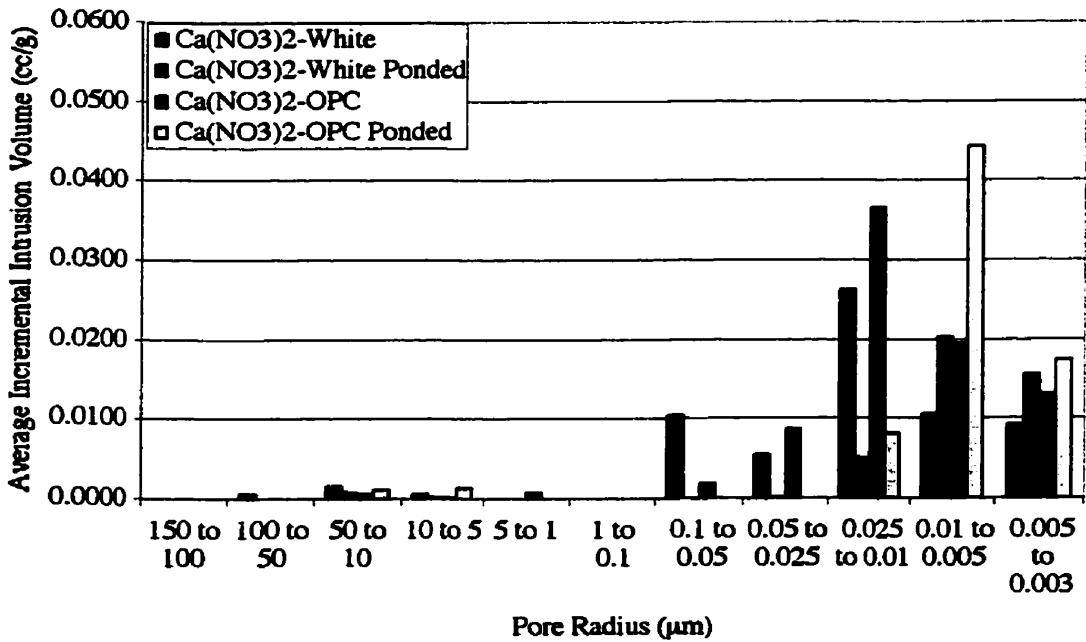


Figure 8.8 Average incremental intrusion volume vs. pore radius for Ca(NO<sub>3</sub>)<sub>2</sub> cylinders

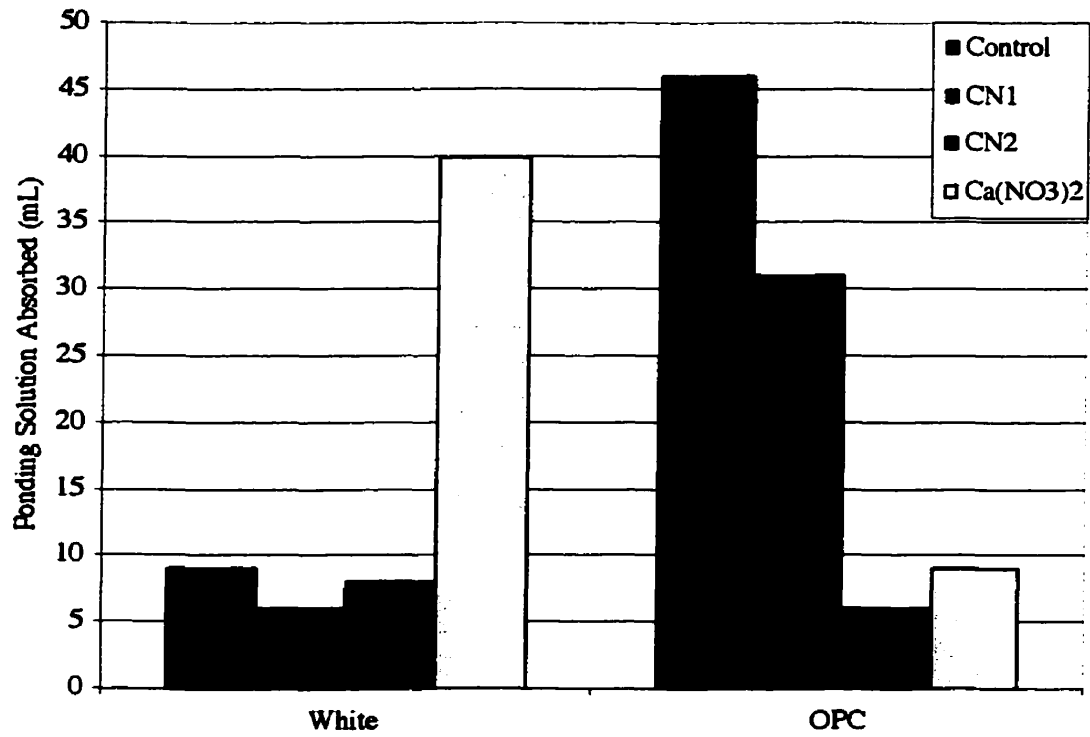


Figure 8.9 Volume of ponding solution absorbed by ponded White Cement and OPC Paste cylinders



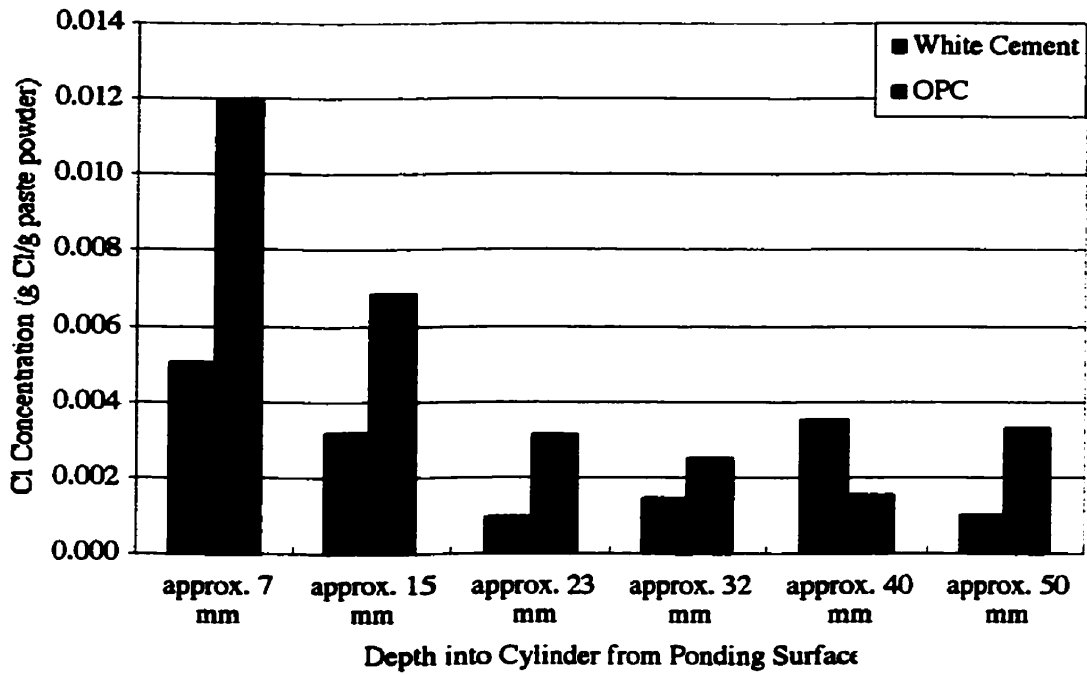


Figure 8.10 Chloride profiles for Control White Cement and OPC Paste cylinders

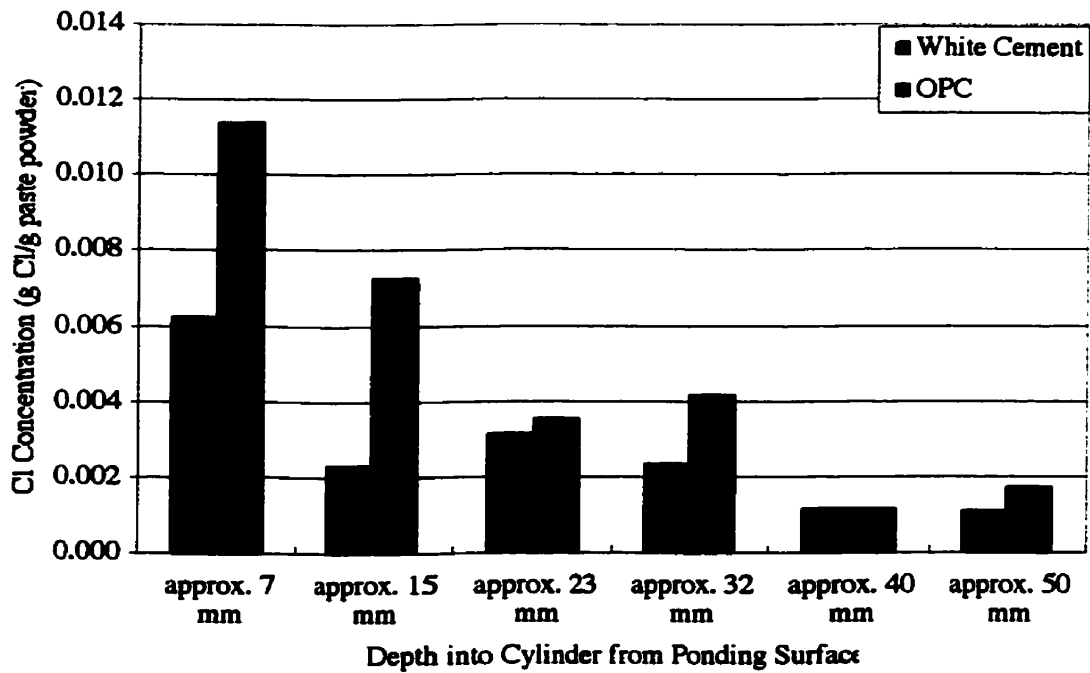


Figure 8.11 Chloride profiles for CN1 White Cement and OPC Paste cylinders

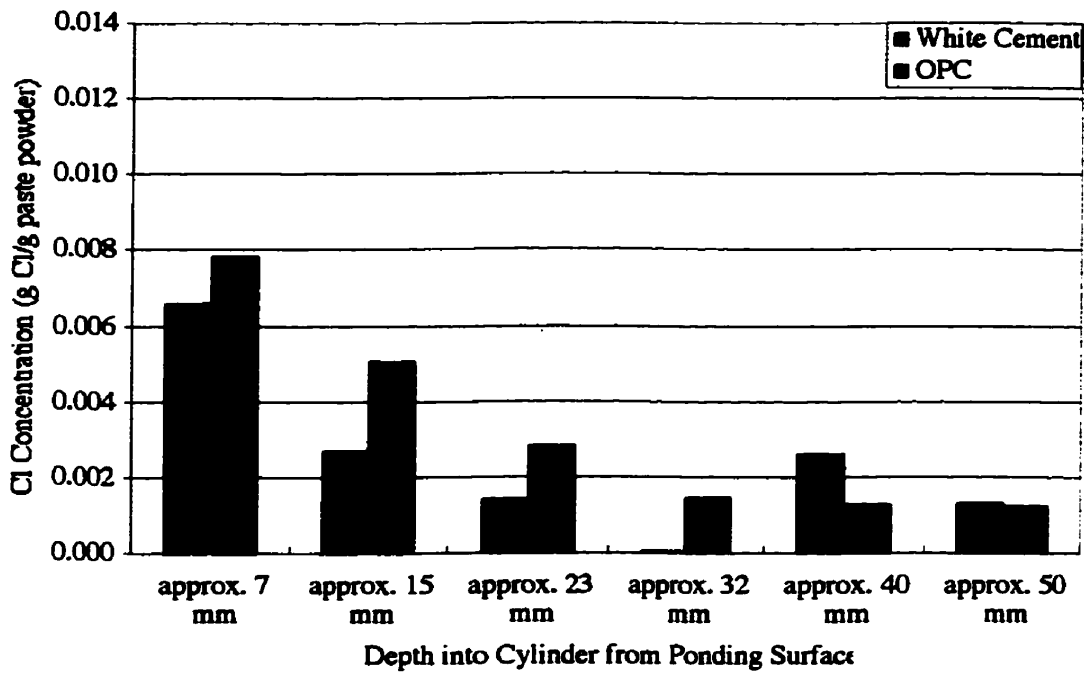


Figure 8.12 Chloride profiles for CN2 White Cement and OPC Paste cylinders

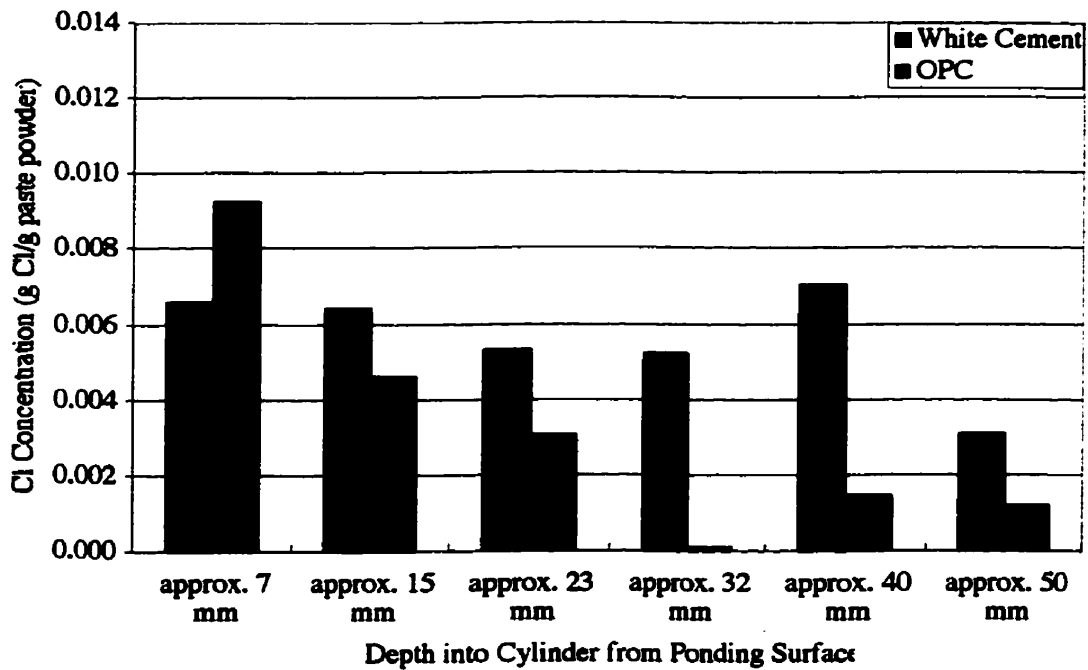


Figure 8.13 Chloride profiles for Ca(NO<sub>3</sub>)<sub>2</sub> White Cement and OPC Paste cylinders

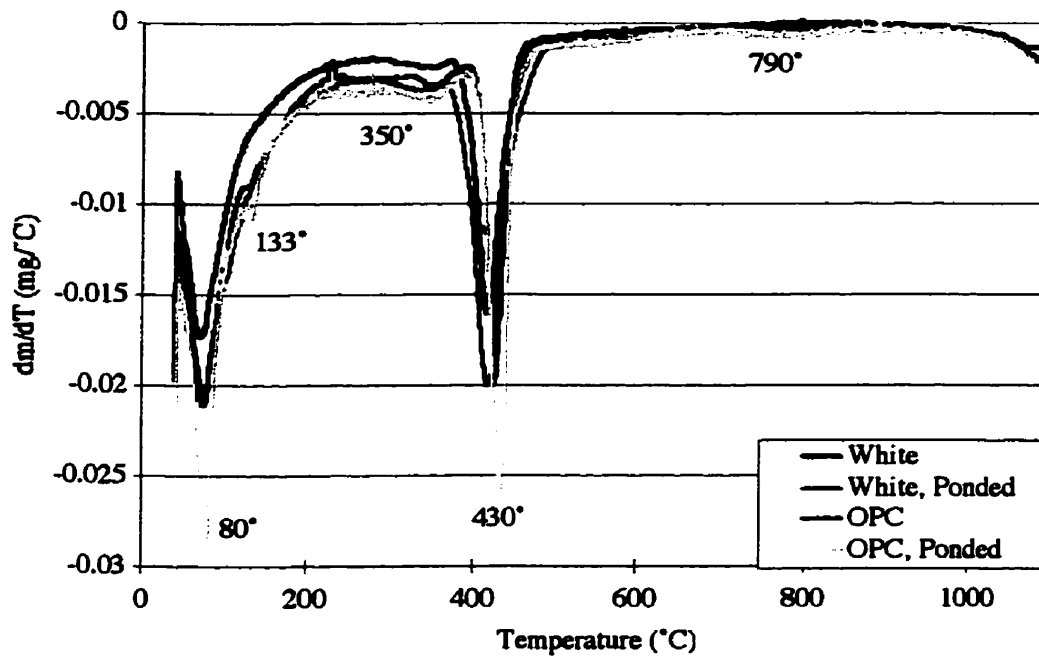


Figure 8.14 DTG of Control cylinders

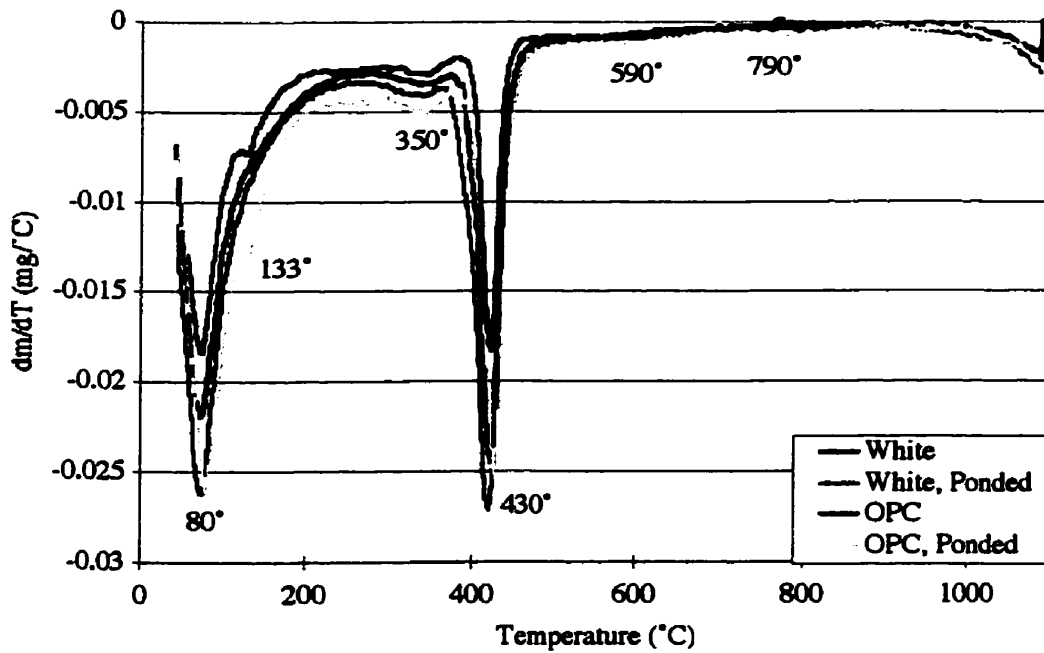


Figure 8.15 DTG of CN1 cylinders

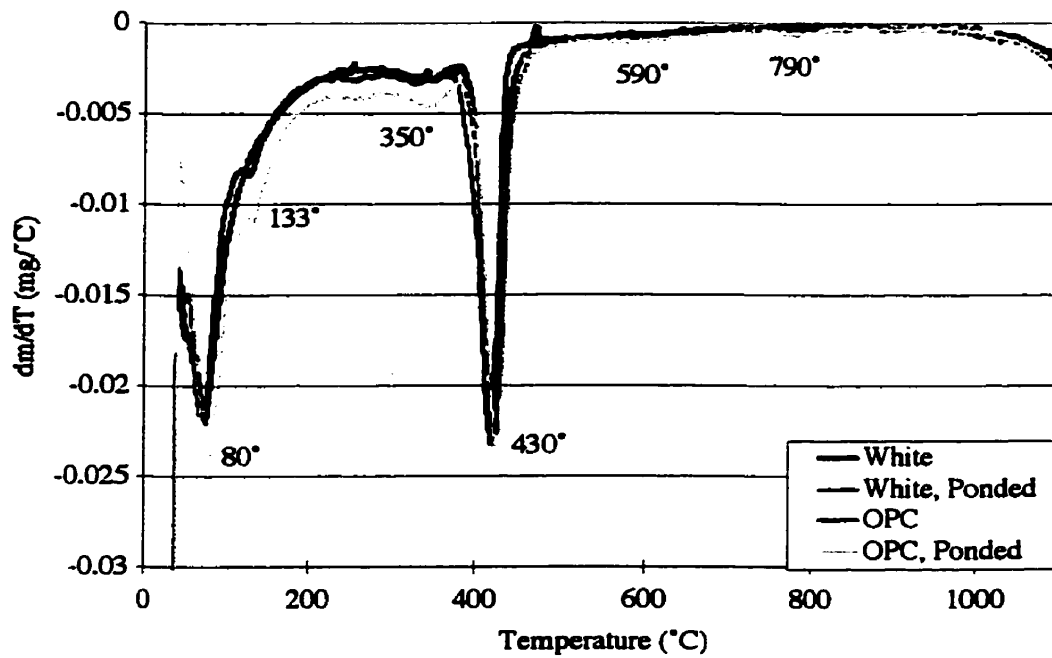


Figure 8.16 DTG of CN2 cylinders

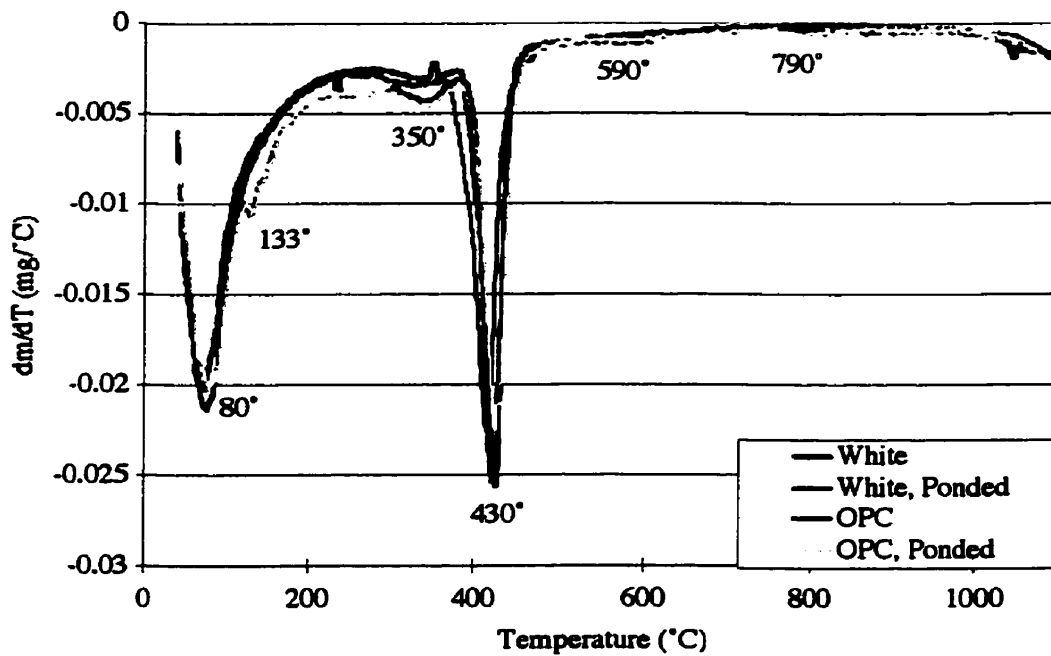


Figure 8.17 DTG of Ca(NO<sub>3</sub>)<sub>2</sub> cylinders

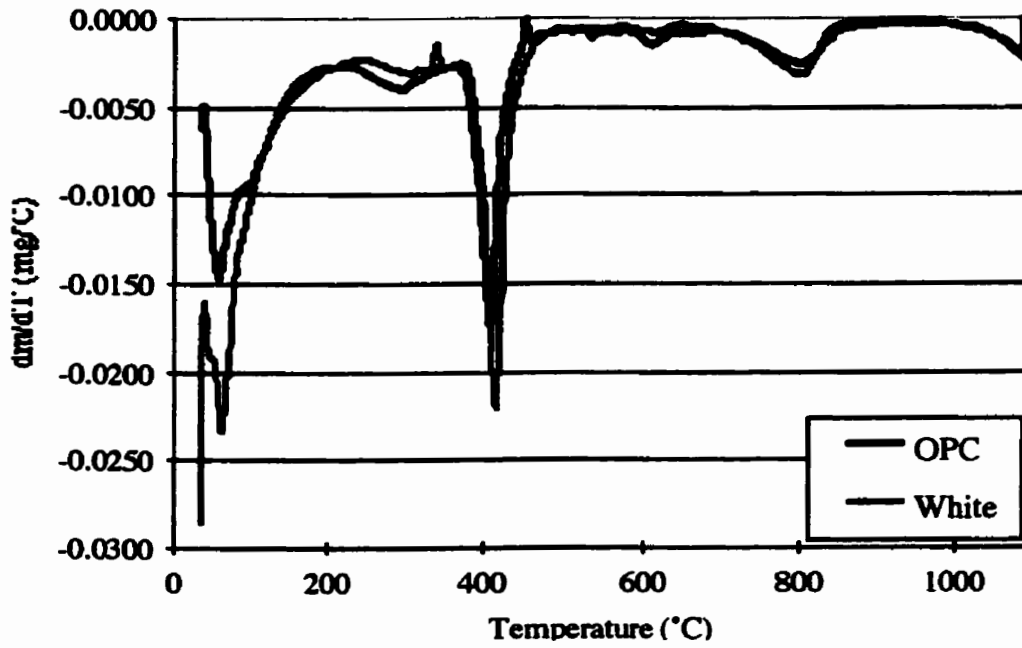


Figure 8.18 DTG of Control cylinders containing 2 % admixed chlorides

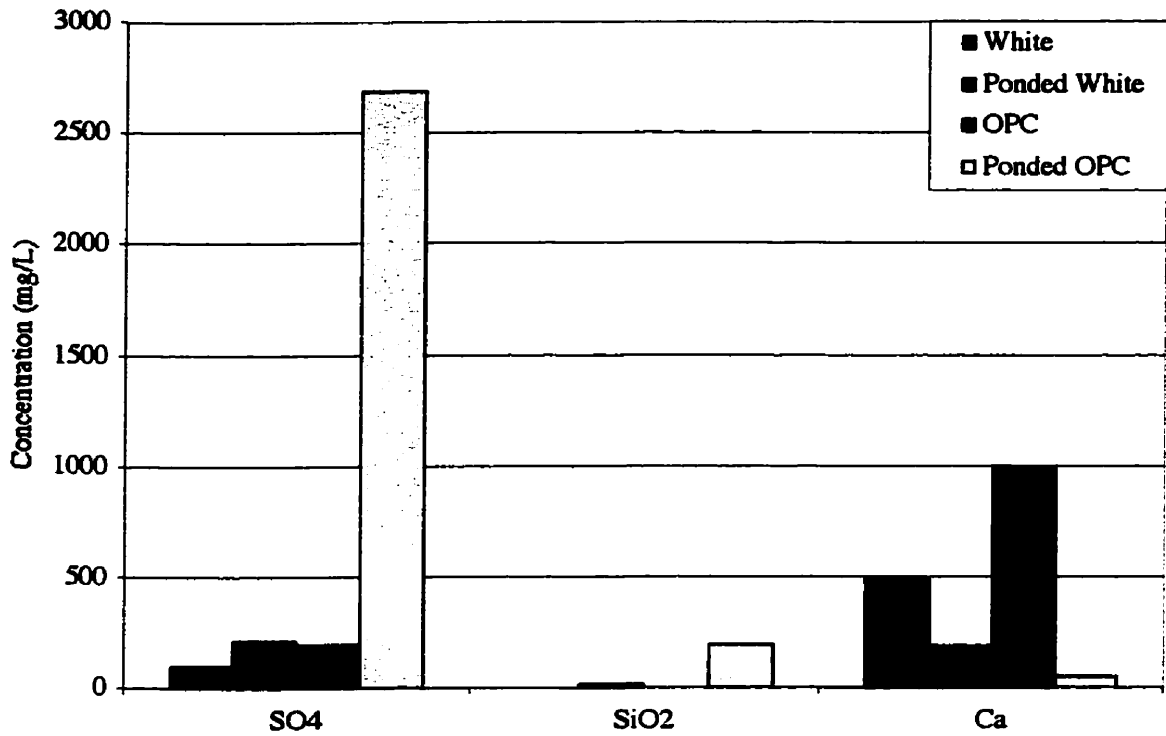


Figure 8.19a Analysis of expressed pore solutions from Control cylinders:  $\text{SO}_4^{2-}$ ,  $\text{SiO}_2^-$  and  $\text{Ca}^{2+}$

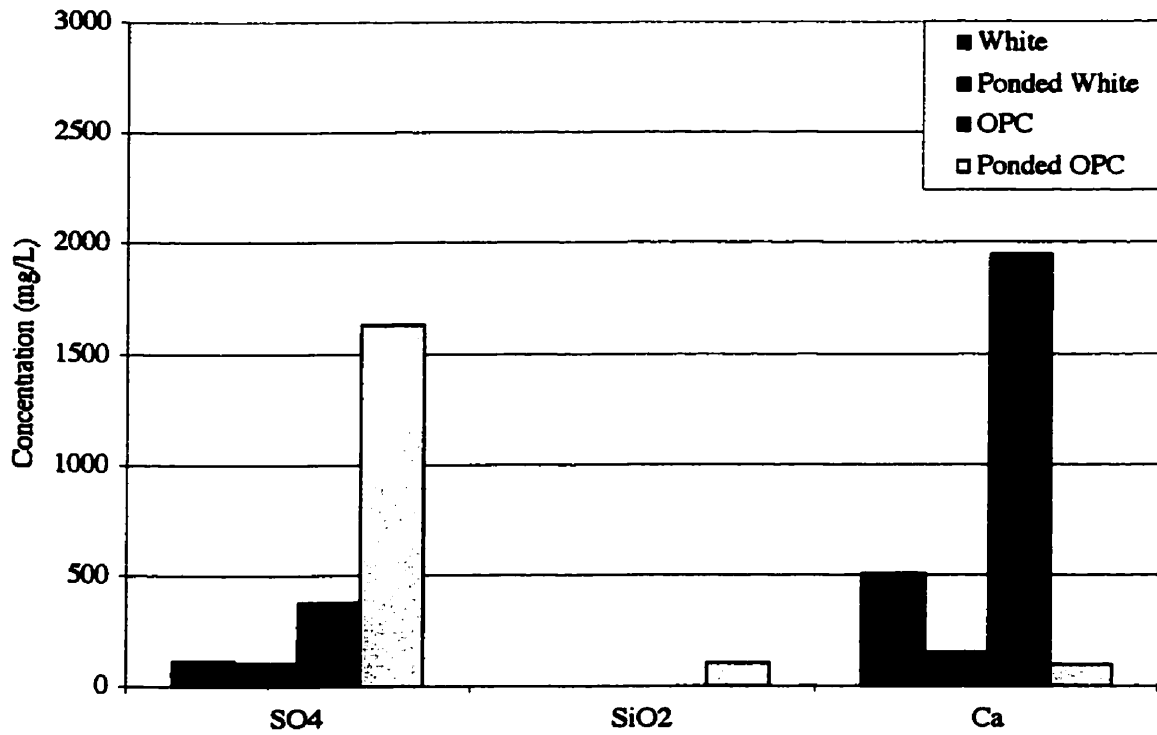


Figure 8.19b Analysis of expressed pore solutions from CN1 cylinders:  $\text{SO}_4^{2-}$ ,  $\text{SiO}_2^-$  and  $\text{Ca}^{2+}$

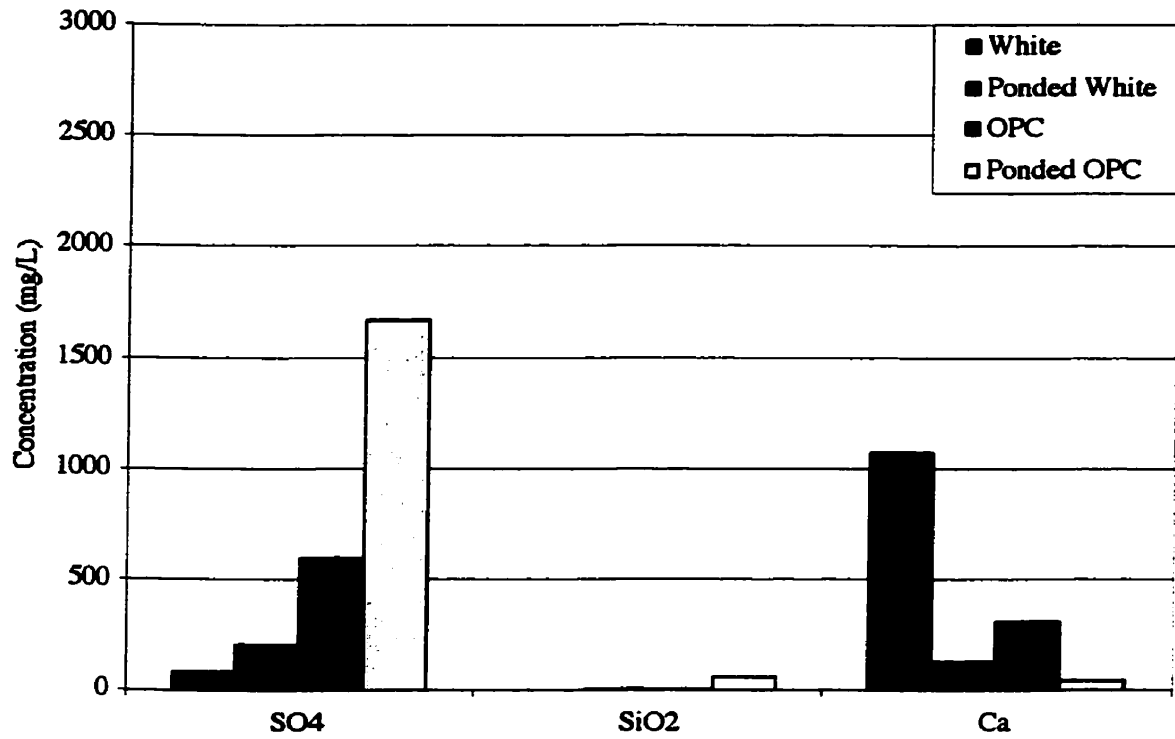


Figure 8.19c Analysis of expressed pore solutions from CN2 cylinders:  $\text{SO}_4^{2-}$ ,  $\text{SiO}_2^-$  and  $\text{Ca}^{2+}$

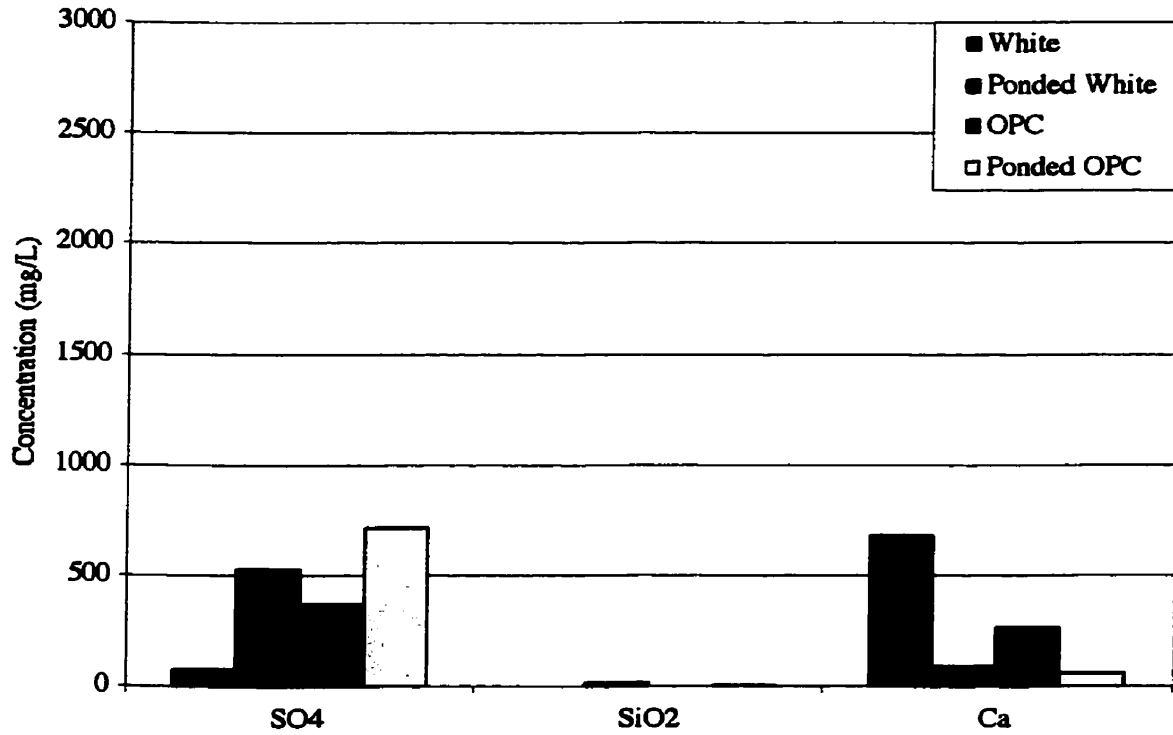


Figure 8.19d Analysis of expressed pore solutions from  $\text{Ca}(\text{NO}_3)_2$  cylinders:  $\text{SO}_4^{2-}$ ,  $\text{SiO}_2^-$  and  $\text{Ca}^{2+}$

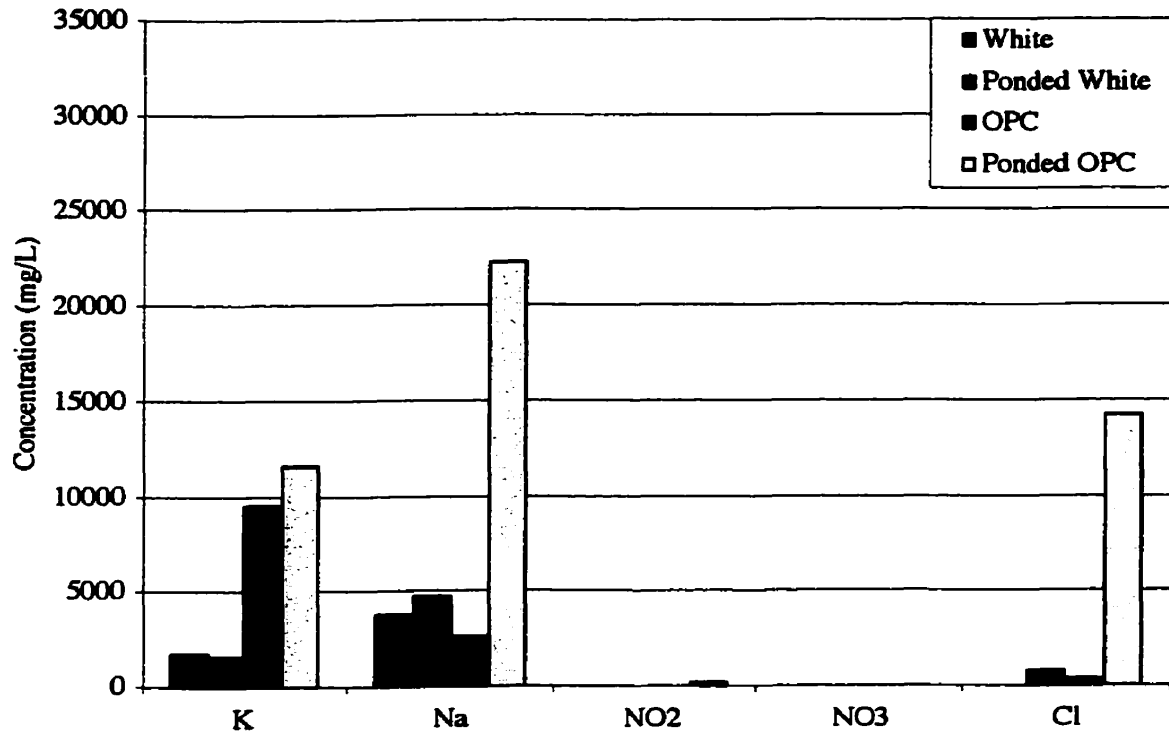


Figure 8.20a Analysis of expressed pore solutions from Control cylinders:  $K^+$ ,  $Na^+$ ,  $NO_2^-$ ,  $NO_3^-$  and  $Cl^-$

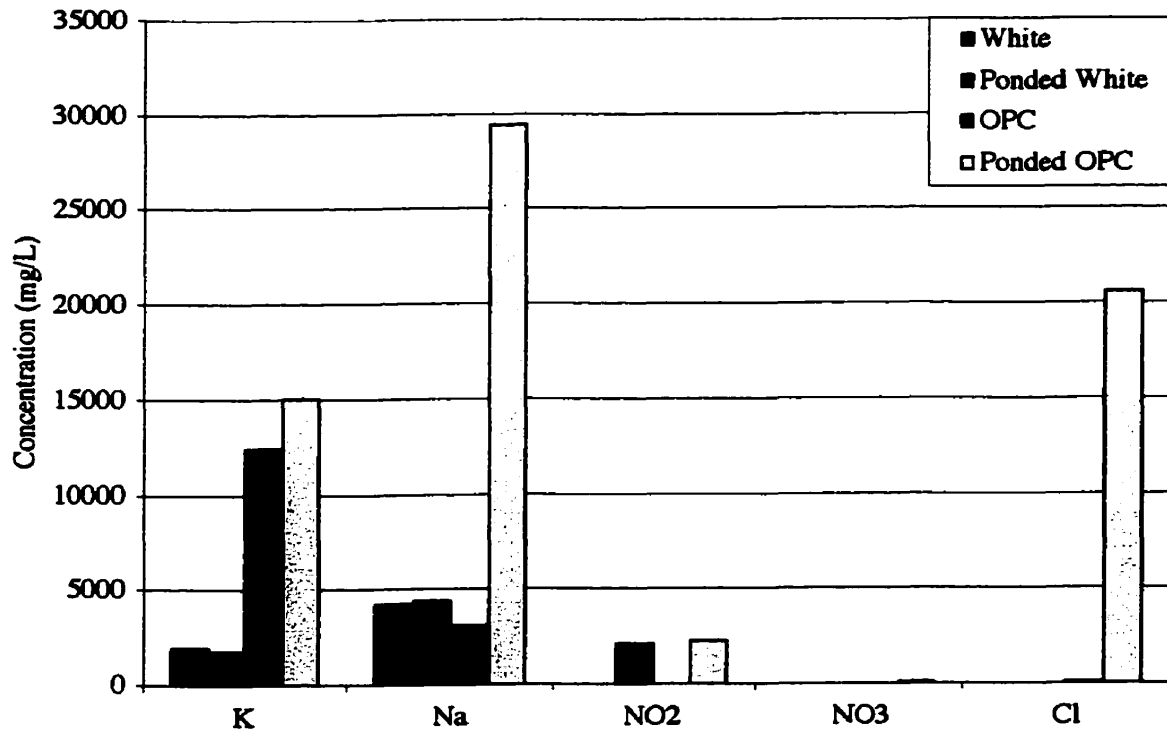


Figure 8.20b Analysis of expressed pore solutions from CN1 cylinders:  $K^+$ ,  $Na^+$ ,  $NO_2^-$ ,  $NO_3^-$  and  $Cl^-$



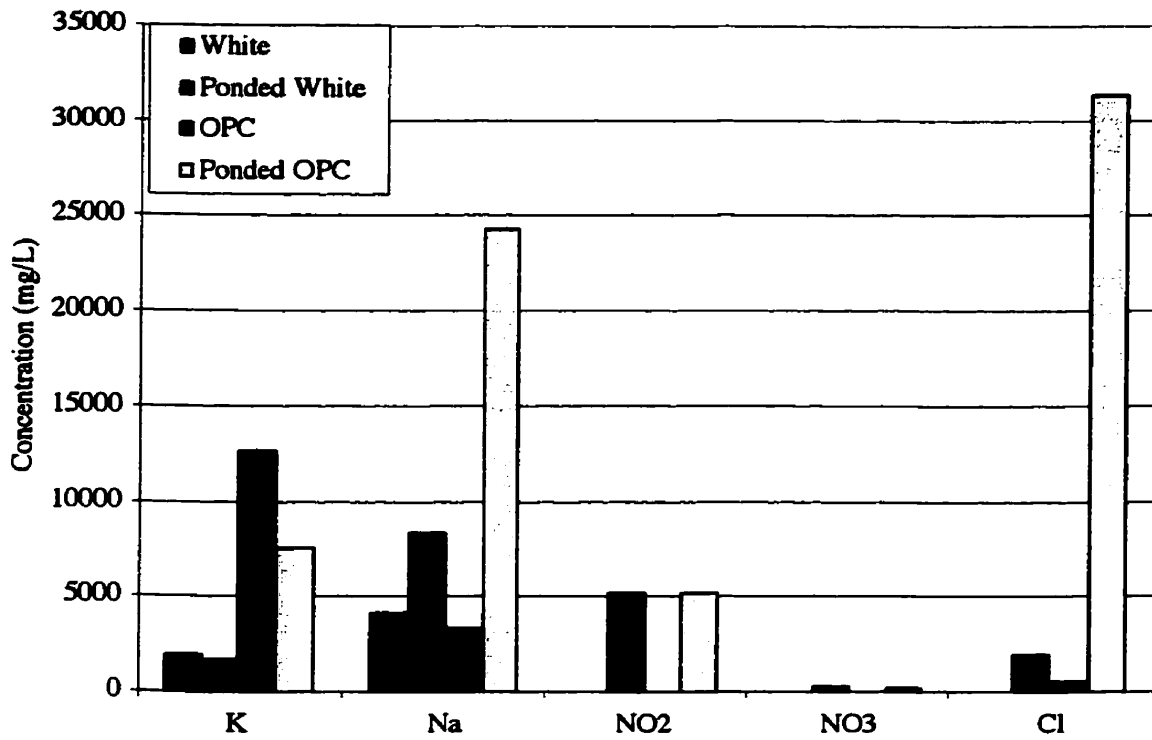


Figure 8.20c Analysis of expressed pore solutions from CN<sub>2</sub> cylinders: K<sup>+</sup>, Na<sup>+</sup>, NO<sub>2</sub><sup>-</sup>, NO<sub>3</sub><sup>-</sup> and Cl<sup>-</sup>

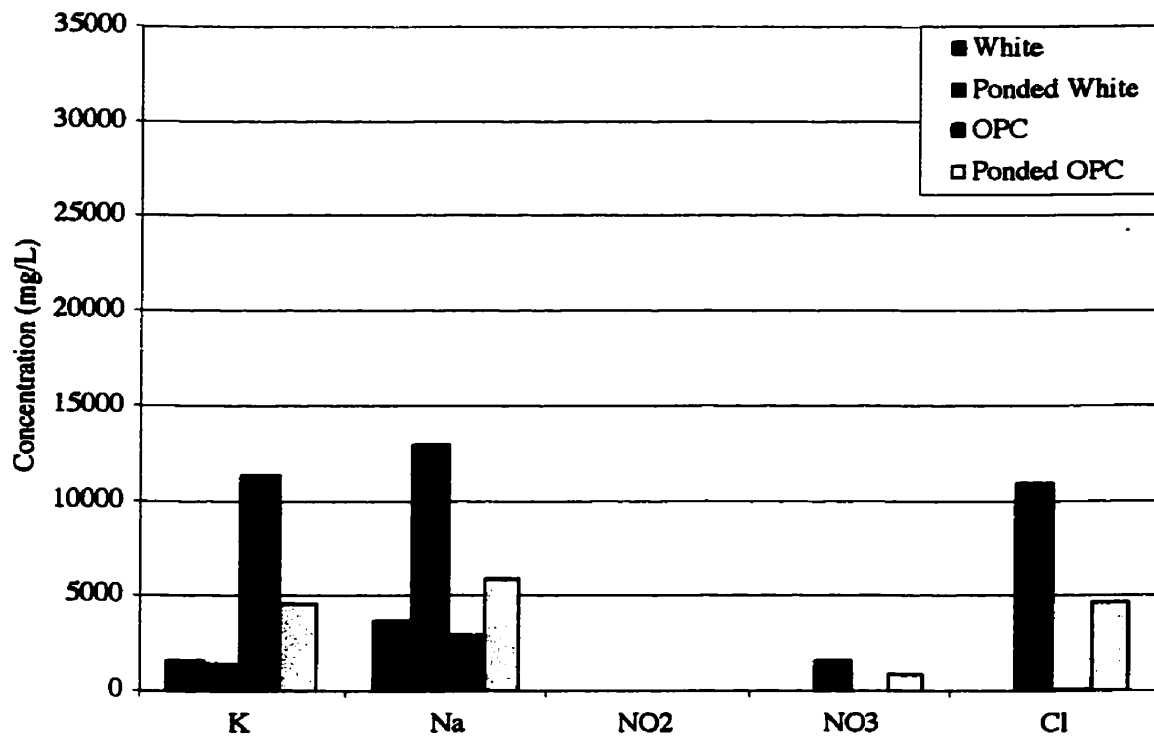


Figure 8.20d Analysis of expressed pore solutions from Ca(NO<sub>3</sub>)<sub>2</sub> cylinders: K<sup>+</sup>, Na<sup>+</sup>, NO<sub>2</sub><sup>-</sup>, NO<sub>3</sub><sup>-</sup> and Cl<sup>-</sup>

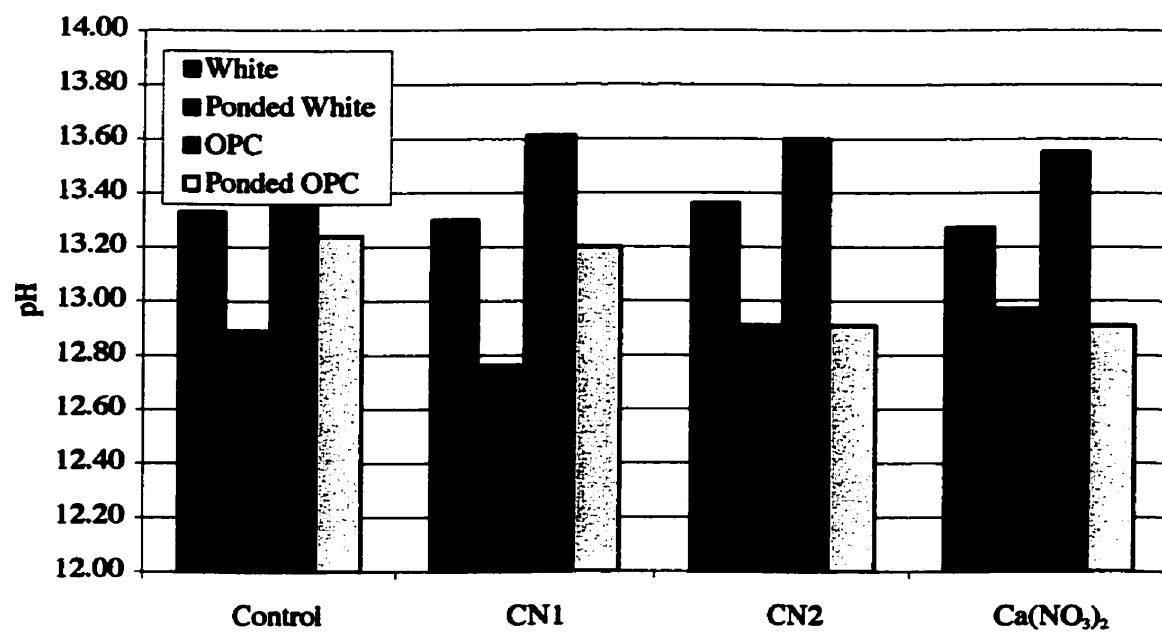


Figure 8.21 pH values of expressed pore solutions

## **Chapter 9**

### **Overall Discussion, Conclusion and Recommendations**

#### **9.1 Overall Discussion**

The primary objective of this investigation was to determine the mechanism of inhibition by calcium nitrite and calcium nitrate in concrete. Integration of the results presented in Chapters 5 through 7 suggests that the mechanism of inhibition by both calcium nitrite and calcium nitrate is the enhanced chemical binding of the chlorides, with the effect being weakest in the CN2 and  $\text{Ca}(\text{NO}_3)_2$  mixes. The compounds involved in the binding are not only the well-recognized Friedel's salt, but also calcium hydroxychloride ( $\text{Ca-OH-Cl}$ ) and the incorporation of chlorides into the C-S-H by replacement of  $\text{OH}^-$  in the interlayer structure of the hydrate. The formation of these products will effectively remove free chlorides from the pore solution and, by changing both the gel and capillary pore structures, affect the transport of aqueous solutions containing deleterious components to the reinforcing steel.

Studies investigating the corrosion behaviour of steel immersed in synthetic pore solutions with and without inhibitor confirmed that the addition of CN1, CN2 and  $\text{Ca}(\text{NO}_3)_2$  did not provide any decrease in corrosion which could be attributed to a more protective film. In fact, localized forms of corrosion were more likely to occur on samples immersed in these solutions. Examination of the passive film by Raman spectroscopy also found no evidence of passive film enhancement due to calcium nitrite as CN1.

While the analysis of the Control synthetic pore solution showed that 100% of the added chlorides remains dissolved in the solution, both synthetic solutions containing nitrite have

lower dissolved chloride concentrations than theoretically calculated. This indicates that some of the chlorides added to the solutions containing nitrite precipitate out in solid form. This is in spite of the lack of components normally associated with bound chlorides in cement, namely the calcium aluminate compounds. Therefore, it is logical to conclude that another type of chloride-binding compound is precipitating in the synthetic pore solutions containing calcium nitrite. The exact composition of this solid is up to interpretation. The most likely candidate, on the basis of these and thermal analysis experiments, is calcium hydroxychloride. Moreover, the high potassium content of the “tuber” precipitate and the “bulk” precipitate from the synthetic CN1 solution (Figure 5.13 and Table 5.6) indicates that potassium is substituted for some of the calcium in this structure.

Results of thermal analysis confirm the formation of other chloride binding compounds in cements, namely Ca-OH-Cl and  $\text{Cl}^-$  in C-S-H. The higher levels of these components in pastes containing calcium nitrite and calcium nitrate inhibitors implies that the addition of these chemicals increases the formation of these forms of bound chlorides. The replacement of  $\text{Cl}^-$  for some of the  $\text{OH}^-$  in the C-S-H may also affect the interlayer spacing in the C-S-H, thereby affecting fine porosity. Due to the overlapping of the endotherms in the DTG spectra of Friedel’s salt and other compounds, it is difficult to draw conclusions regarding the influence of the inhibitors on the formation of the Friedel’s salts.

The effect of inhibitor on the porosity of the cement pastes is complicated. Although all of the inhibitors change the amount of total porosity compared with those in the Control mixes, the specific effect is strongly controlled by the type of cement used. The changes became even more varied after the mixes were exposed to NaCl solution. One particularly confusing result is the increase in coarse porosity of OPC cement pastes containing inhibitors when

exposed to ponding solution, while a similar increase did not occur in the parallel white cement paste mixes. It is possible that micro-cracks may have formed in these OPC cylinders due to this exposure. This is further supported by comparison of the volume of ponding solution absorbed by samples that were used for pore solution expression with the volume of ponding solution absorbed by samples subjected to MIP, as shown in Table 9.1. Both sets of OPC cylinders absorbed considerably more ponding solution than comparable white cement cylinders. As it is highly unlikely that the existing coarse pores have grown in diameter or number, the introduction of microcracks appears to be a logical assumption. Substitution of  $\text{Cl}^-$  for  $\text{OH}^-$  in the C-S-H may cause the microcracking, as this ion exchange may lead to a volume expansion due to the larger atomic radius for  $\text{Cl}^-$  compared to  $\text{OH}^-$  (0.181 and 0,137 nm, respectively) (CRC 1994).

Table 9.1 Comparison of ponding duration and volume of ponding solution absorbed of MIP and Pore Solution Expression Samples

Cement Type	Mix	MIP		Pore Solution Expression	
		Duration of Ponding (days)	Vol. Ponding Solution Absorbed (mL)	Duration of Ponding (days)	Vol. Ponding Solution Absorbed (mL)
White	Control	412	9	452	7
	CN1	412	6	452	7
	CN2	412	8	453	9
	$\text{Ca}(\text{NO}_3)_2$	412	40	453	62
OPC	Control	385	46	426	93
	CN1	390	31	432	240
	CN2	390	6	432	115
	$\text{Ca}(\text{NO}_3)_2$	390	9	432	120

Thermal analysis of ponded OPC pastes shows the existence of  $\text{Cl}^-$  in C-S-H and was not observed in ponded white cement pastes, which may explain why an increase in coarse porosity was not observed in the former pastes. Another, or additional, scenario may be that more ponding solution is being absorbed into the fine porosity of the cement paste than in the coarse pores. This is indicated by the greater change in magnitude of the fine porosity than

of coarse porosity in both cements (Tables 6.5 and 6.11, pages 94 and 98). Chloride profiles in the same samples used for MIP investigations show that the OPC mixes also absorbed more chloride than the white mixes, which somewhat correlates with fine porosity observations.

Lack of consistency in porosity measurements determined through MIP is considered an indication of the limitations of the technique. It is generally acknowledged that the pore size distributions determined by MIP are not reliable (Taylor 1997, Diamond 1994) due to the factors mentioned in Chapter 2, page 30, in addition to the problems associated with sample preparation. It is also possible that a large pore will have a small entry, and therefore be registered as a small pore. Additionally, MIP appears to have difficulty in measuring coarse porosity (diameter  $> 1 \mu\text{m}$ ), which is observed in the figures found in Appendix C.

Surprisingly, in the DTG experiments, none of the white cement paste samples exhibited endotherms associated with  $\text{Ca-OH-Cl}$  or  $\text{Cl}^-$  in  $\text{C-S-H}$  even in the cylinder with  $\text{Ca}(\text{NO}_3)_2$  which absorbed a high volume of ponding solution, similar to the volume absorbed by the Control OPC cylinder. However, because the amount of dissolved chlorides in the expressed pore solutions relative to the total chloride concentrations as determined by chloride titration, is significantly lower than would be expected if binding were only by the aluminate phases, other solid phases must be forming in the white cement pastes. Moreover, as shown in Figure 8.18, white cement paste is capable of forming these other forms of bound chloride. Therefore, it is suggested that there is a sequence of binding in the cement paste, shown in Figure 9.1, and that this is accelerated/enhanced in cement pastes that contain calcium nitrite and calcium nitrate inhibitors. This sequence is based on the following observations:

1. there were no detectable endotherms associated with  $\text{Cl}^-$  in C-S-H and Ca-OH-Cl in any of the ponded white cement paste cylinders;
2. endotherms for both  $\text{Cl}^-$  in C-S-H and Ca-OH-Cl were detected in white cement paste cylinders that had admixed chlorides, with the former being the dominant of the two phases;
3. sufficient ponding solution was not absorbed by the white cement paste cylinders to stimulate the development of those other forms of bound chloride in the period of exposure of these samples.



Figure 9.1 Sequence of chloride binding in White Cement and OPC pastes

It is also possible that  $\text{Cl}^-$  in C-S-H and Ca/K-OH-Cl form at the same time and that larger quantities of the former are observed in the white cement paste with admixed chlorides due to the higher volume of C-S-H and  $\text{Ca}(\text{OH})_2$  in the cement matrix. Since thermal decomposition of C-S-H does not occur at a specific temperature giving rise to a sharp endotherm (Taylor 1997) but degrades continuously over several hundreds of degrees, it is reasonable to assume that “dilute” solutions of  $\text{Cl}^-$  in C-S-H would behave likewise. It is also difficult to state whether calcium hydroxychloride complex forms from calcium hydroxide already formed from  $\text{C}_3\text{S}$  hydration or is formed during hydration of the remaining anhydrous  $\text{C}_3\text{S}$ , which subsequently reacts because of the exposure to ponding water. The proposed occasional substitution of potassium for calcium in Ca-OH-Cl is based on the results of precipitate analysis from synthetic pore solutions and from the reduced potassium concentrations with exposure to ponding solution in all expressed solutions from white cement paste cylinders and  $\text{CN}_2$  and  $\text{Ca}(\text{NO}_3)_2$  OPC paste cylinders. It was also noted that in expressed pore solutions that experienced a drop in potassium concentration, the drop in pH was larger in magnitude.

Combined results from tests in synthetic pore solution and alkalinity measurements from expressed pore solutions show that most of the nitrite, and probably most of the nitrate, is in solid form. Tests in synthetic pore solution showed only slightly lower nitrite/nitrate concentrations than calculated, however they also showed a large reduction in pH with addition of calcium nitrite or calcium nitrate. It must be noted, however, that when tests were conducted in synthetic pore solution, it was assumed that 100 % of the inhibitor remained in the capillary water. A much smaller decrease in pH of the pore solutions expressed from the cement pastes is due to the fact that only a small proportion of the inhibitors remains dissolved in the pore solution. Glasser et al. (Glasser 1999) indicates that a variety of anions (e.g. sulphate, hydroxide, chloride, and carbonate) can be incorporated into the AFm phase of cement paste (Figure 9.2). It follows logically that any anion has this possibility. In fact, Renaudin et al. (Renaudin 2000) were successful in synthesizing AFm with nitrate anion incorporation,  $3\text{CaO}\cdot\text{Al}_2\text{O}_3\cdot\text{Ca}(\text{NO}_3)_2\cdot 10\text{H}_2\text{O}$ .

Pore solution expression from all mixes shows a further decrease in pH when cylinders are exposed to ponding solution containing NaCl. This is in contrast to other results, which show that when sodium chloride is added at the time of mixing, the pH of the capillary water increases (Byfors 1986; Enevoldsen 1993; Mammoliti 1999). A similar decrease in pH is observed in synthetic pore solutions with increasing chloride concentration in the form of NaCl. In the case of the cement paste cylinders, the likely explanation for this decrease is shown in Figure 9.3. The pH of pore solution at the surface will be lower than pore solution at a deeper depth, due to the dilution effect of the ponding water. With increasing depth, the dilution effect is reduced while diffusion of sodium ions into the cement paste results in a “spike” in pore solution pH, which is slightly higher than the pore solution pH of the bulk of



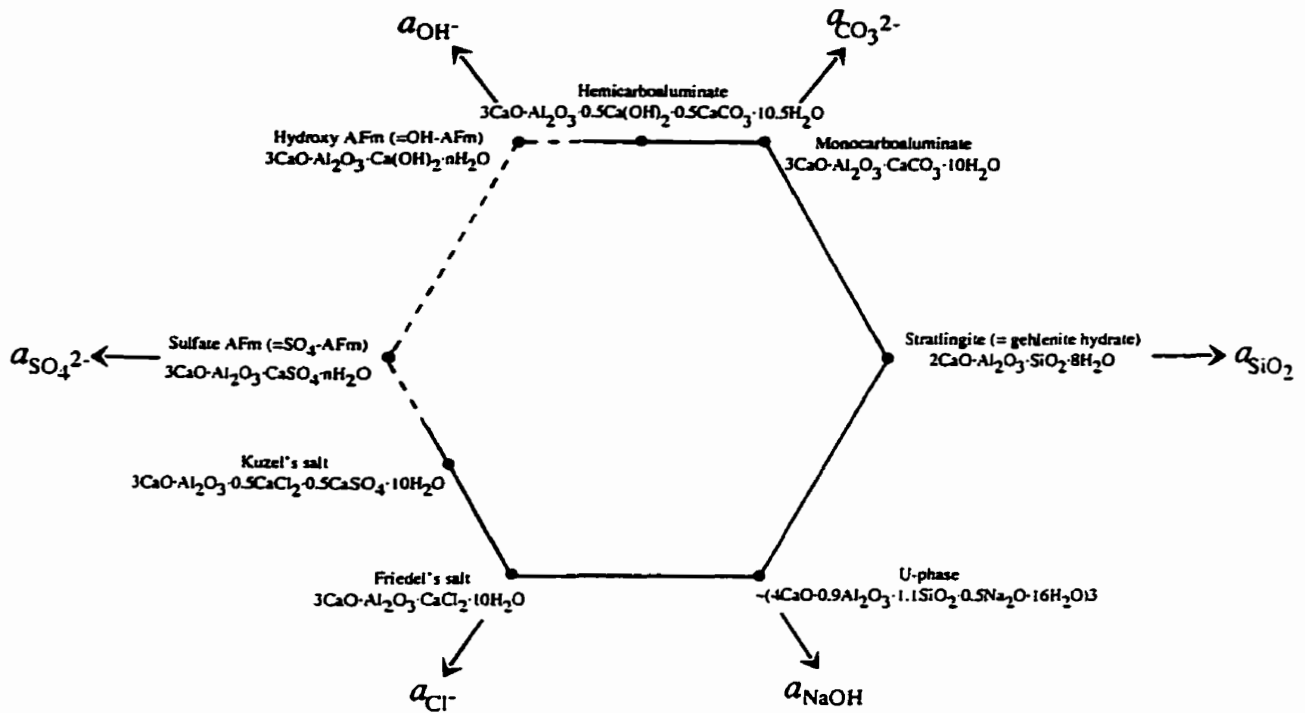


Figure 9.2 Composition-activity diagram of the AFm family at  $-25^{\circ}\text{C}$  (Glasser 1999)

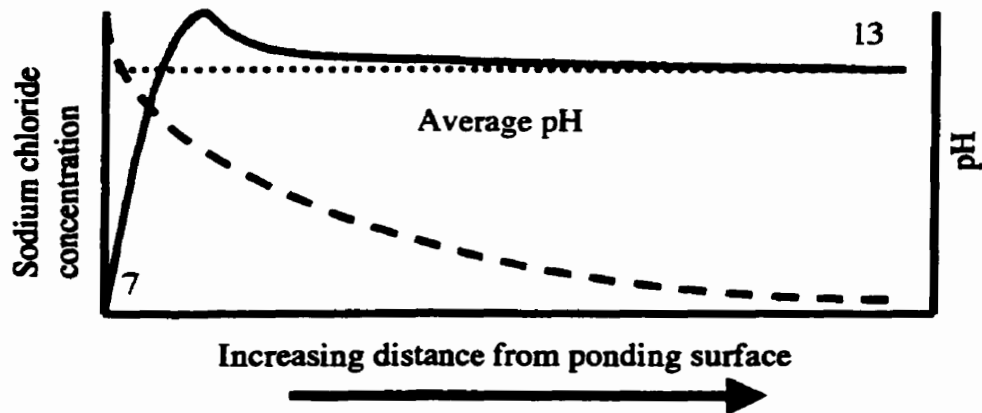


Figure 9.3 Explanation of pH reduction in ponded cement paste cylinders

the cylinder. Therefore, when the pore solution is expressed from the top half of the ponded cylinder, a slightly reduced pH as compared to that expressed from unponded cylinders is observed (Reardon 2001). In synthetic pore solutions, the reduction in pH with increasing chloride concentration is likely a result of the precipitation of potassium, as described in Chapter 5, page 65.

Pore solution expression also indicates that, unlike the other mixes, the CN1 white cement paste solution does not experience an increase in sulphate concentration upon exposure to ponding solution. As the increase in sulphate concentration was initially taken as an indicator of the degree of chloride binding in the form of Friedel's salt, it can be inferred that not as much binding was occurring in this paste. On the other hand, the free sulphate released from the conversion of monosulphate to Friedel's salt may be reacting with unhydrated  $C_3A$  to form AFt, which would gradually convert to monosulphate upon sulphate depletion. Midgley and Illston (Midgley 1984) also propose that Friedel's salt results from the reaction of chlorides with anhydrous  $C_3A$ . Therefore, higher amounts of Friedel's salt would be formed in white cement pastes as compared to those studied presently, particularly in the case of CN1, with equivalent exposure to ponding solution.

The results from chloride titration also present some interesting findings. Lower than expected total chloride concentrations were found given the volume of ponding solution absorbed by each of the ponded cylinders, as shown in Table 9.2. This means that the solution penetrating into the samples has a lower  $Cl^-$  concentration than the original ponding solution. For example, the Control white cylinder absorbed approximately 9 mL of ponding solution and has a total chloride concentration of 0.015 g Cl/g paste compared with that theoretically calculated – 0.029 g Cl/g paste – if the solution penetrating into the sample had the same concentration as the ponding solution. The  $Ca(NO_3)_2$  white cylinder absorbed approximately 4.5 times more solution, but contained only twice as much chloride, 0.034 g Cl/g paste. This is because water penetrates by a “domino effect”, whereas chlorides simply “ride the wave”.

**Table 9.2 Comparison of theoretical and measured total chloride content of White and OPC cylinders exposed to ponding solution**

		<b>Vol. Absorbed Ponding Solution (mL)</b>	<b>Theoretical Total Cl<sup>-</sup> (g Cl<sup>-</sup>/g paste)</b>	<b>Measured Total Cl<sup>-</sup> (g Cl<sup>-</sup>/g paste)</b>
<b>White</b>	<b>Control</b>	9	0.029	0.015
	<b>CN1</b>	6	0.019	0.016
	<b>CN2</b>	8	0.026	0.015
	<b>Ca(NO<sub>3</sub>)<sub>2</sub></b>	40	0.129	0.034
<b>OPC</b>	<b>Control</b>	46	0.148	0.026
	<b>CN1</b>	31	0.100	0.026
	<b>CN2</b>	6	0.019	0.017
	<b>Ca(NO<sub>3</sub>)<sub>2</sub></b>	9	0.029	0.017

Another observation of note is that sole reliance on one or two method(s) of analysis would have resulted in an incomplete picture of the influence of calcium nitrite and calcium nitrate on cement paste chemistry. Each technique provided different and complementary information regarding these interactions:

1. chloride titration yielded information regarding the differences in concentration between the solution absorbed and the bulk concentration of ponding solution as well as total chloride concentration profiles;
2. tests in synthetic pore solution indicated that another form of bound chloride evolved was formed in solutions containing nitrite, specifically CN1 and showed the absence of any apparent enhancement of the passive film;
3. pore solution expression demonstrated that most of nitrite or nitrate did not remain in solution, and therefore is incorporated into the cement matrix;
4. thermal analysis confirmed the existence of other forms of bound chlorides and their tendencies to form in different cements;
5. while limited information was gathered from MIP, the influence of both inhibitors and chlorides on the gel porosity was apparent and it is speculated that micro-cracks were developing in some cement mixes containing inhibitors.

## **9.2 Conclusions**

The use of multiple techniques to analyse the effect of inhibitors on cement paste provided a

more complete picture of the exact mechanism of inhibition. It is felt by this researcher that the use of only one technique would have severely limited the possible analysis and possibly led to erroneous conclusions.

Tests in synthetic pore solution with excess  $\text{Ca}(\text{OH})_2$  indicate no benefit of the addition of either calcium nitrite or calcium nitrate on the corrosion behaviour of reinforcing steel, but did show evidence of some chloride binding in calcium nitrite-inhibited solutions.

Examination of the passive film showed that a more inhomogeneous film formed on the sample immersed in synthetic pore solution containing CN1, again suggesting no benefit to the steel with its addition to pore solution.

Evidence from synthetic pore solution and expressed pore solutions show that nitrite and nitrate are incorporated into the hydrated cement phases.

Calcium nitrite and calcium nitrate increase the chloride binding capacity of the cement paste by increasing the amount or the rate of binding – or both – of  $\text{Cl}^-$  in C-S-H and Ca/K-OH-Cl. Some evidence exists that they also increase the amount of Friedel's salt produced as well, although this evidence is not conclusive.

Calcium nitrite and calcium nitrate have a greater affect on fine porosity than on coarse porosity, which is a result of the formation of various bound chlorides. It is clear that ponding solution is absorbed through fine pores as well as coarse pores, and that water is absorbed faster than chlorides from the ponding solution.

It is also apparent from this investigation that it cannot be assumed that any chemical admixture used with concrete will react the same way in cements of differing chemistry.

### **9.3 Recommendations**

- 1. Further examination of the interactions of nitrite with individual cement components, using the techniques utilized in this study as well as others such as x-ray diffraction (XRD), energy dispersive spectroscopy (EDS), backscatter secondary electrons (BSE), Fourier Transform Infrared Spectroscopy (FTIR), and Raman Spectroscopy, in order to positively identify components such as Ca-OH-Cl and Cl<sup>-</sup> in C-S-H.**
- 2. Examination of profiled ponded samples is necessary to examine changes in porosity and cement paste chemistry with depth from the ponding surface in order to gain a better understanding of the limitations of inhibitors.**
- 3. The effect of calcium nitrite on the cement paste matrix formed by other types of cement, including blended cements, needs further investigation.**
- 4. A sample geometry should be developed which would allow analysis of all material parameters – porosity, cement paste chemistry and pore solution chemistry – on one sample, to minimize the variations, for example, in the amount of absorbed pore solution. This can be most easily accomplished by having a ponded prism large enough to allow coring of a cylinder for pore solution expression and enough remaining sample to allow analysis of porosity and cement chemistry.**
- 5. The same parameter should be examined using different experimental techniques. For example, porosity would be determined using MIP, image analysis and micro-MRI (Magnetic Resonance Imaging), while cement chemistry would utilize thermal analysis, EDS, BSE and Raman Spectroscopy.**
- 6. The study of corrosion inhibitors in cracked concrete is warranted, as the majority of concrete structures have some both shrinkage and loading cracks, which will affect the ingress of harmful species such as chlorides, to the reinforcing steel surface.**
- 7. The concentration of nitrite and nitrate in expressed pore solution should be determined, both prior to and after exposure to chloride containing-ponding solutions to determine if nitrite/nitrate concentrations increase upon exposure to chlorides. This may provide further evidence that nitrite/nitrate is incorporated into the cement phases.**

## References

- ACI (1995). Manual of Concrete Practice. Detroit, Michigan, American Concrete Institute. 1.
- Al-Gahtani, A. S., S. Rasheeduzzafar, E. Hussain (1994). Effect of Alkali Content of Cement on Chloride Binding and Corrosion of Reinforcing Steel. Corrosion and Corrosion Protection of Steel in Concrete. Sheffield, England, Sheffield Academic Press: 472-481.
- Andrade, C., J. A. Gonzalez (1978). "Quantitative Measurements of the Corrosion Rate of Reinforcing Steels Embedded in Concrete using Polarization Resistance Measurements." Werkstoffe und Korrosion 29: 515-519.
- Arup, H. (1983). European Work on Corrosion of Steel in Concrete. Glostrup, Denmark, Danish Corrosion Centre.
- ASTM (1991). C 876-91: Standard Test Method for Half-Cell Potentials of Uncoated Reinforcing Steel in Concrete.
- ASTM (1993). G 61-93: Standard Test Method for Conducting Cyclic Potentiodynamic Polarization Measurements for Localized Corrosion Susceptibility of Iron-, Nickel-, or Cobalt-Based Alloys.
- Arya, C., N. R. Buenfeld, J. B. Newman (1987). "Assessment of Simple Methods of Determining the Free Chloride Ion Content of Cement Paste." Cement and Concrete Research 17(6): 907-918.
- Bakker, R. F. M. (1988). Chapter 3: Initiation Period. Corrosion of Steel in Concrete, RILEM Report 60-CSC. P. Schiessl. New York, N. Y., Chapman & Hall: 22-55.
- Barneyback, R. S., S. Diamond (1981). "Expression and Analysis of Pore Fluids from Hardened Cement Pastes and Mortars." Cement and Concrete Research 11(2): 279-285.
- Benjamin, S. E., J. M. Sykes (1990). Chloride-Induced Pitting Corrosion of Swedish Iron in Ordinary Portland Cement Mortars and Alkaline Solutions: The Effect of Temperature. Corrosion of Reinforcement in Concrete. Wishaw, Warwickshire, UK, Elsevier Science Publishers, Ltd.: 59-64.
- Bensted, J. (1983). Hydration of Portland Cement. Advances in Cement Technology: Critical Reviews and Case Studies on Manufacturing, Quality Control, Optimization and Use. S. N. Ghosh. Toronto, Ontario, Pergamon Press.
- Berke, N. S. (1986). The Use of Anodic Polarization to Determine the Effectiveness of Calcium Nitrite as an Anodic Inhibitor. Corrosion Effect of Stray Currents and the Techniques for Evaluating Corrosion of Rebars in Concrete, ASTM STP 906. V. Chaker. Philadelphia, PA, American Society for Testing and Materials: 78-91.

Berke, N. S. (1989). A Review of Corrosion Inhibitors in Concrete. Materials Performance: 41-44.

Berke, N. S., D. F. Shen, K. M. Sundberg (1990). Comparison of the Polarization Resistance Technique to the Macrocell Corrosion Technique. Corrosion Rates of Steel in Concrete, ASTM STP 1065. V. C. N. S. Berke, D. Whiting. Philadelphia, PA., American Society for Testing and Materials: 38-51.

Berke, N. S., M. C. Hicks (1990). Electrochemical Methods of Determining the Corrosivity of Steel in Concrete. Corrosion Testing and Evaluation: Silver Anniversary Volume, ASTM STP 1000. S. W. D. R. Baboian. Philadelphia, Pa, American Society for Testing and Materials: 425-440.

Berke, N. S., T. G. Weil (1992). World-Wide Review of Corrosion Inhibitors in Concrete. Advances in Concrete Technology: 899-924.

Berke, N. S., M. Hicks, B. I. Abdelrazig, T. P. Lees (1994). A Belt and Braces Approach to Corrosion Protection. Corrosion and Corrosion Protection of Steel in Concrete. Sheffield, England, Sheffield Academic Press: 893-904.

Berke, N. S., M. C. Hicks, R. J. Hoopes, P. J. Tournay (1994). Use of Laboratory Techniques to Evaluate Long-Term Durability of Steel Reinforced Concrete Exposed to Chloride Ingress. Durability of Concrete. Nice, France, ACI: 299-329.

Birnin-Yauri, U. A., F. P. Glasser (1998). "Friedel's Salt,  $\text{Ca}_2\text{Al}(\text{OH})_6(\text{Cl},\text{OH})\cdot 2\text{H}_2\text{O}$ : Its Solid Solutions and Their Role in Chloride Binding." Cement and Concrete Research 28(12): 1713-1723.

Borgard, B. C., C. Warren, S. Somayaji, R. Heidersbach (1990). Mechanisms of Corrosion of Steel in Concrete. Corrosion Rates of Steel in Concrete, ASTM STP 1065. V. C. N. S. Berke, D. Whiting. Philadelphia, PA, American Society for Testing and Materials: 174-188.

Byfors, K. (1986). "Chloride Binding in Cement." Nordic Concrete Research 5(December): 27-38.

Byfors, K., C. M. Hansson, J. Tritthart (1986). "Pore Solution Expression as a Method to Determine the Influence of Mineral Additives on Chloride Binding." Cement and Concrete Research 16(5): 760-770.

Cigna, R., G. Familiari, F. Gianetti, E. Proverbio (1994). Influence of Calcium Nitrite on the Reinforcement Corrosion in Concrete Mixtures Containing Different Cements. Corrosion and Corrosion Protection of Steel in Concrete. Sheffield, England, Sheffield Academic Press: 878-892.

Collins, W. D., R. E. Weyers, I. L. Al-Qadi (1993). "Chemical Treatment of Corroding Steel Reinforcement after Removal of Chloride-Contaminated Concrete." Corrosion 49(1): 74-88.

Cottis, R. A., A. Llewellyn (1996). Electrochemistry for Corrosion: Electrochemical Noise, UMIST. 2001.

CPCA (1995). Chapter 2 Portland Cements. Design and Control of Concrete Mixtures. Ottawa, Canadian Portland Cement Association.

CRC (1994). CRC Handbook of Chemistry and Physics. Boca Raton, Florida, CRC Press, Inc.

Diamond, S. (1988). Methodologies of PSD Measurements in HCP: Postulates, Peculiarities and Problems. Pore Structure and Permeability of Cementitious Materials, Boston, MA, Materials Research Society, Pittsburgh, Pen.

Diamond, S., M. E. Leeman (1994). Pore Size Distributions in Hardened Cement Paste by SEM Image Analysis. Microstructure of Cement-Based Systems/Bonding and Interfaces in Cementitious Materials. Proceedings of the 1994 MRS Fall Meeting, Boston, MA, MRS Materials Research Society.

Eglinton, M. S. (1987). Concrete and Its Chemical Behaviour. London, England, Thomas Telford.

El-Jazairi, B., N. S. Berke (1990). The Use of Calcium Nitrite as a Corrosion Inhibiting Admixture to Steel Reinforcement in Concrete. Corrosion of Reinforcement in Concrete. Wishaw, Warwickshire, UK, Elsevier Science Publishers, Ltd.: 571-585.

Enevoldsen, J. N. (1993). Factors Controlling the Rate of Corrosion of Steel Embedded in Concrete and Mortar. Materials and Metallurgical Engineering. Kingston, Ontario, Queen's University.

Fontana, M. G. (1986). Corrosion Engineering. Toronto, Ont., McGraw-Hill, Inc.

Fordham, C. J., I. J. Smalley (1985). "A Simple Thermogravimetric Study of Hydrated Cement." Cement and Concrete Research 15(1): 141-144.

Genin, J.-M. R., Ph. Refait, A. Raharinaivo (1997). Green Rusts, intermediate corrosion products formed on rebars in concrete in the presence of carbonation or chloride ingress. Corrosion: Conference on Understanding Corrosion Mechanisms in Concrete: A Key to Improving Infrastructure Durability, Massachusetts Institute of Technology, Cambridge, Massachusetts, USA.

Ghosh, S. N., Ed. (1983). Advances in Cement Technology: Critical Reviews and Case Studies on Manufacturing, Quality Control, Optimization and Use. Toronto, Ontario, Pergamon Press.



Glasser, F. P., A. Kindness, S. A. Stronach (1999). "Stability and solubility relationships in AFm phases: Part I. Chloride, sulfate and hydroxide." Cement and Concrete Research **29**: 861-866.

Gui, J., T. M. Devine (1995). "A SERS investigation of the passive films formed on iron in mildly alkaline solutions of carbonate/bicarbonate and nitrate." Corrosion Science **37**(8): 1177-1189.

Hansson, C. M. (1984). "Comments on Electrochemical Measurements of the Rate of Corrosion of Steel in Concrete." Cement and Concrete Research **14**(4): 574-584.

Hansson, C. M., Professor (1999). Personal Communication, Department of Mechanical Engineering, University of Waterloo.

Hansson, C. M., Professor (2000). Personal Communication, Department of Mechanical Engineering, University of Waterloo.

Holly, R. (2001). Characterization of White Cement Paste: Effect of Temperature and Chemical Corrosion Inhibitor. Physics. Waterloo, Ontario, University of Waterloo.

Hope, B. B., A. K. C. Ip (1987). Corrosion Inhibitors for Use in New Concrete Construction. St. Catharines, Ont., Research and Development Branch, Ontario Ministry of Transportation.

Hope, B. B., A. K. C. Ip (1989). "Corrosion Inhibitors for Use in Concrete." ACI Materials Journal **86**(6): 602-608.

Ioannidis, M., Professor (2001). Personal Communication, Department of Chemical Engineering, University of Waterloo.

Jawed, I., J. Skalny, J. F. Young (1983). Chapter 6: Hydration of Portland Cement. Structure and Performance of Cements. P. Barnes. New York, N.Y., Applied Science Publishers.

Jones, D. A. (1992). Principles and Prevention of Corrosion. Toronto, Ont., Maxwell Macmillan Canada.

Justnes, H., E. C. Nygaard (1994). The Influence of Technical Calcium Nitrate Additions on the Chloride Binding Capacity of Cement and the Rate of Chloride Induced Corrosion of Steel Embedded in Mortars. Corrosion and Corrosion Protection of Steel in Concrete. Sheffield, England, Sheffield Academic Press: 491-502.

Karapet'iants, M. K., M. L. Karepet'iants (1970). Thermodynamic constants of inorganic and organic compounds, Ann Arbor, Humphrey Science Publishers.

Katz Analytical Services, I. (2000). Ion Chromatography, [www.katzlabs.com/ic.htm](http://www.katzlabs.com/ic.htm).

- Lea, F. M. (1970). The Chemistry of Cement and Concrete. Glasgow, G. B., Edward Arnold (Publishers), Ltd.
- Leek, D. S., A. B. Poole (1990). The Breakdown of the Passive Film on High Yield Mild Steel by Chloride Ions. Corrosion of Reinforcement in Concrete. Wishaw, Warwickshire, Uk, Elsevier Science Publishers, Ltd.: 65-73.
- Leek, D. S. (1997). A Study of the effects of Chloride and Sulfate in the Hydration of Portland Cement and the Corrosion of Carbon Steel Reinforcement using Electro-optical Techniques and Energy Dispersive X-ray Analysis. University of London (Queen Mary and Westfield College).
- Locke, C. E. (1982). Mechanism of Corrosion of Steel in Concrete. Solving Rebar Corrosion Problems in Concrete. Chicago, Illinois, NACE: 2/1-2/10.
- Locke, C. E. (1986). Corrosion of Steel in Portland Cement Concrete: Fundamental Studies. Corrosion Effect of Stray Currents and the Techniques for Evaluating Corrosion of Rebars in Concrete, ASTM STP 906. V. Chaker. Philadelphia, PA., American Society for Testing and Materials: 5-14.
- Loto, C. A. (1992). "Effect of Inhibitors and Admixed Chloride on Electrochemical Corrosion Behaviour of Mild Steel Reinforcement in Concrete in Seawater." Corrosion 48(9): 759-763.
- Mammoliti, L. (1995). Evaluation of Corrosion Inhibitors in Synthetic Concrete Pore Solutions. Materials and Metallurgical Engineering. Kingston, Ontario, Queen's University.
- Mammoliti, L. T., L. C. Brown, C. M. Hansson, B. B. Hope (1996). "The Influence of Surface Finish of Reinforcing Steel and pH of the Test Solution on the Chloride Threshold Concentration for Corrosion Initiation in Synthetic Pore Solutions." Cement and Concrete Research 26(4): 545-550.
- Mammoliti, L. (1999). Unpublished research.
- Manning, D. G. (1991). Reflections on Steel Corrosion in Concrete. St. Catherines, Ontario, Research and Development Branch, Ontario Ministry of Transportation.
- Marsh, B. K., R. L. Day, D. G. Bonner, J. M. Illston (1985). Principles and Applications of Pore Structural Characterization. RILEM/CNR International Symposium: 365.
- Mehta, P. K. (1986). Concrete: Structures, Properties, and Materials. Englewood Cliffs, New Jersey, Prentice-Hall, Inc.
- Metz, F., D. Knofel (1992). "Systematic mercury porosimetry investigations on sandstones." Materials and Structures 25: 127-136.

- Midgley, H. G., J. M. Illston (1984). "The Penetration of Chlorides into Hardened Cement Pastes." Cement and Concrete Research 14(4): 546-558.

Mindess, S., J. F. Young (1981). Concrete. Englewood Cliffs, N. J., Prentice-Hall, Inc.

Monkman, G. S. P. (1995). The Effect of Corrosion Inhibitors on the Physical and Mechanical Properties of Concrete. Materials and Metallurgical Engineering. Kingston, Ontario, Queen's University.

Monkman, G. S. P. (1999). A Materials Science Investigation of the Early Hydration of Two Types of Cement at Three Different Hydration Temperatures. M. A. Sc. Thesis, Mechanical Engineering. Waterloo, Ontario, University of Waterloo.

Neville, A. M. (1991). Properties of Concrete. New York, N. Y., Longman Scientific & Technical.

Oblonsky, L. J., T. M. Devine (1997). "Corrosion of Carbon Steels in CO<sub>2</sub>-Saturated Brine." Journal of the Electrochemical Society 144(4): 1252-1260.

Odziemkowski, M., J. Flix, D. E. Irish (1994). "Raman Spectral and Electrochemical Studies of Surface Film Formation on Iron and Its Alloys with Carbon in Na<sub>2</sub>CO<sub>3</sub>/NaHCO<sub>3</sub> Solution with Reference to Stress Corrosion Cracking." Electrochimica Acta 39(14): 2225-2236.

Odziemkowski, M. S., T. T. Schuhmacher, R. W. Gillham, E. J. Reardon (1998). "Mechanism of oxide film formation on iron in simulating groundwater solutions: Raman Spectroscopic studies." Corrosion Science 40(2/3): 371-389.

Optics, P. E. (1996). Environmental Scanning Electron Microscopy, An Introduction to ESEM. El Dorado Hills, Ca, Robert Johnson Associates.

Page, C. L. (1988). Chapter 1: Basic Principles of Corrosion. Corrosion of Steel in Concrete, RILEM Report 60-CSC. P. Schiessl. New York, N. Y., Chapman & Hall: 3-21.

Parsons, V., Estimator (1995). Personal Communication, Ministry of Transportation of Ontario.

Pourbaix, M. (1974). Atlas of Electrochemical Equilibria in Aqueous Solutions. Houston, Texas, NACE.

Pyke, R., M. Cohen (1948). "Rate of Breakdown and Mechanism of Nitrite Inhibition of Steel Corrosion." Journal of the Electrochemical Society(March): 63-78.

Ramachandran, V. S. (1971). "Possible States of Chloride in the Hydration of Tricalcium Silicate in the Presence of Calcium Chloride." Materiaux et Constructions 4(19): 3-12.

Reardon, E. J., Professor (1999). Personal Communication, Department of Earth Sciences, University of Waterloo.

Reardon, E. J., Professor (2001). Personal Communication, Department of Earth Sciences, University of Waterloo.

Renaudin, G., J.-P. Rapin, B. Humbert, M. Francois (2000). "Thermal behaviour of the nitrated AFm phase  $\text{Ca}_4\text{Al}_2(\text{OH})_{12}(\text{NO}_3)_2 \cdot 4\text{H}_2\text{O}$  and structure determination of the intermediate hydrate  $\text{Ca}_4\text{Al}_2(\text{OH})_{12}(\text{NO}_3)_2 \cdot 2\text{H}_2\text{O}$ ." Cement and Concrete Research **30**: 307-314.

Research, E. G. & G. (1982). Application Note Corr 1: Basics of Corrosion Measurements.

Sagoe-Crentsil, K. K., V. T. Yilmaz, F. P. Glasser (1991/92). "Properties of inorganic corrosion inhibition admixtures in steel-containing OPC mortars, Part 1: Chemical properties." Advances in Cement Research **4**(15): 91-96.

Shaver, J. (2000). Raman Spectroscopy Explained, [www-personal.umich.edu:80/~jshaver/virtual/labeled/explain.html](http://www-personal.umich.edu:80/~jshaver/virtual/labeled/explain.html).

Skalny, J., I. Odler (1967). "The effect of chlorides upon the hydration of Portland cement and upon some clinker minerals." Magazine of Concrete Research **19**(61): 203-210.

Stern, M., A. L. Geary (1957). "Electrochemical Polarization: A Theoretical Analysis of the Shape of Polarization Curves." Journal of Electrochemical Society **104**(1): 56-63.

Suryavanshi, A. K., J. D. Scantlebury, S. B. Lyon, P. J. Nedwell (1994). Pore Solution Analysis of Normal Portland Cement and Sulphate Resistant Portland Cement Mortars and Their Influence on Corrosion Behaviour of Embedded Steel. Corrosion and Corrosion Protection of Steel in Concrete. Sheffield, England, Sheffield Academic Press: 482-490.

Tarricone, P. (1992). Adding Up Admixtures. Civil Engineering: 48-51.

Taylor, H. F. W. (1997). Cement Chemistry. London, UK, Thomas Telford Publishing.

Thierry, D., D. Persson, C. Leygraf, N. Boucherit, A. Hugot-le Goff (1991). "Raman Spectroscopy and XPS Investigations of Anodic Corrosion Films formed on Fe-Mo Alloys in Alkaline Solutions." Corrosion Science **32**(3): 273-284.

Thompson, S. V. (1991). The Use of Chemical Inhibitors to Prevent Corrosion of Reinforcing Steel in Reinforced Concrete Structures. Civil Engineering. Kingston, Ontario, Queen's University.

Tomosawa, F., Y. Masuda, I. Fukushi, M. Takakura, T. Hori (1990). Experimental Study on the Effectiveness of Corrosion Inhibitor in Reinforced Concrete. RILEM Symposium on Concrete Durability. Barcelona, Spain: 382-391.

Treadaway, K. (1988). Chapter 3: Corrosion Period. Corrosion of Steel in Concrete, RILEM Report 60-CSC. P. Schiessl. New York, N. Y., Chapman & Hall: 56-69.

Trepanier, S. (1994). Effectiveness of Corrosion Inhibitors in Reinforced Concrete. Civil Engineering. Kingston, Ontario, Queen's University.

Tritthart, J. (1989). "Chloride Binding in Cement." Cement and Concrete Research **19**(5): 683-691.

Tritthart, J. (1990). Pore Solution Composition and Other Factors Influencing the Corrosion Risk of Reinforcement in Concrete. Corrosion of Reinforcement in Concrete. New York, N. Y., The Society of Chemical Industry, Elsevier Applied Science: 96-106.

Tullmin, M., Post-Doctoral Fellow (1995). Personal Communication, Department of Materials and Metallurgical Engineering, Queen's University.

Vocka, R., C. Galle, M. Dubois, P. Lovera (2000). "Mercury intrusion porosimetry and hierarchical structure of cement pastes: Theory and experiment." Cement and Concrete Research **30**: 521-527.

Wendlandt, W. W. (1986). Thermal Analysis. Toronto, Ontario, John Wiley & Sons.

Windholz, M., Ed. (1979). The Merck Index: an encyclopedia of chemicals and drugs. Rahway, N.J., Merck & Company, Inc.

Yilmaz, V. T., K. K. Sagoe-Crentsil, F. P. Glasser (1991/92). "Properties of inorganic corrosion inhibition admixtures in steel-containing OPC mortars, Part 2: Electrochemical properties." Advances in Cement Research **4**(15): 97-102.

Yonezawa, T., V. Ashworth, R. P. M. Procter (1988). "Pore Solution Composition and Chloride Effects on the Corrosion of Steel in Concrete." Corrosion Engineering **44**(7): 489-499.

## Appendix A

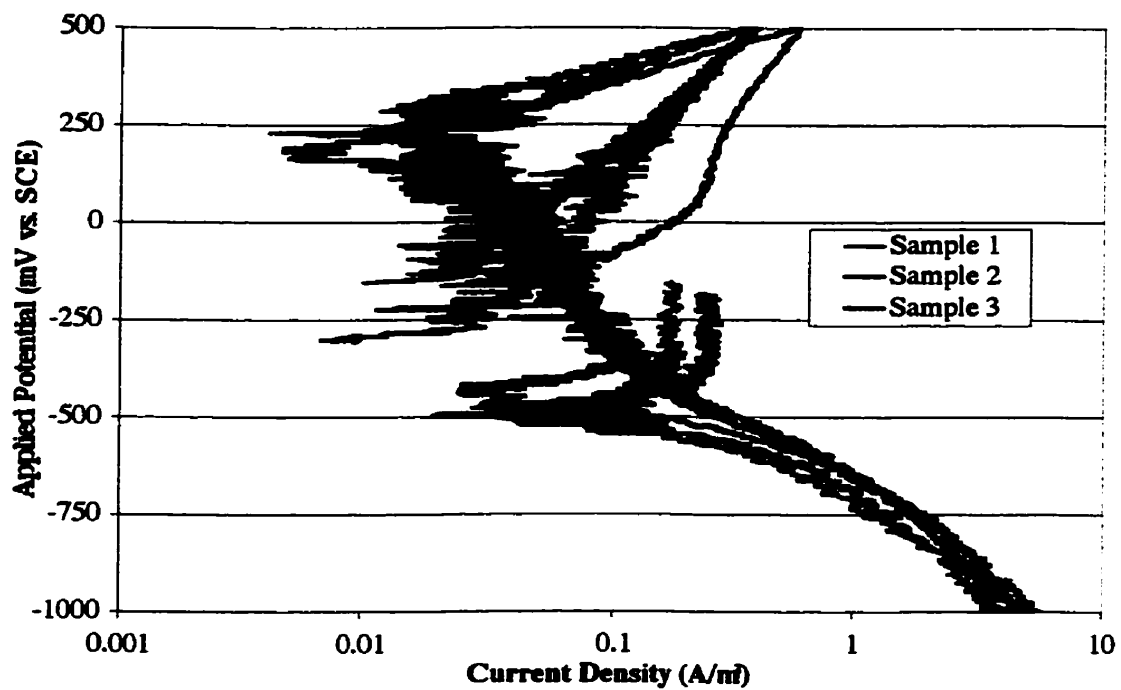


Figure A.1 Cyclic polarization curves of three samples immersed in Control, 0% Cl solution.

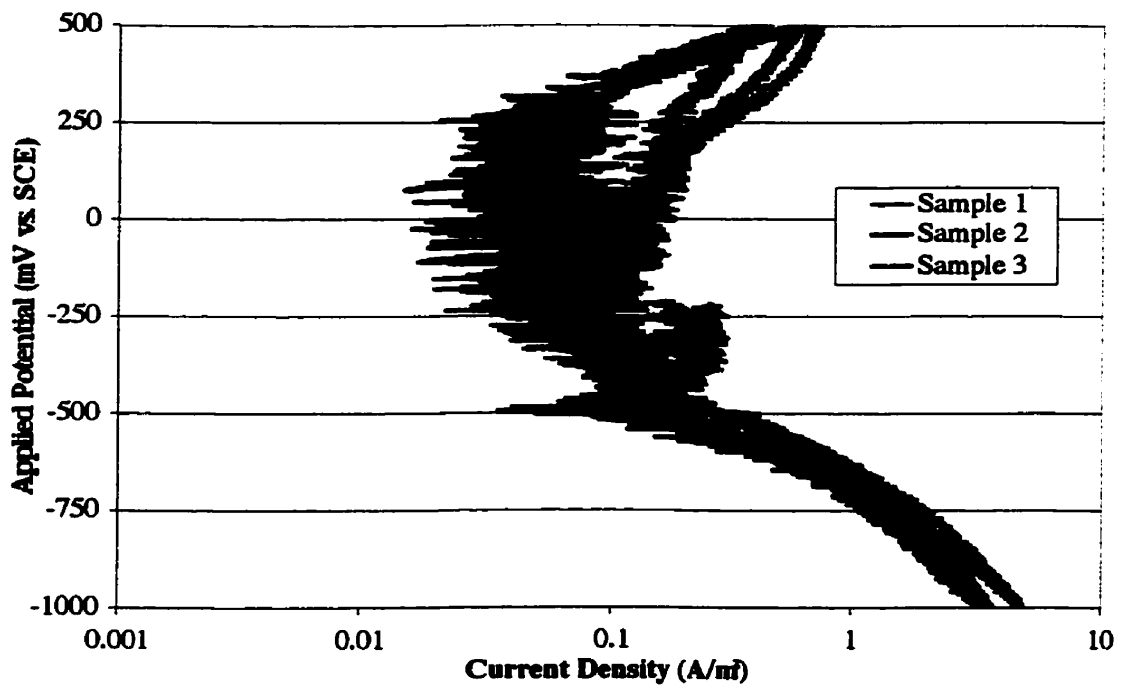


Figure A.2 Cyclic polarization curves of three samples immersed in Control, 1% Cl solution.

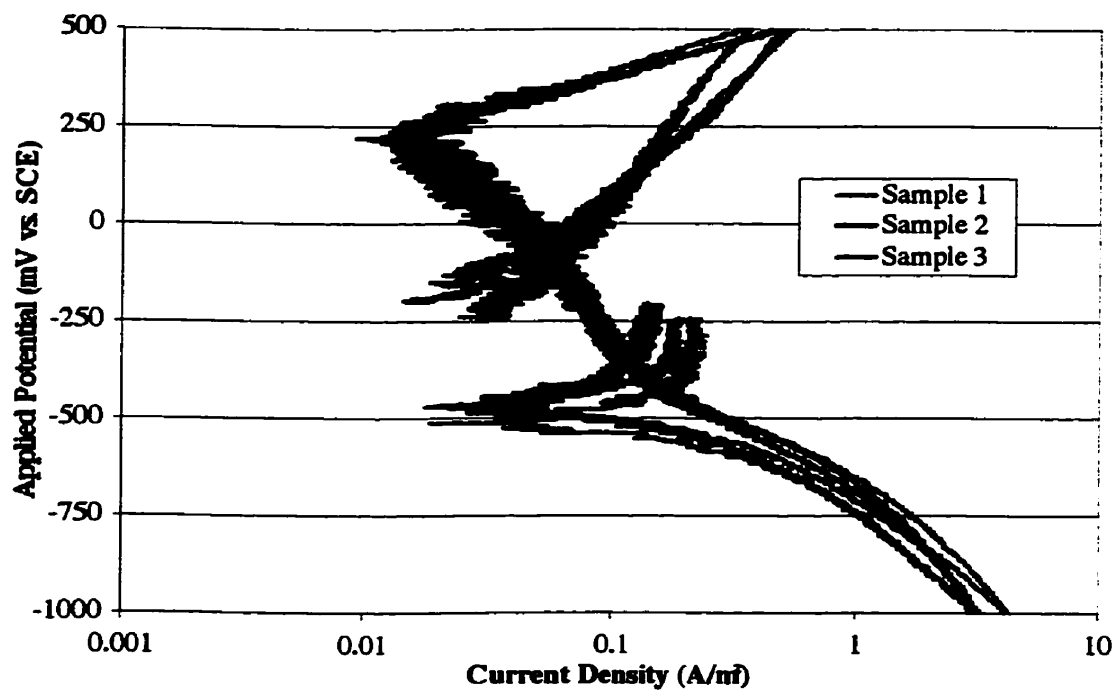


Figure A.3 Cyclic polarization curves for three samples immersed in Control, 2% Cl solutions.

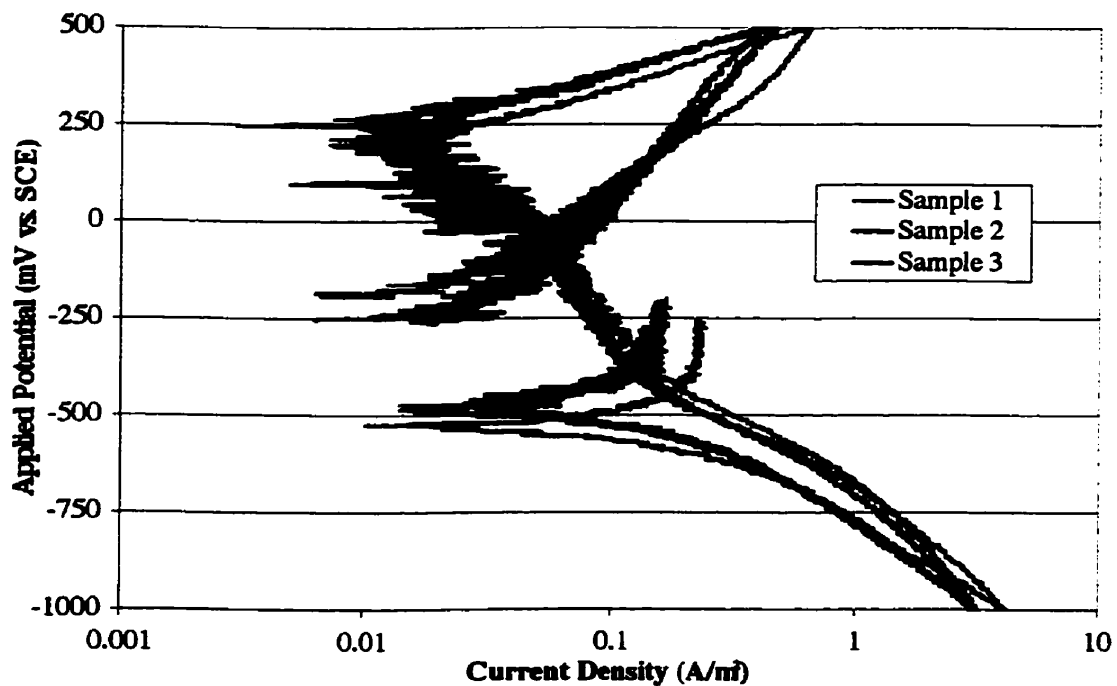


Figure A.4 Cyclic polarization curves for three samples immersed in Control, 3% Cl solutions

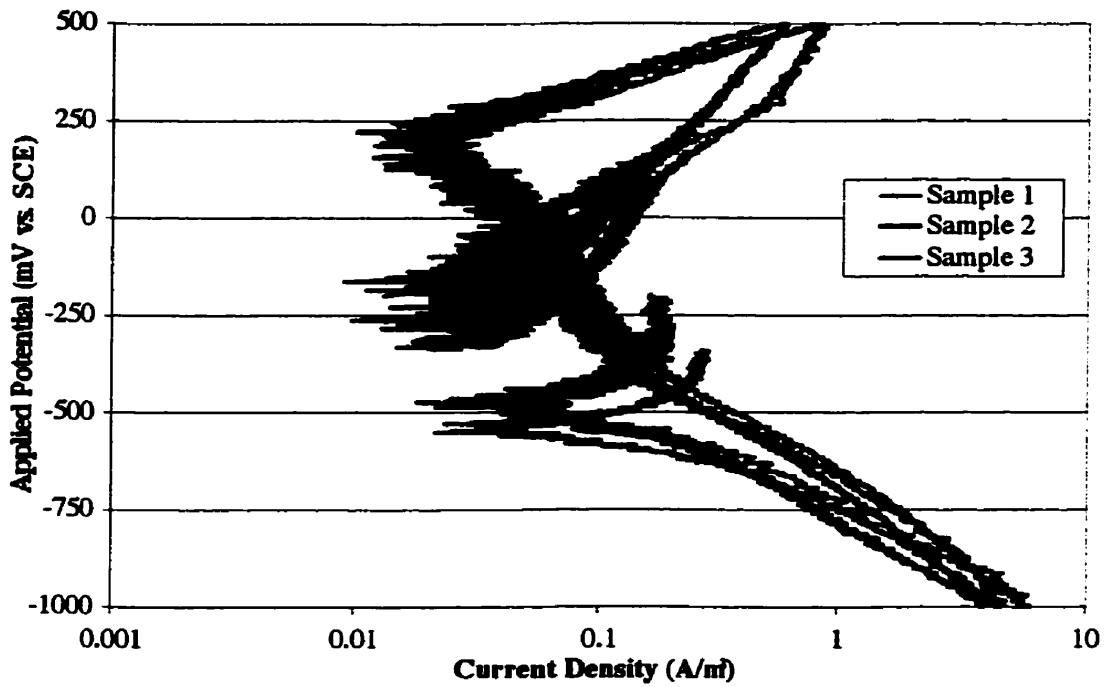


Figure A.5 Cyclic polarization curves for three samples immersed in Control, 4% Cl solution.

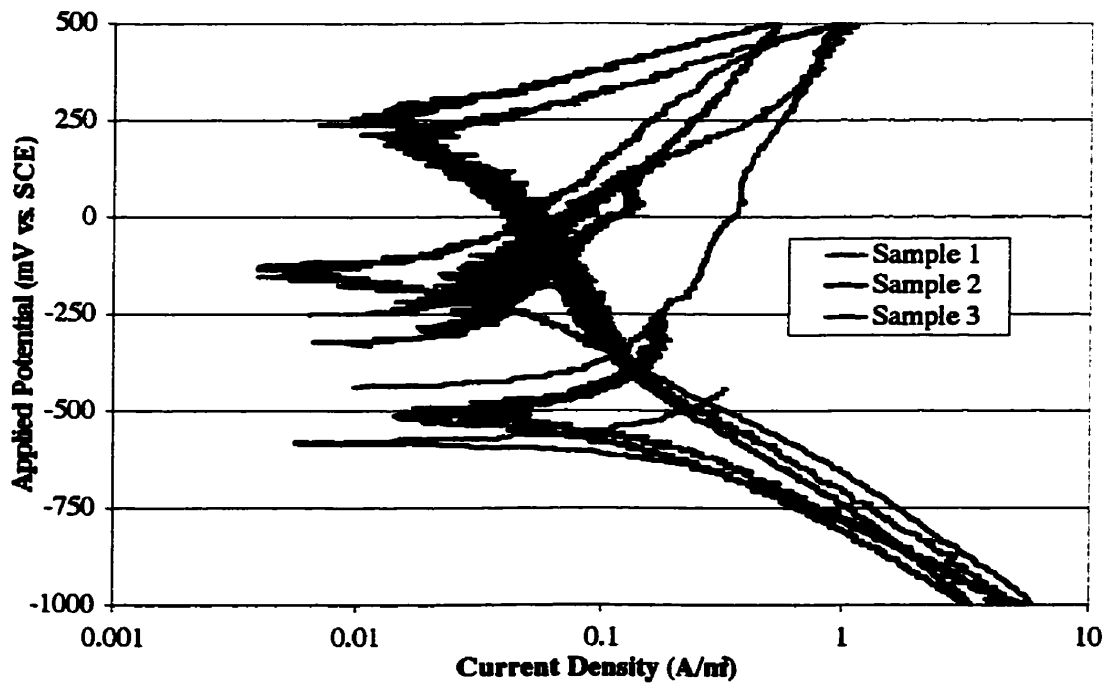


Figure A.6 Cyclic polarization curves for three samples immersed in Control, 5% Cl solution.



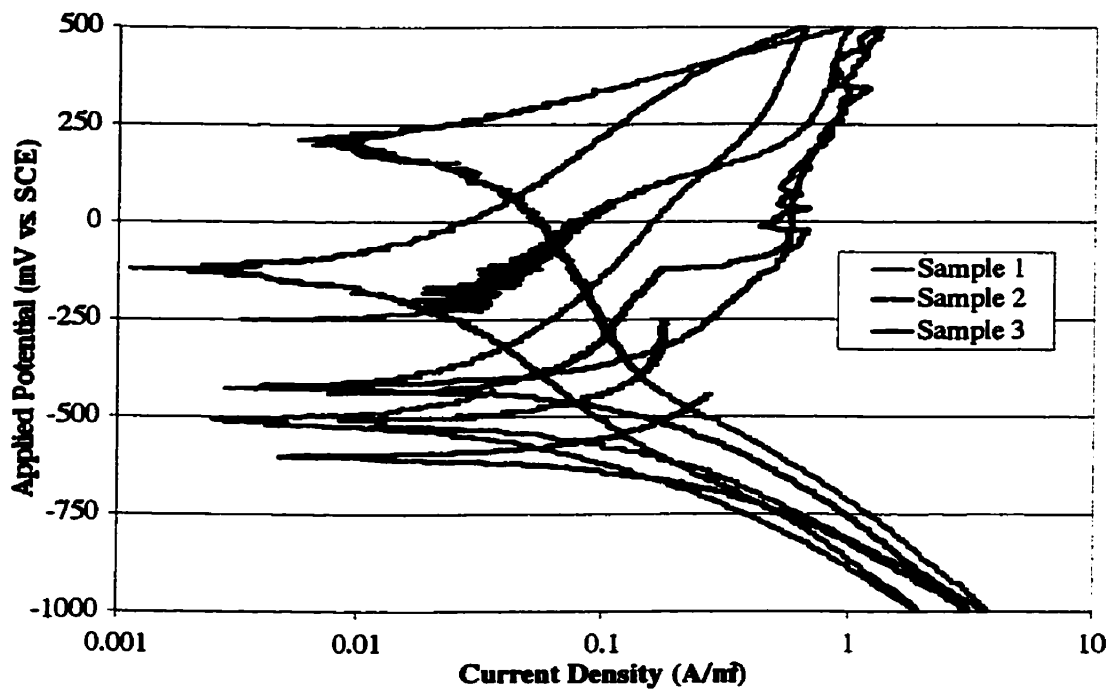


Figure A.7 Cyclic polarization curves for three samples immersed in Control, 6% Cl solution.

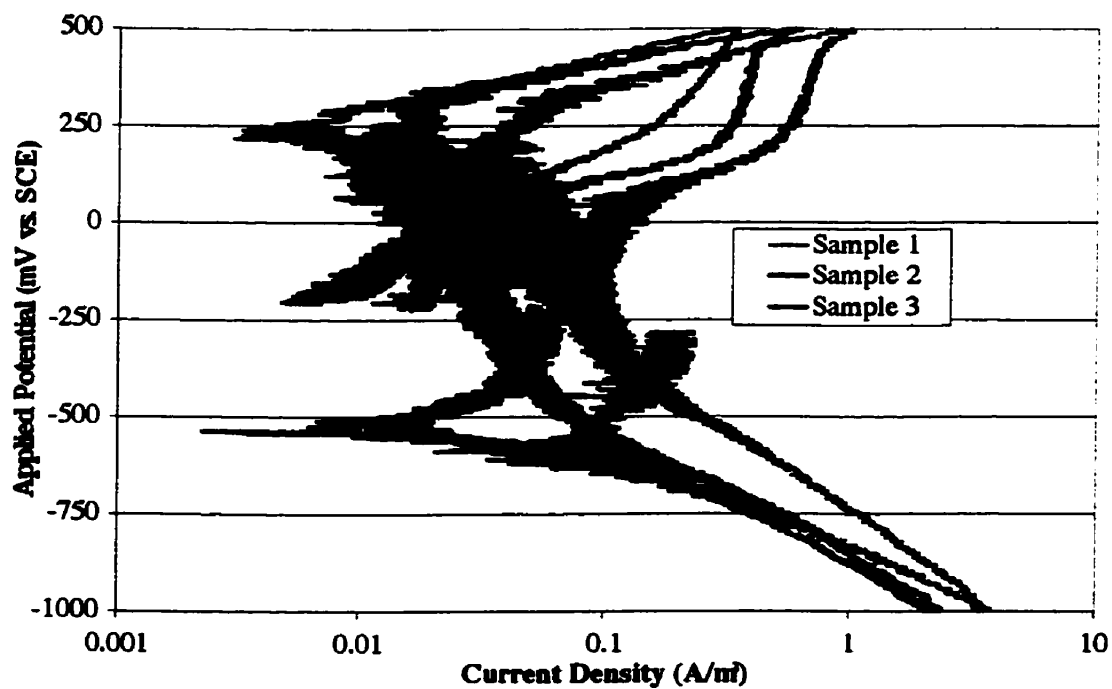


Figure A.8 Cyclic polarization curves for three samples immersed in Control, 7% Cl solution.

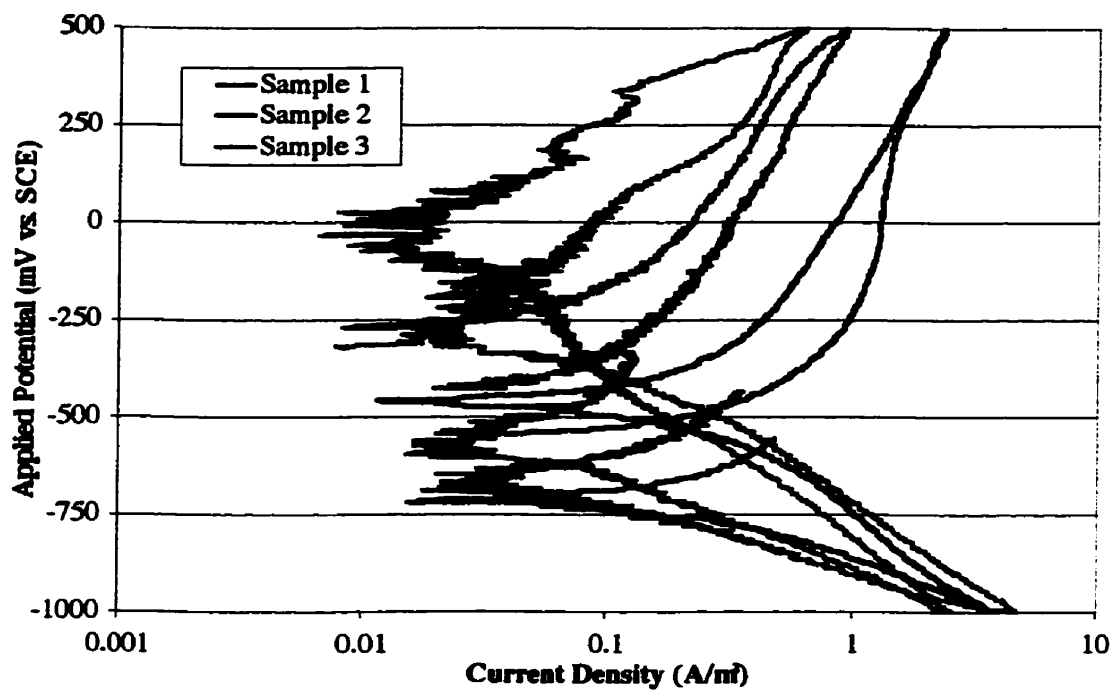


Figure A.9 Cyclic polarization curves for three samples immersed in Control, 8% Cl solution.

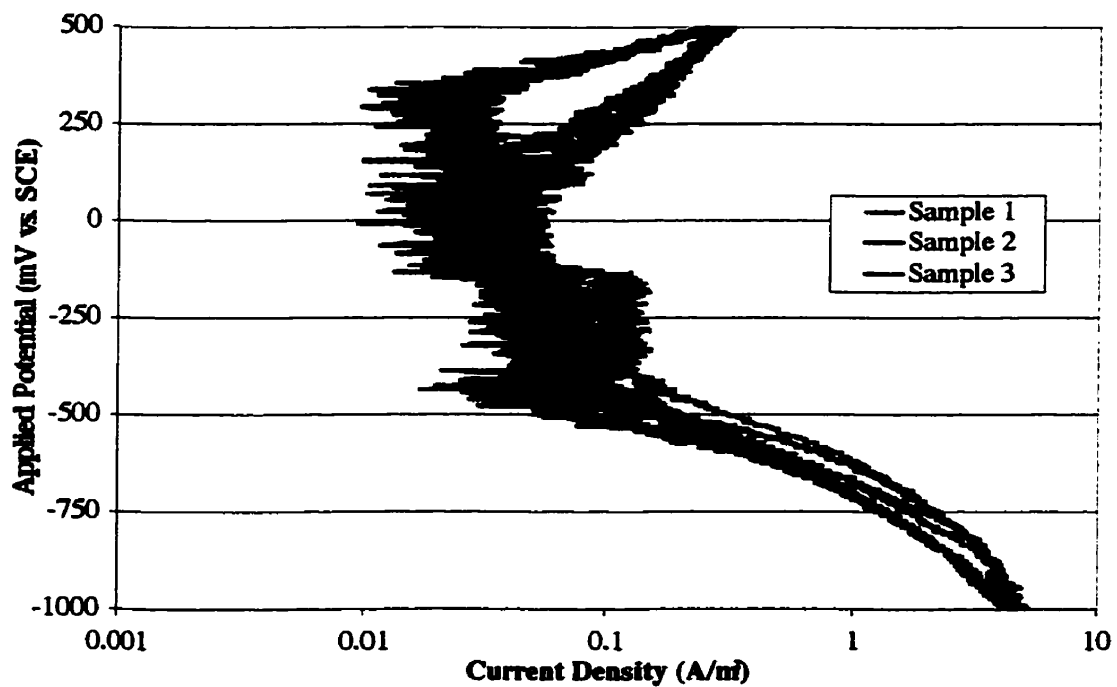


Figure A.10 Cyclic polarization curves for three samples immersed in CN1, 0% Cl solution.

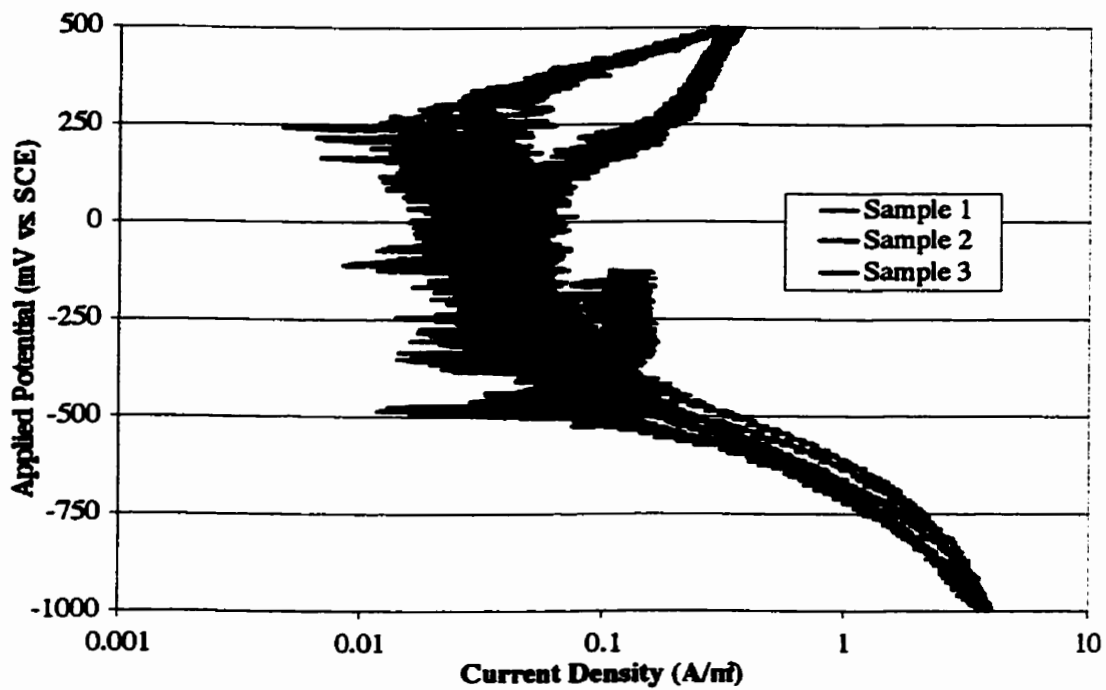


Figure A.11 Cyclic polarization curves for three samples immersed in CN1, 1% Cl solution.

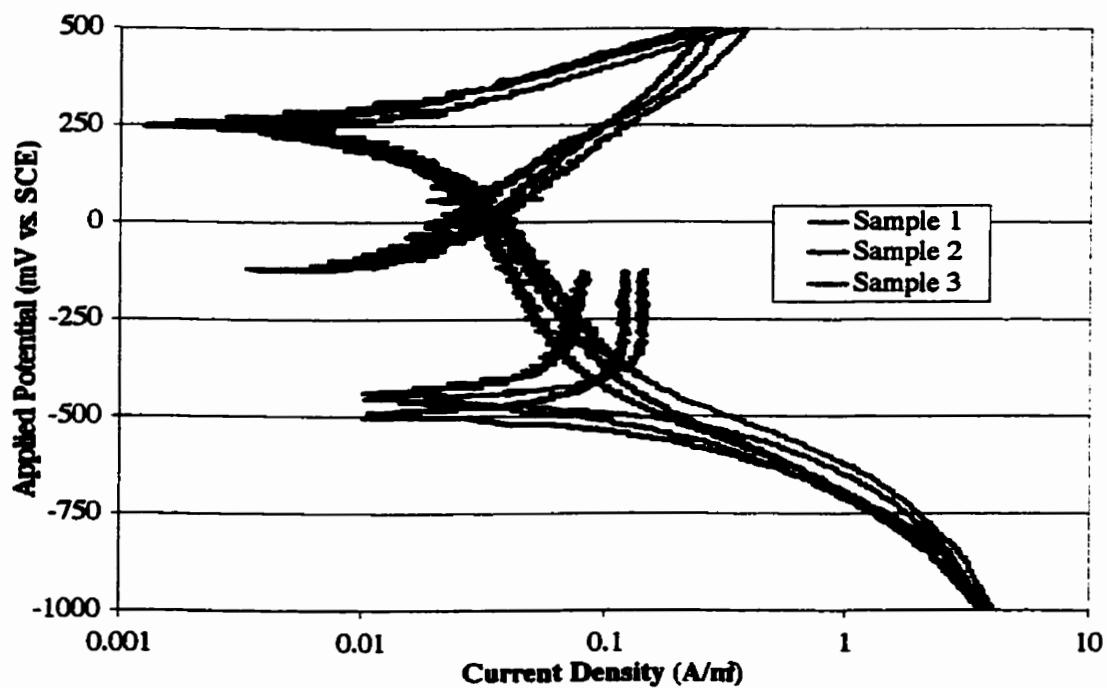


Figure A.12 Cyclic polarization curves for three samples immersed in CN1, 2% Cl solution.

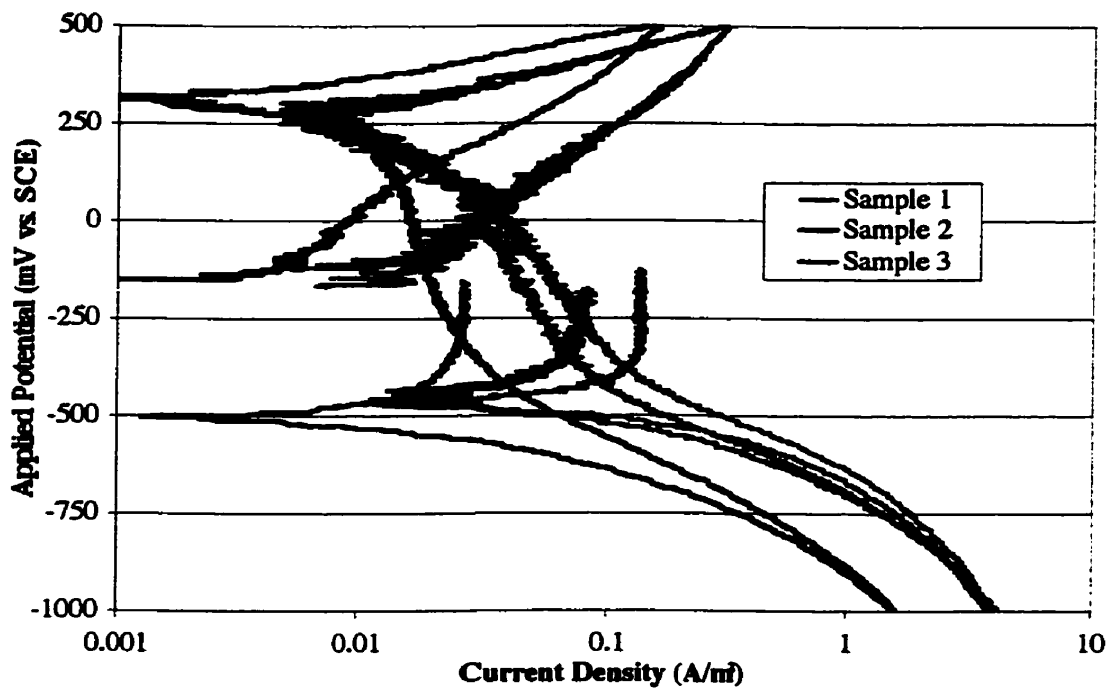


Figure A.13 Cyclic polarization curves for three samples immersed in CN1, 3% Cl solution.

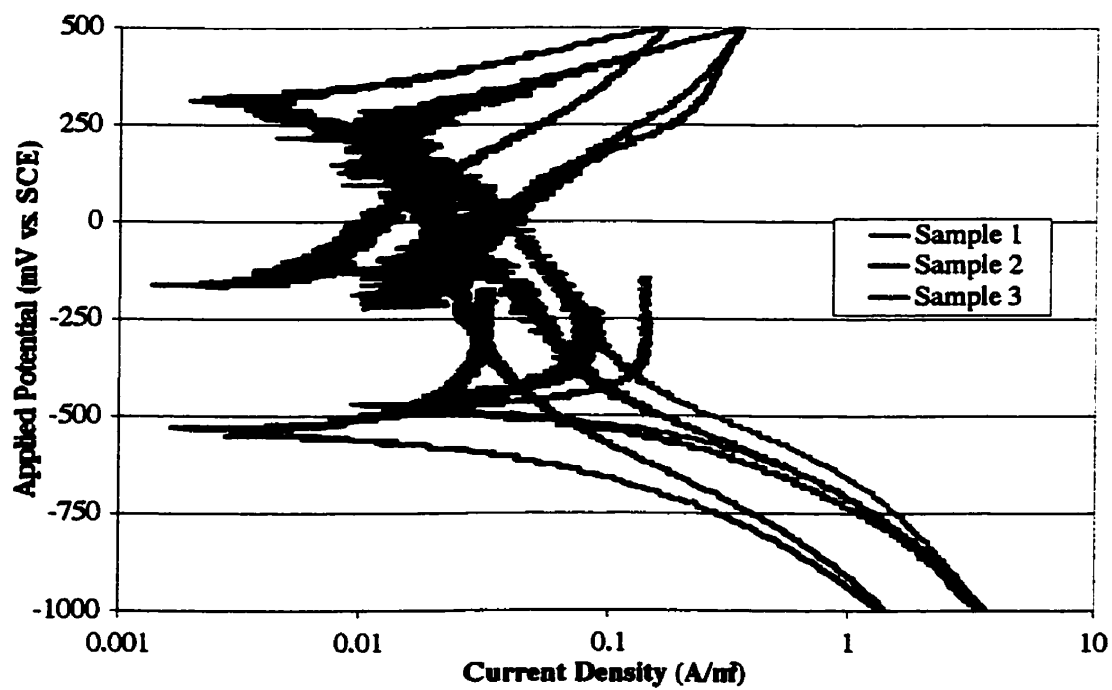


Figure A.14 Cyclic polarization curves for three samples immersed in CN1, 4% Cl solution.

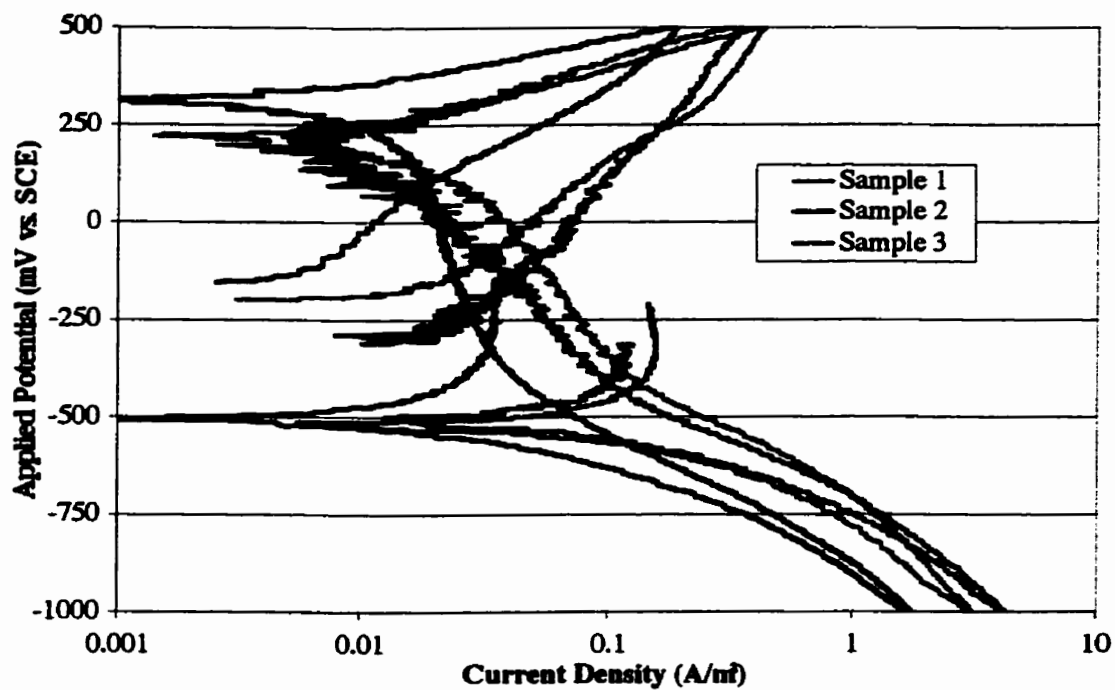


Figure A.15 Cyclic polarization curves for three samples immersed in CN1, 5% Cl solution.

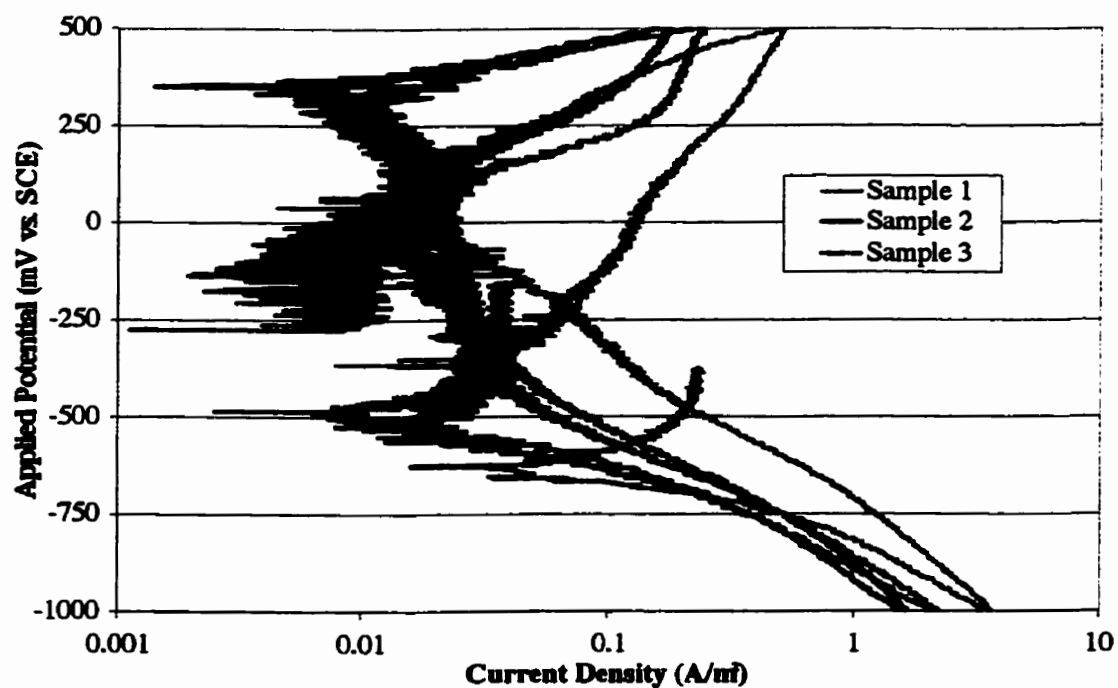


Figure A.16 Cyclic polarization curves for three samples immersed in CN1, 6% Cl solution.

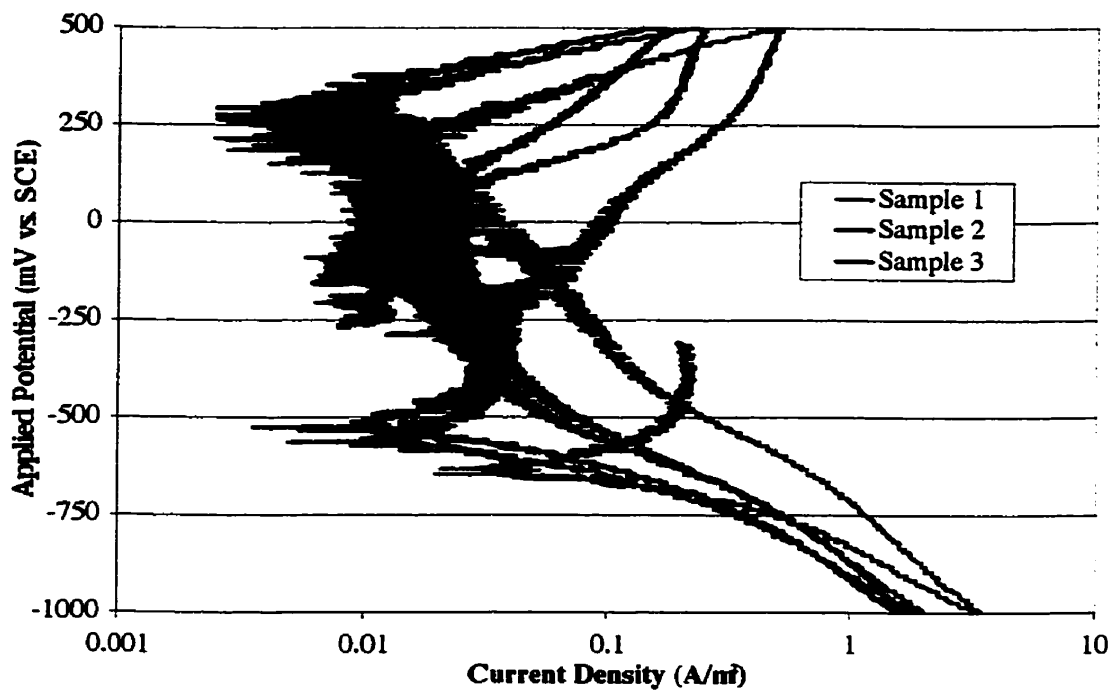


Figure A.17 Cyclic polarization curves for three samples immersed in CN1, 7% Cl solution.

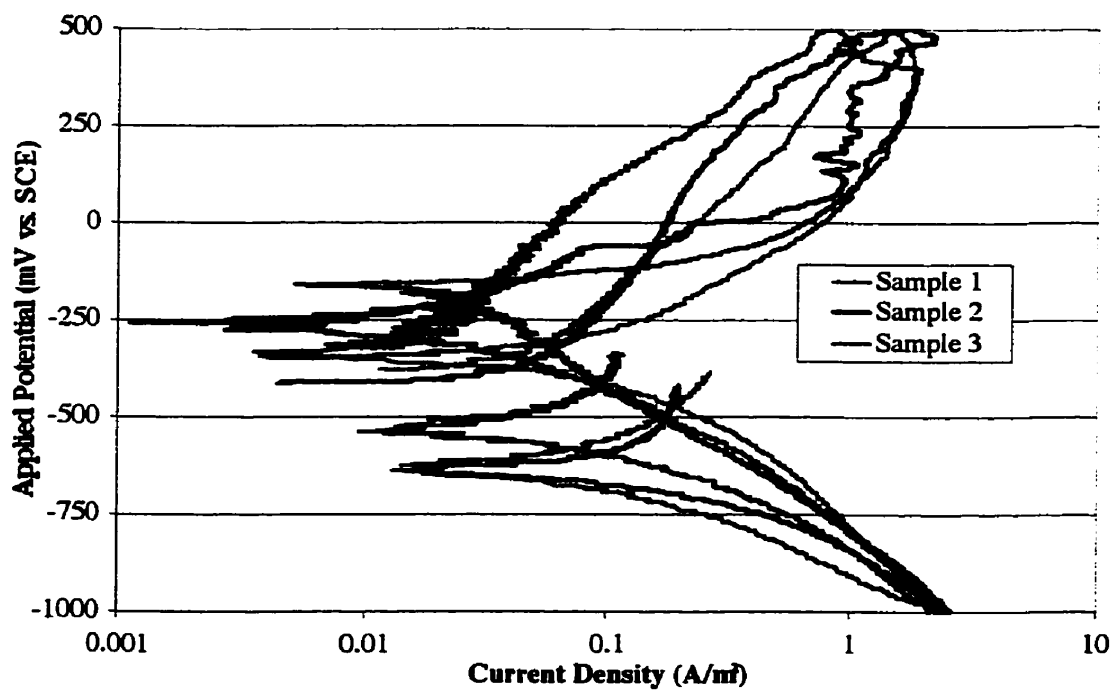


Figure A.18 Cyclic polarization curves for three samples immersed in CN1, 8% Cl solution.

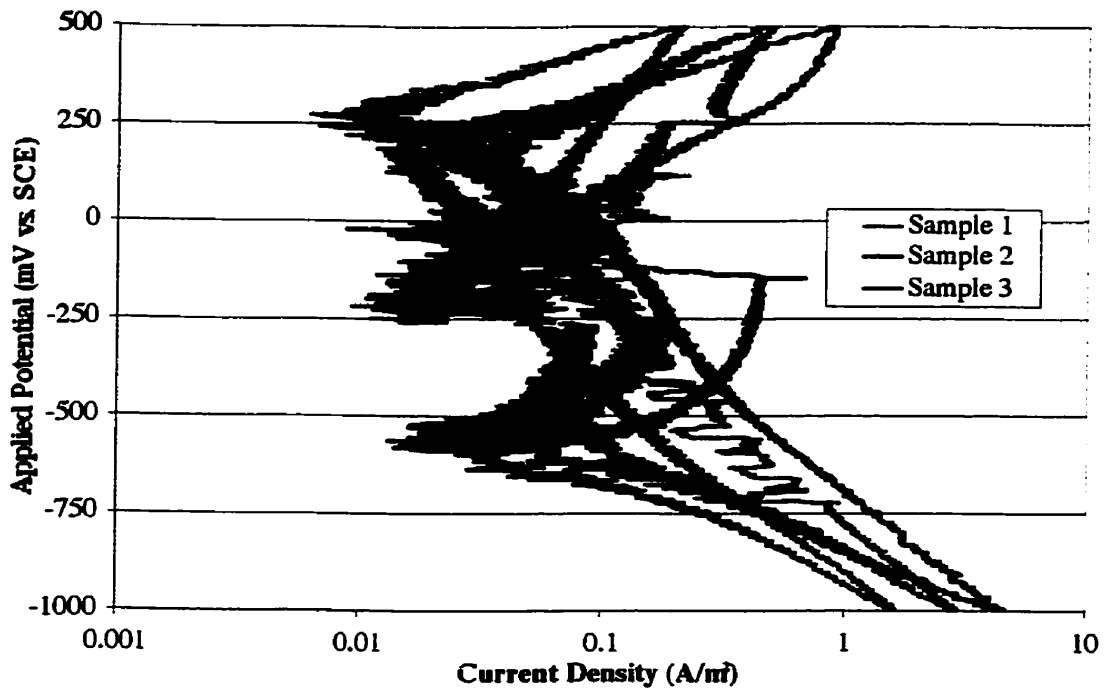


Figure A.19 Cyclic polarization curves for three samples immersed in CN2, 0% Cl solution.

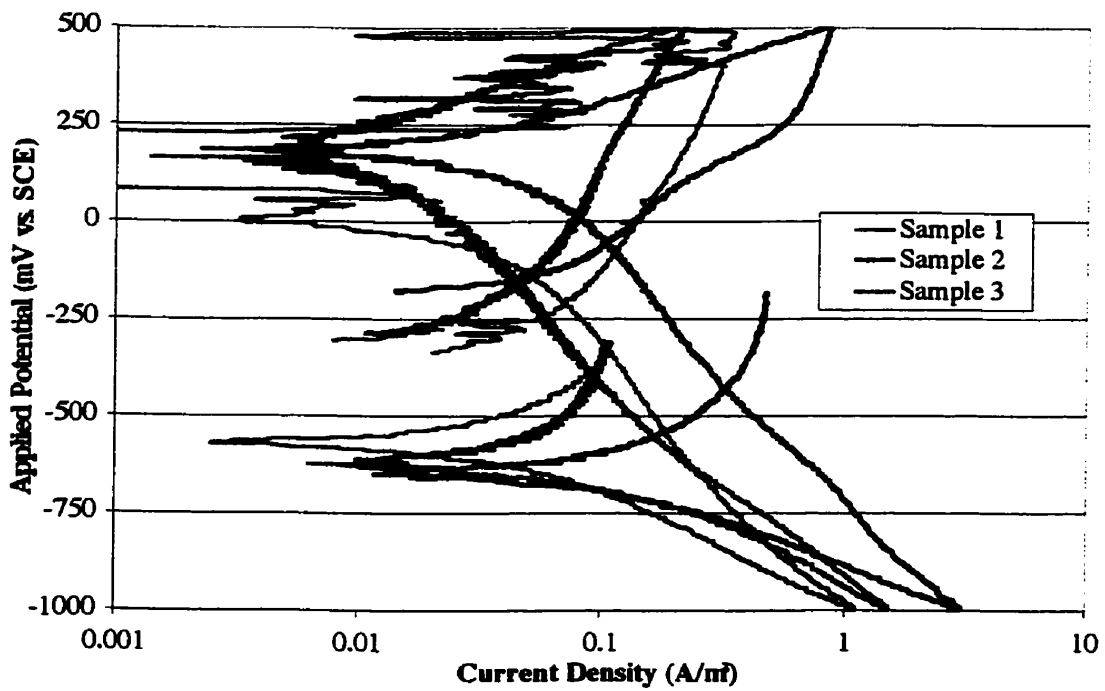


Figure A.20 Cyclic polarization curves for three samples immersed in CN2, 1% Cl solution.

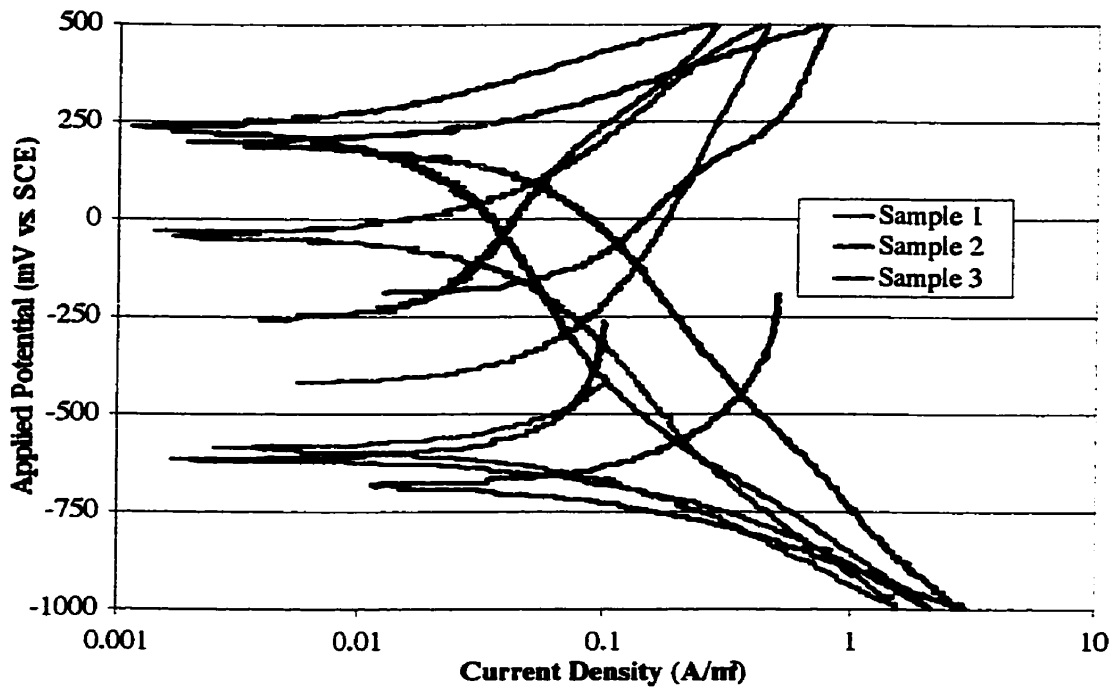


Figure A.21 Cyclic polarization curves for three samples immersed in CN2, 2% Cl solution.

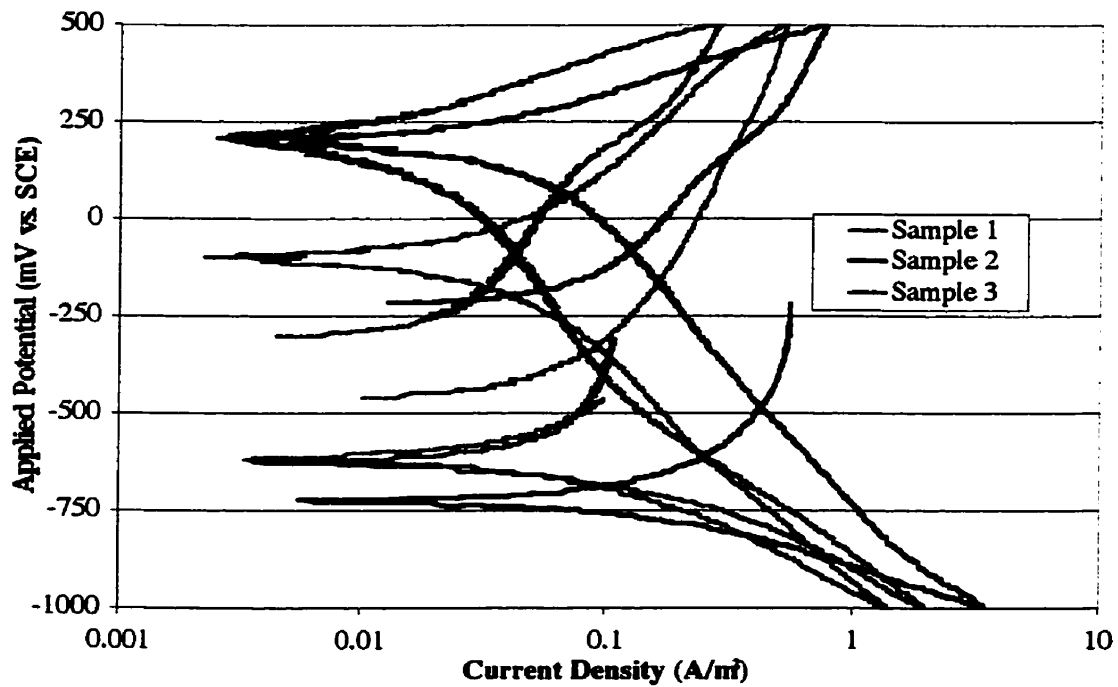


Figure A.22 Cyclic polarization curves for three samples immersed in CN2, 3% Cl solution.



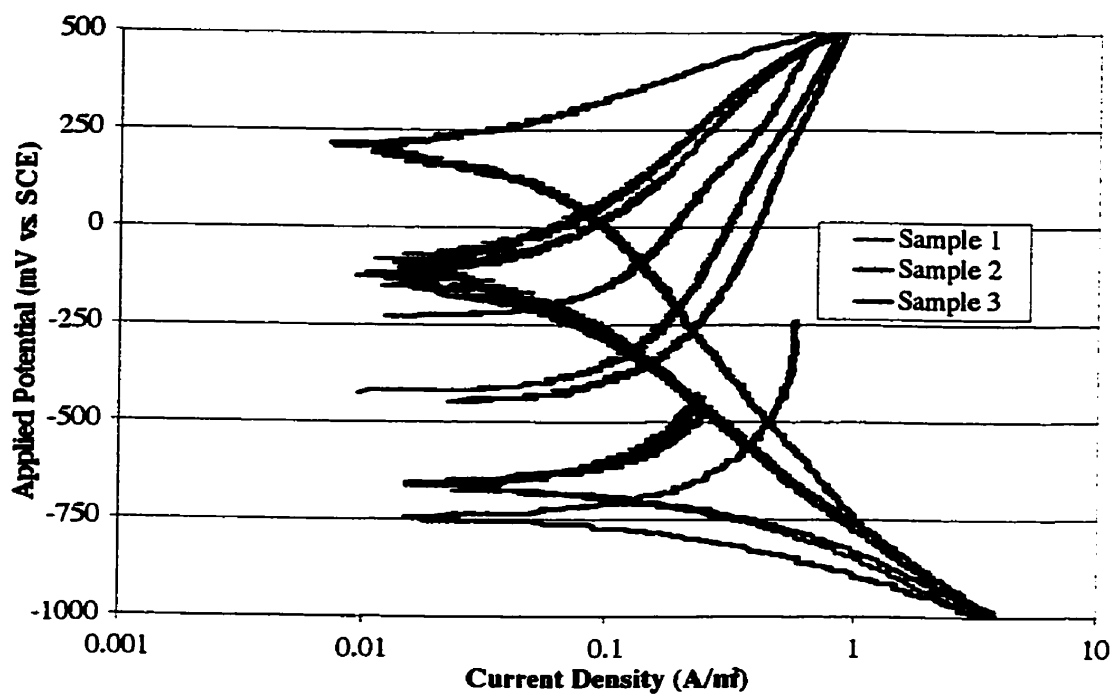


Figure A.23 Cyclic polarization curves for three samples immersed in CN2, 4% Cl solution.

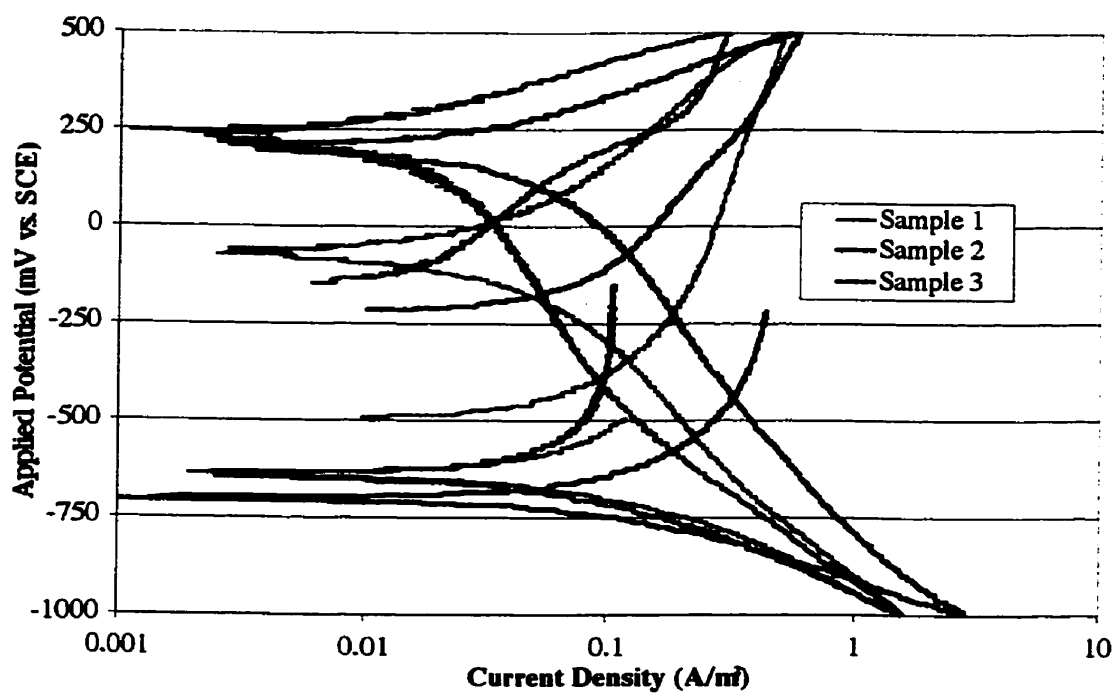


Figure A.24 Cyclic polarization curves for three samples immersed in CN2, 5% Cl solution.

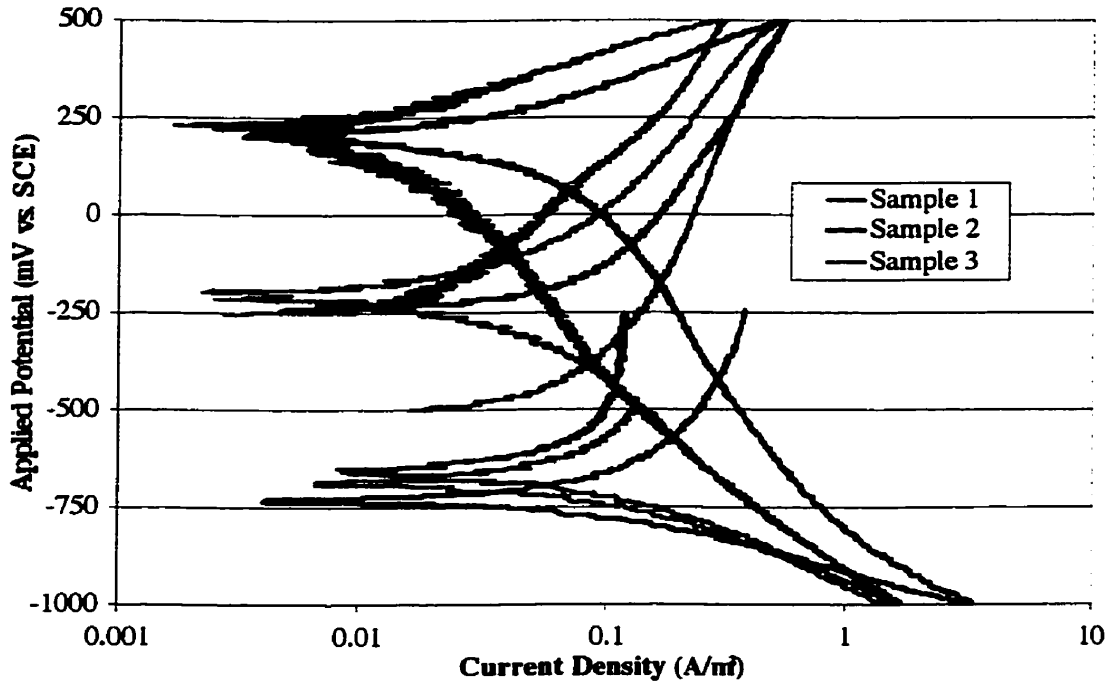


Figure A.25 Cyclic polarization curves for three samples immersed in CN2, 6% Cl solution.

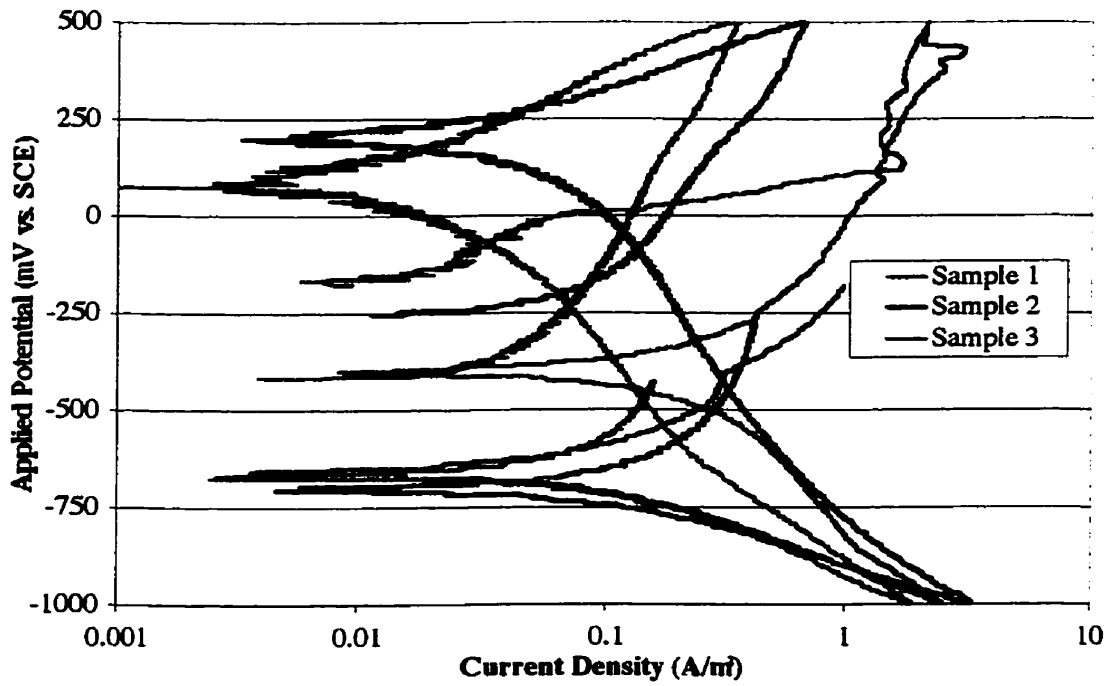


Figure A.26 Cyclic polarization curves for three samples immersed in CN2, 7% Cl solution.

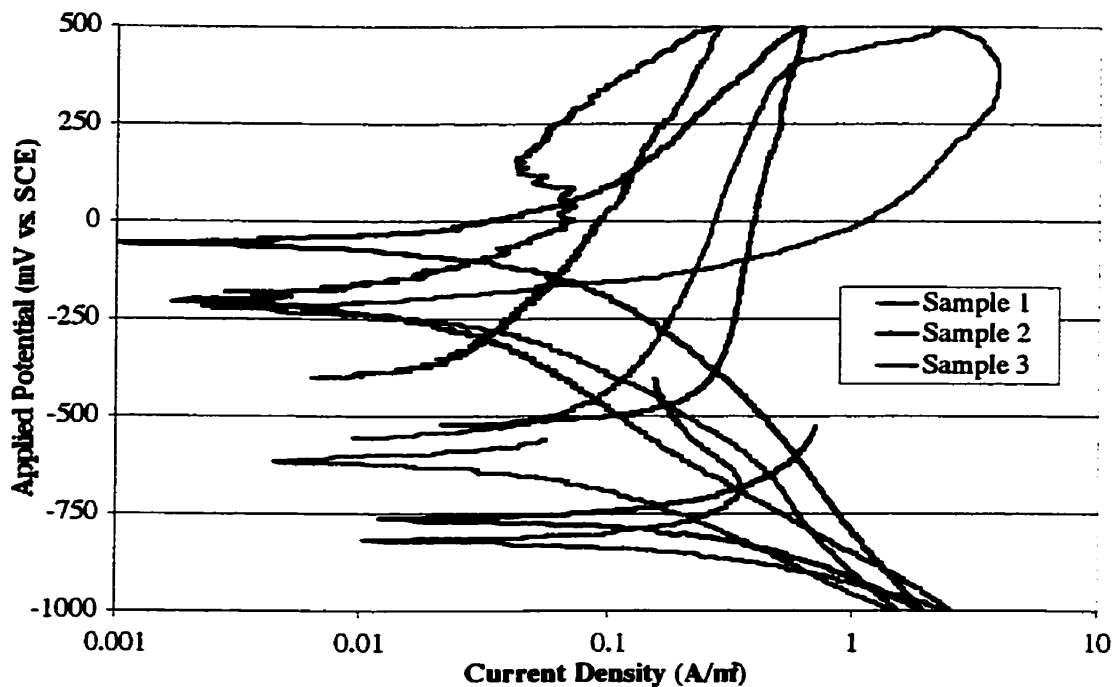


Figure A.27 Cyclic polarization curves for three samples immersed in CN<sub>2</sub>, 8% Cl solution.

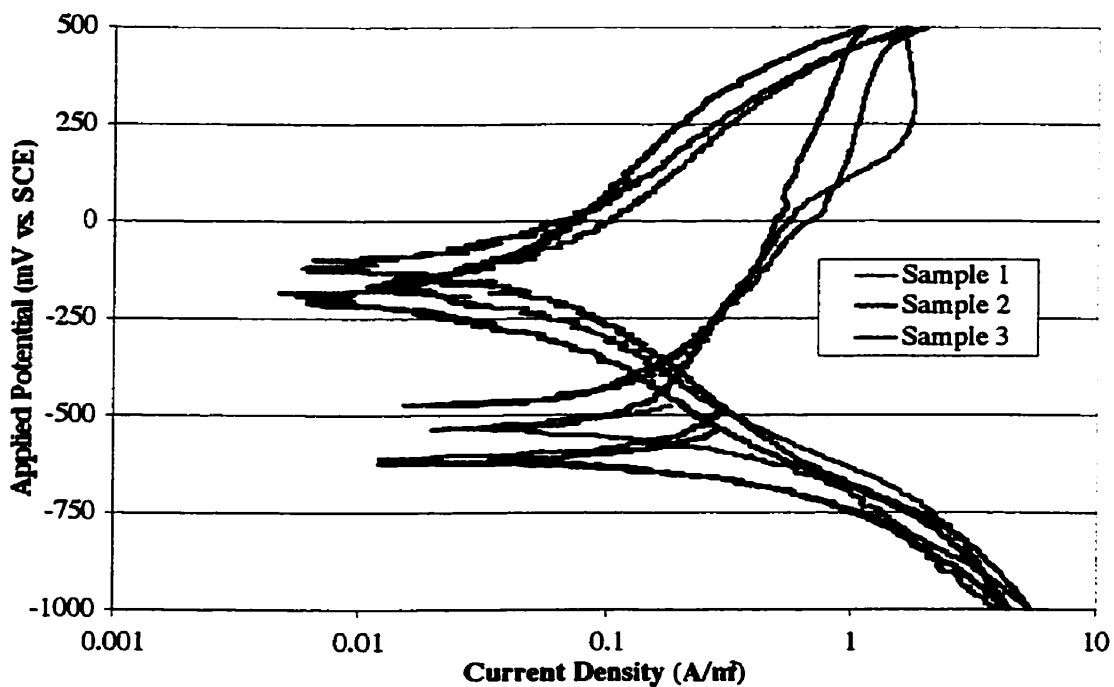


Figure A.28 Cyclic polarization curves for three samples immersed in Ca(NO<sub>3</sub>)<sub>2</sub>, 0% Cl solution.

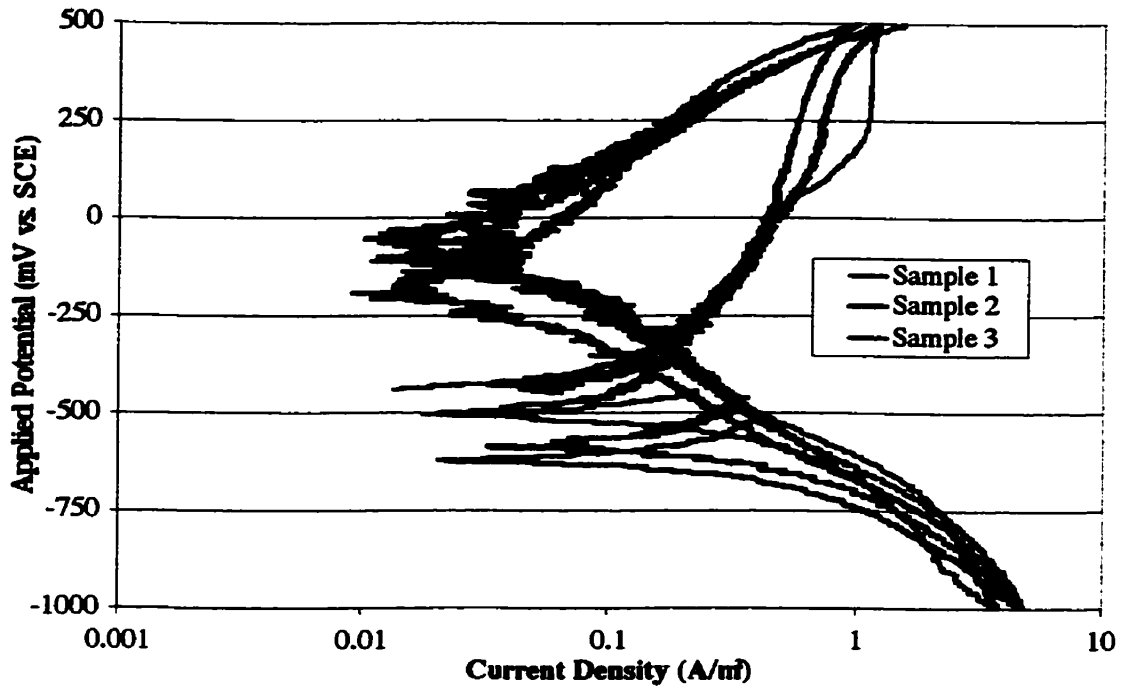


Figure A.29 Cyclic polarization curves for three samples immersed in  $\text{Ca}(\text{NO}_3)_2$ , 1% Cl solution.

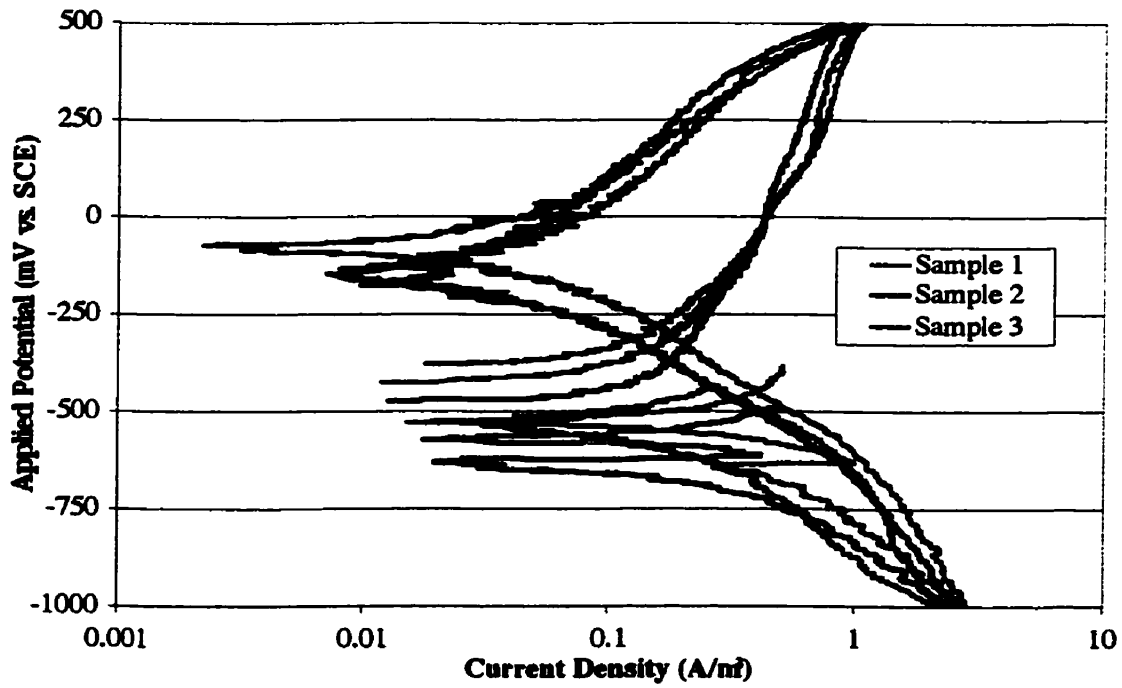


Figure A.30 Cyclic polarization curves for three samples immersed in  $\text{Ca}(\text{NO}_3)_2$ , 2% Cl solution.

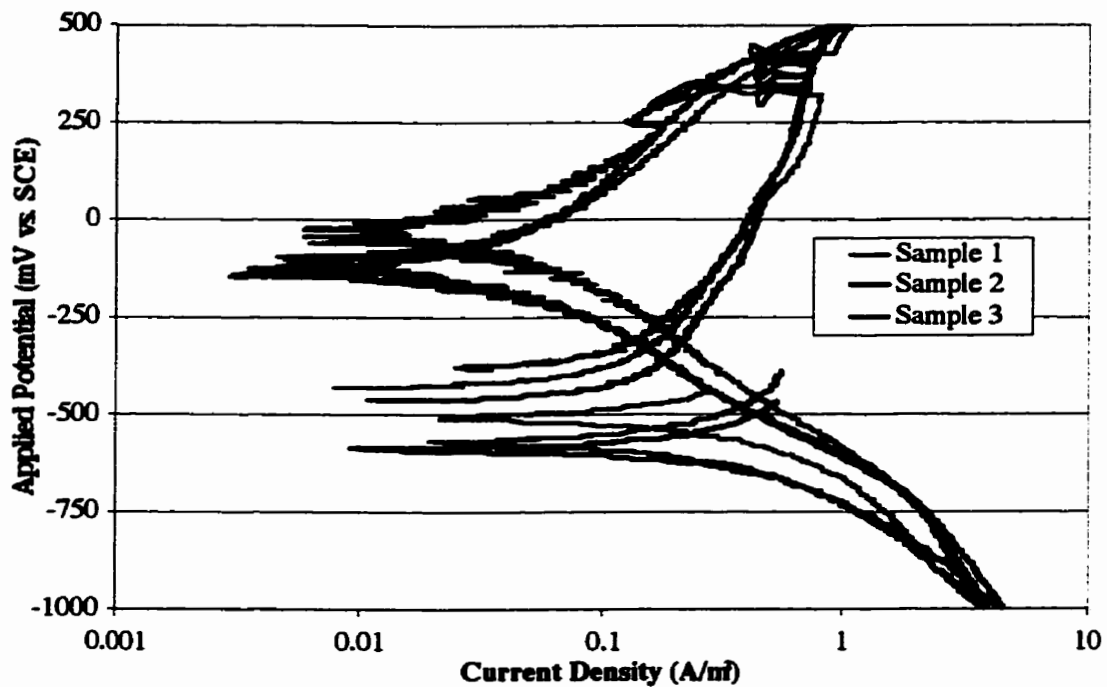


Figure A.31 Cyclic polarization curves for three samples immersed in  $\text{Ca}(\text{NO}_3)_2$ , 3% Cl solution.

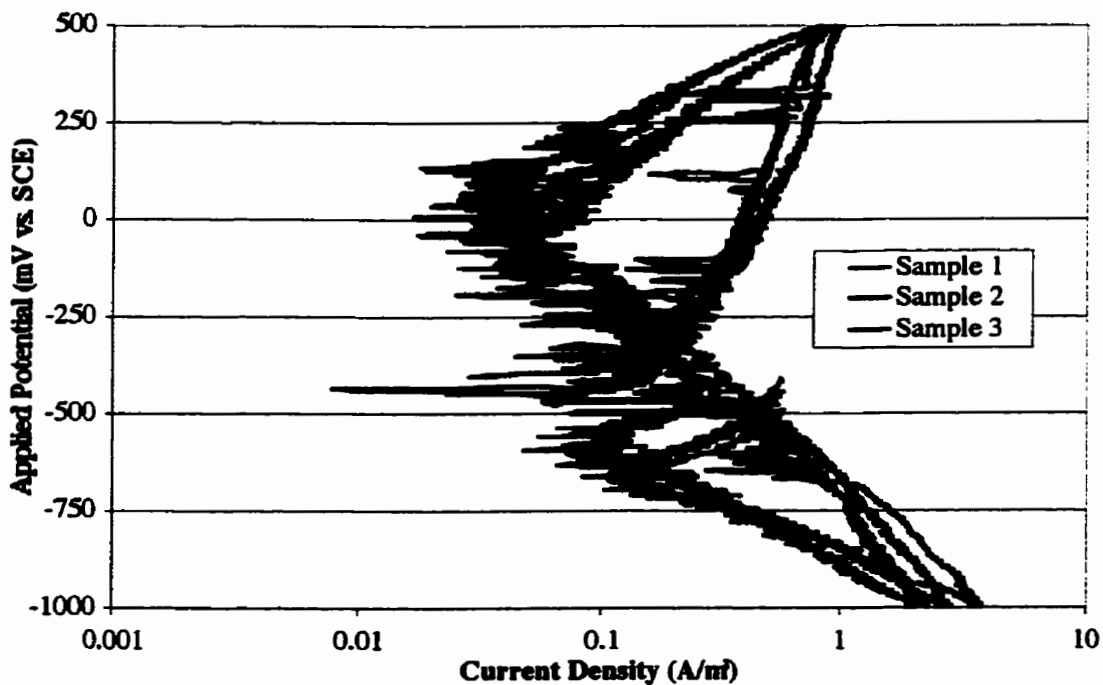


Figure A.32 Cyclic polarization curves for three samples immersed in  $\text{Ca}(\text{NO}_2)_3$ , 4% Cl solution.

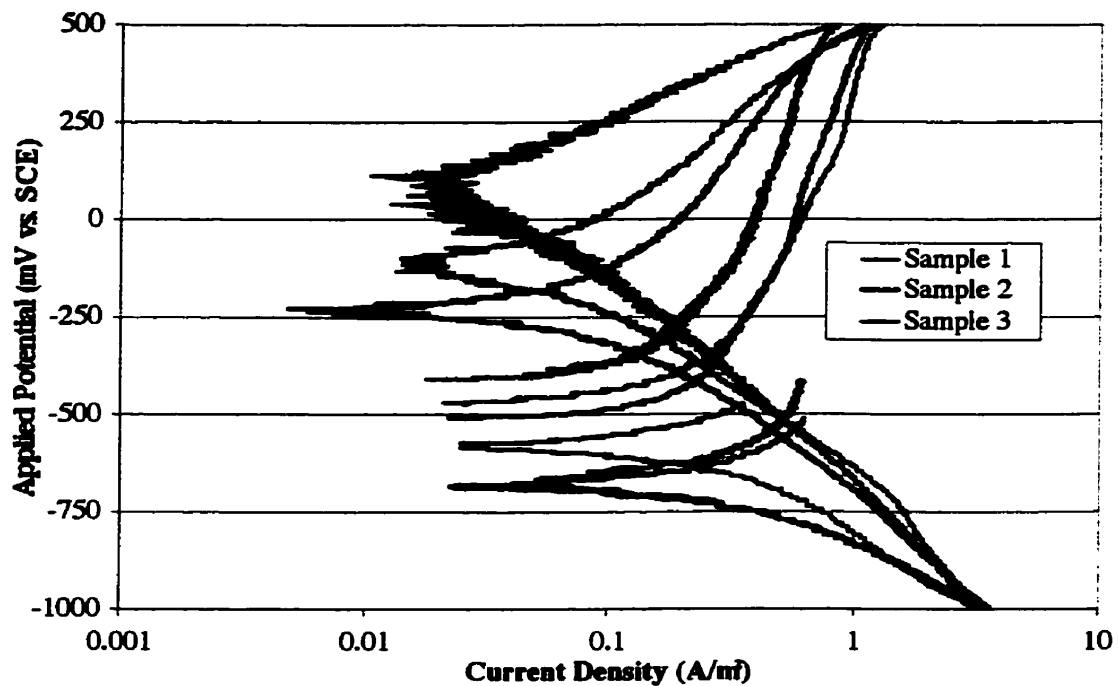


Figure A.33 Cyclic polarization curves for three samples immersed in  $\text{Ca}(\text{NO}_3)_2$ , 5% Cl solution.

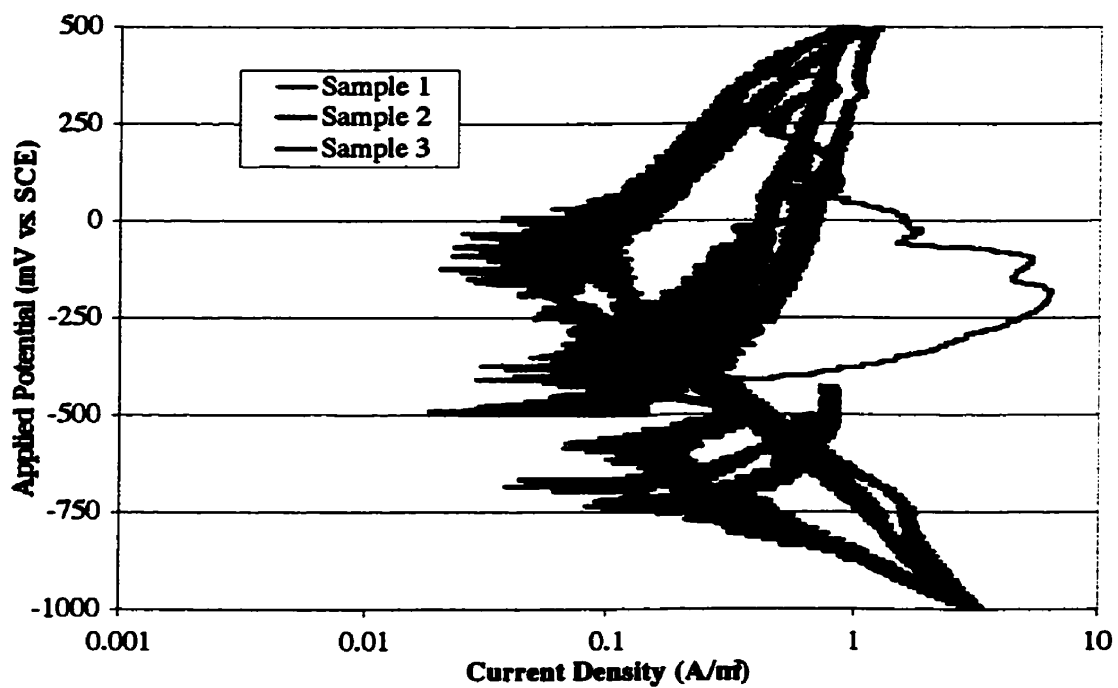


Figure A.34 Cyclic polarization curves for three samples immersed in  $\text{Ca}(\text{NO}_3)_2$ , 6% Cl solution.

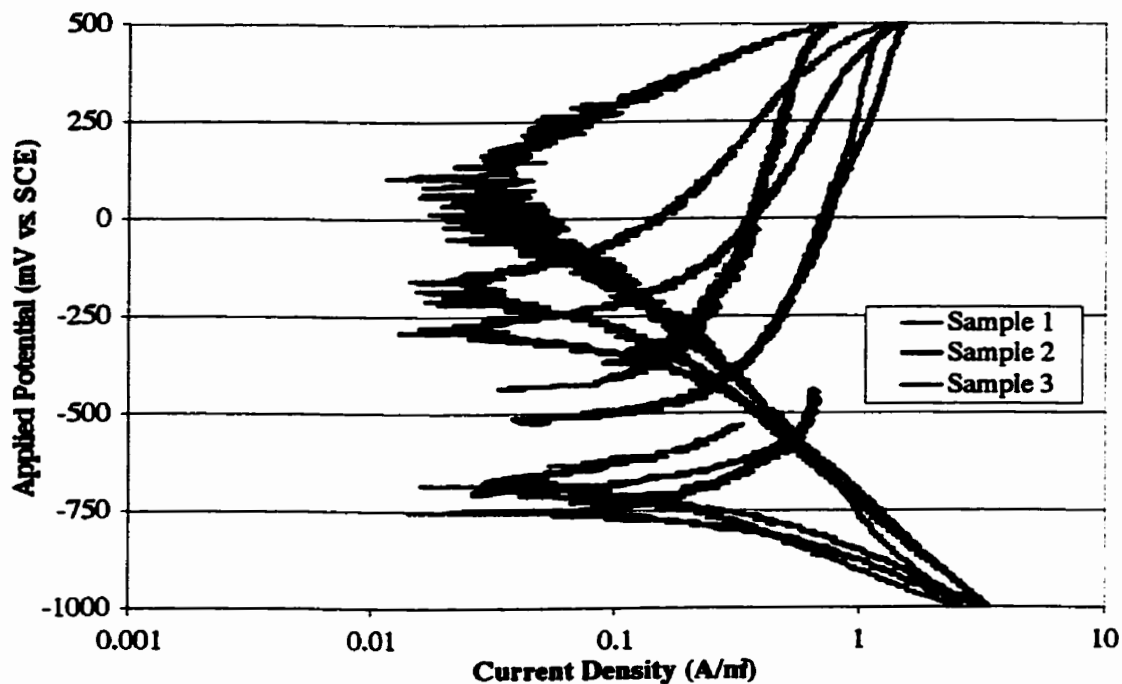


Figure A.35 Cyclic polarization curves for three samples immersed in  $\text{Ca}(\text{NO}_3)_2$ , 7% Cl solution.

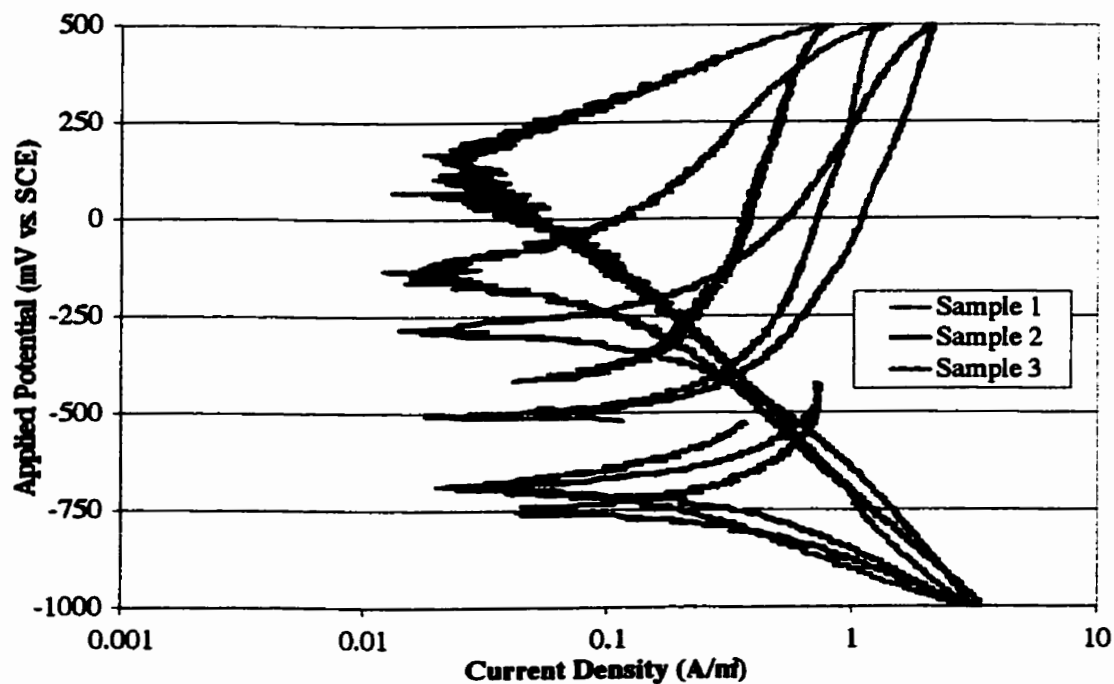


Figure A.36 Cyclic polarization curves for three sample immersed in  $\text{Ca}(\text{NO}_3)_2$ , 8% Cl solution.

## Appendix B

### $\text{NO}_2^-$ in Cells

Density of CN1 = 1.30 g/mL

Density of CN2 = 1.295 g/mL

Volume of inhibitor added: CN1 = 80 mL  
CN2 = 80.1 mL

Therefore, mass of CN1 added =  $80 \times 1.30 = 104 \text{ g} = 104,000 \text{ mg}$   
mass of CN2 added =  $80.1 \times 1.295 = 103.7 \text{ g} = 103,730 \text{ mg}$

Manufacturers of CN1 and CN2 state that inhibitor contains 30%  $\text{Ca}(\text{NO}_2)_2$  by mass

Therefore, mass of  $\text{Ca}(\text{NO}_2)_2$  in CN1 =  $104,000 \text{ mg} \times .30 = 31,200 \text{ mg}$   
mass of  $\text{Ca}(\text{NO}_2)_2$  in CN2 =  $103,730 \text{ mg} \times .30 = 31,119 \text{ mg}$

Total volume in Cell 2 (CN1) = 880 mL

Total volume in Cell 3 (CN2) = 880.1 mL

Therefore, concentration of  $\text{Ca}(\text{NO}_2)_2$  in CN1 cell =  $31,200 \text{ mg}/880 \text{ mL} = 35,455 \text{ mg/L}$   
concentration of  $\text{Ca}(\text{NO}_2)_2$  CN2 cell =  $31,119 \text{ mg}/880.1 \text{ mL} = 35,358 \text{ mg/L}$

Molar mass of  $\text{Ca}(\text{NO}_2)_2 = 40.08 + 2(14.0067 + 2(15.9994)) = 132.09 \text{ g/mol}$

Fraction of  $\text{NO}_2^-$  in  $\text{Ca}(\text{NO}_2)_2 = [2(14.0067 + 2(15.9994))]/132.09 = 0.6966$

Therefore, concentration of  $\text{NO}_2^-$  in CN1 cell =  $35,455 \text{ mg/L} \times 0.6966 = 24,698 \text{ mg/L}$   
concentration of  $\text{NO}_2^-$  in CN2 cell =  $35,358 \text{ mg/L} \times 0.6966 = 24,630 \text{ mg/L}$



## **Cl<sup>-</sup> in Cells**

Mass of each Cl<sup>-</sup> addition as NaCl:                      Cell 1 (Control) = 13.19 g  
   Cell 2 (CN1) = 14.90 g  
   Cell 3 (CN2) = 14.90 g

Total mass of NaCl additions:                              Cell 1 = 13.19 x 8 = 105.52 g  
   Cell 2 = 14.90 x 8 = 119.20 g  
   Cell 3 = 14.90 x 8 = 119.20 g

Total Volume:    Cell 1 = 800 mL  
   Cell 2 = 880 mL  
   Cell 3 = 880.1 mL

Molar mass of NaCl = 22.9898 g/mol + 35.4527 g/mol = 58.4425 g/mol

Fraction of Cl<sup>-</sup> in NaCl = 35.4527/58.4425 x 100 = 0.6066

Mass of total Cl<sup>-</sup>:    Cell 1 = 105.52 g x 0.6066 = 64.01 g  
   Cell 2 = 119.20 g x 0.6066 = 72.31 g  
   Cell 3 = 119.20 g x 0.6066 = 72.31 g

Therefore, expected Cl<sup>-</sup> concentration if complete dissociation of NaCl occurs:

Cell 1 = (64.01 g x 1000 mg/g)/.8 L = 80012.5 mg/L  
Cell 2 = (72.31 g x 1000 mg/g)/.88 L = 82170.5 mg/L  
Cell 3 = (72.31 g x 1000 mg/g)/.8801 L = 82161.1 mg/L

## **K<sup>+</sup> in Cells**

Total Volume:    Cell 1 = 800 mL  
   Cell 2 = 880 mL  
   Cell 3 = 880.1 mL

Concentration of K in pore solution = 0.6 mol/L KOH

Molar mass of K = 39.0983 g/mol

Therefore mass of K = 0.6 mol/L x 39.0983 g/mol = 23.459 g/L

Since each cell contains 800 mL of pure pore solution, mass of K<sup>+</sup> from pore solution in each cell:

= 23459 mg/L x 0.8 L = 18767.2 mg

Therefore, expected K<sup>+</sup> concentration if complete dissociation of KOH occurs:

Cell 1 = 18767.2 mg/0.8 L = 23549 mg/L  
Cell 2 = 18767.2 mg/0.88 L = 21326 mg/L  
Cell 3 = 18767.2 mg/0.8801 L = 21324 mg/L

## Na<sup>+</sup> in Cells

Sources of sodium      (1) NaOH  
                                      (2) NaCl

Molar mass of Na = 22.98977 g/mol

Each cell has the same initial concentration of NaOH due to pore solution = 0.3 mol.L

Therefore, Na<sup>+</sup> from pore solution = 0.3 mol/L x 0.8 L = 0.24 mol

Therefore, mass of Na<sup>+</sup> from NaOH = 0.24 mol x 22.98977 g/mol = 5.5175 g

Total NaCl added to each cell:

Cell 1 = 105.52 g
Cell 2 = 119.20 g
Cell 3 = 119.20 g

Fraction of Na<sup>+</sup> in NaCl =  $22.98977 / (22.98977 + 35.453) = 0.3934$

Therefore, mass Na<sup>+</sup> from NaCl added per cell:

Cell 1 = 105.52 g x 0.3934 = 41.51 g
Cell 2 = 119.20 g x 0.3934 = 46.89 g
Cell 3 = 119.20 g x 0.3934 = 46.89 g

Therefore, total mass of Na<sup>+</sup>:

Cell 1 = 5.5175 g + 41.51 g = 47.03 g
Cell 2 = 5.5175 g + 46.89 g = 52.41 g
Cell 3 = 5.5175 g + 46.89 g = 52.41 g

Therefore, amount of Na<sup>+</sup> per cell, if complete dissociation occurs:

Cell 1 = (47.03 g x 1000 mg/g)/0.8 L = 58787.5 mg/L
Cell 2 = (52.41 g x 1000mg/g)/0.88 L = 59556.8 mg/L
Cell 3 = (52.41 g x 1000mg/g)/0.8801 L = 59550.1 mg/L

## Ca<sup>2+</sup> in Cells

Sources of Ca: (1) Ca(OH)<sub>2</sub>  
(2) Ca(NO<sub>2</sub>)<sub>2</sub>

Mass of Ca(OH)<sub>2</sub> added to each cell = 10.00 g

Molar mass of Ca(OH)<sub>2</sub> = 40.08 + 2(15.9994 + 1.0079) = 74.0946 g/mol

Fraction of Ca<sup>2+</sup> by mass = 40.08/74.09 x 100 = 0.5409

Therefore, mass of Ca<sup>2+</sup> due to Ca(OH)<sub>2</sub> = 10.00 g x 0.5409 = 5.409 g

For Cells 2 and 3, other source of Ca is Ca(NO<sub>2</sub>)<sub>2</sub>.

Volume of inhibitor added to cells: Cell 2 = 80 mL  
Cell 3 = 80.1 mL

Mass of inhibitor added: Cell 2 = 80 mL x 1.30 g/mL = 104 g  
Cell 3 = 80.1 mL x 1.295 g/mL = 104 g

Manufacturers of CN1 and CN2 state that inhibitor contains 30 % Ca(NO<sub>2</sub>)<sub>2</sub> by mass

$$\text{CN1} = 104 \text{ g} \times 1000 \text{ mg/g} \times 30 \% = 31,200 \text{ mg}$$

$$\text{CN2} = 104 \text{ g} \times 1000 \text{ mg/g} \times 30 \% = 31,200 \text{ mg}$$

Fraction of Ca in Ca(NO<sub>2</sub>)<sub>2</sub> = 40.08/[40.08 + 2(14.0067 + 2(15.9994))] = 0.3034

Therefore, mass of Ca in CN1 = 31,200 mg x 0.3034 = 9466 mg  
mass of Ca in CN2 = 31,200 mg x 0.3034 = 9466 mg

Total Ca in cells: Cell 1 = 5409 mg  
Cell 2 = 5409 mg + 9466 mg = 14,875 mg  
Cell 3 = 5409 mg + 9466 mg = 14,875 mg

Total volume: Cell 1 = 800 mL  
Cell 2 = 880 mL  
Cell 3 = 880.1 mL

Therefore, amount of Ca in cells, assuming complete dissociation of all species:

$$\text{Cell 1} = 5409 \text{ mg}/.8 \text{ L} = 6761 \text{ mg/L}$$

$$\text{Cell 2} = 14,875 \text{ mg}/.88 \text{ L} = 16,903 \text{ mg/L}$$

$$\text{Cell 3} = 14,875 \text{ mg}/.8801 \text{ L} = 16,901 \text{ mg/L}$$

## Appendix C

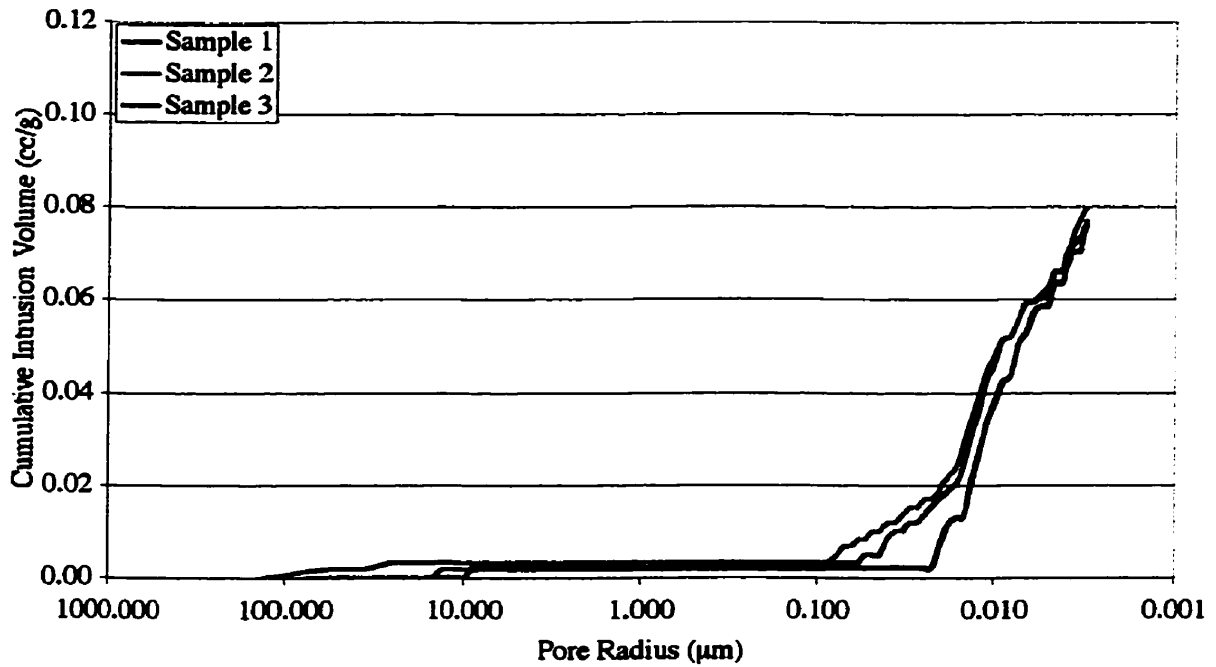


Figure C.1 Cumulative intrusion volume vs. pore radius for three Control White Cement Paste samples

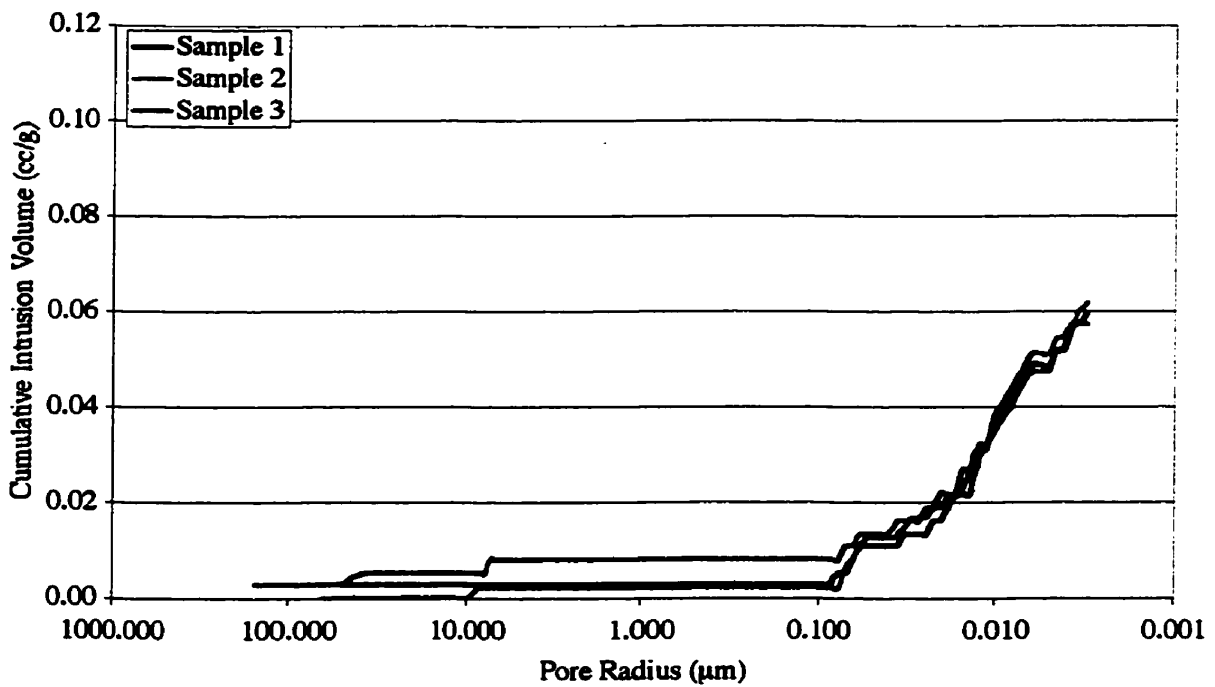


Figure C.2 Cumulative intrusion volume vs. pore radius for three CN1 White Cement Paste samples

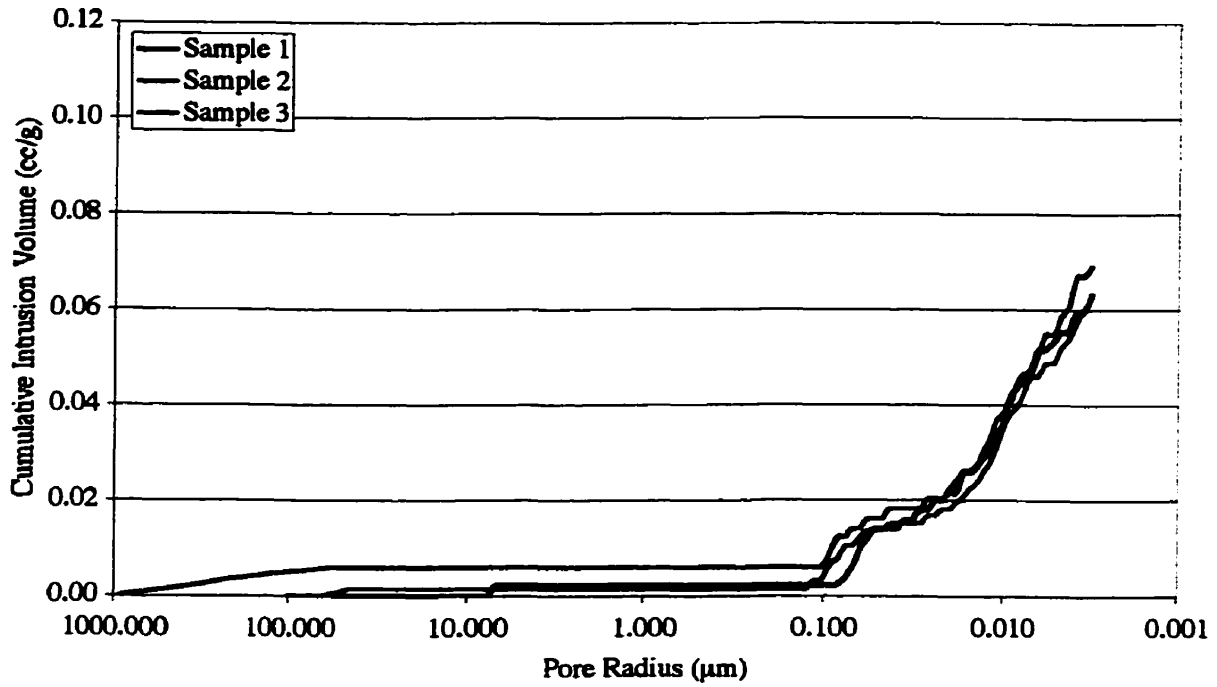


Figure C.3 Cumulative intrusion volume vs. pore radius for three CN2 White Cement Paste samples

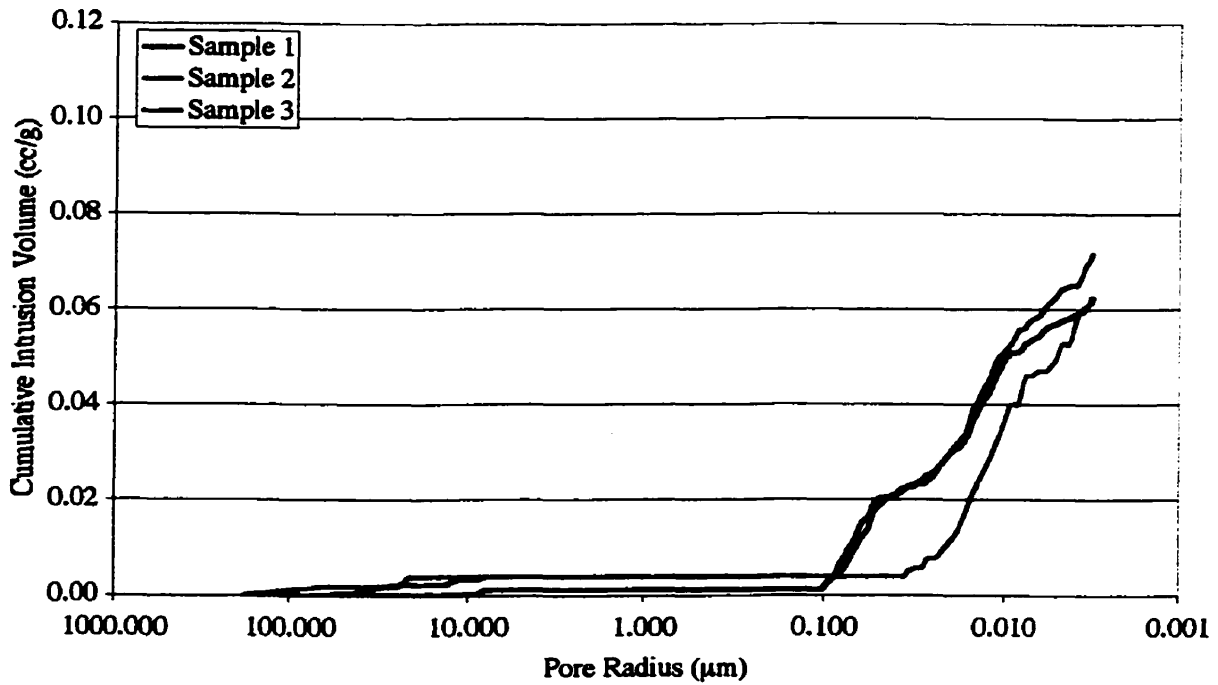


Figure C.4 Cumulative intrusion volume vs. pore radius for three Ca(NO<sub>3</sub>)<sub>2</sub> White Cement Paste samples

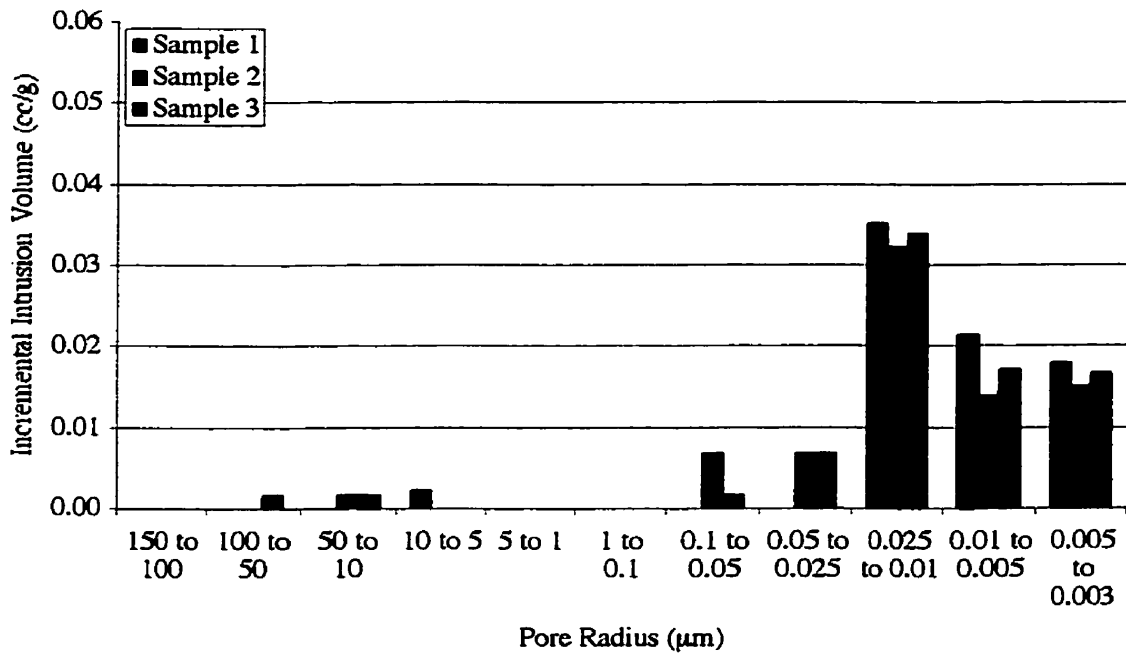


Figure C.5 Incremental intrusion volume vs. pore radius for three Control White Cement Paste samples

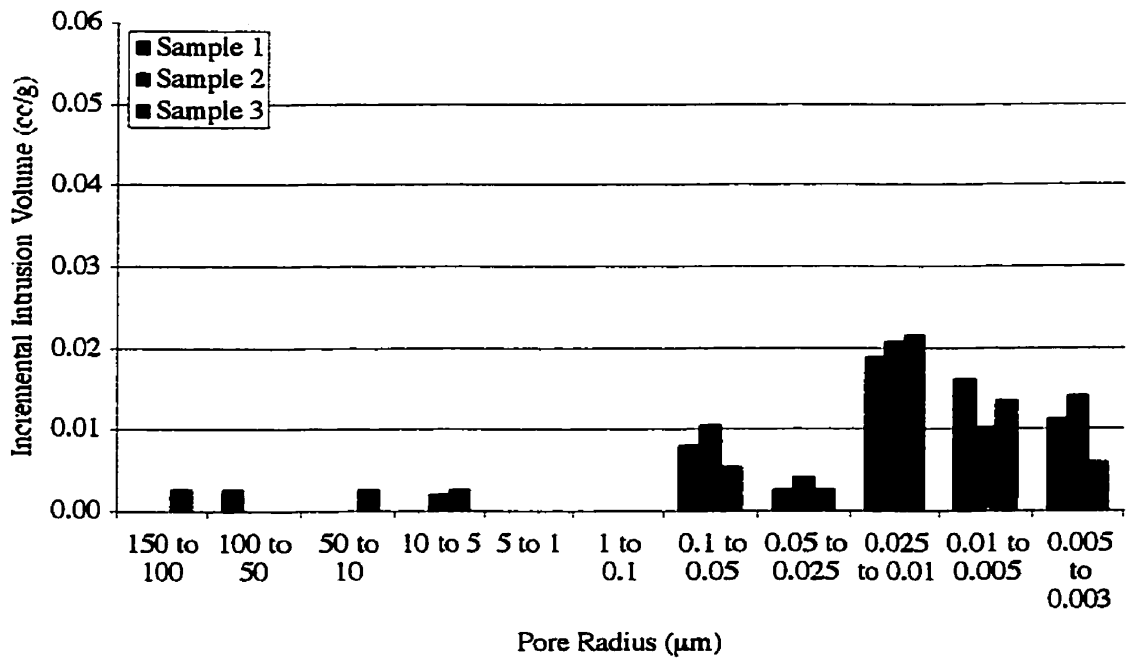


Figure C.6 Incremental intrusion volume vs. pore radius for three CN1 White Cement Paste samples

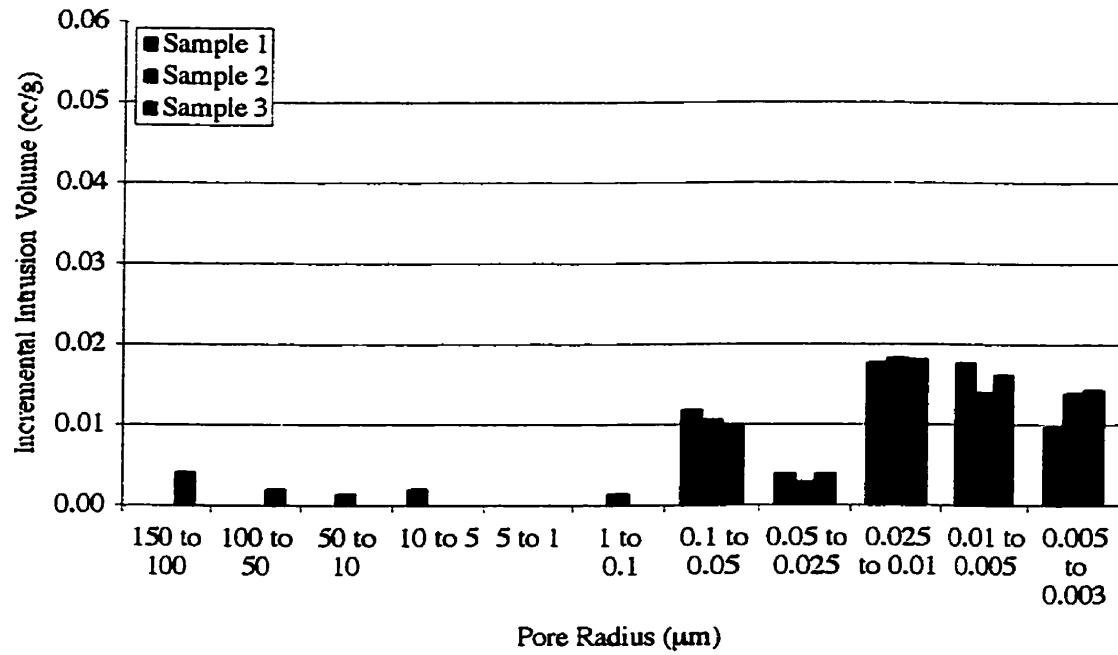


Figure C.7 Incremental intrusion volume vs. pore radius for three CN2 White Cement Paste samples

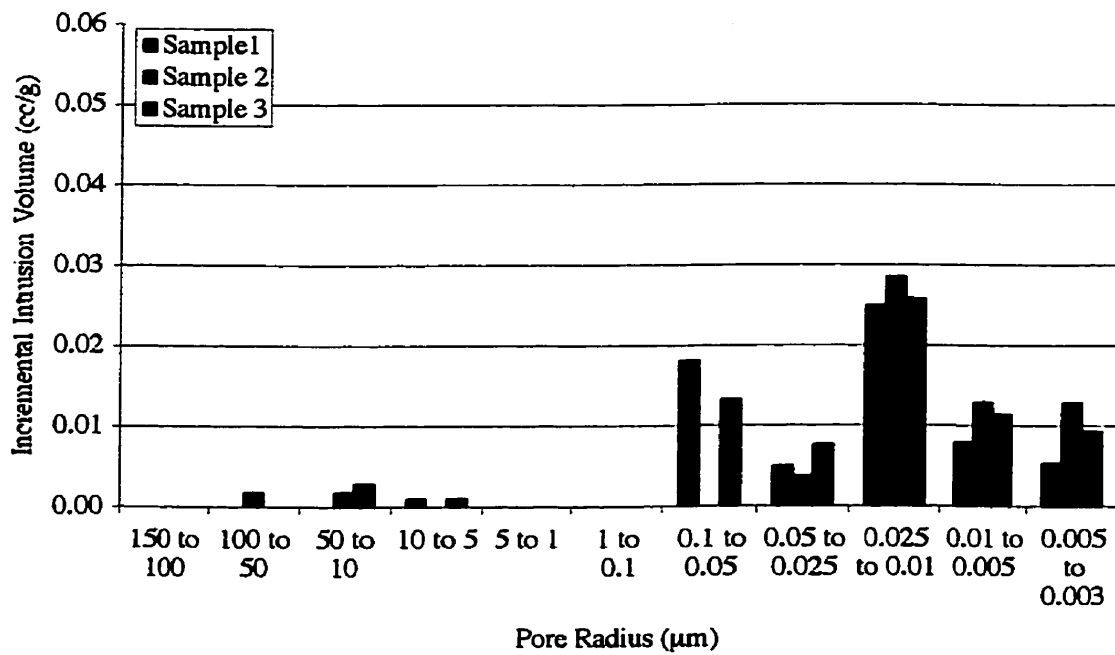


Figure C.8 Incremental intrusion volume vs. pore radius for three Ca(NO<sub>3</sub>)<sub>2</sub> White Cement Paste samples

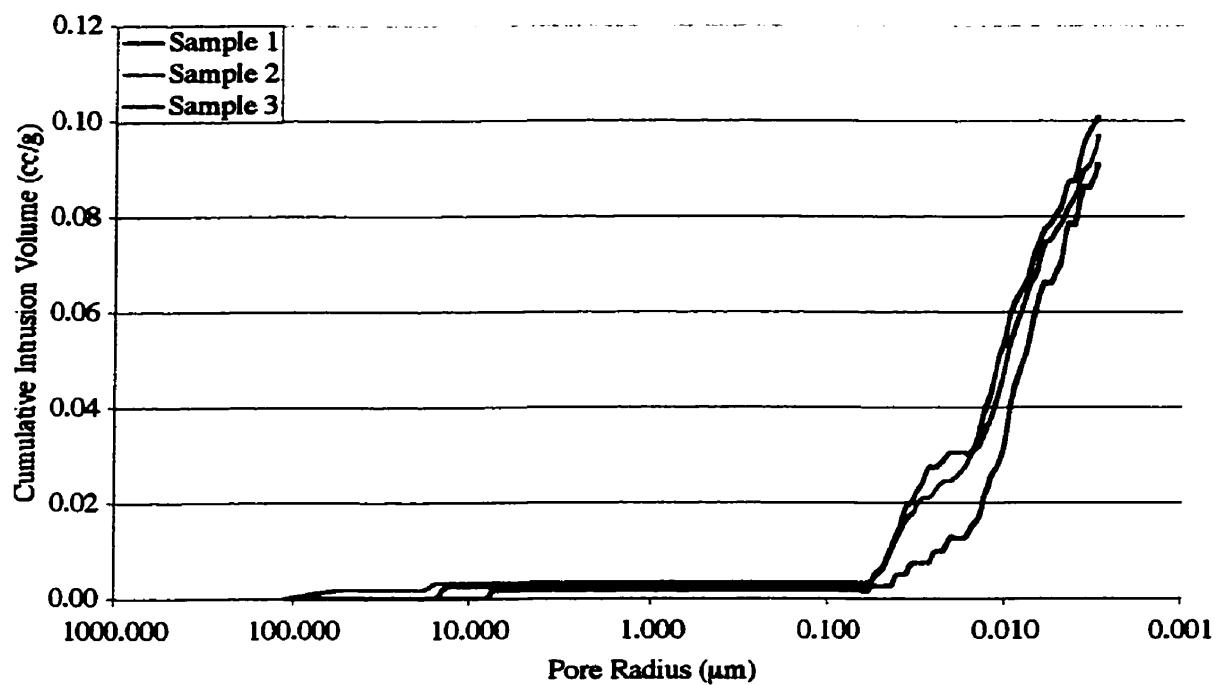


Figure C.9 Cumulative intrusion volume vs. pore radius for three Control OPC Paste samples

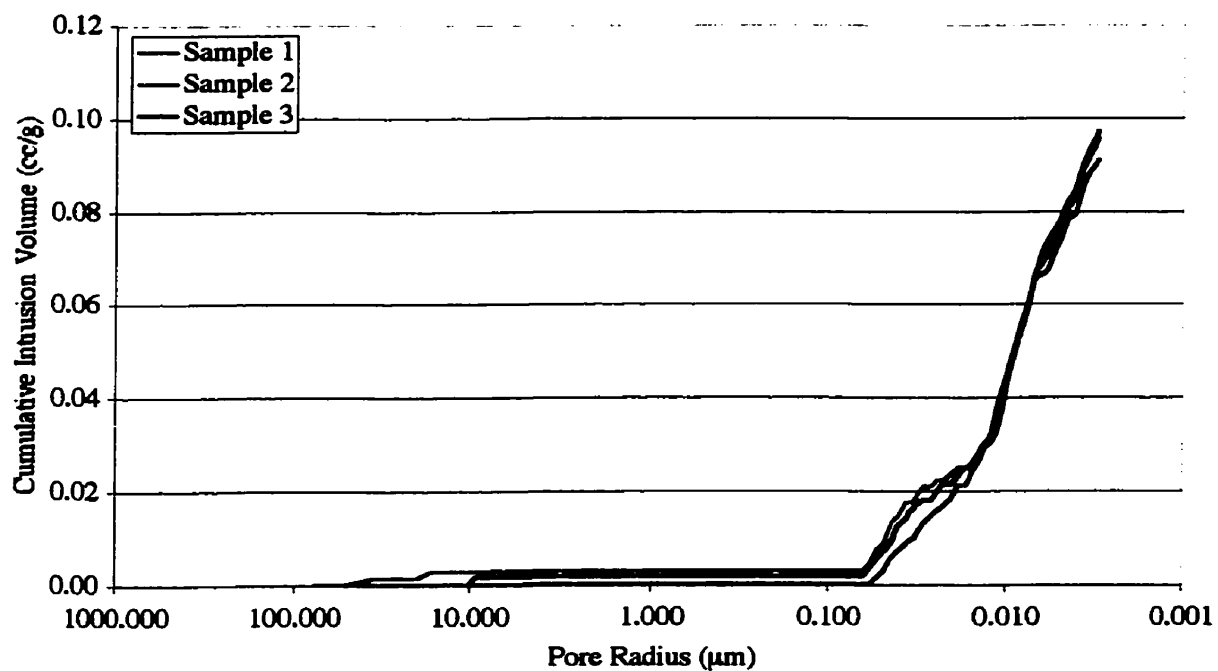


Figure C.10 Cumulative intrusion volume vs. pore radius for three CN1 OPC Paste samples



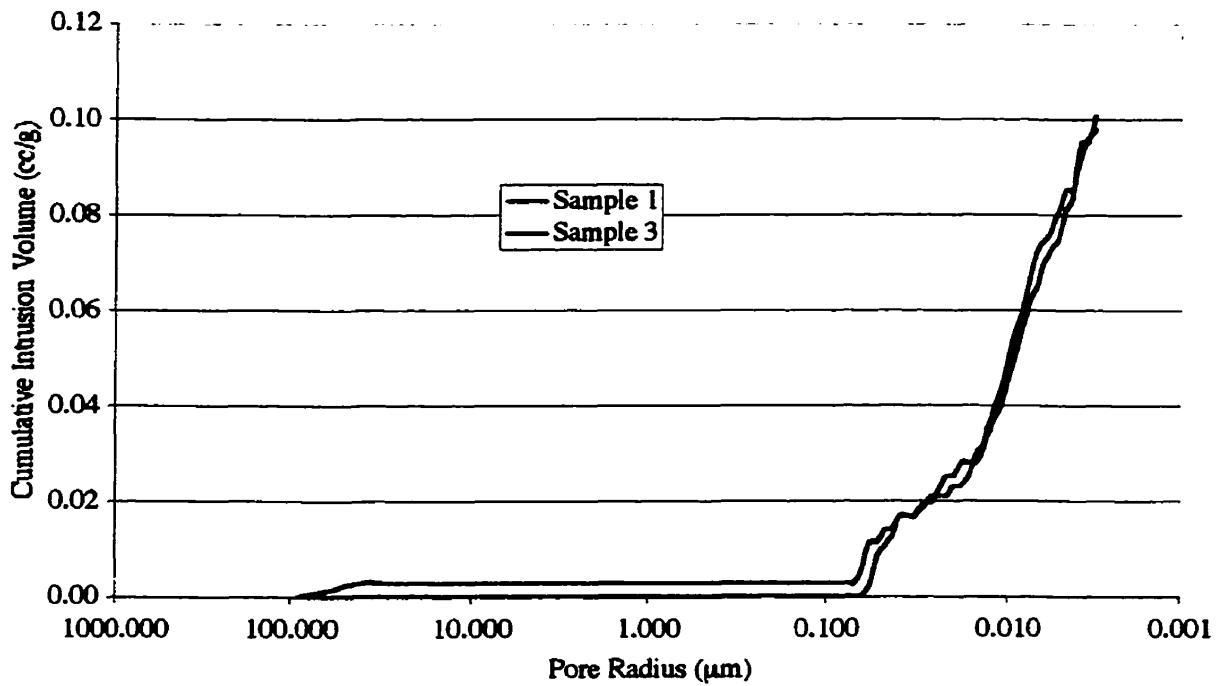


Figure C.11 Cumulative intrusion volume vs. pore radius for two CN2 OPC Paste samples

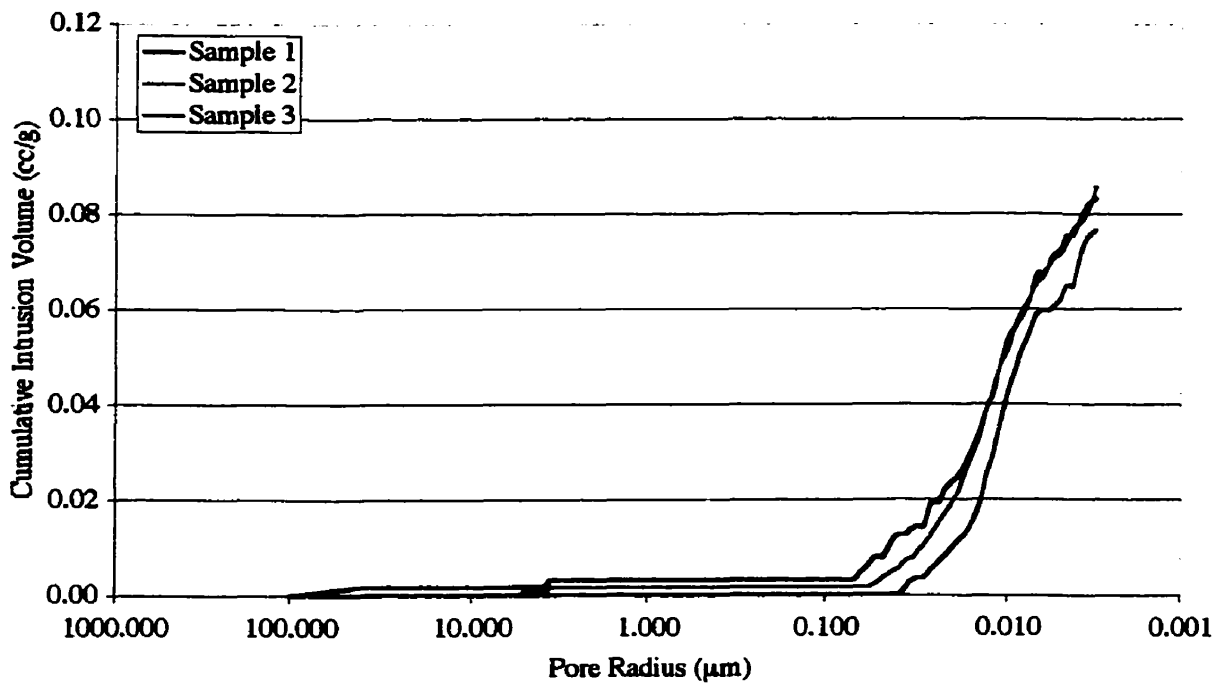


Figure C.12 Cumulative intrusion volume vs. pore radius for three Ca(NO<sub>3</sub>)<sub>2</sub> OPC Paste samples

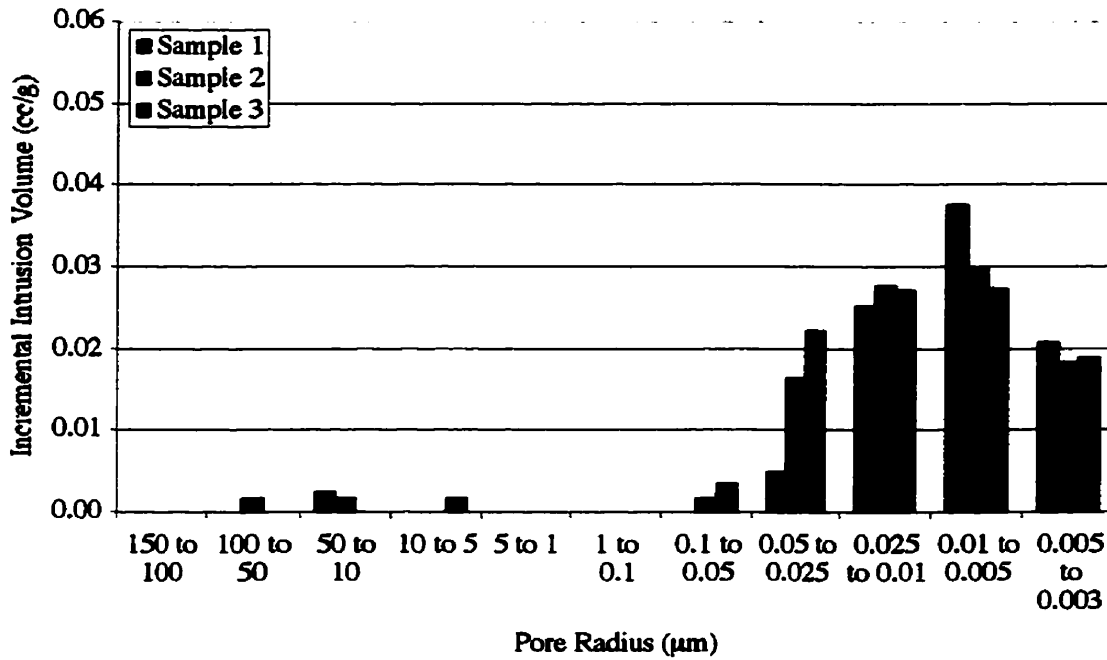


Figure C.13 Incremental intrusion volume vs. pore radius for three Control OPC Paste samples

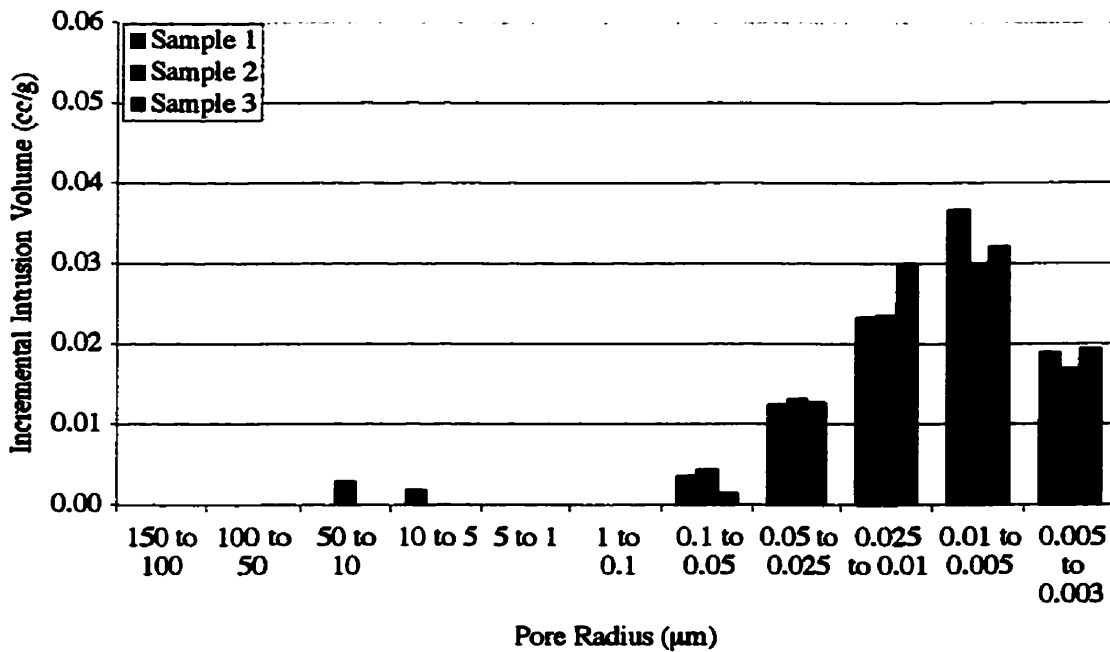


Figure C.14 Incremental intrusion volume vs. pore radius for three CN1 OPC Paste samples

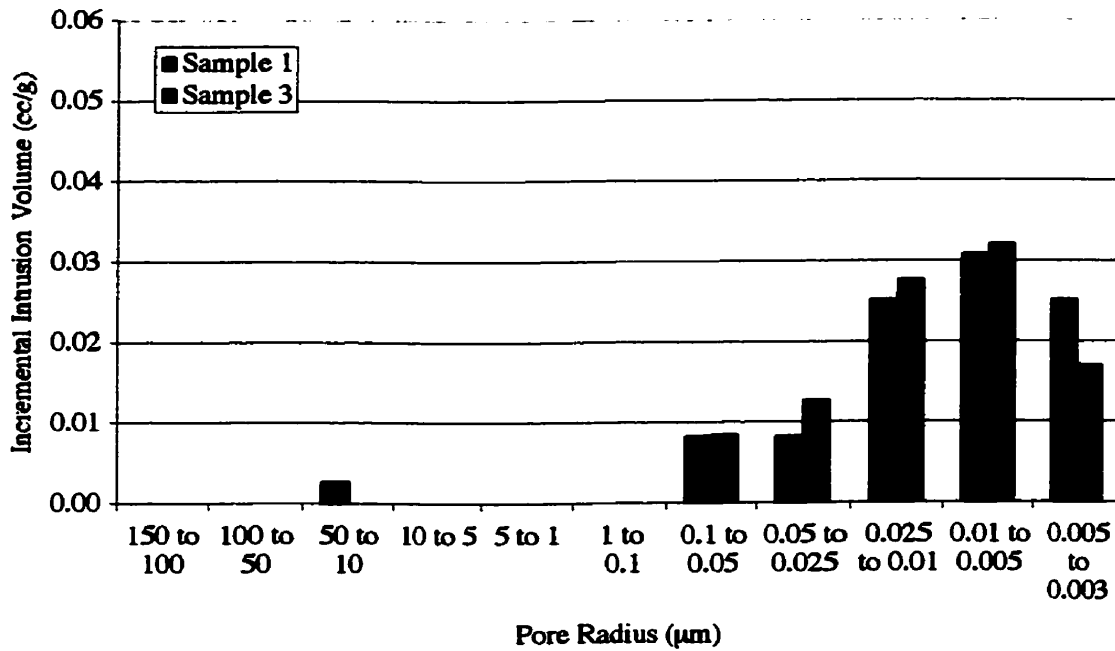


Figure C.15 Incremental intrusion volume vs. pore radius for two CN2 OPC Paste samples

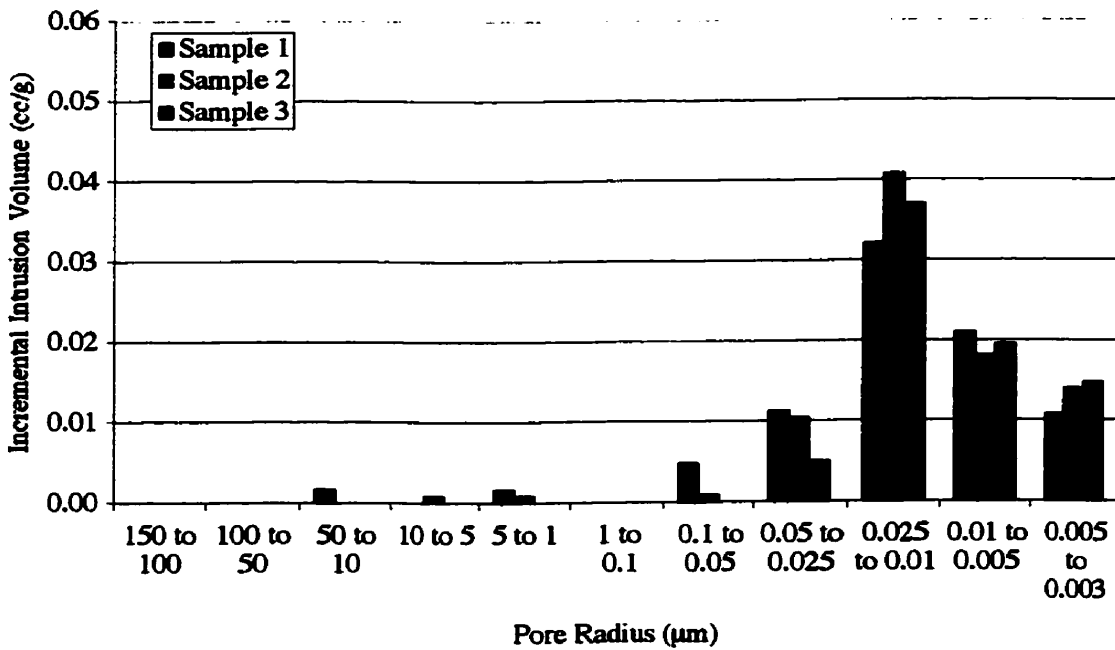


Figure C.16 Incremental intrusion volume vs. pore radius for three Ca(NO<sub>3</sub>)<sub>2</sub> OPC Paste samples

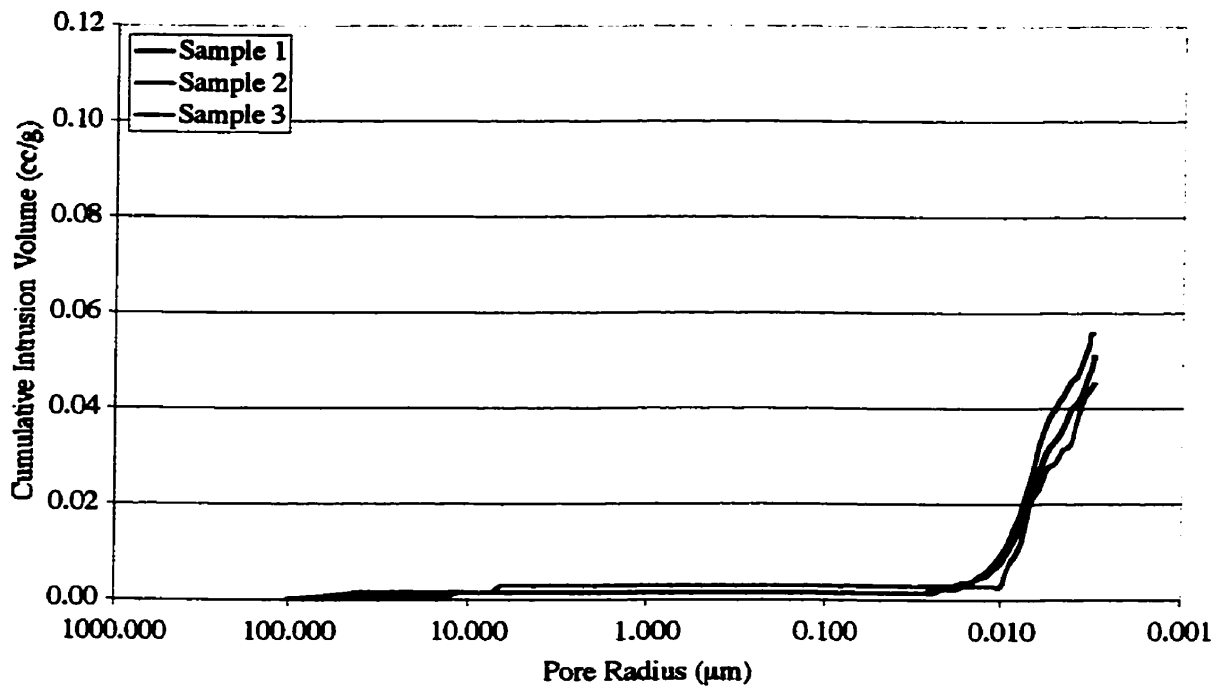


Figure C.17 Cumulative intrusion volume vs. pore radius for three Poned Control White Cement Paste samples

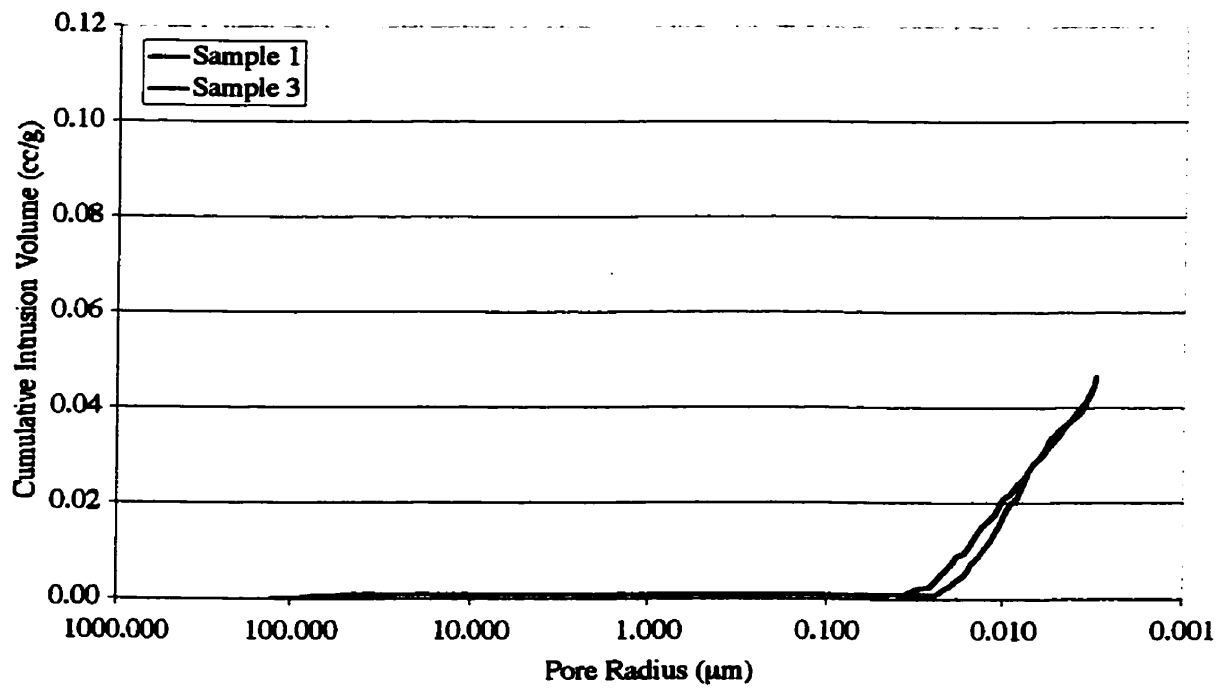


Figure C.18 Cumulative intrusion volume vs. pore radius for two Poned CN1 White Cement Paste samples

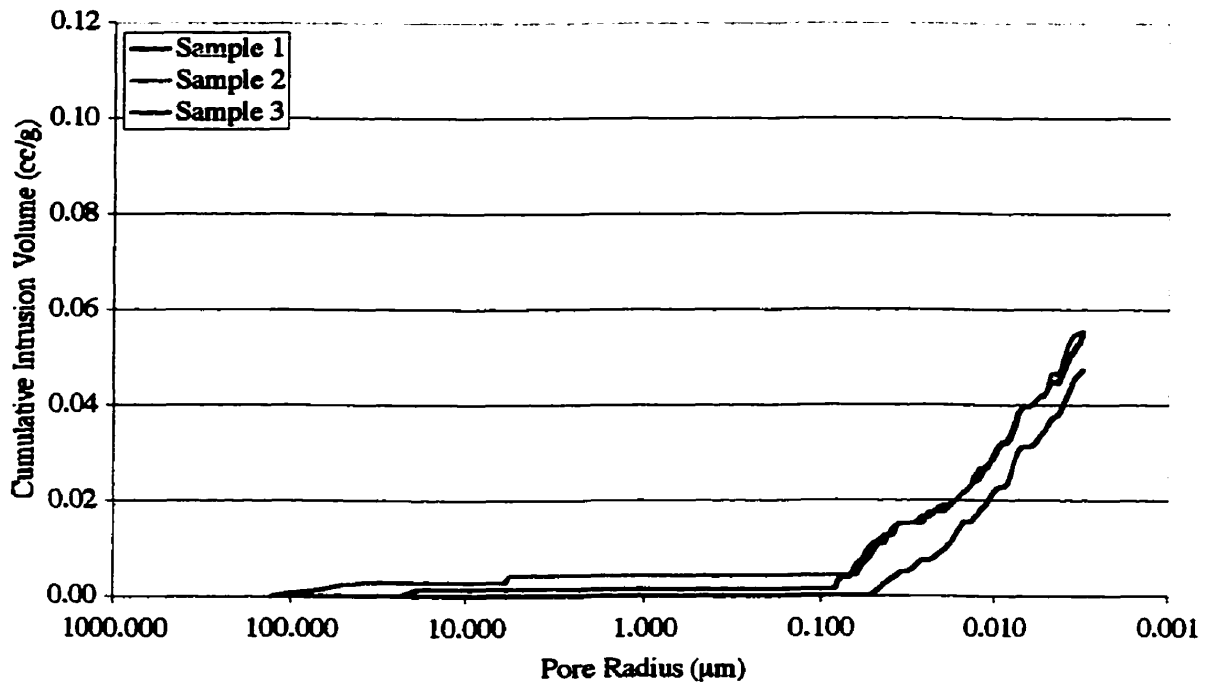


Figure C.19 Cumulative intrusion volume vs. pore radius for three Pondered CN<sub>2</sub> White Cement Paste samples

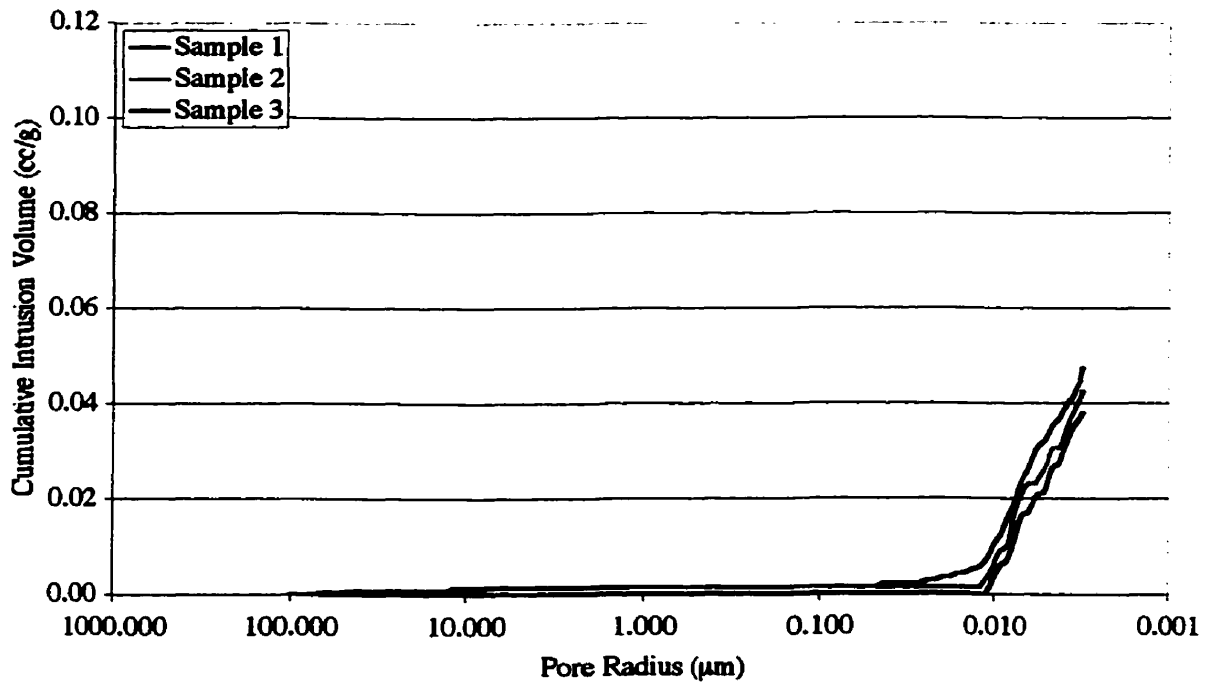


Figure C.20 Cumulative intrusion volume vs. pore radius for three Pondered Ca(NO<sub>3</sub>)<sub>2</sub> White Cement Paste samples

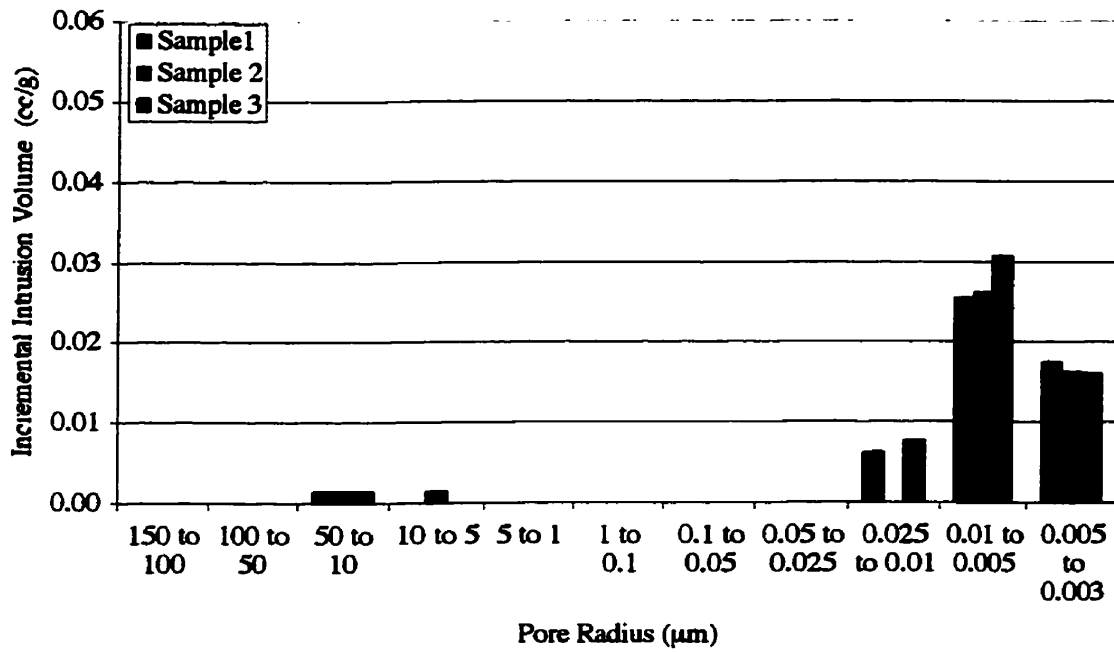


Figure C.21 Incremental intrusion volume vs. pore radius for three Poned Control White Cement Paste samples

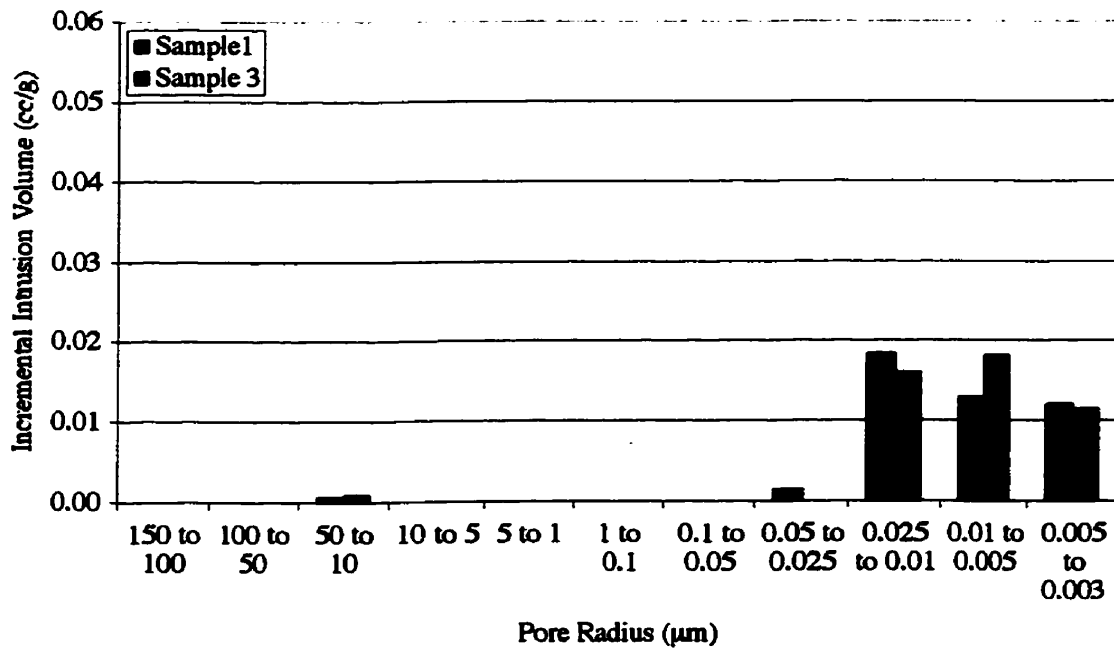


Figure C.22 Incremental intrusion volume vs. pore radius for two Poned CN1 White Cement Paste samples

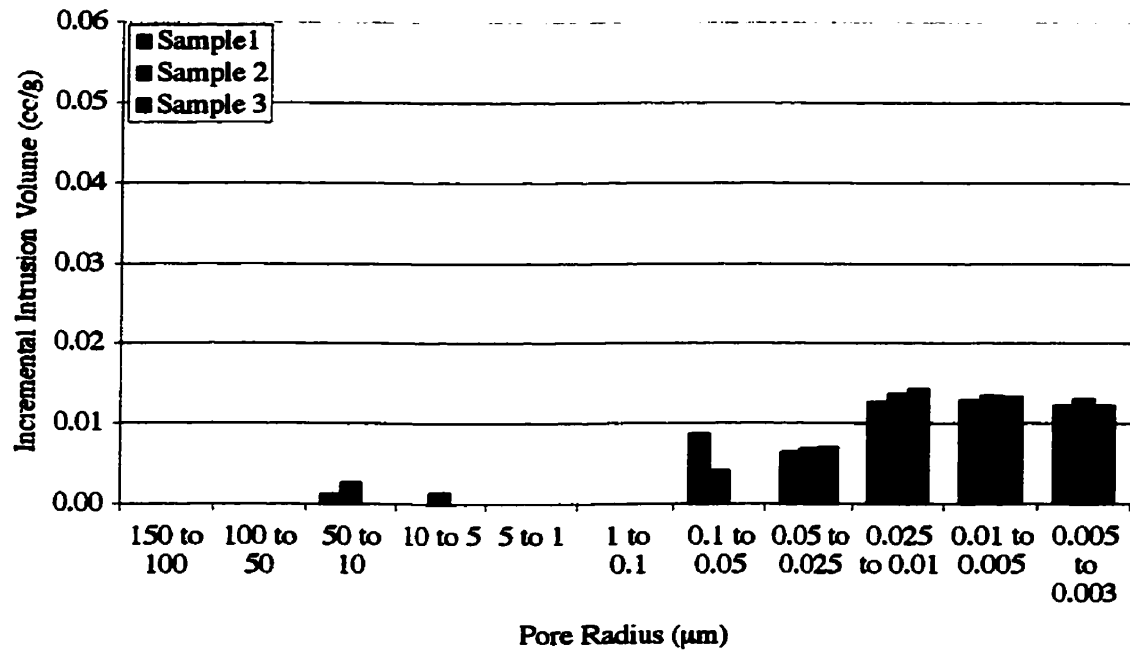


Figure C.23 Incremental intrusion volume vs. pore radius for three Pondered CN2 White Cement Paste samples

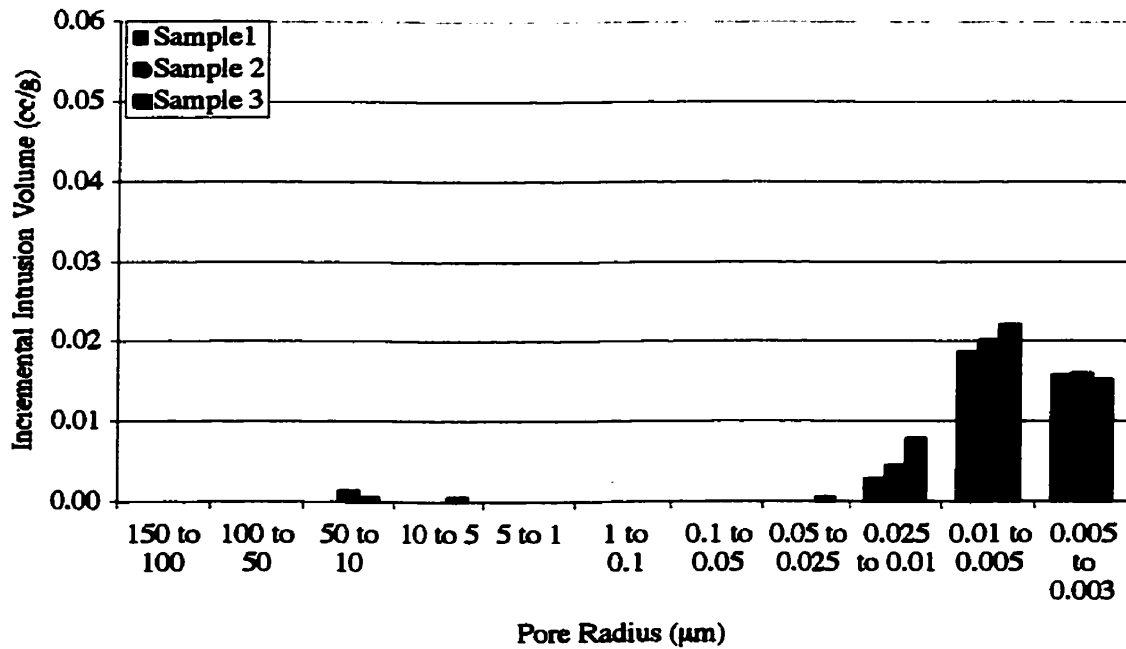


Figure C.24 Incremental intrusion volume vs. pore radius for three Pondered Ca(NO<sub>3</sub>)<sub>2</sub> White Cement Paste samples

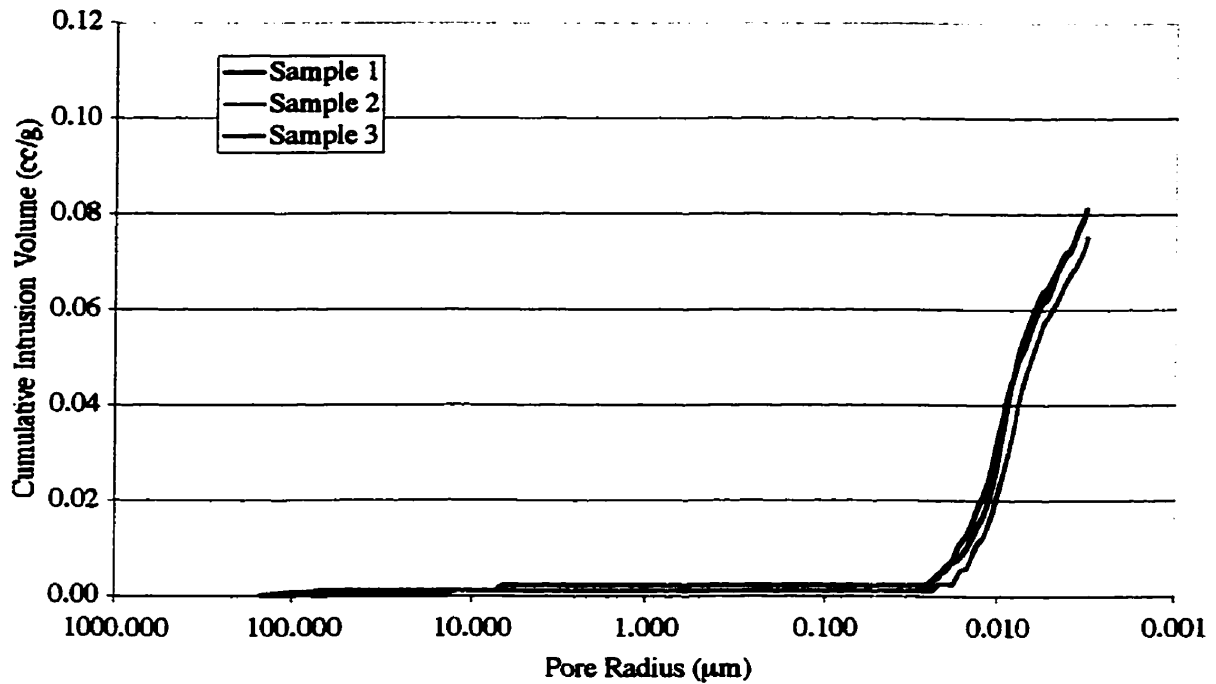


Figure C.25 Cumulative intrusion volume vs. pore radius for three Ponded Control OPC Paste samples

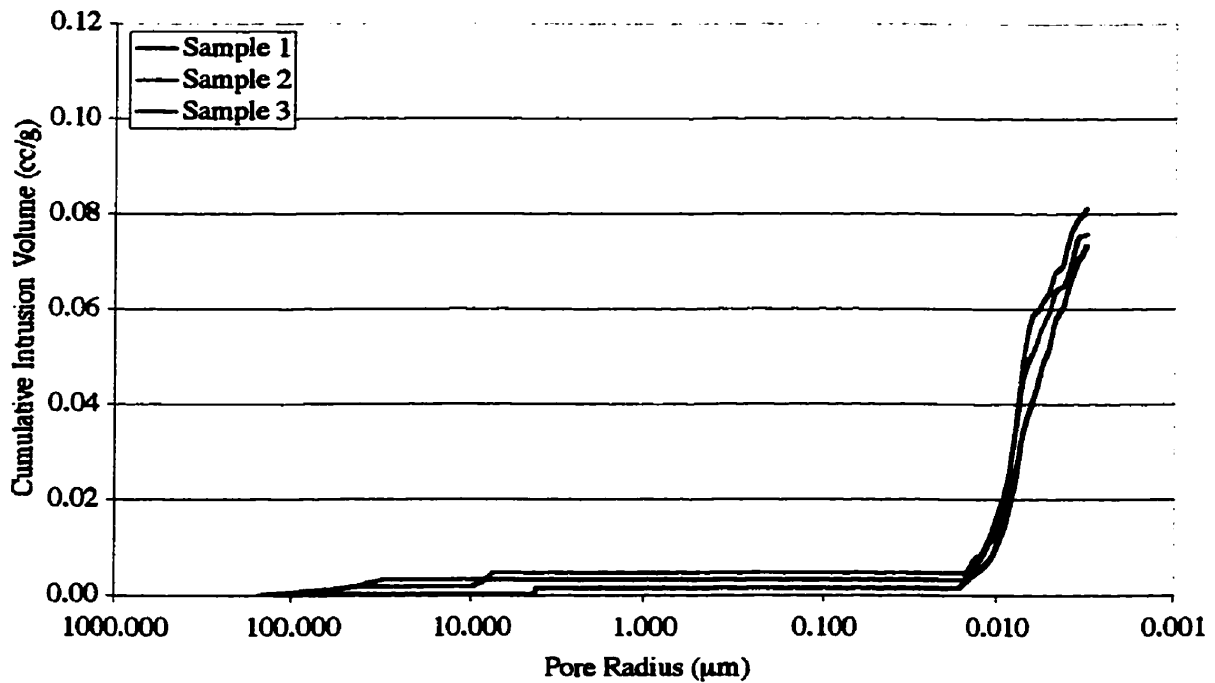


Figure C.26 Cumulative intrusion volume vs. pore radius for three Ponded CN1 OPC Paste samples



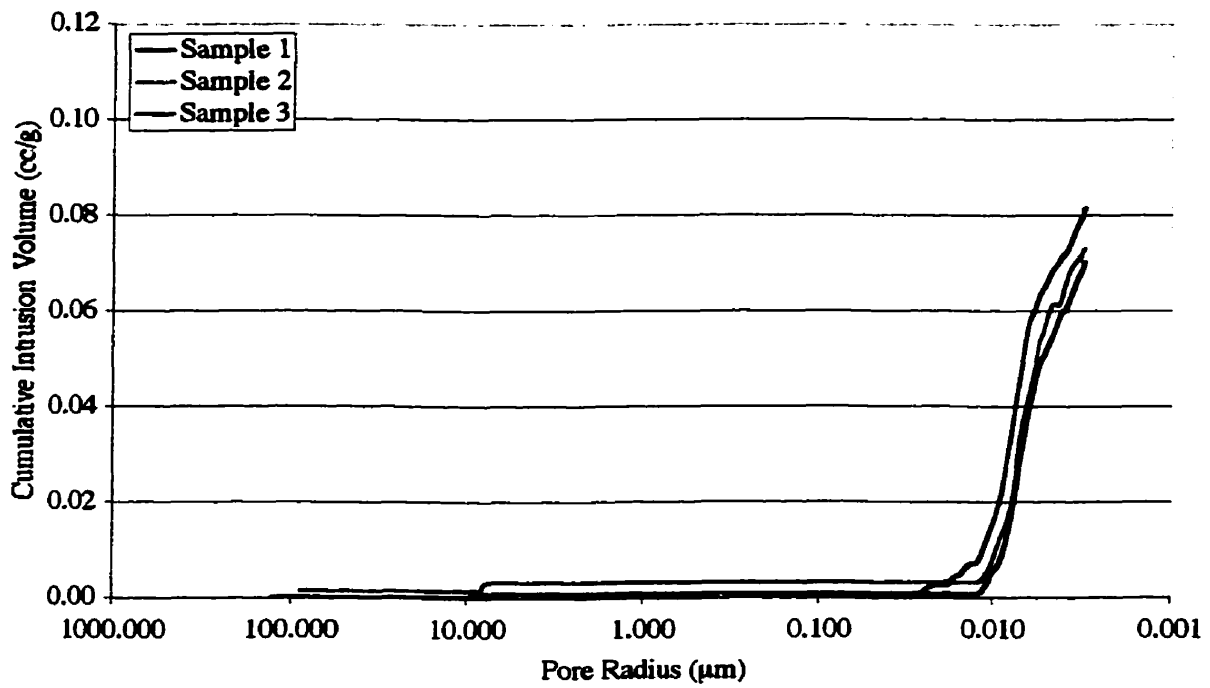


Figure C.27 Cumulative intrusion volume vs. pore radius for three Pondered CN<sub>2</sub> OPC Paste samples

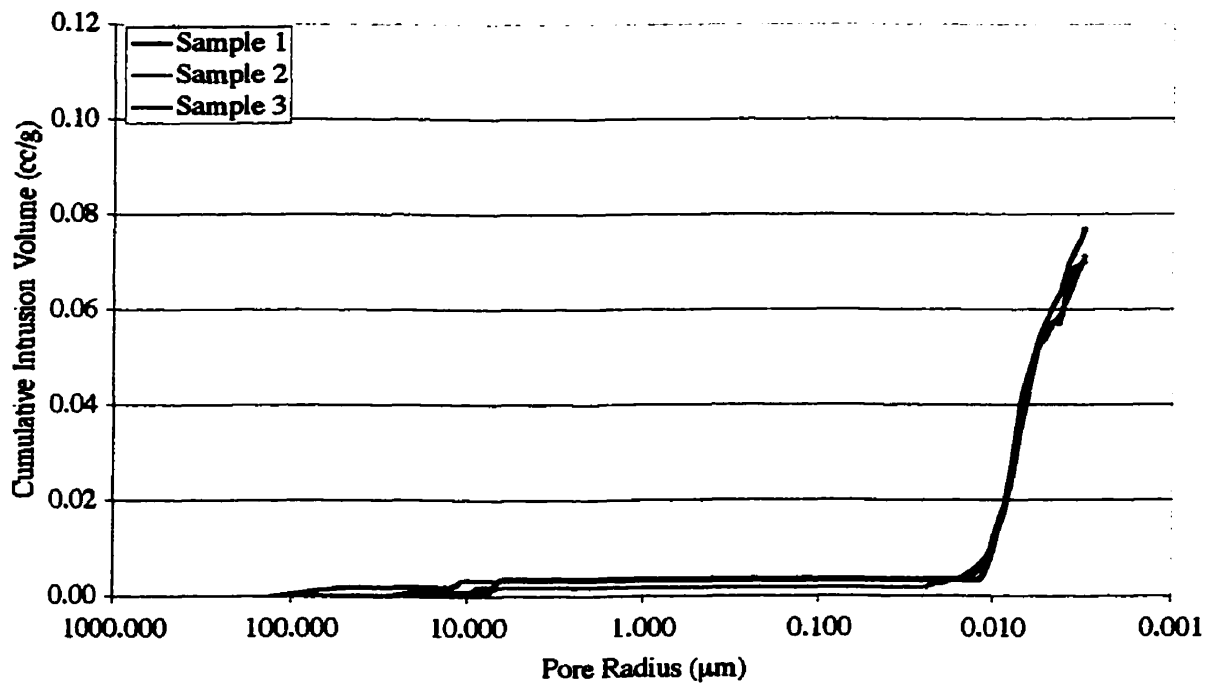


Figure C.28 Cumulative intrusion volume vs. pore radius for three Pondered Ca(NO<sub>3</sub>)<sub>2</sub> OPC Paste samples

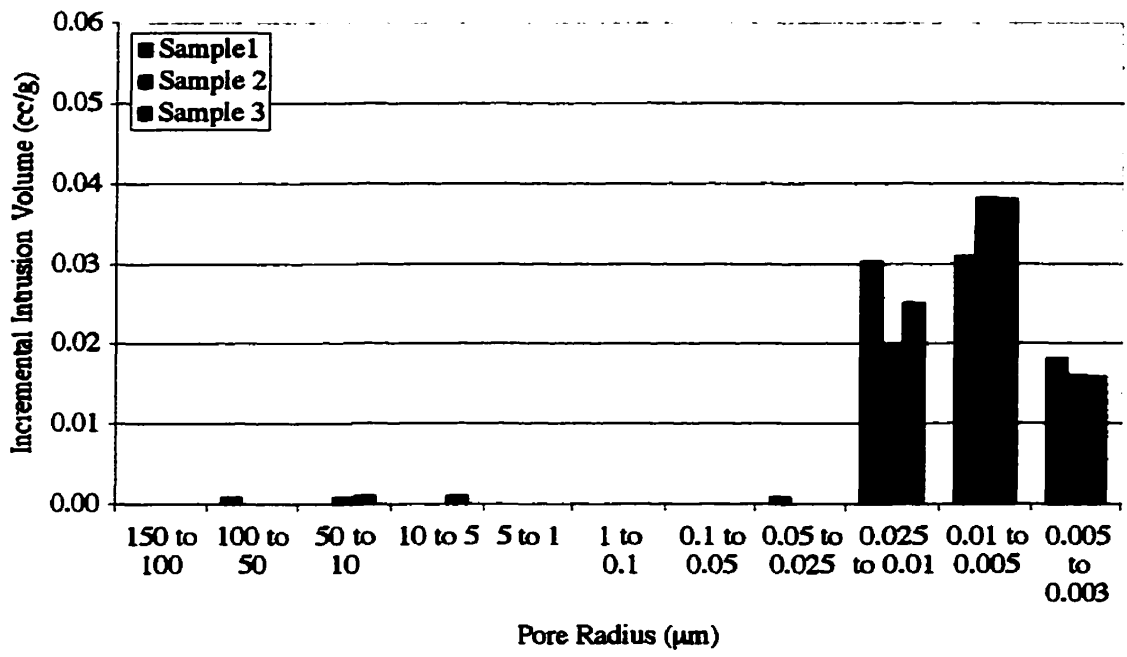


Figure C.29 Incremental intrusion volume vs. pore radius for three Pondered Control OPC Paste samples

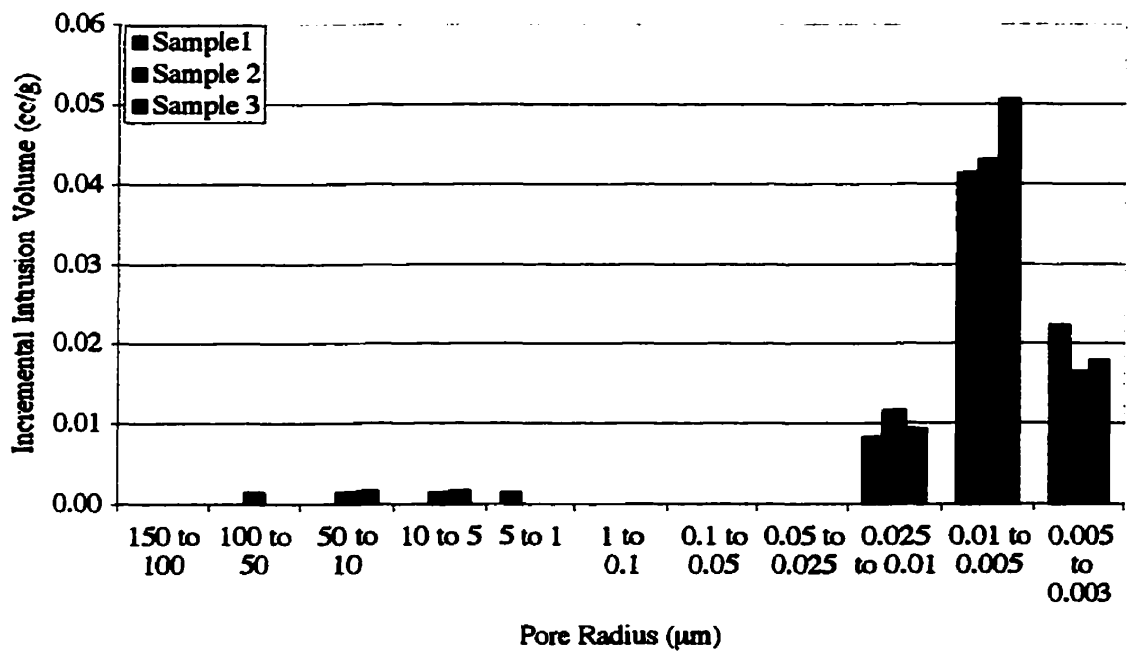


Figure C.30 Incremental intrusion volume vs. pore radius for three Pondered CN1 OPC Paste samples

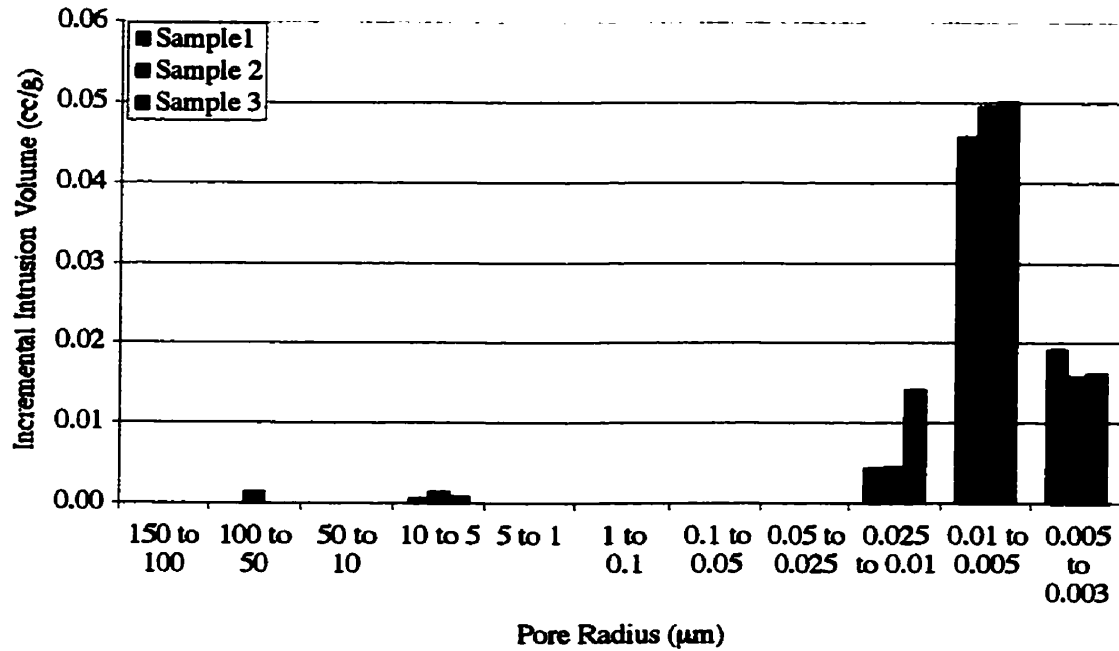


Figure C.31 Incremental intrusion volume vs. pore radius for three Pondered CN2 OPC Paste samples

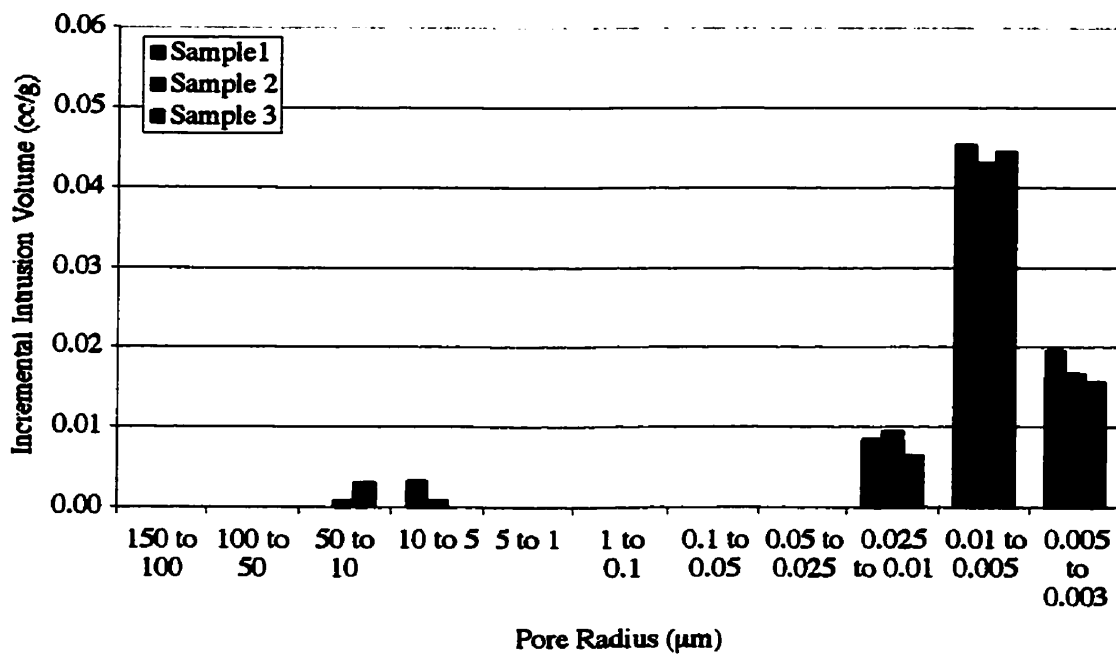


Figure C.32 Incremental intrusion volume vs. pore radius for three Pondered Ca(NO<sub>3</sub>)<sub>2</sub> OPC Paste samples

## Appendix D

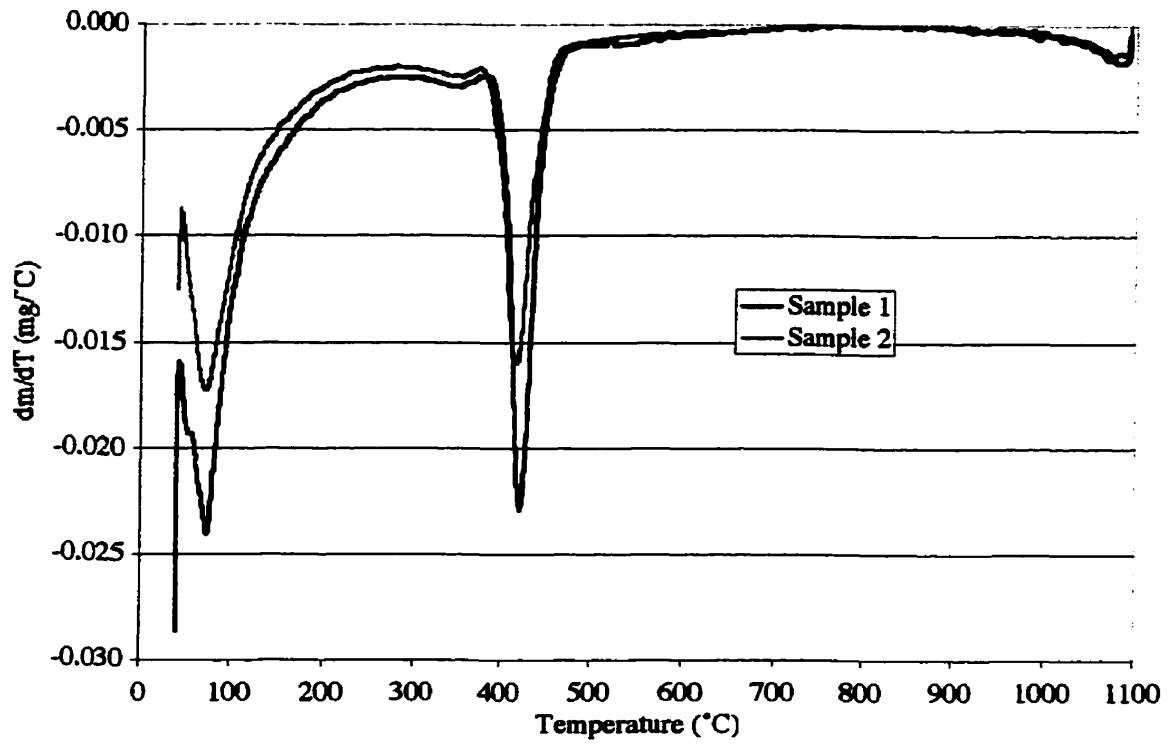


Figure D.1 DTG of two Control White Cement Paste samples

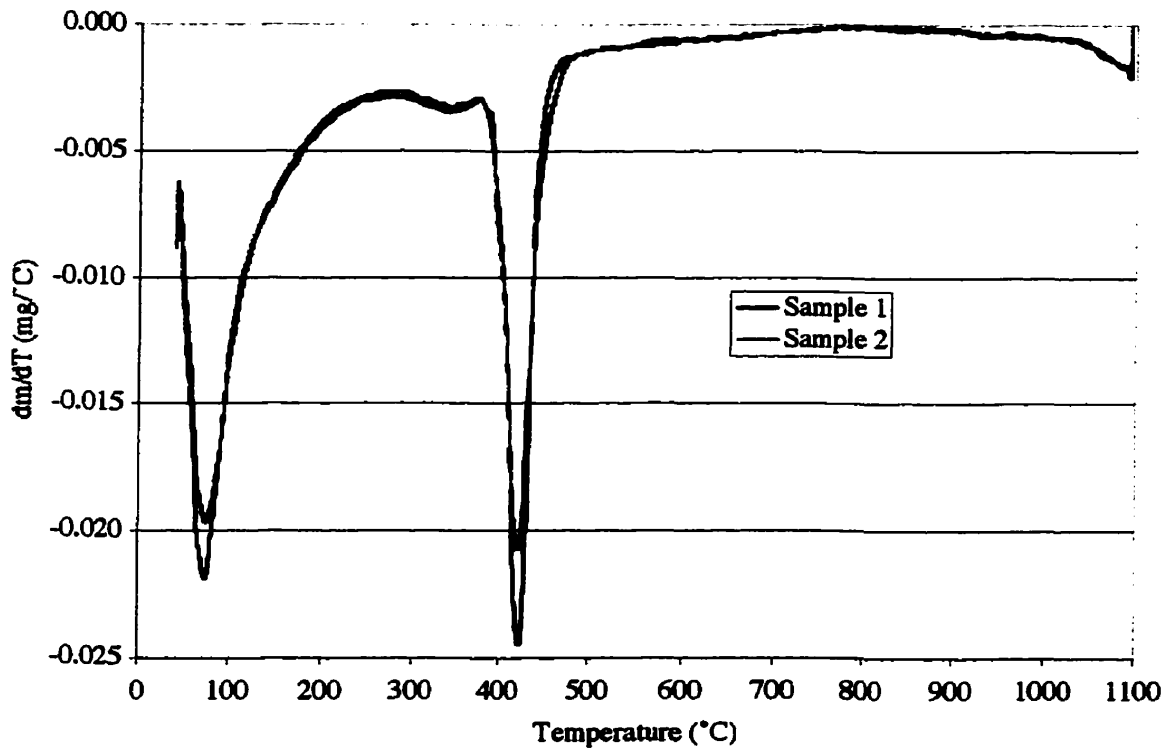


Figure D.2 DTG of two CN1 White Cement Paste samples

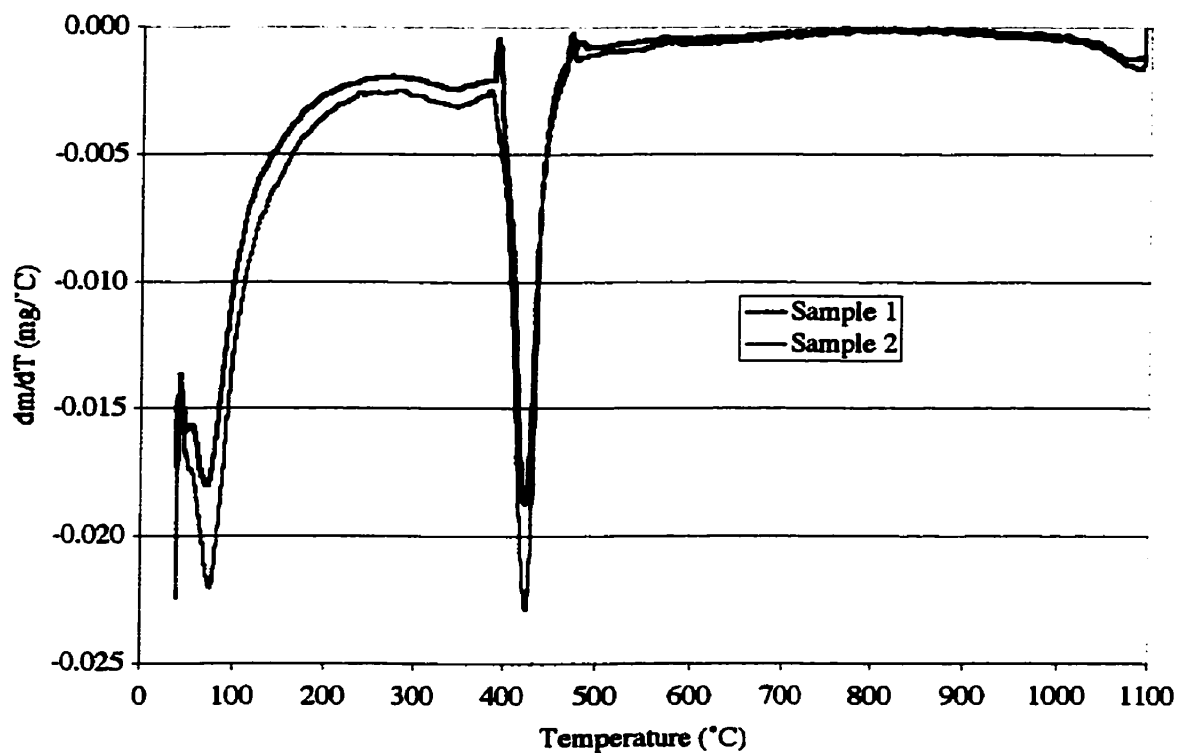


Figure D.3 DTG of two CN<sub>2</sub> White Cement Paste samples

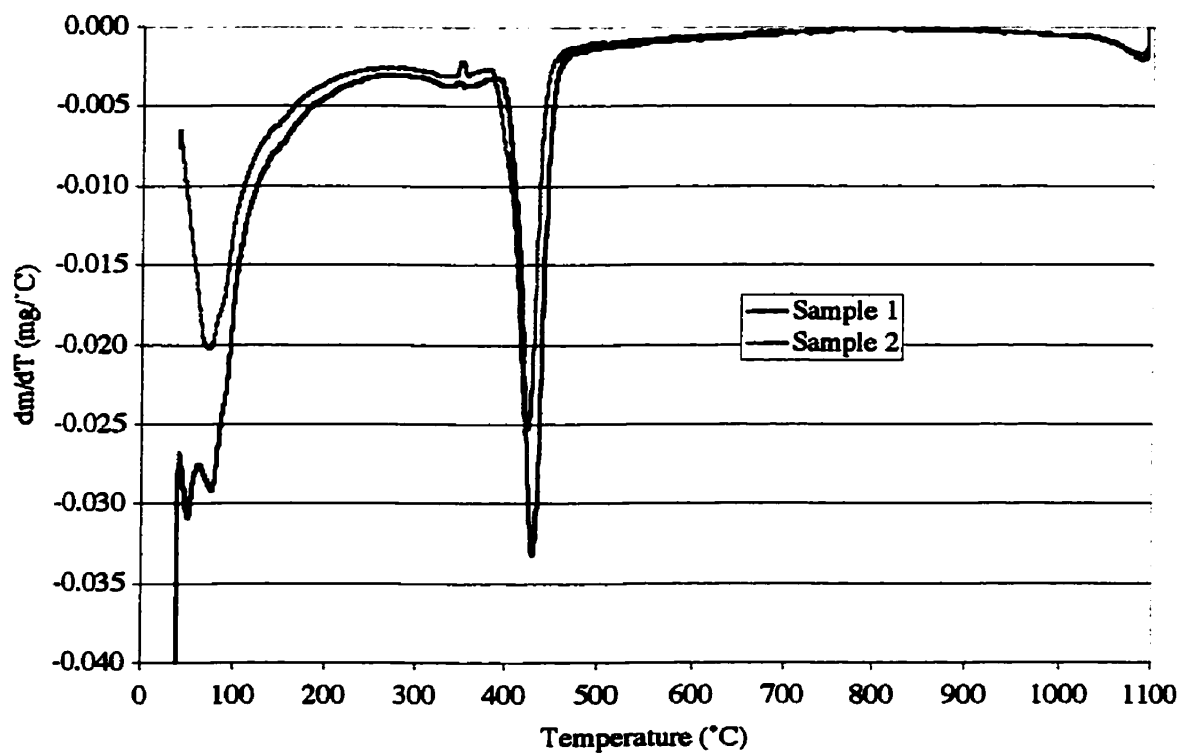


Figure D.4 DTG of two Ca(NO<sub>3</sub>)<sub>2</sub> White Cement Paste Samples

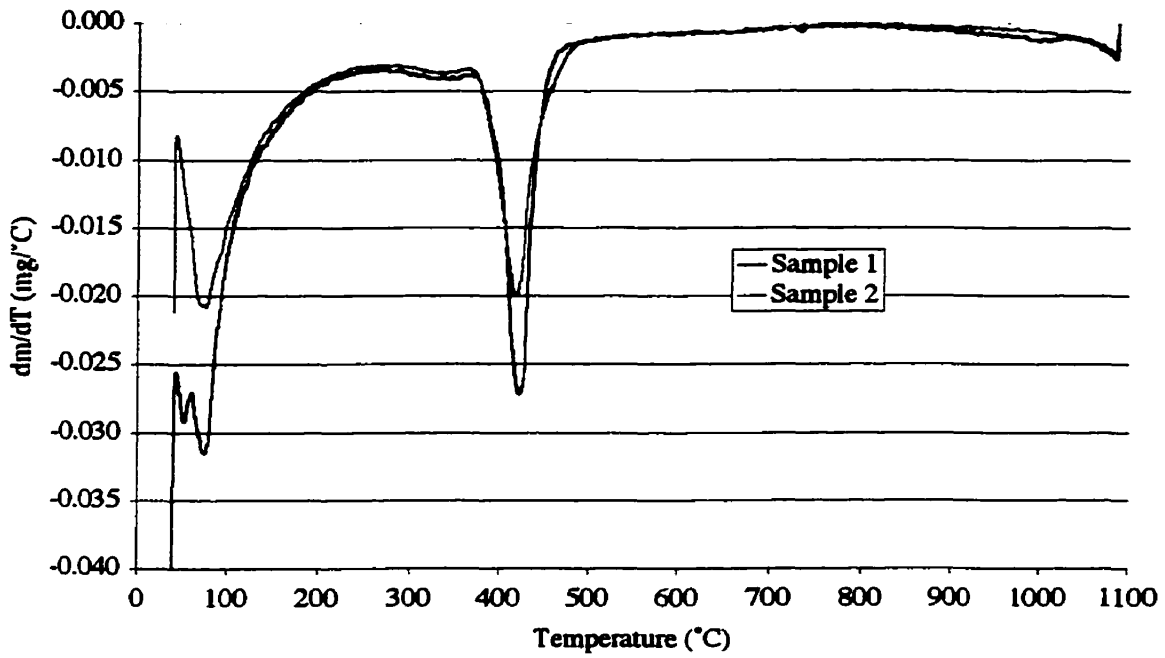


Figure D.5 DTG of two ponded Control White Cement Paste Samples

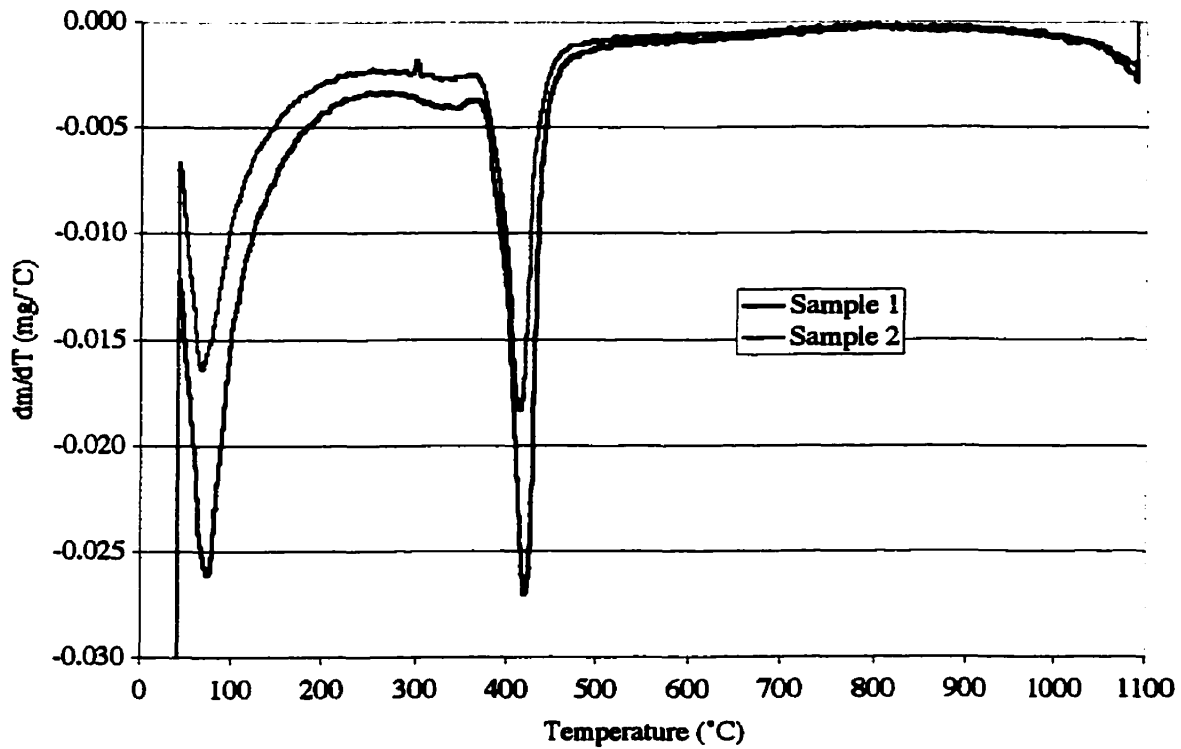


Figure D.6 DTG of two ponded CN1 White Cement Paste Samples

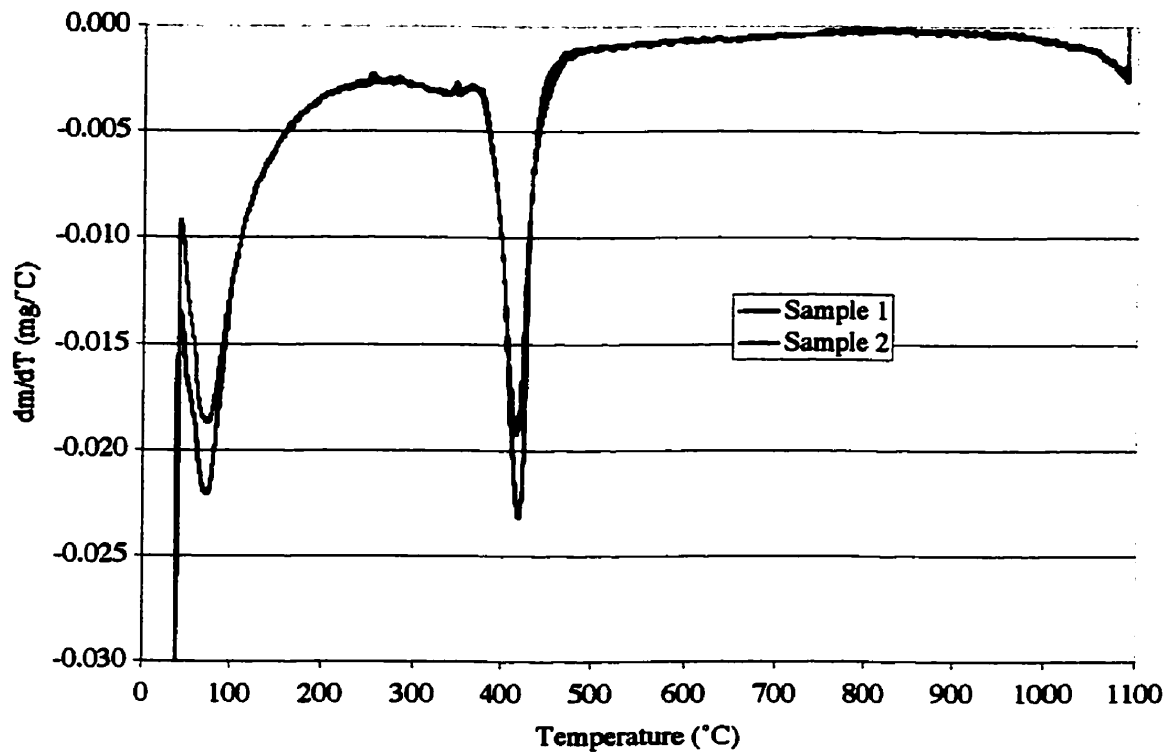


Figure D.7 DTG of two ponded CN2 White Cement Paste Samples

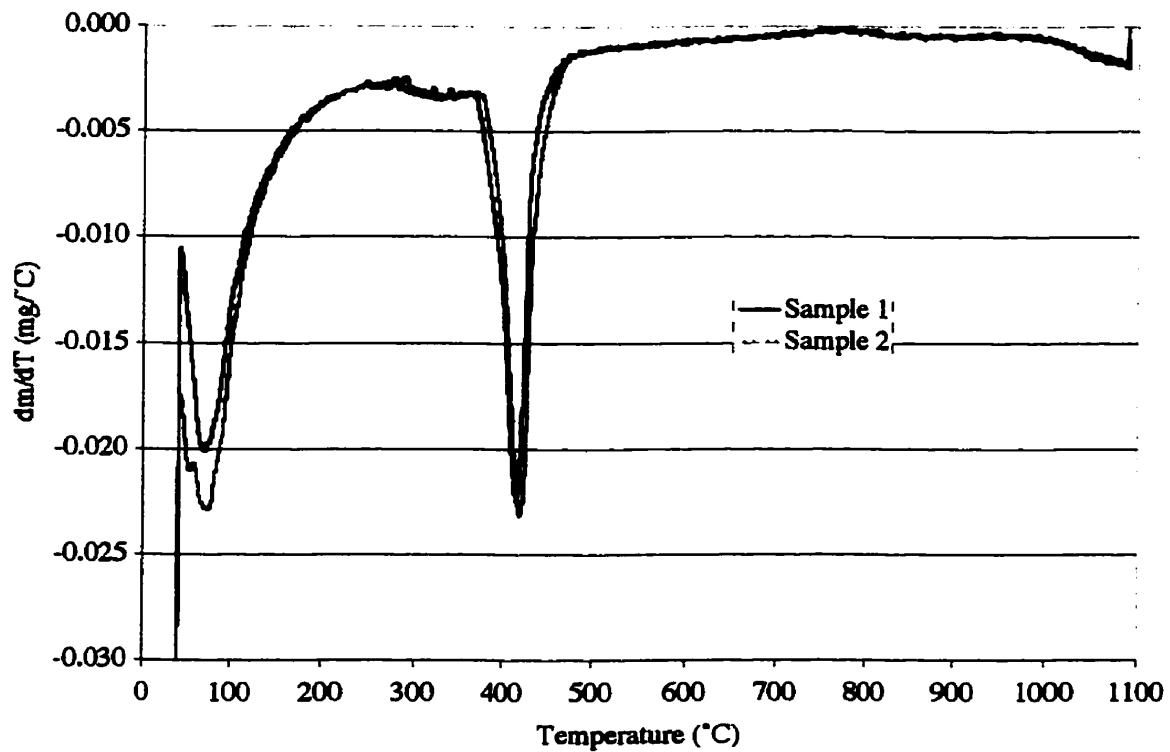


Figure D.8 DTG of two ponded  $Ca(NO_3)_2$  White Cement Paste Samples

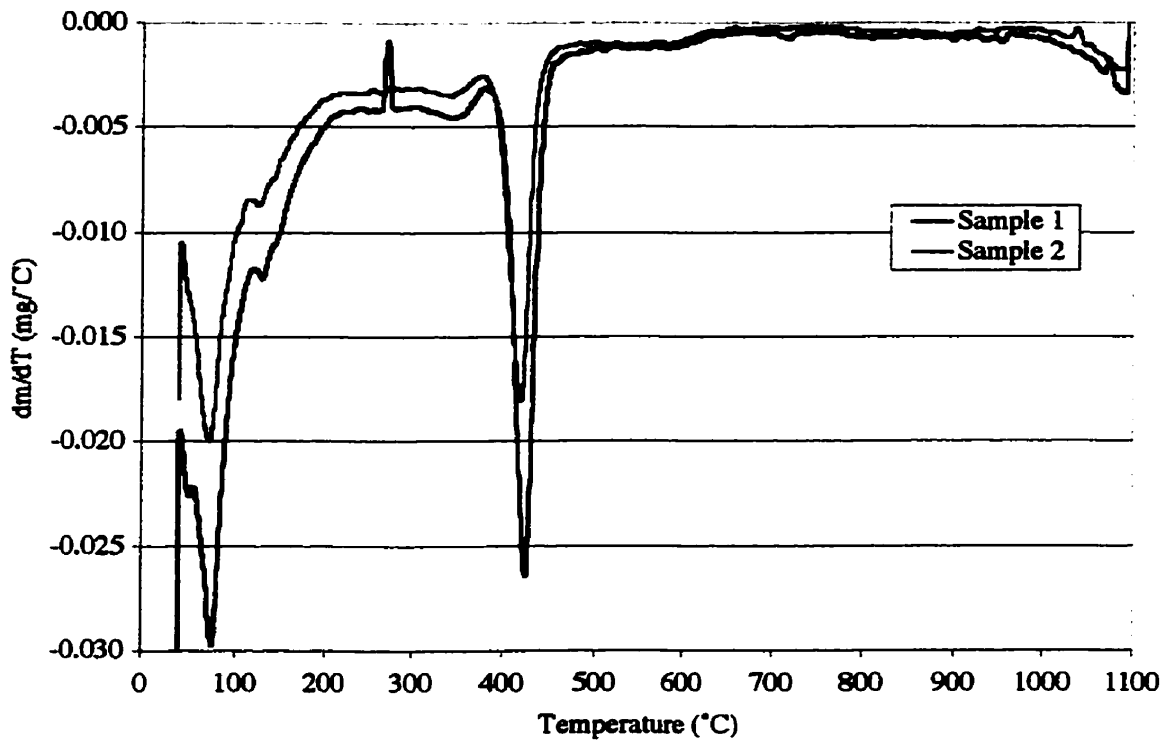


Figure D.9 DTG of two Control OPC Paste Samples

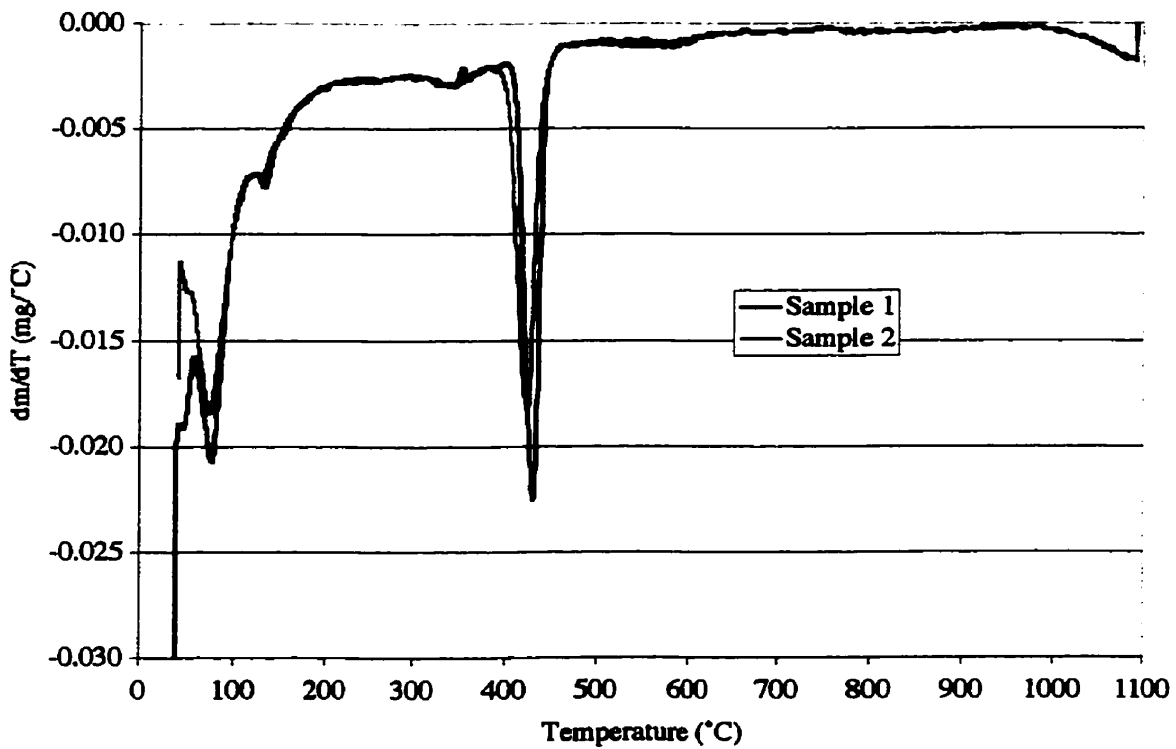


Figure D.10 DTG of two CN1 OPC Paste Samples



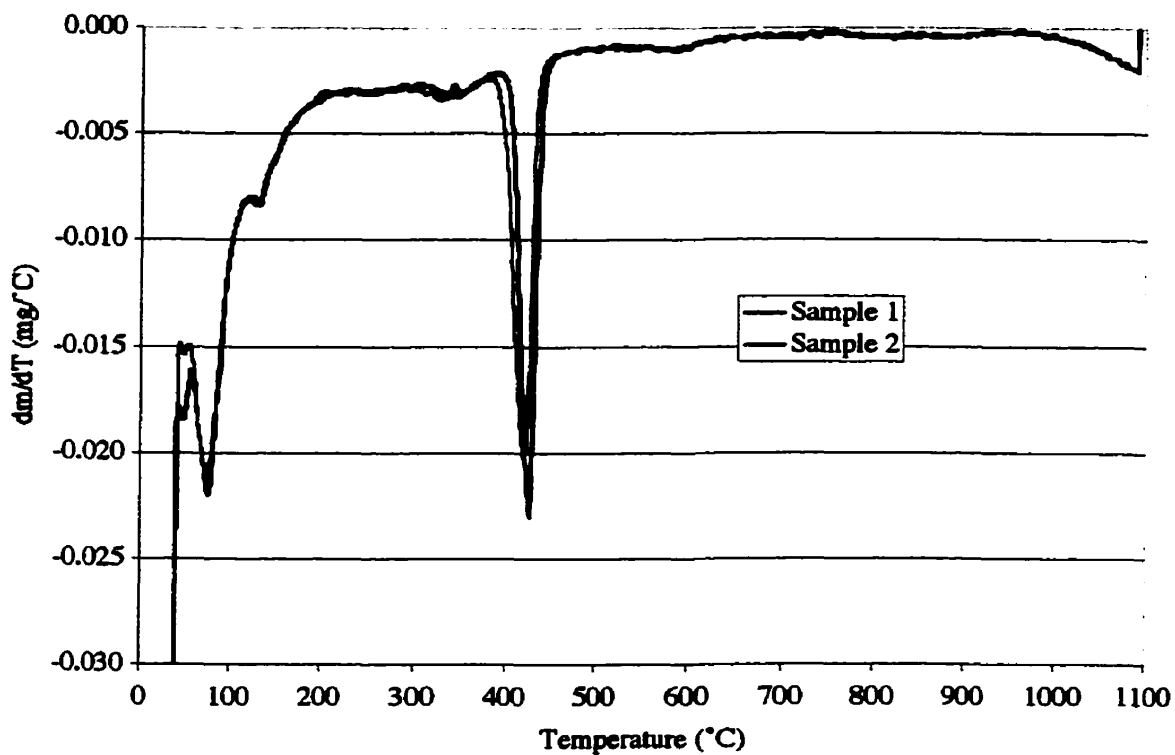


Figure D.11 DTG of two CN2 OPC Paste Samples

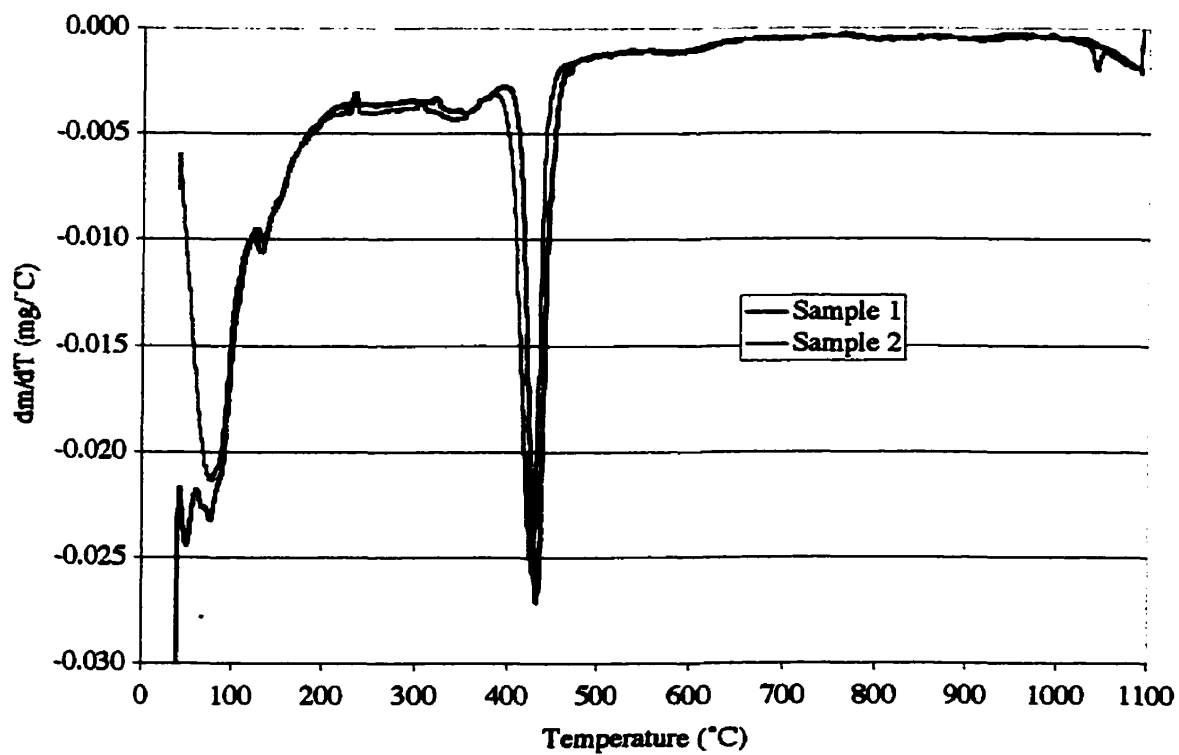


Figure D.12 DTG of two Ca(NO<sub>3</sub>)<sub>2</sub> OPC Paste Samples

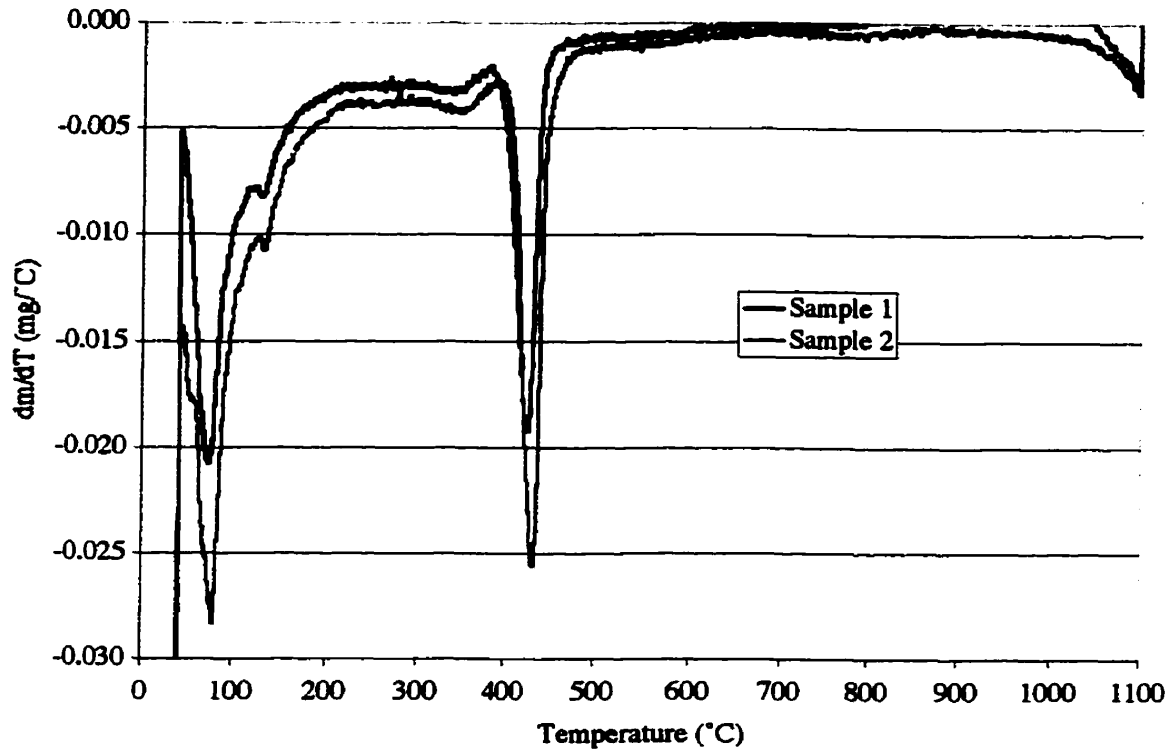


Figure D.13 DTG of two ponded Control OPC Paste Samples

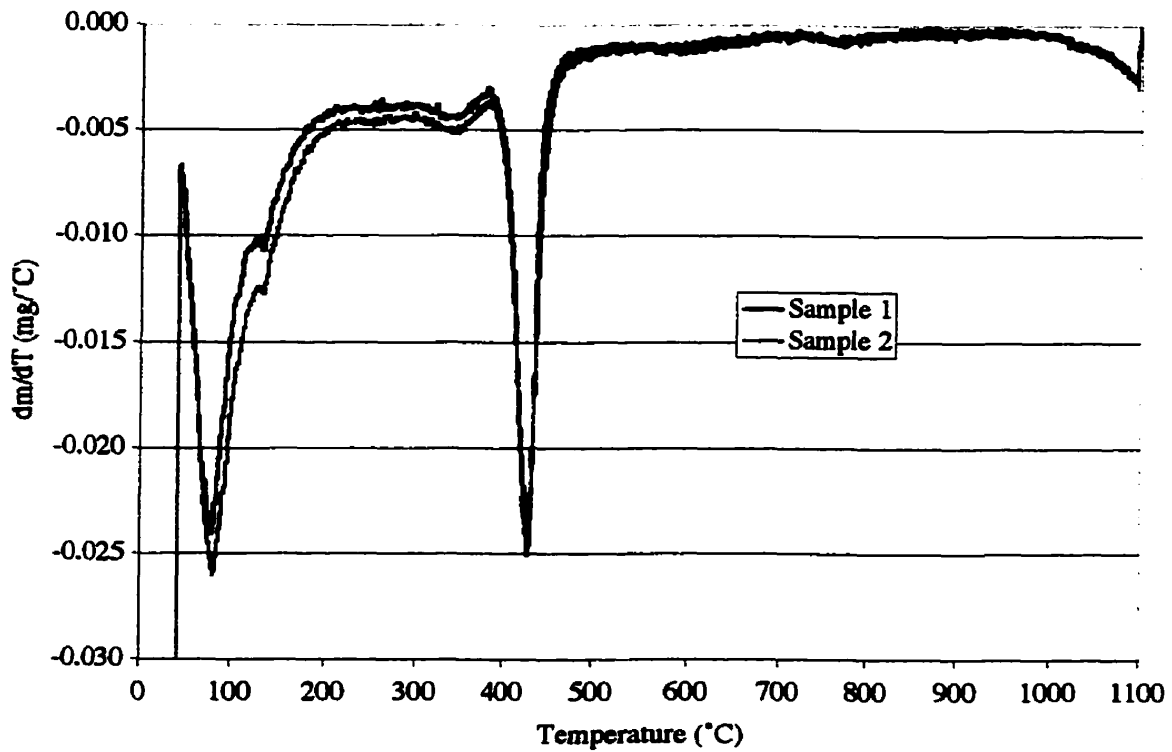


Figure D.14 DTG of two ponded CN1 OPC Paste Samples

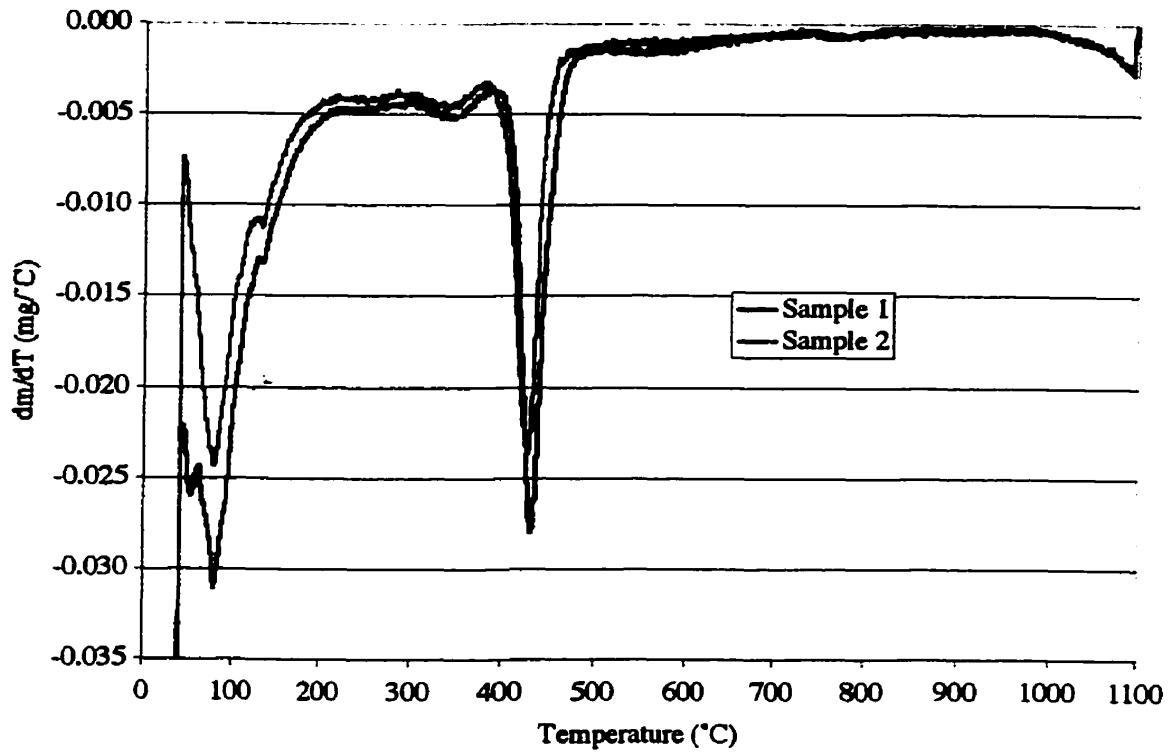


Figure D.15 DTG of two ponded CN2 OPC Paste Samples

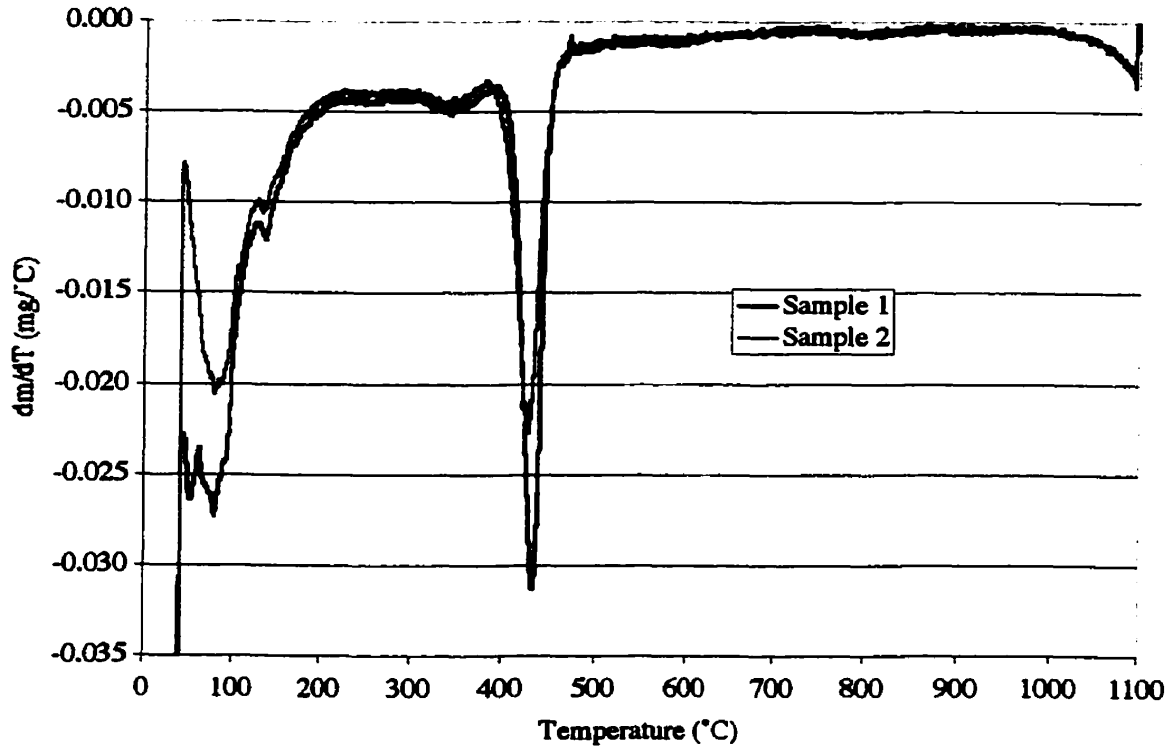


Figure D.16 DTG of two ponded Ca(NO<sub>3</sub>)<sub>2</sub> OPC Paste Samples

## Appendix E

Table E.1 Analysis of expressed pore solution from White Cement Paste cylinders

Anions (mg/L)	Dilution Factors (by mass)							
	Control = 3.353359 CN2 = 3.030347				CN1 = 3.891243 Ca(NO <sub>3</sub> ) <sub>2</sub> = 2.354796			
	Original Values from Solutions Analytical				Adjusted Values due to Dilution Factors			
	Control	CN1	CN2	Ca(NO <sub>3</sub> ) <sub>2</sub>	Control	CN1	CN2	Ca(NO <sub>3</sub> ) <sub>2</sub>
Cl	8.02	4.41	6.07	3.45	26.9	17.2	18.4	8.12
NO <sub>2</sub>	195	608	1180	442	654	2370	3580	1040
Br	<i>0.50</i>	<i>0.50</i>	<i>0.50</i>	<i>0.50</i>	<i>1.68</i>	<i>1.95</i>	<i>1.52</i>	<i>1.18</i>
NO <sub>3</sub>	69.0	70.7	229	317	231	275	694	746
PO <sub>4</sub>	<i>1.00</i>	<i>1.00</i>	<i>1.00</i>	<i>1.00</i>	<i>3.35</i>	<i>3.89</i>	<i>3.03</i>	<i>2.35</i>
SO <sub>4</sub>	29.2	29.0	27.3	33.6	97.9	113	82.7	79.1
<b>Cations</b>								
<b>(mg/L)</b>								
Al	<i>1.00</i>	<i>1.00</i>	<i>1.00</i>	<i>1.00</i>	<i>3.35</i>	<i>3.89</i>	<i>3.03</i>	<i>2.35</i>
As	<i>0.50</i>	<i>0.50</i>	<i>0.50</i>	<i>0.50</i>	<i>1.68</i>	<i>1.95</i>	<i>1.52</i>	<i>1.18</i>
B	<i>0.10</i>	<i>0.10</i>	<i>0.10</i>	<i>0.10</i>	<i>0.34</i>	<i>0.39</i>	<i>0.30</i>	<i>0.24</i>
Ba	0.13	0.12	0.21	0.21	0.44	0.47	0.64	0.49
Ca	146	130	353	289	490	506	1070	681
Cd	<i>0.10</i>	<i>0.10</i>	<i>0.10</i>	<i>0.10</i>	<i>0.34</i>	<i>0.39</i>	<i>0.30</i>	<i>0.24</i>
Co	<i>0.50</i>	<i>0.50</i>	<i>0.50</i>	<i>0.50</i>	<i>1.68</i>	<i>1.95</i>	<i>1.52</i>	<i>1.18</i>
Cr	<i>0.10</i>	<i>0.10</i>	<i>0.10</i>	<i>0.10</i>	<i>0.34</i>	<i>0.39</i>	<i>0.30</i>	<i>0.24</i>
Cu	3.52	5.28	4.71	4.07	11.8	20.5	14.3	9.58
Fe	<i>0.50</i>	<i>0.50</i>	<i>0.50</i>	<i>0.50</i>	<i>1.68</i>	<i>1.95</i>	<i>1.52</i>	<i>1.18</i>
K	527	498	627	690	1770	1940	1900	1620
Li	0.67	0.57	0.81	0.97	2.25	2.22	2.45	2.28
Mg	0.18	<i>0.25</i>	<i>0.25</i>	0.25	<i>0.60</i>	<i>0.97</i>	<i>0.76</i>	<i>0.59</i>
Mn	0.25	0.25	0.25	0.25	0.84	0.97	0.76	0.59
Mo	0.50	0.50	0.50	0.50	1.68	1.95	1.52	1.18
Na	1120	1090	13.80	1580	3760	4240	4180	3720
Ni	0.25	0.25	0.25	0.36	0.84	0.97	0.76	0.85
P	<i>5.00</i>	<i>5.00</i>	<i>5.00</i>	<i>5.00</i>	<i>16.8</i>	<i>19.5</i>	<i>15.2</i>	<i>11.8</i>
Pb	<i>2.50</i>	<i>2.50</i>	<i>2.50</i>	<i>2.50</i>	<i>8.38</i>	<i>9.73</i>	<i>7.58</i>	<i>5.89</i>
Se	<i>2.50</i>	<i>2.50</i>	<i>2.50</i>	<i>2.50</i>	<i>8.38</i>	<i>9.73</i>	<i>7.58</i>	<i>5.89</i>
SiO <sub>2</sub>	<i>0.50</i>	<i>0.50</i>	0.51	0.55	<i>1.68</i>	<i>1.95</i>	1.55	1.30
Sr	6.26	6.42	9.27	10.1	21.0	25.0	28.1	23.8
Zn	4.12	4.99	4.52	3.95	13.8	19.4	13.7	9.3
<b>Alkalinity (meq/L)</b>								
pH 10	64.2	51.7	75.7	78.9	215	201	229	186
pH 8.3	0.5	3.4	0.3	3.8	1.68	13.2	0.91	8.95
pH 4.3	1.9	1.9	3.1	1.8	6.37	7.39	9.39	4.24

\* bold italicized values indicate levels were below detection limits. Numerical values is detection limit

Table E.2 Analysis of expressed pore solution from Ponded White Cement Paste cylinders

Anions (mg/L)	Dilution Factors (by mass)							
	Control = 10.41315 CN2 = 5.133713				CN1 = 10.78468 Ca(NO <sub>3</sub> ) <sub>2</sub> = 5.597794			
	Original Values from Solutions Analytical				Adjusted Values due to Dilution Factors			
	Control	CN1	CN2	Ca(NO <sub>3</sub> ) <sub>2</sub>	Control	CN1	CN2	Ca(NO <sub>3</sub> ) <sub>2</sub>
Cl	79.8	2.94	384	1960	831	31.7	1970	10970
NO <sub>2</sub>	<i>0.10</i>	193	1020	<i>0.20</i>	<i>1.04</i>	2080	2540	<i>1.12</i>
Br	<i>0.10</i>	<i>0.10</i>	<i>0.10</i>	<i>0.53</i>	<i>1.04</i>	<i>1.08</i>	<i>0.51</i>	2.97
NO <sub>3</sub>	0.8	2.74	46.5	286	8.33	29.6	239	1601
PO <sub>4</sub>	<i>0.20</i>	<i>0.40</i>	<i>0.20</i>	<i>0.20</i>	<i>2.08</i>	<i>4.31</i>	<i>1.03</i>	<i>1.12</i>
SO <sub>4</sub>	20	9.9	39.6	94.8	208	107	203	531
<b>Cations</b>								
<b>(mg/L)</b>								
Al	<i>0.03</i>	<i>0.03</i>	<i>0.03</i>	<i>0.03</i>	<i>0.3</i>	<i>0.3</i>	<i>0.1</i>	<i>0.16</i>
As	<i>0.08</i>	<i>0.08</i>	<i>0.08</i>	<i>0.08</i>	<i>0.9</i>	<i>0.9</i>	<i>0.4</i>	<i>0.47</i>
B	<i>0.00</i>	<i>0.00</i>	<i>0.00</i>	<i>0.00</i>	<i>0.0</i>	<i>0.0</i>	<i>0.0</i>	<i>0.0</i>
Ba	0.05	0.07	0.09	0.0012	0.5	0.7	0.4	0.01
Ca	18.0	14.2	25.7	16.4	188	153	132	91.6
Cd	<i>0.00</i>	<i>0.00</i>	<i>0.00</i>	<i>0.00</i>	<i>0.1</i>	<i>0.1</i>	<i>0.0</i>	<i>0.03</i>
Co	<i>0.01</i>	<i>0.01</i>	<i>0.01</i>	<i>0.01</i>	<i>0.1</i>	<i>0.1</i>	<i>0.0</i>	<i>0.05</i>
Cr	<i>0.00</i>	<i>0.00</i>	<i>0.00</i>	<i>0.00</i>	<i>0.0</i>	<i>0.0</i>	<i>0.0</i>	<i>0.02</i>
Cu	<i>0.0034</i>	3.24	<i>0.0034</i>	3.02	<i>0.03</i>	35.0	<i>0.03</i>	16.9
Fe	<i>0.00</i>	<i>0.00</i>	<i>0.00</i>	<i>0.00</i>	<i>0.0</i>	<i>0.0</i>	<i>0.0</i>	<i>0.0</i>
K	148	162	320	244	1550	1750	1640	1370
Li	<i>0.0041</i>	<i>0.0041</i>	0.383	0.293	<i>0.043</i>	<i>0.044</i>	1.97	1.64
Mg	0.0121	0.0091	<i>0.0001</i>	<i>0.0001</i>	0.1	0.1	<i>0.001</i>	<i>0.0006</i>
Mn	<i>0.0006</i>	<i>0.0006</i>	<i>0.0006</i>	<i>0.0006</i>	<i>0.006</i>	<i>0.006</i>	<i>0.003</i>	<i>0.003</i>
Mo	<i>0.02</i>	<i>0.02</i>	<i>0.02</i>	<i>0.02</i>	<i>0.2</i>	<i>0.2</i>	<i>0.1</i>	<i>0.1</i>
Na	454	409	1640	2310	4720	4410	8420	12900
Ni	<i>0.014</i>	<i>0.014</i>	<i>0.014</i>	<i>0.014</i>	<i>0.1</i>	<i>0.2</i>	<i>0.1</i>	<i>0.08</i>
P	<i>0.12</i>	<i>0.12</i>	<i>0.12</i>	<i>0.12</i>	<i>1.2</i>	<i>1.3</i>	<i>0.6</i>	<i>0.7</i>
Pb	<i>0.07</i>	<i>0.07</i>	<i>0.07</i>	<i>0.07</i>	<i>0.7</i>	<i>0.7</i>	<i>0.3</i>	<i>0.4</i>
Se	<i>0.20</i>	<i>0.20</i>	<i>0.20</i>	<i>0.20</i>	<i>2.1</i>	<i>2.2</i>	<i>1.0</i>	<i>1.1</i>
SiO <sub>2</sub>	1.22	<i>0.04</i>	1.86	3.09	12.7	<i>0.4</i>	9.5	17.3
Sr	1.62	2.27	4.03	2.83	16.9	24.5	20.7	15.8
Zn	1.00	0.75	2.01	2.84	10.4	8.1	10.3	15.9
<b>Alkalinity (meq/L)</b>								
pH 10	7.54	5.39	15.9	16.8	78.5	58.1	81.1	94.0
pH 8.3	0.61	0.63	0.8	0.8	6.4	6.8	4.1	4.5
pH 4.3	0.22	0.05	0.9	0.3	2.3	0.5	4.6	1.7

\* bold italicized values indicate levels were below detection limits. Numerical values is detection limit

Table E.3 Analysis of expressed pore solution from OPC Paste cylinders

Anions (mg/L)	Dilution Factors (by mass)							
	Control = 4.811239 CN2 = 5.051018				CN1 = 5.021236 Ca(NO <sub>3</sub> ) <sub>2</sub> = 3.599088			
	Original Values from Solutions Analytical				Adjusted Values due to Dilution Factors			
	Control	CN1	CN2	Ca(NO <sub>3</sub> ) <sub>2</sub>	Control	CN1	CN2	Ca(NO <sub>3</sub> ) <sub>2</sub>
Cl	80.8	9.90	102	28.5	389	49.7	515	103
NO <sub>2</sub>	107	1010	640	74.7	515	5070	3230	269
Br	<b>0.10</b>	<b>0.10</b>	<b>0.10</b>	<b>0.10</b>	<b>0.48</b>	<b>0.50</b>	<b>0.51</b>	<b>0.36</b>
NO <sub>3</sub>	42.7	171	49.9	128	205	859	252	461
PO <sub>4</sub>	2.71	<b>0.20</b>	<b>0.20</b>	<b>0.20</b>	13.0	<b>1.00</b>	<b>1.01</b>	<b>0.72</b>
SO <sub>4</sub>	40.5	75.9	118	102	195	381	596	367
<b>Cations (mg/L)</b>								
Al	<b>1.00</b>	<b>1.00</b>	<b>1.00</b>	1.08	<b>4.81</b>	<b>5.02</b>	<b>5.05</b>	3.89
As	<b>0.50</b>	<b>1.00</b>	<b>1.00</b>	<b>1.00</b>	<b>2.41</b>	<b>5.02</b>	<b>5.05</b>	<b>3.60</b>
B	0.11	<b>0.10</b>	0.11	<b>0.10</b>	0.53	<b>0.50</b>	0.56	<b>0.36</b>
Ba	0.26	0.22	0.14	0.17	1.25	1.10	0.71	0.61
Ca	205	389	62.0	72.6	986	1950	313	261
Cd	<b>0.10</b>	<b>0.10</b>	<b>0.10</b>	<b>0.10</b>	<b>0.48</b>	<b>0.50</b>	<b>0.51</b>	<b>0.36</b>
Co	<b>0.50</b>	<b>0.50</b>	<b>0.50</b>	<b>0.50</b>	<b>2.41</b>	<b>2.51</b>	<b>2.53</b>	<b>1.80</b>
Cr	<b>0.10</b>	<b>0.10</b>	0.19	<b>0.10</b>	<b>0.48</b>	<b>0.50</b>	0.96	<b>0.36</b>
Cu	3.60	3.59	7.33	2.72	17.3	18.0	37.0	9.79
Fe	<b>0.50</b>	<b>0.50</b>	<b>0.50</b>	<b>0.50</b>	<b>2.41</b>	<b>2.51</b>	<b>2.53</b>	<b>1.80</b>
K	1970	2470	2520	3170	9480	12400	12700	11400
Li	3.55	3.11	3.22	4.77	17.1	15.6	16.3	17.2
Mg	0.15	<b>0.25</b>	<b>0.25</b>	<b>0.25</b>	0.72	<b>1.26</b>	<b>1.26</b>	<b>0.90</b>
Mn	<b>0.25</b>	<b>0.25</b>	<b>0.25</b>	<b>0.25</b>	<b>1.20</b>	<b>1.26</b>	<b>1.26</b>	<b>0.90</b>
Mo	<b>0.50</b>	<b>0.50</b>	<b>0.50</b>	<b>0.50</b>	<b>2.41</b>	<b>2.51</b>	<b>2.53</b>	<b>1.80</b>
Na	549	616	668	819	2640	3090	3370	2950
Ni	<b>0.25</b>	<b>0.25</b>	<b>0.25</b>	<b>0.25</b>	<b>1.20</b>	<b>1.26</b>	<b>1.26</b>	<b>0.90</b>
P	<b>5.00</b>	<b>5.00</b>	<b>5.00</b>	<b>5.00</b>	<b>24.1</b>	<b>25.1</b>	<b>25.3</b>	<b>18.0</b>
Pb	10.0	3.18	2.52	<b>2.50</b>	48.1	16.0	12.7	<b>9.00</b>
Se	<b>2.50</b>	<b>2.50</b>	<b>2.50</b>	<b>2.50</b>	<b>12.0</b>	<b>12.6</b>	<b>12.6</b>	<b>9.00</b>
SiO <sub>2</sub>	0.59	0.57	1.88	0.72	2.84	2.86	9.50	2.59
Sr	1.66	1.15	0.93	1.13	7.99	5.77	4.70	4.07
Zn	6.04	5.86	11.6	8.11	29.1	29.4	58.6	29.2
<b>Alkalinity (meq/L)</b>								
pH 10	68.8	81.0	78.9	99.4	331	407	399	358
pH 8.3	6.1	3.3	4.8	0	29.3	16.6	24.2	0
pH 4.3	3.5	4.3	3.8	0.4	16.8	21.6	19.2	1.44

\* bold italicized values indicate levels were below detection limits. Numerical values is detection limit

Table E.4 Analysis of expressed pore solution from Poned OPC Paste cylinders

Anions (mg/L)	Dilution Factors (by mass)							
	Control = 7.07224 CN2 = 5.398913				CN1 = 6.463641 Ca(NO <sub>3</sub> ) <sub>2</sub> = 7.583576			
	Original Values from Solutions Analytical				Adjusted Values due to Dilution Factors			
	Control	CN1	CN2	Ca(NO <sub>3</sub> ) <sub>2</sub>	Control	CN1	CN2	Ca(NO <sub>3</sub> ) <sub>2</sub>
Cl	2020	3180	5820	617	14300	20600	31400	4680
NO <sub>2</sub>	21.9	355	957	<i>0.10</i>	155	2290	5170	<i>0.76</i>
Br	<i>0.20</i>	<i>0.20</i>	<i>0.20</i>	<i>0.10</i>	<i>1.41</i>	<i>1.29</i>	<i>1.08</i>	<i>0.76</i>
NO <sub>3</sub>	1.05	7.47	27.5	112	7.43	48.3	48	849
PO <sub>4</sub>	3.25	<i>0.40</i>	<i>0.40</i>	<i>0.20</i>	23.0	<i>2.59</i>	<i>2.16</i>	<i>1.52</i>
SO <sub>4</sub>	381	252	3.9	94.6	2690	1630	1670	717
<b>Cations (mg/L)</b>								
Al	<i>0.03</i>	<i>0.03</i>	2.41	<i>0.03</i>	<i>0.3</i>	<i>0.3</i>	12.4	<i>0.16</i>
As	<i>0.08</i>	<i>0.08</i>	<i>0.08</i>	<i>0.08</i>	<i>0.9</i>	<i>0.9</i>	<i>0.4</i>	<i>0.5</i>
B	<i>0.00</i>	<i>0.00</i>	<i>0.00</i>	<i>0.00</i>	<i>0.0</i>	<i>0.0</i>	<i>0.0</i>	<i>0.0</i>
Ba	<i>0.0012</i>	0.07	<i>0.0012</i>	0.0929	<i>0.008</i>	0.8	<i>0.006</i>	0.52
Ca	5.38	9.22	9.03	10.3	56.0	99.5	46.4	57.3
Cd	<i>0.00</i>	<i>0.00</i>	<i>0.00</i>	<i>0.00</i>	<i>0.0</i>	<i>0.0</i>	<i>0.0</i>	<i>0.0</i>
Co	<i>0.01</i>	<i>0.01</i>	<i>0.01</i>	<i>0.01</i>	<i>0.1</i>	<i>0.1</i>	<i>0.05</i>	<i>0.07</i>
Cr	<i>0.00</i>	<i>0.00</i>	0.27	0.08	<i>0.0</i>	<i>0.0</i>	1.4	0.47
Cu	2.80	0.19	<i>0.0034</i>	0.25	29.2	2.1	<i>0.02</i>	1.38
Fe	0.23	0.36	0.37	<i>0.00</i>	2.4	3.9	1.9	<i>0.0</i>
K	1120	1390	1480	826	11600	15000	7590	4620
Li	1.58	1.82	2.14	1.59	16.4	19.7	11.0	8.92
Mg	<i>0.0001</i>	<i>0.0001</i>	0.0104	<i>0.0001</i>	<i>0.0</i>	<i>0.0</i>	0.1	<i>0.0</i>
Mn	0.0679	0.0907	0.079	0.0461	0.7	1.0	0.4	0.3
Mo	0.26	<i>0.00</i>	<i>0.00</i>	<i>0.00</i>	2.7	<i>0.0</i>	<i>0.0</i>	<i>0.0</i>
Na	2140	2730	4750	1050	22300	29500	24400	5870
Ni	<i>0.014</i>	<i>0.014</i>	<i>0.014</i>	<i>0.014</i>	<i>0.1</i>	<i>0.2</i>	<i>0.1</i>	<i>0.1</i>
P	3.92	<i>0.12</i>	4.02	<i>0.12</i>	40.8	<i>1.3</i>	20.6	<i>0.67</i>
Pb	<i>0.07</i>	<i>0.07</i>	<i>0.07</i>	<i>0.07</i>	<i>0.7</i>	<i>0.7</i>	<i>0.3</i>	<i>0.4</i>
Se	<i>0.20</i>	<i>0.20</i>	<i>0.20</i>	<i>0.20</i>	<i>2.1</i>	<i>2.2</i>	<i>1.0</i>	<i>1.1</i>
SiO <sub>2</sub>	18.7	9.48	12.1	1.17	194	102	62.2	6.57
Sr	0.21	0.53	0.48	0.54	2.2	5.7	2.5	3.0
Zn	6.43	3.10	6.81	2.67	66.9	33.5	35.0	15.0
<b>Alkalinity (meq/L)</b>								
pH 10	16.6	14.7	15.7	14.5	173	159	80.6	81.2
pH 8.3	1.8	0.8	2.1	0.4	18.7	8.6	10.8	2.24
pH 4.3	2.4	1.5	2.5	0.8	25.0	16.2	12.8	4.48

\* bold italicized values indicate levels were below detection limits. Numerical values is detection limit

Table E.5 Molar quantities of cement components

White Cement Molar Quantities							
Compound	Wt. %	Molar Mass (g/mol)	Fraction of Ion in Molar Mass*	Mass in 2000 g (g)	Ion Mass* (g)	Moles in Mix (mol)	Moles per cylinder
SiO <sub>2</sub>	25.01	60.08	1.00	500.2	500.20	8.32	1.19E+00
Al <sub>2</sub> O <sub>3</sub>	1.91	101.96	0.53	38.2	20.22	0.75	1.07E-01
Fe <sub>2</sub> O <sub>3</sub>	0.32	159.69	0.70	6.4	4.48	0.08	1.15E-02
CaO	69.34	56.08	0.71	1386.8	991.15	24.73	3.53E+00
MgO	0.56	40.30	0.60	11.2	6.75	0.28	3.97E-02
Na <sub>2</sub> O	0.17	61.98	0.74	3.4	2.52	0.11	1.57E-02
K <sub>2</sub> O	0.12	94.20	0.83	2.4	1.99	0.05	7.28E-03
SO <sub>3</sub>	2.1	80.06	0.40	42	16.82	0.52	7.49E-02
TiO <sub>2</sub>	0.09	79.90	0.60	1.8	1.08	0.02	3.22E-03
Cl	0.008	35.45	1.00	0.16	0.16	0.00	6.45E-04

OPC Molar Quantities							
Compound	Wt. %	Molar Mass (g/mol)	Fraction of Ion in Molar Mass*	Mass in 2000 g (g)	Ion Mass* (g)	Moles in Mix (mol)	Moles per cylinder
SiO <sub>2</sub>	21.15	60.08	1.00	423	423.00	7.04	1.01E+00
Al <sub>2</sub> O <sub>3</sub>	5.01	101.96	0.53	100.2	53.03	1.97	2.81E-01
Fe <sub>2</sub> O <sub>3</sub>	2.46	159.69	0.70	49.2	34.41	0.62	8.80E-02
CaO	64.16	56.08	0.71	1283.2	917.10	22.88	3.27E+00
MgO	2.19	40.30	0.60	43.8	26.41	1.09	1.55E-01
Na <sub>2</sub> O	0.12	61.98	0.74	2.4	1.78	0.08	1.11E-02
K <sub>2</sub> O	0.43	94.20	0.83	8.6	7.14	0.18	2.61E-02
SO <sub>3</sub>	3.08	80.06	0.40	61.6	24.67	0.77	1.10E-01

\*For SiO<sub>2</sub> and Cl, the ion referred to is SiO<sub>2</sub> and Cl. In all other cases, the cation is considered the ion.

Table E.6 Molar contributions of inhibitors

Moles of Ca & NO <sub>2</sub> added as CN1	Moles of Ca & NO <sub>2</sub> added as CN2	Moles of Ca and NO <sub>3</sub> added as Ca(NO <sub>3</sub> ) <sub>2</sub>
<p>ρ(CN1) = 1.3 g/mL                      Vol. added to paste = 26 mL                      Mass CN1 added = 33.8 g                      % Ca(NO<sub>2</sub>)<sub>2</sub> in CN1 = 30%                      mass Ca(NO<sub>2</sub>)<sub>2</sub> added = 10.14 g                      m.m. Ca(NO<sub>2</sub>)<sub>2</sub> = 132.09 g/mol                      m.m. Ca = 40.08 g/mol                      m.m. NO<sub>2</sub> = 46.01 g/mol                      NO<sub>2</sub> in Ca(NO<sub>2</sub>)<sub>2</sub> = 0.69657282                      mass NO<sub>2</sub> added = 7.063 g                      mass Ca added = 3.077 g                      Moles NO<sub>2</sub> added = 1.54E-1                      Moles Ca added = 7.68E-2                      Moles NO<sub>2</sub>/cylinder = 2.19E-2                      Moles Ca/cylinder = 1.10E-2</p>	<p>ρ(CN2) = 1.295 g/mL                      Vol. added to paste = 26 mL                      Mass CN1 added = 33.67 g                      % Ca(NO<sub>2</sub>)<sub>2</sub> in CN1 = 30%                      mass Ca(NO<sub>2</sub>)<sub>2</sub> added = 10.10 g                      m.m. Ca(NO<sub>2</sub>)<sub>2</sub> = 132.09 g/mol                      m.m. Ca = 40.08 g/mol                      m.m. NO<sub>2</sub> = 46.01 g/mol                      NO<sub>2</sub> in Ca(NO<sub>2</sub>)<sub>2</sub> = 0.69657282                      mass NO<sub>2</sub> added = 7.036 g                      mass Ca added = 3.065 g                      Moles NO<sub>2</sub> added = 1.53E-1                      Moles Ca added = 7.65E-2                      Moles NO<sub>2</sub>/cylinder = 2.18E-2                      Moles Ca/cylinder = 1.09E-2</p>	<p>mass Ca(NO<sub>3</sub>)<sub>2</sub> added = 9.87 g                      purity of Ca(NO<sub>3</sub>)<sub>2</sub> = 99%                      mass Ca(NO<sub>3</sub>)<sub>2</sub> added = 9.77 g                      m.m. Ca(NO<sub>3</sub>)<sub>2</sub> = 164.09 g/mol                      m.m. Ca = 40.08 g/mol                      m.m. NO<sub>3</sub> = 62.00 g/mol                      NO<sub>3</sub> in Ca(NO<sub>3</sub>)<sub>2</sub> = 0.75574350                      mass NO<sub>3</sub> added = 7.385 g                      mass Ca added = 2.387 g                      Moles NO<sub>3</sub> added = 1.19E-1                      Moles Ca added = 5.95E-2                      Moles NO<sub>3</sub>/cylinder = 1.70E-2                      Moles Ca/cylinder = 8.51E-3</p>



Table E.7 Molar quantities of expressed pore solutions from Control White and OPC Unponded and Ponded Cylinders

<b>Mass of Expressed Solutions (g)</b>				
<b>White = 4.5059</b>			<b>OPC = 3.4096</b>	
<b>White, Ponded = 1.9975</b>			<b>OPC, Ponded = 0.966</b>	
	<b>Molar Mass (g/mol)</b>	<b>Concentration (mg/L)</b>	<b>Mass (mg)</b>	<b>Moles (moles)</b>
<b>White Control Expressed Solution</b>				
SiO <sub>2</sub>	60.0843	<i>1.68</i>	<i>0.00756991</i>	<i>1.25988E-07</i>
Al	26.98154	<i>3.35</i>	<i>0.01509477</i>	<i>5.59448E-07</i>
Fe	55.847	<i>1.68</i>	<i>0.00756991</i>	<i>1.35547E-07</i>
Ca	40.08	490	2.207891	8.80871E-05
Mg	24.305	0.6	0.00240354	1.11234E-07
Na	22.98977	3760	16.942184	0.000736944
K	39.0983	1770	7.975443	0.000203984
S	32.06	43.6	0.19645724	601278E-06
Cl	35.453	26.9	0.12120871	3.41886E-06
<b>Ponded White Control Expressed Solution</b>				
SiO <sub>2</sub>	60.0843	12.7	0.02536825	4.22211E-07
Al	26.98154	<i>0.3</i>	<i>0.00059925</i>	<i>2.22096E-08</i>
Fe	55.847	<i>0</i>	<i>0</i>	<i>0</i>
Ca	40.08	188	0.37553	9.36951E-06
Mg	24.305	0.1	0.00019975	8.21847E-09
Na	22.98977	4720	9.4282	0.000410104
K	39.0983	1550	3.096125	7.91882E-05
S	32.06	75.6	0.151011	4.71026E-06
Cl	35.453	831	1.6599225	4.68204E-05
<b>OPC Control Expressed Solution</b>				
SiO <sub>2</sub>	60.0843	2.84	0.00968326	1.61161E-07
Al	26.98154	<i>4.81</i>	<i>0.01640018</i>	<i>0.000442502</i>
Fe	55.847	<i>2.41</i>	<i>0.00821714</i>	<i>0.000458902</i>
Ca	40.08	986	3.3618656	0.134743573
Mg	24.305	0.72	0.00245491	5.96666E-05
Na	22.98977	2640	9.001344	0.206938828
K	39.0983	9480	32.323008	1.263774664
S	32.06	104	0.3545984	0.011368425
Cl	35.453	389	1.3263344	0.047022533
<b>Ponded OPC Control Expressed Solution</b>				
SiO <sub>2</sub>	60.0843	194.2	0.1875972	3.12223E-06
Al	26.98154	<i>0.3</i>	<i>0.0002898</i>	<i>1.07407E-08</i>
Fe	55.847	2.4	0.0023184	4.15134E-08
Ca	40.08	56	0.054096	1.3497E-06
Mg	24.305	<i>0</i>	<i>0</i>	<i>0</i>
Na	22.98977	22300	21.5418	0.000937017
K	39.0983	11600	11.2056	0.000286601
S	32.06	1522	1.470252	4.58594E-05
Cl	35.453	14300	13.8138	0.000389637

Bold italicized values indicate levels below detection limit

Table E.8 Molar quantities of expressed pore solution CN1 White and OPC Unponded and Pounded Cylinders

Mass of Expressed Solutions (g)				
White = 4.1634 White, Pounded = 0.9349			OPC = 2.8584 OPC, Pounded = 2.0559	
	Molar Mass (g/mol)	Concentration (mg/L)	Mass (mg)	Moles (moles)
<b>White CN1 Expressed Solution</b>				
SiO <sub>2</sub>	60.0843	<i>1.95</i>	<i>0.00811863</i>	<i>1.35121E-07</i>
Al	26.98154	<i>3.89</i>	<i>0.01619563</i>	<i>6.00278E-07</i>
Fe	55.847	<i>1.95</i>	<i>0.00811863</i>	<i>1.45373E-07</i>
Ca	40.08	506	2.1066804	5.25619E-05
Mg	24.305	<i>0.97</i>	<i>0.0040385</i>	<i>1.66159E-07</i>
Na	22.98977	4240	17.652816	0.000767855E0.
K	39.0983	1940	8.076996	000206582
S	32.06	45.1	0.18776934	5.85681E-06
Cl	35.453	17.2	0.07161048	2.01987E-06
NO <sub>2</sub>	46.0055	2370	9.867258	0.00021448
NO <sub>3</sub>	62.0049	375	0.561275	2.51799E-05
<b>Pounded White CN1 Expressed Solution</b>				
SiO <sub>2</sub>	60.0843	<i>0.4</i>	<i>0.00037396</i>	<i>6.22393E-09</i>
Al	26.98154	<i>0.3</i>	<i>0.00028047</i>	<i>1.03949E-08</i>
Fe	55.847	<i>0</i>	<i>0</i>	<i>0</i>
Ca	40.08	153	0.1430397	3.56885E-06
Mg	24.305	0.1	0.00009349	3.84653E-09
Na	22.98977	4410	4.122909	0.000179337
K	39.0983	1750	1.636075	4.18452E-05
S	32.06	46.6	0.04356634	1.3589E-06
Cl	35.453	31.7	0.02963633	8.35933E-07
NO <sub>2</sub>	46.0055	2080	1.944592	4.22687E-05
NO <sub>3</sub>	62.0049	29.6	0.02767304	4.46304E-07
<b>OPC CN1 Expressed Solution</b>				
SiO <sub>2</sub>	60.0843	2.86	0.00817502	1.36059E-07
Al	26.98154	<i>5.02</i>	<i>0.01434917</i>	<i>0.000387163</i>
Fe	55.847	<i>2.51</i>	<i>0.00717458</i>	<i>0.000400679</i>
Ca	40.08	1950	5.57388	0.22340111
Mg	24.305	<i>1.26</i>	<i>0.00360158</i>	<i>8.75365E-05</i>
Na	22.98977	3090	8.832456	0.203056132
K	39.0983	12400	35.44416	1.385806401
S	32.06	177	0.5059368	0.016220334
Cl	35.453	50	0.14292	0.005066943
NO <sub>2</sub>	46.0055	5070	14.492088	0.666715754
NO <sub>3</sub>	62.0049	859	2.4553656	0.152244698
<b>Pounded OPC CN1 Expressed Solution</b>				
SiO <sub>2</sub>	60.0843	102	0.2097018	3.49013E-06
Al	26.98154	<i>0.3</i>	<i>0.00061677</i>	<i>2.2859E-09</i>
Fe	55.847	3.9	0.00801801	1.43571E-07
Ca	40.08	99.5	0.20456205	5.10384E-06
Mg	24.305	<i>0</i>	<i>0</i>	<i>0</i>
Na	22.98977	39500	60.64905	0.002638089
K	39.0983	15000	30.8385	0.000788743
S	32.06	1080	2.220372	6.92568E-05
Cl	35.453	20600	42.35154	0.001194583
NO <sub>2</sub>	46.0055	2290	4.708011	0.000102336
NO <sub>3</sub>	62.0049	48.3	0.09929997	1.60149E-06

Bold italicized values indicate levels below detection limit

Table E.9 Molar quantities of expressed pore solution CN2 White and OPC Unponded and Ponded Cylinders

Mass of Expressed Solutions (g)				
White = 5.1867			OPC = 1.621	
White, Ponded = 2.3857			OPC, Ponded = 2.5953	
	Molar Mass (g/mol)	Concentration (mg/L)	Mass (mg)	Moles (moles)
<b>White CN2 Expressed Solution</b>				
SiO <sub>2</sub>	60.0843	1.55	0.00803939	1.33802E-07
Al	26.98154	<i>3.03</i>	<i>0.0157157</i>	<i>5.82461E-07</i>
Fe	55.847	<i>1.52</i>	<i>0.00788378</i>	<i>1.41168E-07</i>
Ca	40.08	1070	5.549769	0.000138467
Mg	24.305	<i>0.76</i>	<i>0.00394189</i>	<i>1.62184E-07</i>
Na	22.98977	4180	21.680406	0.000943046
K	39.0983	1900	9.85473	0.00025205
S	32.06	47.3	0.24533091	7.65224E-06
Cl	35.453	18.4	0.09543528	2.69188E-06
NO <sub>2</sub>	46.0055	3580	18.568386	0.000403612
NO <sub>3</sub>	62.0049	694	3.5995698	5.8053E-05
<b>Ponded White CN2 Expressed Solution</b>				
SiO <sub>2</sub>	60.0843	9.5	0.02266415	3.77206E-07
Al	26.98154	<i>0.1</i>	<i>0.00023857</i>	<i>8.84197E-09</i>
Fe	55.847	<i>0</i>	<i>0</i>	<i>0</i>
Ca	40.08	132	0.3149124	7.8571E-06
Mg	24.305	<i>0</i>	<i>0</i>	<i>0</i>
Na	22.98977	8420	20.087594	0.000873762
K	39.0983	1640	3.912548	0.00010007
S	32.06	84.7	0.20206879	6.30283E-06
Cl	35.453	1970	4.699829	0.000132565
NO <sub>2</sub>	46.0055	52400	125.01068	0.002717299
NO <sub>3</sub>	62.0049	239	0.5701823	9.19576E-06
<b>OPC CN2 Expressed Solution</b>				
SiO <sub>2</sub>	60.0843	9.5	0.0153995	2.56298E-07
Al	26.98154	<i>5.05</i>	<i>0.00818605</i>	<i>0.000220872</i>
Fe	55.847	<i>2.53</i>	<i>0.00410113</i>	<i>0.000229036</i>
Ca	40.08	313	0.507373	0.2033551
Mg	24.305	<i>1.26</i>	<i>0.00204246</i>	<i>4.9642E-05</i>
Na	22.98977	3370	5.46277	0.125587826
K	39.0983	12700	20.5867	0.804904973
S	32.06	225	0.364725	0.011693084
Cl	35.453	515	0.834815	0.029596696
NO <sub>2</sub>	46.0055	3230	5.23583	0.240876977
NO <sub>3</sub>	62.0049	252	0.408492	0.025328506
<b>Ponded OPC CN2 Expressed Solution</b>				
SiO <sub>2</sub>	60.0843	62.2	0.16142766	2.68669E-06
Al	26.98154	12.4	0.03218172	1.19273E-06
Fe	55.847	1.9	0.00493107	8.82961E-08
Ca	40.08	46.4	0.12042192	3.00424E-06
Mg	24.305	0.1	0.00025953	1.0678E-08
Na	22.98977	24400	63.32532	0.0027545
K	39.0983	7590	19.698327	0.000503815
S	32.06	674	1.7492322	5045612E-05
Cl	35.453	31400	81.49242	0.002298604
NO <sub>2</sub>	46.0055	5170	13.417701	0.000291654
NO <sub>3</sub>	62.0049	148	0.3841044	6.19474E-06

Italicized values indicate levels below detection limit

Table E.10 Molar quantities of expressed pore solution  $\text{Ca}(\text{NO}_3)_2$  White and OPC Unponded and Ponded Cylinders

Mass of Expressed Solutions (g)				
White = 7.2126 White, Ponded = 2.2752			OPC = 4.1655 OPC, Ponded = 1.851	
	Molar Mass (g/mol)	Concentration (mg/L)	Mass (mg)	Moles (moles)
<b>White <math>\text{Ca}(\text{NO}_3)_2</math> Expressed Solution</b>				
$\text{SiO}_2$	60.0843	1.3	0.00937638	1.56054E-07
Al	26.98154	2.35	<i>0.01694961</i>	<i>6.28193E-07</i>
Fe	55.847	1.18	<i>0.00851087</i>	<i>1.52396E-07</i>
Ca	40.08	681	4.9117806	0.000122549
Mg	24.305	0.59	0.00425543	1.75085E-07
Na	22.98977	3720	26.830872	0.001167079
K	39.0983	1620	11.684412	0.000298847
S	32.06	37.7	0.27191502	8.48144E-06
Cl	35.453	8.12	0.05856631	1.65194E-06
$\text{NO}_2$	46.0055	1040	7.501104	0.000163048
$\text{NO}_3$	62.0049	746	5.3805996	8.6777E-05
<b>Ponded White <math>\text{Ca}(\text{NO}_3)_2</math> Expressed Solution</b>				
$\text{SiO}_2$	60.0843	17.3	0.03936096	6.55096E-07
Al	26.98154	<i>0.16</i>	<i>0.00036403</i>	<i>1.34919E-08</i>
Fe	55.847	<i>0.02</i>	<i>4.5504E-05</i>	<i>8.14798E-10</i>
Ca	40.08	91.6	0.20840832	5.19981E-06
Mg	24.305	0	0	0
Na	22.98977	12900	29.35008	0.001276658
K	39.0983	1370	3.117024	7.97228E-05
S	32.06	195	0.443664	1.38386E-05
Cl	35.453	11000	25.0272	0.000705926
$\text{NO}_2$	46.0055	<i>1.12</i>	<i>0.00254822</i>	<i>5.53896E-08</i>
$\text{NO}_3$	62.0049	1601	3.6425952	5.87469E-05
<b>OPC <math>\text{Ca}(\text{NO}_3)_2</math> Expressed Solution</b>				
$\text{SiO}_2$	60.0843	2.59	0.01078865	1.79558E-07
Al	26.98154	3.89	<i>0.0162038</i>	<i>0.000437203</i>
Fe	55.847	1.8	<i>0.0074979</i>	<i>0.000418735</i>
Ca	40.08	261	1.0871955	0.043574796
Mg	24.305	0.9	<i>0.00374895</i>	<i>9.11182E-05</i>
Na	22.98977	2950	12.288225	0.282503466
K	39.0983	11400	47.4867	1.856649243
S	32.06	146	0.608163	0.019497706
Cl	35.453	103	0.4290465	0.015210986
$\text{NO}_2$	46.0055	269	1.1205195	0.05155006
$\text{NO}_3$	62.0049	461	1.9202955	0.11906773
<b>Ponded OPC <math>\text{Ca}(\text{NO}_3)_2</math> Expressed Solution</b>				
$\text{SiO}_2$	60.0843	6.57	0.01216107	2.024E-07
Al	26.98154	<i>0.16</i>	<i>0.00029616</i>	<i>1.09764E-08</i>
Fe	55.847	<i>0.02</i>	<i>0.00003702</i>	<i>6.62883E-10</i>
Ca	40.08	57.4	0.1062474	2.65088E-06
Mg	24.305	0	0	0
Na	22.98977	5870	10.86537	0.000472618
K	39.0983	4620	8.55162	0.000218721
S	32.06	221	0.409071	1.27295E-05
Cl	35.453	4680	8.66268	0.000244343
$\text{NO}_2$	46.0055	<i>0.76</i>	<i>0.00140676</i>	<i>3.05781E-08</i>
$\text{NO}_3$	62.0049	849	1.571499	2.53448E-05

Bold italicized values indicate levels below detection limit

## Appendix F

Corrections for compression and thermal expansion of mercury, sample compression and volume changes of glass penetrometer

### A. Mercury intrusion porosimetry without sample (i.e. blank run)

$$\Delta V_b = \Delta V_{Hg,b} - \Delta V_g \quad (F.1)$$

where  $\Delta V_b$  = the change in volume due to the blank run

$\Delta V_{Hg,b}$  = reduction in mercury volume

$\Delta V_g$  = reduction in penetrometer volume

$$\begin{aligned} dV &= \left( \frac{\partial V}{\partial P} \right)_T dP + \left( \frac{\partial V}{\partial T} \right)_P dT \\ &= -\beta V dP + \alpha V dT \\ &\quad \text{or} \\ d \ln V &= -\beta dP + \alpha dT \quad (F.2) \end{aligned}$$

where  $\beta$  = isothermal compressibility coefficient

$$\beta = -\frac{1}{V} \left( \frac{\partial V}{\partial P} \right)_T$$

where  $\alpha$  = thermal expansion coefficient

$$\alpha = \frac{1}{V} \left( \frac{\partial V}{\partial T} \right)_P$$

Integration of (F.2) gives:

$$\begin{aligned} \ln \frac{V_{Hg}(P)}{V_{Hg}(P_a)} &= -\int_{P_a}^P \beta_{Hg} dP' + \int_{T_a}^T \alpha_{Hg} dT' \\ \Delta V_{Hg}(P) &= V_{Hg}(P_a) - V_{Hg}(P) = V_p \left[ 1 - \exp \left\{ -\int_{P_a}^P \beta_{Hg} dP' + \int_{T_a}^T \alpha_{Hg} dT' \right\} \right] \quad (F.3) \end{aligned}$$

where  $V_p = V_{Hg}(P_a, T_a)$  = penetrometer volume at ambient conditions.

Similarly for glass,

$$\Delta V_g(P) = V_g(P_a) - V_g(P) = V_g \left[ 1 - \exp \left\{ -\int_{P_a}^P \beta_g dP' + \int_{T_a}^T \alpha_g dT' \right\} \right] \quad (F.4)$$

where  $V_g = V_g(P_a, T_a)$  = glass volume at ambient conditions.

Substitution into of F.3 and F.4 into F.1 gives:

$$\Delta V_b(P) = V_p \left[ 1 - \exp \left\{ - \int_{P_c}^P \beta_{Hg} dP' + \int_{T_c}^T \alpha_{Hg} dT' \right\} \right] - V_g \left[ 1 - \exp \left\{ - \int_{P_c}^P \beta_g dP' + \int_{T_c}^T \alpha_g dT' \right\} \right]$$

**B. Mercury intrusion porosimetry with non-porous sample of volume  $V_s$**

$$\Delta V_{exp}(P) = \Delta V_{Hg}(P) - \Delta V_g(P) + \Delta V_s(P) \quad (F.5)$$

where  $\Delta V_s(P)$  is the reduction in volume of the non-porous sample

$$\Delta V_{Hg}(P) = (V_p - V_s) \left[ 1 - \exp \left\{ - \int_{P_c}^P \beta_{Hg} dP' + \int_{T_c}^T \alpha_{Hg} dT' \right\} \right] \quad (F.6)$$

$$\Delta V_g(P) = V_g \left[ 1 - \exp \left\{ - \int_{P_c}^P \beta_g dP' + \int_{T_c}^T \alpha_g dT' \right\} \right] \quad (F.7)$$

$$\Delta V_s(P) = V_s \left[ 1 - \exp \left\{ - \int_{P_c}^P \beta_s dP' + \int_{T_c}^T \alpha_s dT' \right\} \right] \quad (F.8)$$

Substituting F.6, F.7 and F.8 into F.5 gives:

$$\begin{aligned} \Delta V_{exp}(P) &= (V_p - V_s) \left[ 1 - \exp \left\{ - \int_{P_c}^P \beta_{Hg} dP' + \int_{T_c}^T \alpha_{Hg} dT' \right\} \right] \\ &\quad + V_s \left[ 1 - \exp \left\{ - \int_{P_c}^P \beta_s dP' + \int_{T_c}^T \alpha_s dT' \right\} \right] \\ &\quad - V_g \left[ 1 - \exp \left\{ - \int_{P_c}^P \beta_g dP' + \int_{T_c}^T \alpha_g dT' \right\} \right] \quad (F.9) \end{aligned}$$

Algebraic combination of F.1 and F.9 gives:

$$\frac{\Delta V_{exp}}{V_p - V_s} - \frac{\Delta V_b}{V_p} = \frac{V_s}{V_p - V_s} - \left[ \frac{1 - \exp \left\{ - \int_{P_c}^P \beta_s dP' + \int_{T_c}^T \alpha_s dT' \right\}}{\left( \frac{V_g}{V_p} - \frac{V_g}{V_p - V_s} \right) \left( 1 - \exp \left\{ - \int_{P_c}^P \beta_g dP' + \int_{T_c}^T \alpha_g dT' \right\} \right)} \right]$$

or

$$\frac{\Delta V_{exp}(P) - \Delta V_b(P)}{V_s} + \frac{\Delta V_b(P)}{V_p} = \Gamma(P)$$

where  $\Gamma(P) = 1 - \exp\left\{-\int_{P_0}^P \beta_s dP' + \int_{T_0}^T \alpha_s dT'\right\} - \frac{V_g}{V_p} \left[1 - \exp\left\{-\int_{P_0}^P \beta_g dP' + \int_{T_0}^T \alpha_g dT'\right\}\right]$

Therefore, correction value at each intruded pressure for cement paste specimens is given by:

$$\Delta V_{ccm}(P) = \left(1 - \frac{V_{ccm}}{V_p}\right) \Delta V_b(P) + V_{ccm} \Gamma(P)$$

Corrected incremental intrusion volume is given by:

$$\Delta V_{uncorrected}(P) - \Delta V_{ccm}(P) = \Delta V_{corrected}(P)$$